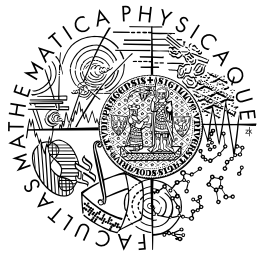

FACULTY
OF MATHEMATICS
AND PHYSICS
Charles University

DOCTORAL THESIS

Jiří Procházka

Elastic proton-proton collisions at high energies

Institute of Particle and Nuclear Physics

Supervisor of the doctoral thesis: RNDr. Vojtěch Kundrát, DrSc.
Study programme: Physics
Study branch: Subnuclear Physics

Prague 2016

Acknowledgement

First of all I would like to thank to my supervisor Vojtěch Kundrát for his kind advice and tireless help during my doctoral research studies. His guidence throughout literature and hitherto knowledge concerning elastic collisions has been very valuable.

I would like to express my sincere gratitude also to Valentina Avati, Mirko Berretti, Mario Deile, Karsten Eggert, Adrian Fiergolski, Frigyes J. Nemes, Simone Gianni, Leszek Grzanka, Hubert Niewiadomski, Jan Kašpar, Josef Kopal, Kenneth Österberg, Michele Quinto, Nicola Turini and all other members of the TOTEM collaboration for many discussions which I had with them in past several years during my stay at CERN and which helped me to better understand not only the measurement of particle collisions.

I am very grateful that I had quite unique opportunity to get familiar with both theoretical and experimental aspects of the given physical process (particle collisions in general) which strongly influenced the structure of this thesis. I am fully convinced that it will be possible to obtain further interesting results in the future if assumptions often not sufficiently mentioned in theoretical descriptions (models) will be analysed simultaneously with corresponding experimental conditions.

Last but not least I would like to express my deep gratitude to my family for permanent support as well as to all other people who directly or indirectly helped and inspired me during my studies.

I declare that I carried out this doctoral thesis independently, and only with the cited sources, literature and other professional sources.

I understand that my work relates to the rights and obligations under the Act No. 121/2000 Coll., the Copyright Act, as amended, in particular the fact that the Charles University in Prague has the right to conclude a license agreement on the use of this work as a school work pursuant to Section 60 paragraph 1 of the Copyright Act.

In Prague, July 29, 2016

Jiří Procházka

Title: Elastic proton-proton collisions at high energies

Author: Jiří Procházka

Department: Institute of Particle and Nuclear Physics

Supervisor: RNDr. Vojtěch Kundrát, DrSc.; Institute of Physics AS CR

Abstract:
The proton, one of the basic constituents of atoms, was discovered around 1920. Its structure has been intensively studied since that time mainly with the help of proton-proton collision experiments. Main progress has started when corresponding experiments at the world's first hadron collider ISR at CERN which ran from 1971 to 1984 were performed. The understanding of the structure and interactions of this subatomic particle protons has been, however, rather incomplete. Only some very general models have been available especially in the case of higher collision energies when very different kinds of collisions have existed. Some very simplifying assumptions of unclear physical meaning have been then involved in models concerning elastic processes. The influence of these assumptions on physical interpretation has started to be studied and some progress has been made when the eikonal model has been proposed, i.e., the dependence of elastic collisions on corresponding impact parameter values has been taken into account from the beginning. However, even if some new results have been obtained many unanswered questions have remained. For example, the collision process has been denoted generally as probabilistic but corresponding probabilities have not been sufficiently defined and determined. The given thesis contains, therefore, summary of different contemporary descriptions of elastic hadron collisions concerning the influence of impact parameter and the discussion of consequences and justification of some important assumptions. The eikonal model has been generalized and demonstrated on experimental data at 53 GeV and then applied also to newly obtained data at 8 TeV. Consequently, the contemporary TOTEM experiment at the LHC accelerator at CERN devoted to measurement of elastic pp scattering and diffractive processes at the highest ever reached energies has been described. In the given thesis several important open problems blocking the progress in the given area of research have been identified. A new probabilistic model of particle collisions has been then shortly described; the dependence of elastic collisions on impact parameter having been systematically taken into account in analyses of corresponding experimental data. It has been demonstrated that with the help of it deeper understanding of characteristics and interactions of fundamental particles might be obtained.

Keywords: proton-proton collisions, models of elastic collisions, impact parameter, central or peripheral scattering, probabilistic scattering, TOTEM experiment at the LHC at CERN

Název práce: Pružné srážky protonů s protony při vysokých energiích

Autor: Jiří Procházka

Katedra: Ústav částicové a jaderné fyziky

Vedoucí disertační práce: RNDr. Vojtěch Kundrát, DrSc.; Fyzikalní ústav AV ČR, v. v. i.

Abstrakt:
Proton, jeden ze základních stavebních kamenů atomů, byl objeven okolo roku 1920. Jeho struktura byla od té doby intensivně studována zejména s pomocí srážkových proton-protonových experimentů. K hlavnímu pokroku došlo, když byly provedeny experimenty na světově prvním srážeči hadronů ISR v CERN, který byl v provozu v letech 1971 až 1984. Porozumění struktuře a vzájemnému působení této subatomární částici však zůstávalo značně neúplné. Pouze velice obecné modely byly k disposici, zejména v případě vyšších srážkových energiích, kdy existovaly velmi rozdílné druhy srážek. Modely pružných srážek zahrnovaly některé velice zjednodušující předpoklady nejasného fyzikálního významu. Vliv těchto předpokladů na fyzikální interpretaci se začal studovat, a určitého pokroku se dosáhlo, když byl navržen eikonálový model, který mimo jiné umožnil studovat závislost pružných srážek na hodnotách příslušného srážkového parametru od samého počátku. Avšak i když některé nové výsledky byly získány, mnoho nezodpovědených otázek zůstalo. Srážkový proces byl, např., označen jako pravděpodobnostní, ale příslušné pravděpodobnosti nebyly dostatečně definovány a určeny. Předkladaná práce proto obsahuje přehled současných různých popisů pružných srážek hadronů týkajících se vlivu srážkového parametru a příslušnou diskuzi ohledně důsledků a oprávněnosti několika důležitých předpokladů. Eikonálový model byl zobecněn a demonstrován na experimentálních datech při 53 GeV a pak aplikován také na nově získané výsledky při 8 TeV. Je proto popsán i současný experiment TOTEM (na urychlovači LHC v CERN) určený k měření pružných srážek protonů a difrakčních procesů při nejvyšších energiích, kterých kdy bylo dosaženo. Dále je identifikováno několik důležitých otevřených problémů omezujících pokrok v dané oblasti výzkumu. Krátce je pak popsán nový pravděpodobnostní kolizní model částic, s jehož pomocí lze vzít do úvahy systematicky závislost pružných srážek na srážkovém parametru v analýzách příslušných experimentálních dat. Je také ukázáno, že s jeho pomocí by se mohlo dosáhnout nového a hlubšího porozumění vlastnostem a interakcím fundamentálních částic.

Klíčová slova: srážky protonů, modely pružných srážek protonů, srážkový parameter, centrální či periferální rozptyl, pravděpodobnostní rozptyl, experiment TOTEM na LHC v CERN

Contents

Introduction

According to the contemporary knowledge the macroscopic matter world we live in consists of atoms with dimensions of the order 10^{-10} m. The basic constituents of atomic nuclei ($\approx 10^{-15}$ m) are nucleons: protons and neutrons. Better understanding of nucleon characteristics and their interactions may, therefore, immediately improve our knowledge of the whole atomic (microscopic) physics. One of the nowadays standard methods how to study properties of some particles is to analyze their collisions at various energies and observe corresponding result. This method was pioneered by Rutherford in the beginning of 20th century [1] who also discovered the proton around 1920.

Two-particle collisions may be divided into elastic and inelastic. In *elastic* collision energy and magnitude of momentum of each of the particles are conserved during the motion and no new particles are created (the particles may change only direction of their motion during the collision); all the other types of collisions may be denoted as *inelastic*. Inelastic processes having "similar" dynamical characteristics are called quasi-elastic or more generally diffractive production processes. They have been introduced for the first time in 1950s [2, 3]. Together with the elastic scattering they are often called *diffractive* processes. The presented thesis is devoted mainly to proton-proton (pp) elastic collisions (at high energies) but many discussed aspects are similar to other particles, namely to (charged) hadrons.

Detection of pp collisions has already quite long tradition. Two beams of protons collided for the first time in the Intersecting Storage Rings (ISR) at European Organization for Nuclear Research (CERN); it was the first world hadron collider. It ran from 1971 to 1984 and it was one of very successful projects that opened the way to new technological development and physics discoveries with an impact up to the present [4]. Part of the ISR is shown in fig. 1. In the ISR the protons collided at energy $\sqrt{s}$ in the range of approximately $20 - 60$ GeV.

The pp collisions have been measured and studied later also in several other experiments which helped to extend important information about protons and, of course, about other particles produced during the collisions. The present day accelerator where pp collisions are observed in several experiments is the Large Hadron Collider (LHC) at CERN which has been designed (after some upgrades) to ultimately reach collision energy of 14 TeV. It has provided important experimental data at lower energies already now. The first pp collisions at LHC were recorded during LHC Run 1 from November 2009 till February 2013, before Long Shutdown 1 (LS1). The TOTal, Elastic and diffractive cross section Measurement (TOTEM) experiment which has been dedicated to measurement of diffractive processes including elastically (diffractively) scattered protons.

However, even thought a lot of data have been accumulated at various collision energies, the description and understanding of the structure, interactions and characteristics of protons (hadrons) is still not complete in many aspects. For example, the range of

Figure 1: The world's first proton-proton collider - ISR. Two beam pipes cross at large crossing angle (Image: CERN).

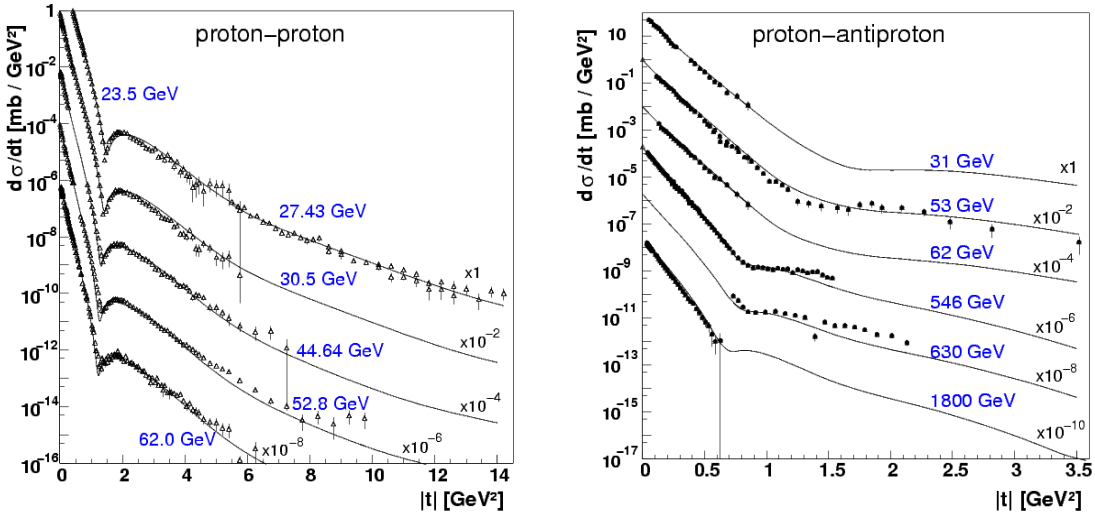

(a) proton-proton **(b)** proton-antiproton

Figure 2: Measured energy dependent elastic differential cross sections (multiplied by different factors for better readability). The full lines are only indicative (corresponding to a model prediction, see [5]).

hadronic interaction, dimensions (shape) of proton, distribution of electric charge inside proton, distribution of hadronic matter inside proton etc. are still not sufficiently known. In fact, the description of the kinematically simplest process, i.e., elastic scattering of protons (diffractive processes in general) is still very limited.

The first measurement of pp elastic collisions (beam-beam) has been performed at ISR; the experimental result in form of measured elastic differential cross section has been plotted as a function of momentum transfer (scattering angle) at some selected energies in fig. 2 where one may see a clear non-trivial *dip-bump* structure which has been measured for the first time at ISR in pp collisions at energies of 23.5, 30.7, 44.9 and 53 GeV in 1974 [6]. Such a t-dependent structure has been later discovered in elastic collisions of several other hadrons [7–12]. Only one diffractive dip has been observed in collisions of hadrons up to now while more than one dip has been observed even earlier in collisions of light nuclei. In the case of ($\bar{\text{p}}$p) elastic collisions no dip has been observed, only a *shoulder* - see fig. 2. Similar diffractive structure has been observed at ISR also in some non-elastic interaction, e.g., in single diffraction pp $\rightarrow$ p ($\text{n}\pi^+$) at 45 GeV as discussed in [13] (from 1975), see fig. 3. Even thought these dip-bump structures in differential cross sections of diffractive processes varying with collision energy and particle type are known for relatively long time, their explanation (relation to the structure and interaction of the colliding particles) represents, however, still an open question.

Two fundamental interactions are usually used for description of elastic scattering of two charged hadrons: the long-ranged Coulomb interaction (electromagnetic) and much stronger but short-ranged hadronic interaction (also known as nuclear or strong). While the former one is supposed to be well known, the determination of the latter one is more complicated. The simultaneous action of both the interactions already in the case of elastic collisions represents, therefore, quite delicate problem even thought some models exist (as we will see later).

Better understanding of diffractive collision processes of protons (mainly those with at least one proton surviving the collision) could bring new and important light in description of their structure and interactions as the diffractive processes are quite frequent ones (they always represent a significant part of total hadronic cross section).

The result of a collision of two objects (particles) depends on their structure, interaction type, collision energy and also on the value of so-called *impact parameter* b, see fig. 4. It is mainly the dependence on the impact parameter which is usually not respected in descriptions of collisions. However, there are at least three effects which may significantly influence the collision result of two hadrons

1. There is surely a big difference in interaction of two particles colliding head-on at $b = 0$ or at some higher value of b (e.g., corresponding to the boundary of short-ranged or contact hadronic collisions). The collision of two particles mainly at small relative distances may be regarded as a probabilistic process (depending on geometrical configuration of colliding particles, their spins, etc.). One may, therefore, introduce probability $P(s, b)$ that two colliding particles will produce a given type of process at impact parameter b and collision energy $\sqrt{s}$. This probability function may be, of course, very different for different types of processes (interactions) and particles.

2. The initial states of two particle collisions distinguished by impact parameter

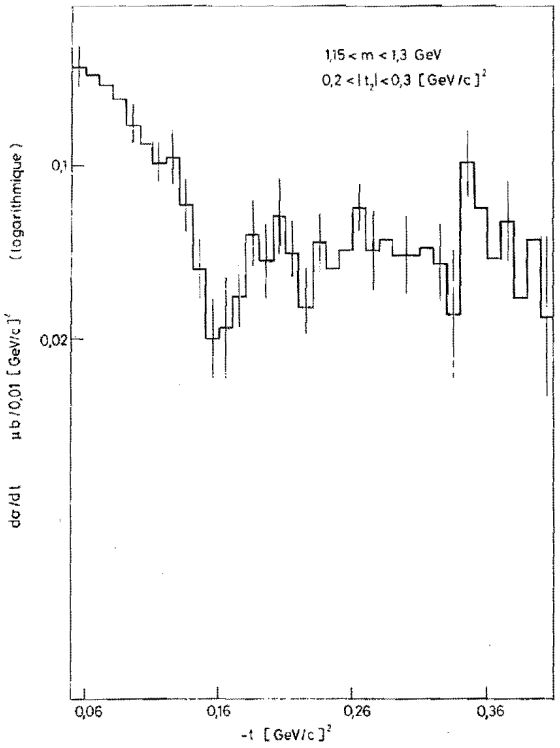

Figure 3: Differential cross section of reaction pp $\to$ p ($n\pi^+$) at the ISR energy of $\sqrt{s} = 45$ GeV in diffractive mass range (1.15, 1.3) GeV and momentum transfer of the neutron in the range $0.2 < |t_2| < 0.3$ GeV^2. A dip at $-t = 0.16$ GeV^2 is followed by a bump [13].

have always different frequencies in collision experiments (see, e.g., fig. 5). The corresponding distribution of impact parameter must be taken into account in order to study the physically interesting dependence of collisions on impact parameter mentioned in the previous point.

3. The actual minimum mutual distance (in collision instant) of colliding charged hadrons may be significantly influenced by long-ranged Coulomb interaction especially at very low collision energy values where it may even happen that the Coulomb interaction may deflect the colliding particles at impact parameter so that they do not even enter to a region of short-ranged interaction. If this effect of long-ranged Coulomb interaction is not taken into account then the established value of total hadronic cross section may be different than it corresponds to reality (depending on collision energy). In the case of attractive (repulsive) Coulomb force it may be lower (higher).

Until now only some phenomenological models have been applied to in interpreting experimental data represented by elastic differential cross sections. For example the description of elastic collisions of charged hadrons proposed by West and Yennie (WY) [14] in 1968 (having been commonly used for determination of total hadronic cross section since ISR era) has not taken impact parameter into account at all. One of the first discussion concerning the character of hadronic collisions in impact parameter space has been presented by Miettinen in 1974 [15] (see also [16] from 1975). According to his calculations a rather great ratio of elastic processes should correspond to central collisions (even at impact parameter $b = 0$) and average impact parameter of elastic collisions should be smaller than that of inelastic ones; which is to be denoted as surprising in the case of matter particles.

The central character of elastic collisions has been even more confusing due to the fact that the single inelastic diffraction seemed to be peripheral (see again [15] or, e.g.,

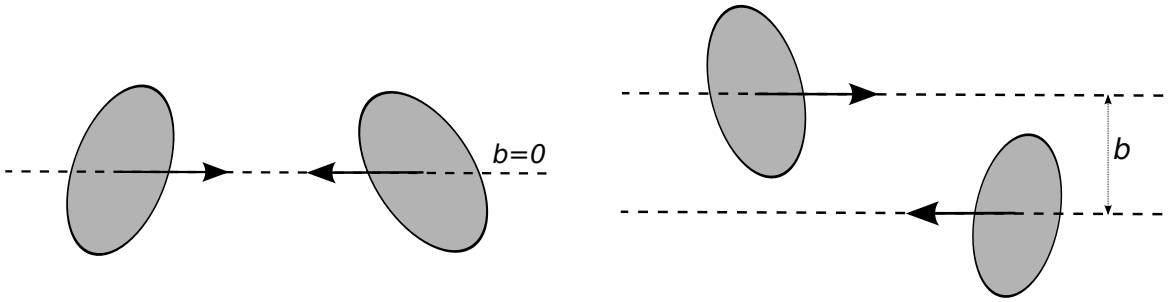

(a) central collision: small values of b **(b)** peripheral collision: higher values of b

Figure 4: Example of a central and peripheral collision of two particles of finite dimensions; one may expect that the result of a collision depends strongly on the value of impact parameter b which represents transversal distance of the two particles before collision.

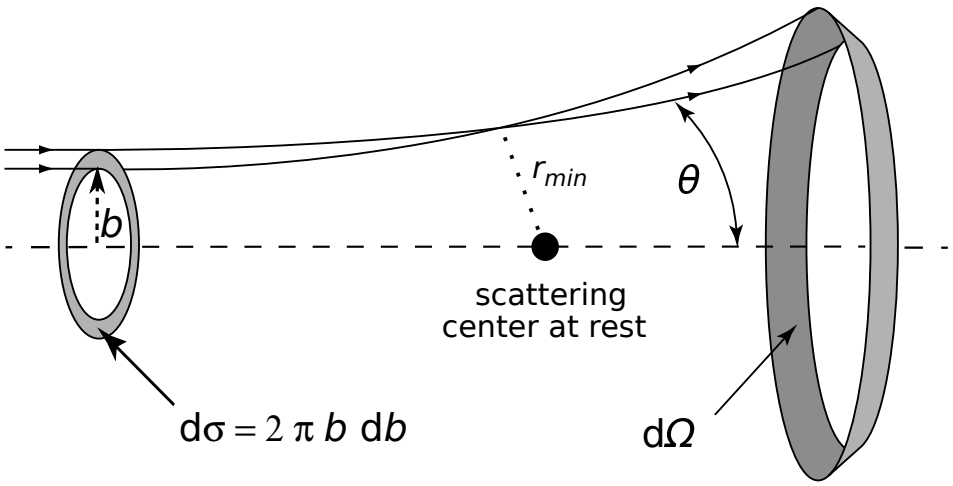

Figure 5: Potential elastic scattering (e.g., Coulomb) of a particle on a scattering centre at rest. Particles hitting the ring between b and $b + \mathrm{d}b$ are scattered by an angle between θ and $\theta + \mathrm{d}\theta$. The element of cross section $\mathrm{d}\sigma = 2\pi b\,\mathrm{d}b$ represents the area of a ring of radius b and width $\mathrm{d}b$. The b-dependent factor $2\pi b$, therefore, represents a weight of initial states corresponding to a given impact parameter (assuming independently and uniformly distributed two particle collisions in cross plane).

Giovannini et al. [17] from 1979). Such significant difference between both the kinds of diffractive collisions may be hardly brought to agreement with other experimental data as the elastic and mentioned inelastic diffraction processes should have very similar dynamics. This kind of "transparency" of protons (in elastic collisions) was, therefore, denoted as a puzzling question already at that time (see, e.g., Giacomelli and Jacob [18] from 1979).

It was then shown in [19] (1981) that the central character of elastic collisions has been derived due to some assumptions in corresponding collision models that have been strongly limiting. It has been shown, too, that very different (peripheral) behaviour of elastic collisions may be obtained if one admits arbitrary change of t-dependence of elastic hadronic phase that has been admitted in standard approaches to change only very slightly.

A new more general formula for description of elastic scattering for both the Coulomb and hadronic interactions has been then derived on the basis of eikonal model in 1994 [20] as an alternative to that of WY. It has allowed taking into account and further study the dependence of (elastic) hadronic collisions on impact parameter. However, even if the elastic processes prevailed significantly at higher values of impact parameter (and elastic collisions could be denoted as peripheral) the non-zero probability at $b = 0$ has remained as other (commonly used) assumptions have been applied to. It means that the problem of physical interpretation is to be studied and analyzed further to a greater detail. The eikonal model approach and its possibilities have been recently revisited and summarized in [21] (2016).

Several fundamental open problems in contemporary descriptions of elastic collisions have been explicitly identified and discussed in [22] (2015). It is possible to say that it is mainly the dependence of elastic collisions on impact parameter which has not been systematically taken into account and which should be carefully analyzed. To overcome the limitations contained in previous descriptions of elastic collisions new probabilistic collision model has been proposed. It is introducing probability of elastic collision in dependence on impact parameter b. First ideas of the model have been formulated in 2009 in [23] and later significantly improved in 2013 [24].

The presented thesis represents continuation of two previous theses (bachelor and diploma) [25, 26] of the author which have been devoted also to elastic scattering. To explain the story outlined in the preceding about evolution of description of elastic pp collisions in dependence on impact parameter in more detail this thesis is structured as follows (main contributions of the author to the given results are also mentioned together with corresponding publications which he co-authored):

Chapter 1

The aim of this chapter is to provide a reader basic information concerning the way how pp collisions are produced at the LHC at CERN. The whole LHC accelerating chain is, therefore, very briefly explained together with purpose of several experiments devoted to the measurement of the collisions. Some widely known accelerator physics principles are summarized. It is mainly transverse linear beam motion and concept of luminosity which are discussed in slightly more details as they are very important for understanding several aspects of measurement of (elastic) pp scattering discussed in next chapters.

Chapter 2

A diffractively scattered proton is scattered at very small angle. It moves along proton beam where its motion is influenced by magnetic field (it stays in beam pipe for quite long distance) before it may be detected by special detectors. One of the main experimental difficulties is then detection of such protons and reconstruction of their kinematics after the scattering. Corresponding measurement techniques are, therefore, outlined in this chapter with the help of detector apparatus of TOTEM experiment at the LHC dedicated to measurement of mainly diffractive processes. This chapter contains also brief summary of several published physics results characterizing pp (diffractive) collisions determined from data obtained during LHC Run 1 (before LHC LS1) by TOTEM collaboration [27–44].

The author of this thesis, as a member of TOTEM collaboration, has contributed to the results concerning mainly elastic scattering and its interpretation; it concerns also measurement of total pp cross section as corresponding hitherto methods are based on measurement of elastic scattering, see below. He has contributed mainly to [36] concerning measurement and interpretation of elastic pp scattering in Coulomb-hadronic interference region at 8 TeV. Some of the results have been presented by the author on behalf of the whole collaboration in [45–47].

Chapter 3

This chapter summarizes contemporary theoretical description of elastic scattering of charged hadrons (e.g., pp or $\bar{\text{p}}$p). One may find here more detailed discussion of the WY and the eikonal model approach together with corresponding assumptions. In [20] only *electric* form factors have been taken into account in the eikonal model. In this chapter the model is generalized to study also the influence of *effective electromagnetic* form factors on determination of elastic hadronic amplitude $F^{\text{N}}(s,t)$ on the basis of experimental data. It is further shown how b-dependent total, elastic and inelastic profile functions and corresponding mean impact parameter values may be calculated at finite energies on the basis of elastic amplitude $F^{\text{N}}(s,t)$. Contemporary widely used models (or parameterizations) of elastic hadronic amplitude $F^{\text{N}}(s,t)$ contain several a priory limitations leading to the mentioned central character of elastic collisions. These limitations are discussed in this chapter, too. The understanding of the description of elastic collisions is also of key importance for understanding of, e.g., contemporary methods of total hadronic cross section measurement; the corresponding discussion may be, therefore, found also in this chapter.

The whole eikonal model approach has been generalized and revisited by the author of the thesis with the aim to prepare it for analysis of experimental data of elastic pp collisions at LHC energies measured by TOTEM, i.e., at the highest ever reached pp collision energies, see also chapter 4.

Chapter 4

In this chapter the eikonal model described in chapter 3 is applied to older experimental ISR data at 53 GeV and also to data at 8 TeV recently measured by TOTEM [36]. At 53 GeV a fit corresponding to widely used assumptions and leading to central behaviour of hadronic collisions is shown. It is then demonstrated that one may fit the same data and obtain peripheral (i.e., completely different) character of elastic collisions; several new peripheral alternatives are discussed

to demonstrate different interpretation possibilities. These fits are performed taking into account *electric* form factors and then also *effective electromagnetic* form factors to see the impact on the results. Similar analysis is then performed at 8 TeV and two interesting fits, one leading to central and the second one to the peripheral behaviour, are shown. At both the energies cross sections, b-dependent profile functions, corresponding values of mean impact parameters and other interesting quantities characterizing pp collisions are calculated for each alternative corresponding to different assumptions. The results obtained on the basis of this eikonal model analysis at two very different high energies are then compared.

The analysis of the 53 GeV data has been made by the author of the thesis and together with the description of the revisited eikonal model may be found in [21] (see also [22]). The performed analysis at 8 TeV aiming to compare and test various assumptions and interpretation possibilities (such as demonstrating the possibility of peripheral alternative) at this new energy together with study of the whole theoretical background discussed in this thesis has represented significant contribution of the author of this thesis to [36] published by the TOTEM collaboration. Main results from [36] have been presented by the author in [47].

Chapter 5

This chapter is devoted to more detailed discussion (including historical context) regarding the centrality and peripherality of elastic collisions and corresponding calculations (approaches) leading to the given character. The results concerning b-dependent profile functions obtained by Miettinen at 53 GeV are compared to the results at the same energy performed in chapter 4. Central character of several contemporary models of hadronic amplitude analyzed in [48, 49] is commented here, too. Discussion from this chapter has been published in [22].

Chapter 6

This chapter contains list of several newly identified open problems in all contemporary descriptions of elastic collisions of (charged) hadrons. This chapter has been published as part of [22]. Some of the mentioned problems have been pointed out also earlier in, e.g., [24, 50, 51].

Chapter 7

In this chapter new probabilistic model of elastic pp collisions which aims to overcome limitations contained in contemporary descriptions of elastic scattering is described and applied to experimental pp data at energy of 53 GeV. Probabilities of total, elastic and inelastic hadronic collisions at given impact parameter together with several other interesting quantities characterizing structure of protons and their interactions are determined. It is demonstrated that with the help of it deeper understanding of characteristics and interactions of fundamental particles might be obtained. Some newly opened questions concerning structure of hadrons are mentioned at the end of this chapter. The probabilistic model has been published in [24] and explained to greater details in this thesis. It has been also extended and applied to broader t-interval of measured data than in [24].

Concluding remarks may be found in Conclusion. Summary of all the main results concerning dependence of elastic hadronic collisions on impact parameter has been

recently published in [22]. The thesis covers both experimental and theoretical aspects of (elastic) pp collisions and may be, therefore, useful for experimentally as well as theoretically oriented readers. Both the aspects (theoretical and experimental) are, of course, important for better understanding of corresponding matters of the given physical process. Many explanatory comments concerning motivations and historical context have been added, too. In the course of preparation of this thesis it has been necessary to go through literature to find out and study many details and origins of various models, techniques and methods. Many valuable references are, therefore, provided throughout the whole thesis for convenience of readers, particularly students.

Fitting of the models of elastic scattering to experimental data (discussed in details in chapter 4 and chapter 7) has been performed by the author of this thesis. For this purpose, the models have been implemented in Python programming language (and partially in C++ for performance reasons) with the help of ROOT [52] and SciPy [53] libraries. The actual fitting has been done with the help of mainly Minuit2 minimization package that is part of ROOT (see also [54]) and which allows a user to have more control on various aspect of the fitting (which has been essential). Version control system Subversion [55], Python testing tool pytest [56], automation server Jenkins [57] and other widely available open source software tools have been used to simplify and speed up the software development.

Chapter 1

Production of pp collisions - LHC accelerator at CERN

1.1 The LHC accelerator chain

The LHC at CERN is a successor of ISR mentioned in Introduction which may collide protons at much higher energies. The protons which collide in LHC origin from hydrogen atom - bounded system of electron and proton. A simple bottle of hydrogen gas provides molecules H_2 to duoplasmatron which uses electric field to strip hydrogen atoms of their electrons to obtain protons, see fig. 1.1. These protons are then accelerated by the chain of accelerators before they are injected into the LHC where dedicated particle detectors may detect products of the collisions. The corresponding collision data represent very important experimental input for studying the structure and interaction of protons which is useful for the whole atomic physics, including mainly the simplest atom - the hydrogen from which the protons originated.

The first accelerator in the LHC accelerator chain during the LHC Run 1 was LINear ACcelerator 2 (LINAC2) which accelerated the protons to the energy of 50 MeV. They were then injected into the Proton Synchrotron Booster (PSB) which accelerated them further to 1.4 GeV, followed by the Proton Synchrotron (PS) which pushed the proton energy to 25 GeV. Protons were then sent to the Super Proton Synchrotron (SPS) where they were accelerated to 450 GeV and injected finally into the LHC. Photos of the 4 LHC pre-accelerators are in fig. 1.3.

The LHC has been operational since 2010 and was able to provide proton collisions at energy up to 8 TeV during LHC Run 1. The LHC machine in the tunnel is shown in fig. 1.4 where one can see also a (small) curvature of the tunnel and the machine. The circumference of the LHC is about 27 km which makes it the biggest circular accelerator in the world. The LHC is located underground approximately 100 m below the surface as it is shown in fig. 1.2. The whole quite complex system of interconnected accelerators in CERN is shown in fig. 1.6. Detailed description of the LHC with all the necessary infrastructure (including various devices for beam diagnostics) may be found, e.g., in [58] (see also [59–62]). Useful information about LHC beam instrumentation may be found also in conceptual design report [63].

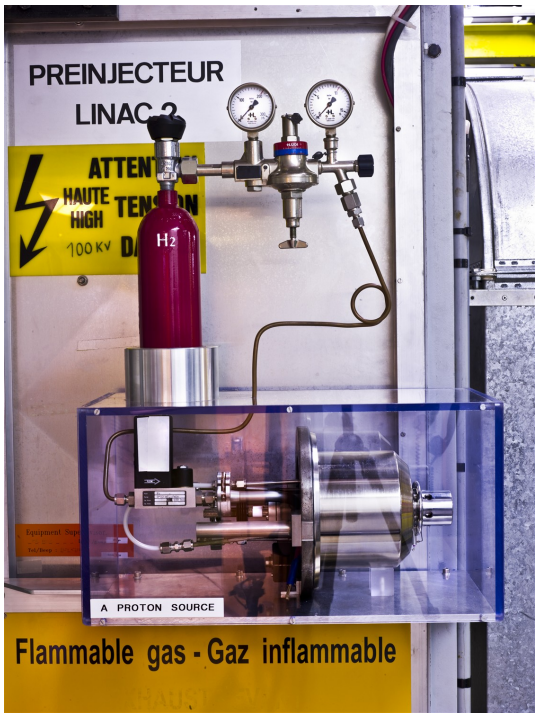

Figure 1.1: Proton source - pre-injector to LINAC2 (part of an exhibition at CERN). The red bottle is filled with hydrogen and duoplasmatron (bellow the bottle in the transparent box) uses an electric field to separate protons from hydrogen. The created protons are injected to LINAC2 (not shown in the photo) for further acceleration (Image: CERN).

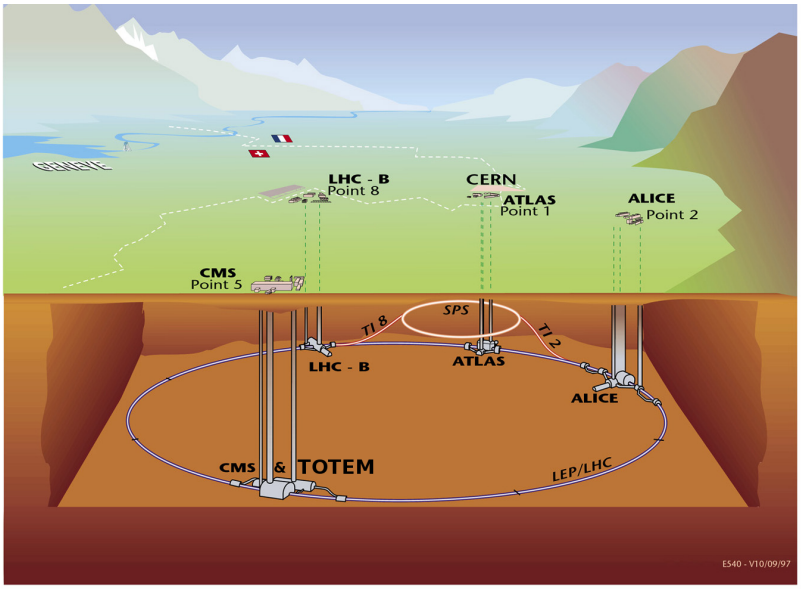

Figure 1.2: Schematic layout of LHC experiments at CERN. The LHC accelerator is underground approximately 100 m below the surface (Image: CERN).

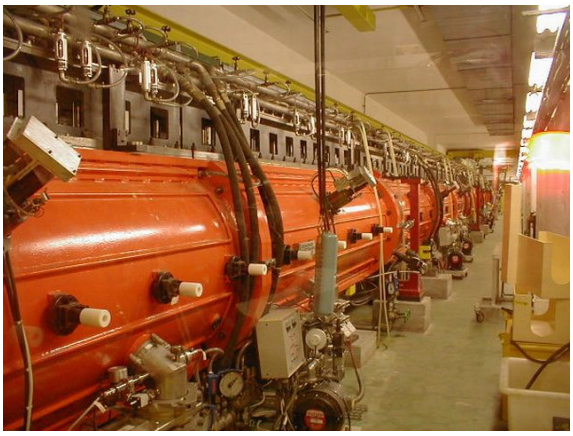

(a) LINear ACcelerator 2 (Image: CERN).

(b) Proton Synchrotron Booster (photo taken from [64]).

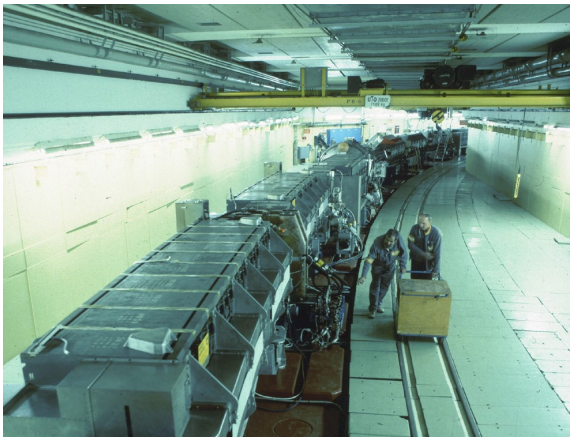

(c) Proton Synchrotron (Image: CERN).

(d) Super Proton Synchrotron (Image: CERN).

Figure 1.3: Preinjectors of LHC used to pre-accelerate protons before they are injected into the LHC.

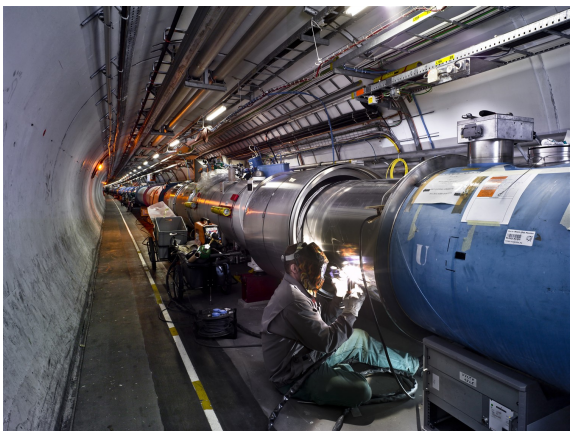

Figure 1.4: View of the LHC machine in the LHC tunnel (Image: CERN).

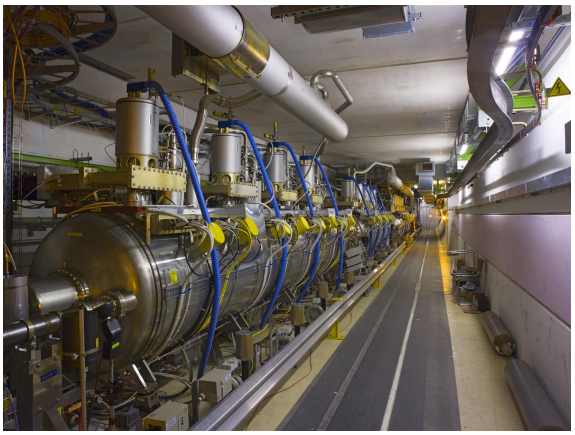

Figure 1.5: LHC superconducting radio-frequency (RF) cavity in the LHC tunnel (Image: CERN).

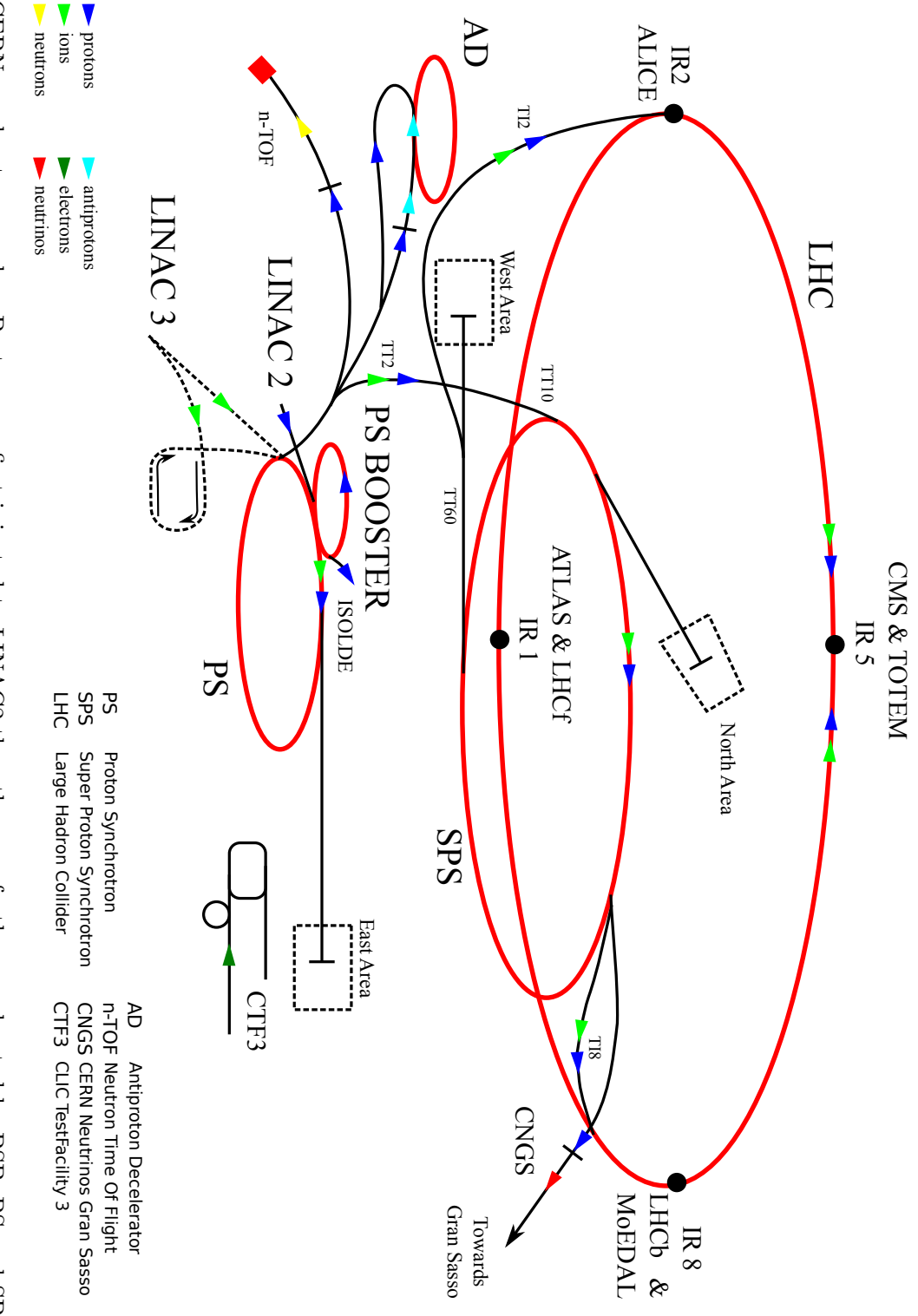

Figure 1.6: CERN accelerator complex. Protons are first injected to LINAC2 then they are further accelerated by PSB, PS and SPS before they are injected to the LHC where they can be even yet more accelerated before they are brought into collisions and then observed by dedicated detectors (Image: CERN).

1.2 Experiments at the LHC

Seven particle detector experiments have been constructed at the LHC. They are located at different interaction regions, see fig. 1.7 (and also figs. 1.2 and 1.6). They detect particles produced during collisions of beams circulating in LHC at various energies higher than 450 GeV (LHC injection energy). They differ in used detector technology according to corresponding physics purposes. The physics programs of the individual experiments are partially overlapping and also complementary to each other:

ALICE
: A Large Ion Collider Experiment. A detector specialised mainly in study of heavy ions (Pb-Pb) collisions but it also studies pp (and p-Pb) collisions [65].

ATLAS
: A Toroidal LHC ApparatuS. A general purpose particle detector designed to cover the widest possible range of physics at the LHC from search of Higgs boson to supersymmetry (SUSY), extradimensions, tests of quantum chromodynamics (QCD) and many others as stated in [66]. It is able to detect products of pp, A-p or A-A collisions where A stands for heavy ion. The purpose of the detector is similar as the CMS one.

CMS
: Compact Muon Solenoid. A general purpose particle detector similar to ATLAS [67]. ATLAS and CMS detectors differ in chosen detector technology and design.

LHCb
: Large Hadron Collider beauty. A detector dedicated to study of asymmetry between matter and antimatter in the interaction of b-hadrons (heavy particles containing a bottom quark) produced in collisions of protons or heavy ions [68].

LHCf
: Large Hadron Collider forward. A special purpose small experiment for astroparticle (cosmic ray) physics [69]. The aim of the experiment is to measure particle produced in the direction very close to the beam (in forward region) in the proton-proton collisions and provide experimental data at LHC energies which could help to explain the origin of ultra-high-energy cosmic rays.

MoEDAL
: Monopole and Exotics Detector at the LHC. A small experiment with primary motivation to search for the magnetic monopole and other highly ionizing Stable (or pseudo-stable) Massive Particles (SMPs) at LHC, see [70].

TOTEM
: TOTal, Elastic and diffractive cross section Measurement. A special purpose experiment focusing on detection of particles produced in forward region including diffractively scattered protons which may provide very important information about structure of protons [71]. The experiment will be discussed in more details in chapter 2.

Some experiments with their own detectors share the same Interaction Region (IR) (also called Interaction Point (IP)) and have, therefore, common physics program, such

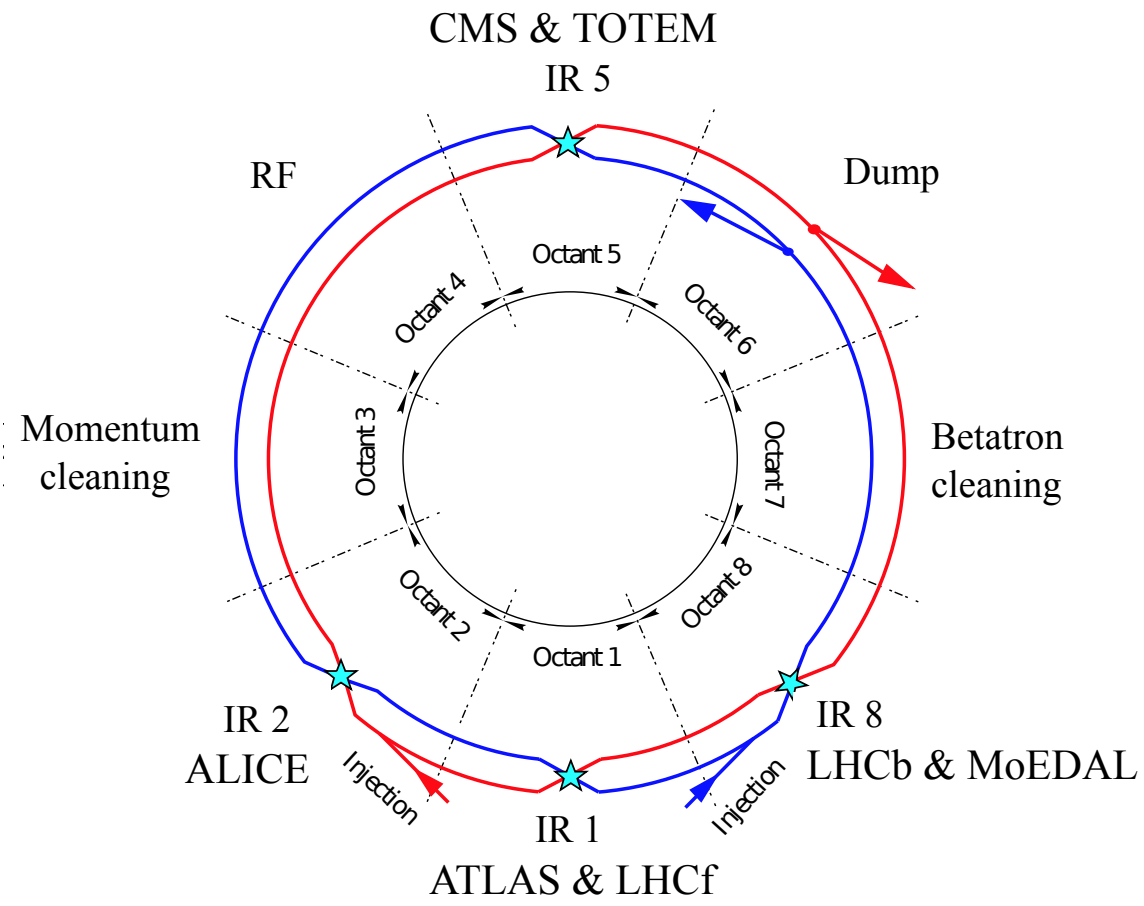

Figure 1.7: Schematic layout of LHC (Image: CERN).

as TOTEM and CMS experiments which are located in IR5, see fig. 1.7. Namely, beam parameters during data taking at given time are, therefore, the same for both the experiments (for this reason, e.g., measurement of instantaneous luminosity by one experiment may be then used by the second one). One of the ATLAS projects is Absolute Luminosity For ATLAS (ALFA) project [72] which has similar physics aim as TOTEM.

1.3 Accelerator physics principles

In this section we remind some basic physics principles of particle accelerators, much more details can be found, e.g., in [73–76]. The beam parameters may influence essentially measurement of characteristics of proton-proton collisions. Namely, detection of diffractive protons very close to the beam is influenced by them significantly. Monitoring and precise measurement of beam parameters is always essential for operation of any accelerator.

The force (Lorentz's force) acting on a particle of charge q moving with velocity $\vec{v}$ in the presence of an external electric field $\vec{E}$ and a magnetic field $\vec{B}$ is given by

$$\vec{F} = q(\vec{E} + \vec{v} \times \vec{B}) = \dot{\vec{p}}\,. \tag{1.1}$$

It is the electric field $\vec{E}$ which is used to accelerate charged particles in accelerators while the magnetic field $\vec{B}$ is used to change direction of motion of charged particles. In

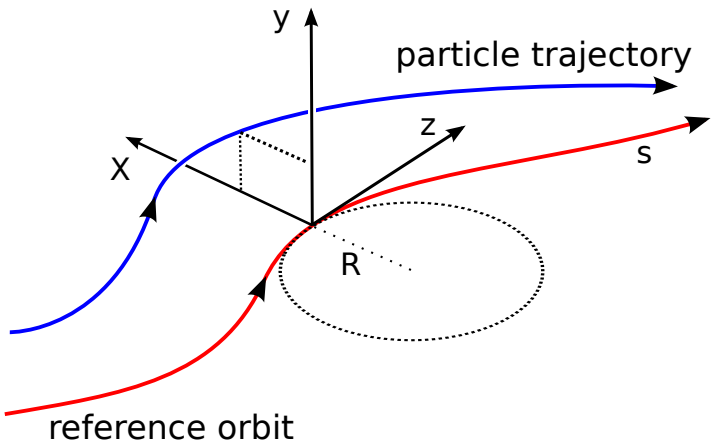

Figure 1.8: LHC co-moving coordinate system to describe the beam motion relative to the orbit. The red line represents nominal beam trajectory (reference orbit) and defines also s-coordinate with local curvature R. Transversal displacement of a particle trajectory (blue line) from the nominal beam trajectory (red line) is then described in the horizontal direction by x-coordinate and by y-coordinate in the vertical direction.

the case of LHC the corresponding acceleration system (Radio Frequency (RF) system) is installed at one place, see figs. 1.5 and 1.7. This system is also focussing the beam in longitudinal direction and keeps bunch structure of the LHC beam. The LHC (or any other similar accelerator) consists then of many magnets of several types. The accelerator magnetic elements are designed to guide and focus the particle beam along the reference circular orbit. The dipole magnets are used to bend the path of the charged particles as they travel around the ring while several other types of magnets (namely quadrupole magnets, see bellow) are designed for focusing of the beam. The physical fundamentals of beam steering and focusing are standardly called *beam optics* due to the fact that charged particle beam can be guided using magnets similarly as the guiding of a light beam by optical lenses.

1.3.1 Transverse linear beam motion

The coordinate system used for the description of the particle motion inside a beam pipe of an accelerator may be chosen as it is plotted in fig. 1.8. The particles travel along the beam nominal closed orbit represented by red line (s-coordinate) and perform transversal oscillation with respect to this reference orbit in horizontal x and vertical y direction due to magnetic field.

Let us consider for the sake of simplicity only the horizontal oscillations of one particle in the x-direction to show the most basic character of the transversal movement of particles in the presence of a magnetic field of several quadrupole magnets periodically displaced along the accelerator rings as these are the principal focusing elements in modern synchrotrons. The strength k of the quadrupole is characterized by gradient of its magnetic field $\mathrm{d}B_y/\mathrm{d}x$

$$k = \frac{1}{BR}\frac{\mathrm{d}B_y}{\mathrm{d}x} \tag{1.2}$$

where the quantity BR is called magnetic rigidity and it is related to momentum p of a

beam particle of charge e by relation $BR = p/e$. The particle trajectory may have an angle with respect to the reference orbit which may be expressed as

$$\theta_x \approx \frac{\mathrm{d}x}{\mathrm{d}s} = x'(s)\,. \tag{1.3}$$

The angular deflection given to a particle with nominal momentum p and passing through a short quadrupole of strength k and length $\mathrm{d}s$ at a displacement x is in a linear approximation (hence the term *linear beam motion*)

$$\mathrm{d}x' = -kx\mathrm{d}s\,. \tag{1.4}$$

It may be rewritten to

$$x''(s) + k_x(s)x = 0 \tag{1.5}$$

which is so-called homogeneous Hill's equation of the motion (a second order linear differential equation). The solution of this equation may be written in the form

$$x(s) = \sqrt{\beta_x(s)\epsilon_x}\cos[\phi_x(s) + \phi_{x0}] \tag{1.6}$$

where $\beta_x(s)$ is so-called *beta function*, also known as the amplitude function. The constant ϵ_x is termed the *emittance*. The trajectory function $x(s)$, therefore, describes transverse oscillations about the orbit known as betatron oscillations (for historical reasons) whose amplitude $\sqrt{\beta_x(s)\epsilon_x}$ and phase $\phi_x(s)$ depend on the position s along the orbit. Both the function $\phi_x(s)$ and β_x must have the same periodicity as the magnet lattice represented by strength $k(s)$; they are linked by condition

$$\frac{\mathrm{d}\phi_x(s)}{\mathrm{d}s} = \frac{1}{\beta_x} \quad \text{or} \quad \phi_x(s) = \int_0^s \frac{\mathrm{d}s'}{\beta_x(s')}\,. \tag{1.7}$$

The divergence equation of the particle's motion can be obtained by differentiating solution of the Hill's equation (1.5)

$$x'(s) = -\sqrt{\frac{\epsilon_x}{\beta_x(s)}}\sin[\phi_x(s) + \phi_{x0}] + \frac{\beta_x'(s)}{2}\cos[\phi_x(s) + \phi_{x0}]. \tag{1.8}$$

Up to now, we have been describing a motion of only one particle in the presence of a magnetic field. However, the beam is an ensemble of many particles and it is, therefore, important to know its parameters, too. The most basic beam parameters are the *beam size* $\sigma_x(s)$ and the *beam divergence* $D_x(s)$ which can be expressed in terms of the *beam emittance* ϵ_x^b and the betatron amplitude $\beta_x(s)$ as follows

$$\sigma_x(s) = \sqrt{\epsilon_x^b\beta_x(s)} \tag{1.9}$$

$$D_x(s) = \sqrt{\frac{\epsilon_x^b}{\beta_x(s)}}\,. \tag{1.10}$$

Such a definition of beam size is sometimes called the *betatron beam size* as it doesn't include the dispersion related beam size component (effect of off-momentum particles which is not taking into account in this section). The so-called *normalized emittance* is defined as

$$\epsilon_\mathrm{N} = \beta\gamma\epsilon \tag{1.11}$$

where β and γ are relativistic factors. The reason for introducing the normalized emittance is that it does not change during beam acceleration. The fact that the beam emittance ϵ_x^b may be constant (s-independent) is (theoretically) related to the Louville's theorem which states that every element of a volume of phase space is constant with respect to time if the particles obey the canonical equation of motions [74]. This is in first approximation the case of circulating proton beams in LHC during a circulation, however, the emittance of a bunch (beam) may blow-up in time in real machines due to several effects [77]. More details about the concept of the emittance and technical details about its measurement at the LHC can be found in [78]. In the case of LHC the corresponding measurement of beam profiles is based on Wire Scanner (WS) (or Beam Synchrotron Radiation Telescope (BSRT)) and measurement of β at the place s where the bunch profiles are measured, see again [78].

Some properties of the beam or characteristics of particle collisions may be strongly energy dependent. It is, therefore, necessary to measure energy of the colliding beams (particles), corresponding details about energy calibration at LHC can be found, e.g., in [79] and papers quoted there.

1.3.2 Concept of luminosity

If two beams collide at certain energy then a number of particle interactions of a given type per unit of time (rate) is produced. This rate N_{proc} is proportional to the corresponding cross section of the given process σ_{proc} (in area units) and so-called luminosity L (in per time and per area units)

$$N_{\text{proc}} = L\sigma_{\text{proc}} \tag{1.12}$$

(if they are not integrated over a time period as it is also common). Both the luminosity L and observed rate N_{proc} of a given process generally depend on time but their ratio, i.e., corresponding cross section, is always constant in time - it is a property of the colliding particles. The symbols N_{proc} and L have sometimes meaning of corresponding quantities integrated over time (the meaning should be always clear from the context). In order to experimentally determine the cross section one needs, therefore, to measure the rate and the luminosity. The way how the rate of, e.g., elastically scattered protons may be measured will be discussed in chapter 2. In the following we will summarize the main steps how the luminosity may be defined and measured.

In the case of the LHC the colliding beams consists of certain number of bunches (bunched beams, as opposite to the ISR beams which were coasting - no bunch structure, see, e.g., [80] for some comments concerning luminosity at ISR). In the following we will consider only two colliding bunches for the sake of simplicity (the overall luminosity is just summed over all the colliding bunches). We will take into account only head-on collisions of the two bunches moving with velocities $\vec{v}_{1,2}$ ($\vec{v}_1 \parallel \vec{v}_2$) and assuming that all the particles in a bunch have the same velocity $\vec{v}_{1,2}$ (also during collision). We may assume without further lost of generality that only the second bunch is moving ($\vec{v}_1 = 0$, $\vec{v}_2 = \Delta\vec{v}$; $\Delta\vec{v}$ being the relative velocity) parallel to z-axis.

Each of the two colliding bunches has certain number of particles $N_{1,2}$ (intensity) with corresponding distribution functions $\rho_1(x, y, z)$ (for the first bunch at rest) and $\rho_2(x, y, z - z_0)$ (for the second bunch displaced by longitudinal distance z_0 from the first bunch), see fig. 1.9. The distance z_0 depends on time according to $z_0 = |\Delta\vec{v}|t$. The

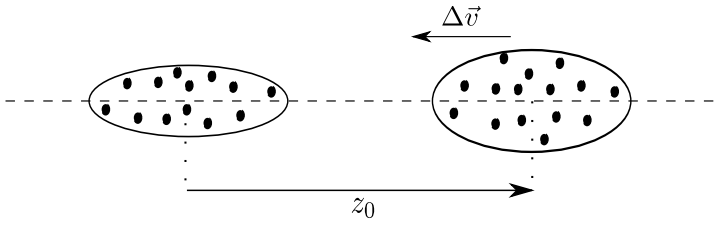

Figure 1.9: Schematic view of two bunches colliding head-on. Relative longitudinal distance z_0 of the bunches is changing in time according to $z_0 = |\Delta\vec{v}|t$. One bunch at rest with N_1 particles with density distribution $\rho_1(x, y, z)$ collide with another one which has N_2 particles distributed according to $\rho_2(x, y, z - z_0)$ distribution function.

particle distributions are taken as normalized so that $\int \rho_{1,2}(x, y, z)\mathrm{d}x\mathrm{d}y\mathrm{d}z = 1$ at any z_0 (or time t).

The luminosity corresponding to single pair of counter-rotating bunches colliding at one interaction region is defined as [81–85]

$$L = N_1 N_2 f_{\mathrm{rev}} \iiiint_{-\infty}^{+\infty} \rho_1(x, y, z)\rho_2(x, y, z - z_0)\mathrm{d}x\mathrm{d}y\mathrm{d}z\mathrm{d}z_0 \tag{1.13}$$

where f_{rev} is a revolution frequency of the two bunches (i.e., how often they collide per unit of time in a circular accelerator at certain interaction region). An *effective transverse area* A_{eff} in which the collisions take place may be defined using the convolution integral as

$$\frac{1}{A_{\mathrm{eff}}} = \iiiint_{-\infty}^{+\infty} \rho_1(x, y, z)\rho_2(x, y, z - z_0)\mathrm{d}x\mathrm{d}y\mathrm{d}z\mathrm{d}z_0. \tag{1.14}$$

Using this definition, the luminosity may be also written in the form

$$L = \frac{N_1 N_2 f_{\mathrm{rev}}}{A_{\mathrm{eff}}}. \tag{1.15}$$

The luminosity corresponding to single pair of counter-rotating bunches may be expressed using explicitly the time variable t (see, e.g., [85] and also [81–84])

$$L = N_1 N_2 f_{\mathrm{rev}} K \iiiint_{-\infty}^{+\infty} \rho_1(x, y, z)\rho_2(x, y, z - |\Delta\vec{v}|t)\mathrm{d}x\mathrm{d}y\mathrm{d}z\mathrm{d}t \tag{1.16}$$

where the relativistic kinematic factor K for bunches with arbitrary velocities $\vec{v}_{1,2}$ introduced by Møller [86] is

$$K = \sqrt{(\vec{v}_1 - \vec{v}_2)^2 - (\vec{v}_1 \times \vec{v}_2)^2/c^2}. \tag{1.17}$$

In our case of exactly head-on collisions ($\vec{v}_1 \parallel \vec{v}_2$), the kinematic factor $K = |\Delta\vec{v}|$ and eq. (1.16) can be rewritten into the form given by eq. (1.13) (using substitution $z_0 = |\Delta\vec{v}|t$ with corresponding Jacobian being equal to $1/|\Delta\vec{v}|$).

The overlap integral (convolution of the time dependent particle distribution functions of the two bunches) in eq. (1.13) or eq. (1.16) can be calculated analytically for certain bunch profiles. We may assume, e.g., uncorrelated Gaussian profiles of bunches in all

dimensions of the form

$$\rho_{iu}(u) = \frac{1}{\sqrt{2\pi}\,\sigma_{iu}} \exp\left(-\frac{u^2}{2\sigma_{iu}^2}\right) \quad \text{where } i = 1,2; \quad u = x, y; \tag{1.18}$$

$$\rho_{1z}(z) = \frac{1}{\sqrt{2\pi}\,\sigma_{1z}} \exp\left(-\frac{z^2}{2\sigma_{1z}^2}\right); \tag{1.19}$$

$$\rho_{2z}(z) = \frac{1}{\sqrt{2\pi}\,\sigma_{2z}} \exp\left(-\frac{(z-z_0)^2}{2\sigma_{2z}^2}\right). \tag{1.20}$$

Such bunch profiles are generally taken as a good first approximation; the determination of the real bunch profiles is generally much more delicate problem. The distribution functions $\rho_{1,2}$ may be, therefore, factorized as follows

$$\rho_1(x, y, z) = \rho_{1x}(x)\rho_{1y}(y)\rho_{1z}(z)\,, \tag{1.21}$$

$$\rho_2(x, y, z - z0) = \rho_{2x}(x)\rho_{2y}(y)\rho_{2z}(z - z_0). \tag{1.22}$$

In the simplified case when the bunches have equal sizes ($\sigma_{1x} = \sigma_{2x} = \sigma_x$, $\sigma_{1y} = \sigma_{2y} = \sigma_y$ and $\sigma_{1z} = \sigma_{2z} = \sigma_z$) the integral in eq. (1.13) can be rewritten to the form

$$L = \frac{N_1 N_2 f_{\text{rev}}}{(\sqrt{2\pi})^6 \sigma_x^2 \sigma_y^2 \sigma_z^2} \iiiint_{-\infty}^{+\infty} \mathrm{e}^{-\frac{x^2}{\sigma_x^2}} \mathrm{e}^{-\frac{y^2}{\sigma_y^2}} \mathrm{e}^{-\frac{z^2}{2\sigma_z^2}} \mathrm{e}^{-\frac{(z-z_0)^2}{2\sigma_z^2}} \,\mathrm{d}x\mathrm{d}y\mathrm{d}z\mathrm{d}z_0 \tag{1.23}$$

and after a substitution $\tilde{z}_0 = z - z_0$ with corresponding Jacobian equal to 1 we may obtain (writing again z_0 instead of $\tilde{z}_0$)

$$L = \frac{N_1 N_2 f_{\text{rev}}}{(\sqrt{2\pi})^6 \sigma_x^2 \sigma_y^2 \sigma_z^2} \iiiint_{-\infty}^{+\infty} \mathrm{e}^{-\frac{x^2}{\sigma_x^2}} \mathrm{e}^{-\frac{y^2}{\sigma_y^2}} \mathrm{e}^{-\frac{z^2}{2\sigma_z^2}} \mathrm{e}^{-\frac{z_0^2}{2\sigma_z^2}} \,\mathrm{d}x\mathrm{d}y\mathrm{d}z\mathrm{d}z_0\,. \tag{1.24}$$

Taking into account relation for the Gaussian integral ($a > 0$)

$$\int_{-\infty}^{+\infty} \mathrm{e}^{-\frac{t^2}{a}} \,\mathrm{d}t = \sqrt{\pi a} \tag{1.25}$$

the integral in eq. (1.24) can be analytically calculated with the result

$$L = \frac{N_1 N_2 f_{\text{rev}}}{4\pi \sigma_x \sigma_y}. \tag{1.26}$$

In the case that the transversal sizes of the two bunches are different $\sigma_{1x} \neq \sigma_{2x}$, $\sigma_{1y} \neq \sigma_{2y}$ and that longitudinal sizes are equal $\sigma_{1s} = \sigma_{2s}$ more general formula can be derived

$$L = \frac{N_1 N_2 f_{\text{rev}}}{2\pi \Sigma_x \Sigma_y} \tag{1.27}$$

where

$$\Sigma_x = \sqrt{\sigma_{1x}^2 + \sigma_{2x}^2}\,, \tag{1.28}$$

$$\Sigma_y = \sqrt{\sigma_{1y}^2 + \sigma_{2y}^2}\,. \tag{1.29}$$

The quantities $\Sigma_{x,y}$ characterize the horizontal and vertical *convoluted beam widths*. It is worth mentioning that the luminosity given by eq. (1.26) or eq. (1.27) does not depend on the longitudinal bunch size σ_s.

The formula (1.26) can be rewritten in terms of bunch emittance and beta function at interaction point using eq. (1.9) as

$$L = \frac{N_1 N_2 f_{\text{rev}}}{4\pi\sqrt{\beta_x^* \epsilon_x^b \beta_y^* \epsilon_y^b}}. \tag{1.30}$$

In the even more symmetric case when $\epsilon_x^b = \epsilon_y^b = \epsilon^b$ and $\beta_x = \beta_y = \beta^*$ we may write

$$L = \frac{N_1 N_2 f_{\text{rev}}}{4\pi\beta^* \epsilon^b}. \tag{1.31}$$

The luminosity, therefore, depends on β^* as $L \propto 1/\beta^*$.

The revolution frequency f_{rev} in a collider is known quite precisely and the number of particles in a given bunch can be continuously measured (it decreases with time). The concept of the methods how bunch (or beam) charge can be measured is described, e.g., in [87]. Two types of devices are used to measure the bunch intensities at LHC: Fast Bunch Current Transformers (FBCT) which are measuring just a relative bunch intensities without a normalization and Direct Current Current Transformers (DCCT) which are measuring intensity of a beam (the relative bunch intensities are then cross normalized with respect to that value). However, it is technically quite difficult measurement when relatively precise values are required, for more technical details about the measurement needed for the absolute determination of the luminosity see [88–91]. The main problem of the absolute luminosity determination is generally the determination of the convolution integral (effective transverse area A_{eff}), see eq. (1.14)). They are several methods how to determine the effective transverse area A_{eff}.

The transversal (convolved) bunch sizes $\Sigma_{x,y}$ (effective transverse area) needed to calculate the luminosity according to eq. (1.27) may be determined using so-called *beam-separation scans* (also called *van der Meer (VDM) scans* according to Simon van der Meer who pioneered this method at ISR [92]): one beam is swept stepwise across the other while measuring a collision rate as a function of the beam displacement. Performing this measurement in the two transverse planes then allows to determine the (convolved) bunch sizes.

This type of scans are performed at LHC in dedicated runs at all interaction points at each collision energy (few times to study also the variation between the scans and to determine more precisely the precision of the measurement). In normal runs only the relative luminosity is measured and the calibration constant is taken from the dedicated runs where the absolute luminosity has been determined.

Determination of the absolute luminosity from the machine parameters (at LHC) based on the *beam-separation scans* has been summarized in detail in [84] where one can found also explicit formulas and discussion for the luminosity if the bunches, e.g., do not collide head on (collision offset), the bunches collide with a certain crossing angle or some other effects which need to be taken into account, too; see also [81–83, 85, 86, 92–95].

Conceptually interesting is also a method for determination of the absolute luminosity in a colliding-beam experiment at circular accelerators by measuring *interaction vertices*

of beam–gas interaction to determine the beam shapes and overlap which was originally proposed for LHC by M. Ferro-Luzzi [96]. This *beam-gas imaging method* does not require displacing the beams (like the separation scan method) and can be thus used during normal data taking. This method was first tried at ISR but it has been successfully applied for the first time in LHCb [97] as the method requires dedicated detector apparatus for precise reconstruction of the vertices, see also [98].

Another quite different method of determination of (transversal) beam sizes needed for the luminosity calculation is based on measurement of so-callled *luminous region*. When two bunches collide with revolution frequency f_{rev}, particles may inelastically interact producing some particles at a given interaction vertex. The distribution of these vertices in space - luminous region - can be measured (typically using an inner tracker such as the one of CMS which can reconstruct the vertex of an inelastic event from detected tracks with good spacial resolution). The luminous region has certain center and size ($\sigma_{x,y;L}$) which is in general equal neither to the size of a bunch nor the convoluted beam sizes $\Sigma_{x,y}$ (in transversal direction). For the Gaussian profiles of bunches with pair-wise equal bunch sizes the relation between (transversal) beam, convoluted beam and luminous region sizes is given by known formula

$$\sigma_{x,y;L} = \frac{\sigma_{x,y}}{\sqrt{2}} = \frac{\Sigma_{x,y}}{2}. \tag{1.32}$$

The concept of luminous region and it's relation to the luminosity may be found, e.g., in sect. 3.3 of [83]. Measuring the luminous region from reconstructed interaction vertices provides another way of the measurement (estimation) of transverse beam sizes needed for the absolute luminosity calculation.

Last but not least there is also a possibility to calculate the transversal bunch sizes for the luminosity calculation from the corresponding measured beam emittances (see sect. 1.3.1), which in principle provide yet another independent measurement of the luminosity (see eq. (1.30)).

All the (different) methods of determination of the convolution integral (effective transverse area A_{eff}, see eq. (1.14)) have their advantages and disadvantages (different precision and systematics). The main problem is generally the determination of the underlying bunch profiles as, e.g., the formula (1.27) or (1.26) was derived only for certain (specific) bunch profiles and the determination of the transverse area A_{eff} should also correspond to these profiles or it is necessary to start again from the general expression (1.13). The primary method of the luminosity determination at LHC is currently based on the beam-separation (VDM) scans determining the transverse area which are considered to be the most reliable for that purpose.

The determination of the luminosity based, e.g., on the separation scans has the advantage that it is determined from beam and machine parameters only. In such a case one can measure rates of some processes and determine experimentally corresponding cross sections using eq. (1.12) which may be then compared to the ones predicted by some models (or used to constrain some models).

In this section we have shown just the most basic formulas concerning the luminosity measured from beam and machine parameters. In practice the actual determination of the (absolute) luminosity in real machines like LHC is more complex than one could expect at first glance and it requires a lot of effort if a precision at the level of few percent is to be reached, see, e.g., luminosity determination at IP5 [99–105] (see also [106–109]). Last but not least very useful and quite detailed review of luminosity determination at proton colliders including the ISR and LHC may be found in [110].

As we have already mentioned, the primary absolute luminosity determination at LHC is currently based on the VDM scans. The more precise determination of the luminosity calibration should be reached the more difficult the measurement is. It is, therefore, always necessary to have strong physics motivation for it, see also [80].

Chapter 2

Measurement of pp collisions - TOTEM experiment at LHC

2.1 Physics program and objectives

When two particle beams collide one may observe corresponding products. TOTEM experiment is one of the LHC experiments at CERN [37, 71] (see also [111–114]) which may measure some of these collision events. The TOTEM acronym stands for TOTal, Elastic and diffractive cross section Measurement which reflects some of its main physics aims - measurement of pp (diffractive) collisions at LHC energies:

- *elastic pp scattering* in the largest possible interval of scattering angle (including extremely low scattering angles where Coulomb interaction has dominant effect)
- the *total* and *inelastic pp cross section*,
- *diffractive processes* including single, double diffraction and central production.

TOTEM is, therefore, dedicated experiment to measure mainly processes with at least one proton surviving a collision. Measurement of these processes provides very important data for studying proton structure and interactions which are still poorly understood. There is also common measurement and analysis with CMS to extend further physics potential of both the experiments which share the same interaction point (IP5), see fig. 1.7 and fig. 1.2. TOTEM detectors are located in forward region while the CMS ones are mainly in the central region, see fig. 2.1. There is also a physics program related to collisions between proton and lead ions but it is not covered here.

2.2 Detector apparatus

To achieve TOTEM physics goals dedicated detector apparatus has been needed. The one described in this chapter corresponds to the first LHC data taking period *before* LS1 (for upgrades see [39, 41], for a new common CMS-TOTEM Precision Proton Spectrometer (CT-PPS) project see [40]).

TOTEM detector apparatus consists of Telescope 1 (T1) and Telescope 2 (T2) for tracking of charged particles from inelastic collisions and of a system of so-called Roman Pots (RPs) equipped by dedicated detectors for detection of elastically and diffractively scattered protons close to outgoing beam (the scattering angles being so low that the

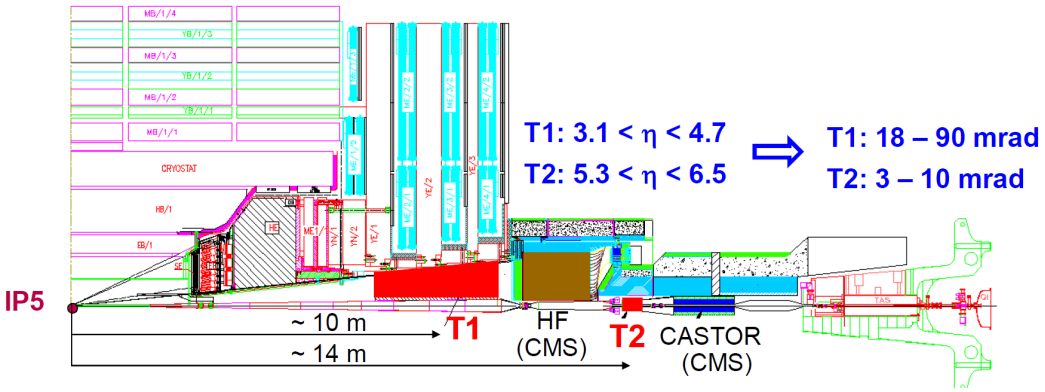

Figure 2.1: The TOTEM forward trackers T1 and T2 embedded in the CMS detector; right side of IP5 only (left side being symmetric).

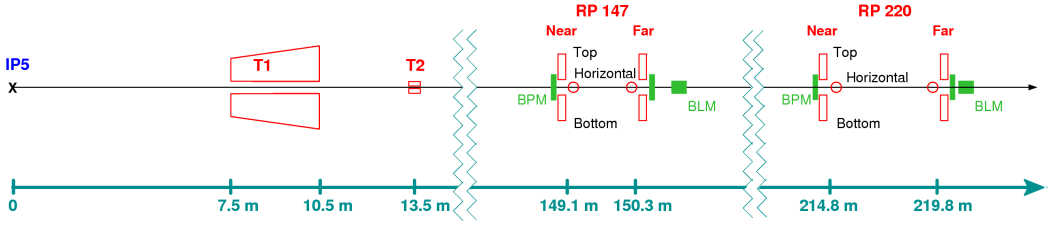

Figure 2.2: The TOTEM forward trackers T1, T2 and two Roman Pot (RP) stations at distances of about 147 m (RP147) and 220 m (RP220); right side of IP5 only (left side being symmetric).

protons stay in the beam pipe). All the TOTEM detectors are located symmetrically on both sides of IP5 (see figs. 2.1 and 2.2 for right side of IP5 only) and are trigger capable trackers. In the following we shall summarize only some basic aspects of the TOTEM detector system, detailed description of the used technology may be found in [71].

The detectors T1 and T2 detect charged particles only in certain limited range of the angle θ between trajectory of a particle and the beam axis (z). The so-called *pseudorapidity* is then defined as

$$\eta = -\ln\left[\tan\left(\frac{\theta}{2}\right)\right]. \tag{2.1}$$

For zero angle the pseudorapidity is diverging $\eta = +\infty$ while $\eta = 0$ for particles perpendicular to the beam axis ($\theta = \pi/2$). It is used often in the forward region to distinguish between particles with (very) small angles. Pseudorapidity is odd about $\theta = \pi/2$ ($\eta(\theta) = -\eta(\pi - \theta)$).

2.2.1 Telescopes T1

Two detectors T1 are installed in two cone-shaped regions in the endcaps of CMS, one on either side of IP5, at a distance between 7.5 m and 10.5 m from the interaction point, see figs. 2.1 and 2.4. T1 is made of 5 planes per arm, each plane consist of 6 trapezoidal

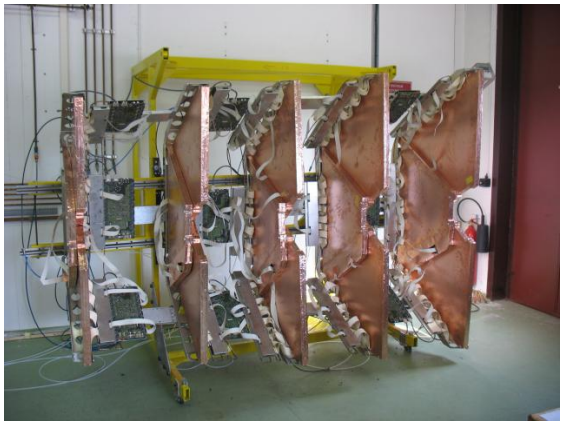

Figure 2.3: One T1 quarter consisting of 5 planes; each of them containing 3 trapezoidal CSC detectors.

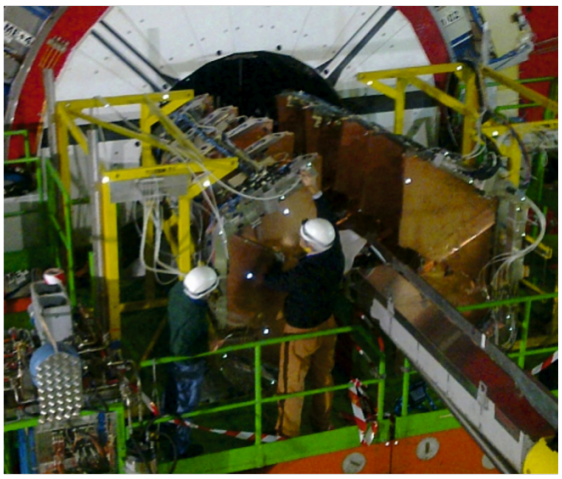

Figure 2.4: T1 (one arm) during an installation to a cone-shaped region in the endcaps of CMS.

Cathode Strip Chambers (CSCs) (multi wire proportional chambers with segmented cathode read-out), see fig. 2.3. The η-acceptance of T1 is $3.1 < |\eta| < 4.7$. This detector has full azimuthal coverage $\Delta\varphi = 2\pi$ (it surrounds the beam pipe). T1 may detect charged particles with transverse momentum $p_{\mathrm{T}} > 100$ MeV.

2.2.2 Telescopes T2

Each of two T2 telescopes is made of 20 half circular sectors of Gas Electron Multipliers (GEMs) (10 plains), see figs. 2.5 and 2.6. They are located at ± 13.5 m on both sides of IP5, see figs. 2.1 and 2.2. The η-acceptance of T2 is $5.3 < |\eta| < 6.5$ which allows to detect particles in even more forward region then the one of T1. T2 has also full azimuthal coverage $\Delta\varphi = 2\pi$ as T1. T2 is able to detect charged particles with transverse momentum $p_{\mathrm{T}} > 40$ MeV.

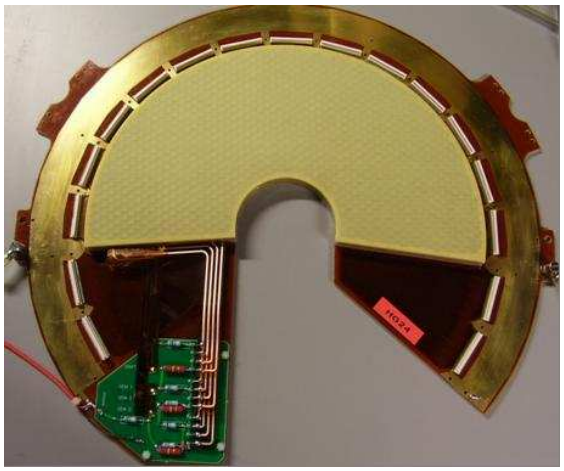

Figure 2.5: One semi-circular sector of the TOTEM T2 GEM detector plane without front-end electronics and cooling pipes.

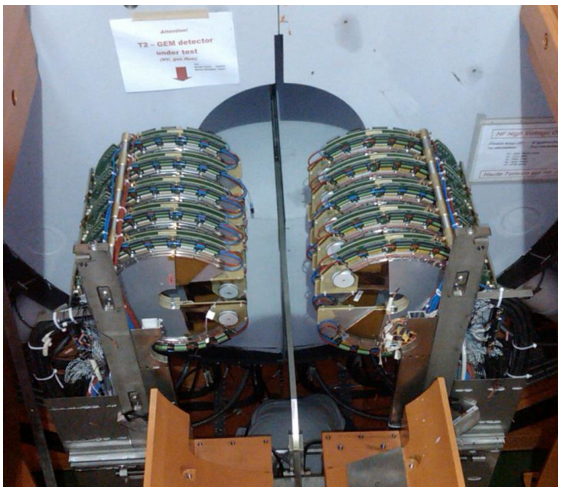

Figure 2.6: T2 detector (one arm) before an installation in CMS.

2.2.3 System of Roman Pots

Diffractive protons at high energies are scattered to very small angles such that they move close to the beam and may gradually deviate from it with distance from the interaction region in dependence also on the magnetic field along the path. They may be quite separated from the proton beam sufficiently far away from the interaction point, so that they may be detected by detectors which are put close to the beam. To detect particles in the beam pipe the detectors are placed in movable beam insertions called *Roman Pots* (RPs) so that the detectors inside the RP can be moved near or far from the beam. They are placed inside a secondary vacuum vessel (called a pot, see fig. 2.12) and moved into the primary vacuum of the machine through vacuum bellows. The primary vacuum is then preserved against an uncontrolled out-gassing of the detector's materials by a thin window as it is shown in fig. 2.12. If the beam does not have stable position and shape (before stabilization) then it is necessary to hold detectors far from the beam. After stabilization of the beam the detectors may be moved near to the beam for measurement. The detection of very forward protons in the movable beam insertions is an experimental technique introduced at ISR [115]. It has been successfully used in other colliders like the Sp$\bar{p}$S, TEVATRON, RHIC, HERA and it is used also at LHC.

The specific constraints of the LHC such as the thin high-intensity beam, the ultra high vacuum and the high radiation fluxes have required the development of new RPs for TOTEM. In order to improve the detector acceptance, the new RPs have thin window and the bottom face towards the beam is 150 μm thick as shown in fig. 2.12. Another difference to RPs designed for earlier machines is in the driving mechanism which must have high precision and radiation hardness. Even newer type of RP has been also proposed for TOTEM detector upgrade [39].

To detect protons as close to the beam as possible novel planar silicon detectors with so-called Current Terminating Structure (CTS) have been developed, see [71, 113]. All TOTEM RP silicon detectors have the CTS on one edge which faces the beam. The CTS collects the current generated in the highly damaged region at the cut edge and so avoids its diffusion into the sensitive detector volume. Full detection efficiency starts already at ≈ 50 μm from the physical edge. This is the reason why this kind of detectors is sometimes called "edgeless". Such detector technology improves acceptance of protons moving very close to the beam. Each detector has 512 strips with pitch of 66 μm. The strips in the detectors are at angle of 45° with respect to the edge facing the beam. The detail of the edge of one plane of the silicon strip detector is shown in fig. 2.7.

Each TOTEM RP is equipped with a stack of 10 edgeless silicon strip detectors, see figs. 2.10 and 2.11. Half of them have their strips oriented at angle of +45° with respect to the edge facing the beam, and the other half at angle of −45°. The measurement of each track projection in 5 planes is advantageous for the reduction of uncorrelated background via programmable coincidences, requiring, e.g., collinear hits in a majority of the planes and so selecting only particles at small angles with respect to the beam axis. The disadvantage of having only two readout projections is the difficulty of reconstruction of more tracks than one. However, if the whole RP units are tilted with respect to each other than the reconstruction of events with higher multiplicities may be significantly improved, see TOTEM upgrade proposal [39] (the RPs were not rotated before LS1).

To reconstruct protons in very forward region from both sides of the IP5, TOTEM uses RP system which is symmetric with respect to the IP. TOTEM RP system consisted of 4 RP stations during LHC Run 1, 2 stations on both sides of the IP at distances

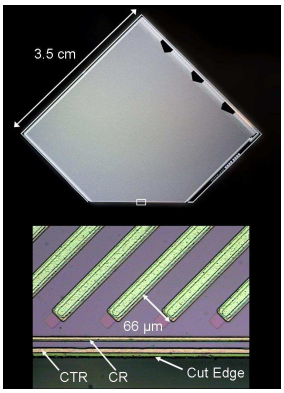

Figure 2.7: Planar silicon strip detector with 512 strips with pitch of 66 μm. The magnification of a portion of the edge region (bottom) shows the details of the CTS [71].

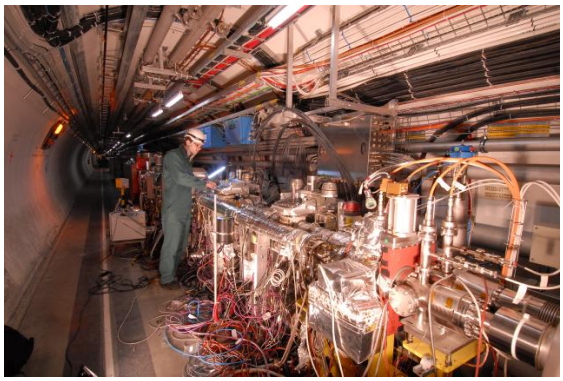

Figure 2.8: One of the RP station in the LHC tunnel during installation of necessary infrastructure.

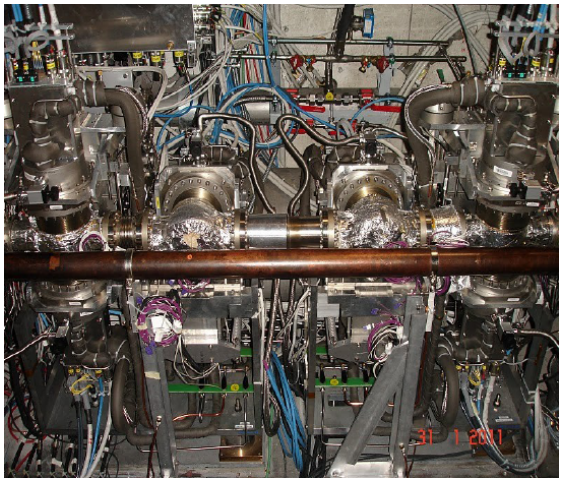

Figure 2.9: A RP station (two RP units, see fig. 2.13) installed in the LHC tunnel. Each of the 6 pots is housing a package of silicon detectors, see fig. 2.11. One can see also two separated beam pipes in the figure; the pots are mounted only on the beam pipe corresponding to the beam coming from the interaction point.

of $\pm$147 m and $\pm$220 m[1], see figs. 2.2 and 2.14. A RP station is an ensemble of 2 RP units, each unit consists of two vertical and one horizontal RP as it is visible on fig. 2.13 (see also fig. 2.2). The TOTEM RP system has thus 24 RPs in total. A RP station installed in the LHC tunnel is shown in figs. 2.8 and 2.9. All the TOTEM pots are housing trigger capable tracker detectors and they can be (individually) moved far and near the beam as needed for measurement.

[1]Mainly the stations at $\pm$220 have been used for measurement and data analysis.

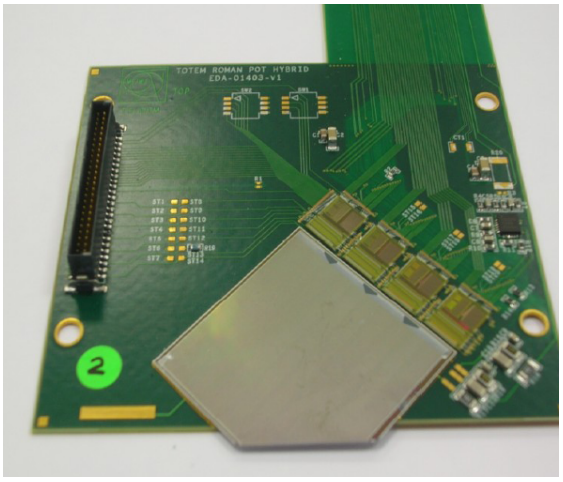

Figure 2.10: One planar silicon strip detector (see fig. 2.7) mounted on a RP hybrid with four readout chips.

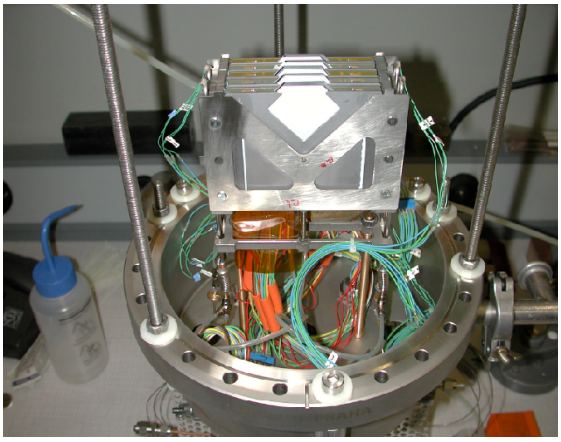

Figure 2.11: A package of 10 silicon strip detector planes (one of them is shown in fig. 2.10).

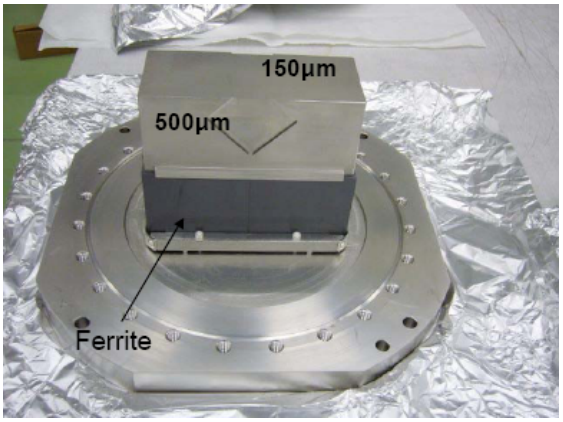

Figure 2.12: A Roman Pot which hosts a package of detectors, see fig. 2.11. The beam is passing through the front face window which is 500 μm thick while the bottom face (towards the beam) is 150 μm thick. The Ferrite collar (black) is needed to reduce the beam coupling impedance.

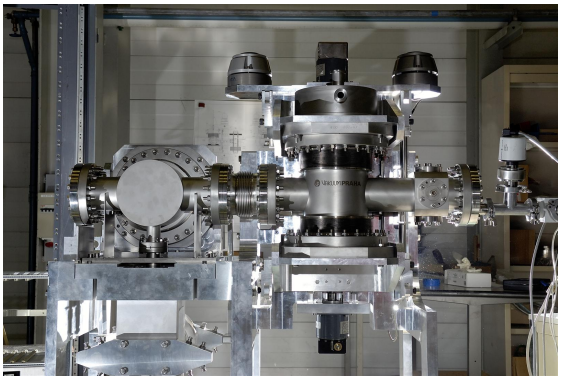

Figure 2.13: A RP unit with one horizontal and two vertical pots.

2.3 Proton transport IP → RP

A proton may survive an interaction at the IP but it may lose some energy and/or change (slightly) direction of motion. Such a proton is then passing through LHC magnet lattice between IP and RPs which changes its kinematic variables before it may be detected by RPs (as we have discussed also in sect. 1.3.1), see fig. 2.14.

Understanding and determination of the proton transport is, therefore, essential for determination of the proton kinematics *just after an interaction at the interaction region* from corresponding measured tracks by RPs located quite far from the IP (this procedure is sometimes denoted as *proton reconstruction*). The good knowledge of the *optics* (magnet settings between IP and position of a RP which detect the proton) is one of the key experimental problems; the basic concept will be, therefore, summarized in the following (see [38, 44, 71, 116–120] for more details).

Proton inside a beam pipe may be characterized by transverse position x and y as function of distance s from the interaction point, as it was mentioned in sect. 1.3.1. Momentum of the proton in spherical coordinates may be written as

$$\vec{p} = p \begin{pmatrix} \sin\theta\cos\varphi \\ \sin\theta\sin\varphi \\ \cos\theta \end{pmatrix} \tag{2.2}$$

where φ is azimuthal angle and θ is angle relative to the beam axis. A diffractive proton after an interaction at IP may lose some momentum which may be denoted as $\xi = \Delta p/p$ where p is momentum of the proton before a collision and Δp is the momentum loss. The quantity ξ is, therefore, by definition dimensionless quantity lying in the interval $\langle 0, 1\rangle$ and it is equal to zero for elastically scattered protons. The energy of the protons guided by LHC magnetic field during transport from IP (after an interaction) to a RP station is conserved, therefore, $p_{\mathrm{RP}} = p_{\mathrm{IP}}$ and $\xi_{\mathrm{RP}} = \xi_{\mathrm{IP}}$ (a star superscript will be also frequently used to denote corresponding quantities at IP, as it is common). One may define projection of the angle θ to the transversal directions (see also eq. (1.3))

$$\theta_x = \theta\cos\varphi, \qquad \theta_y = \theta\sin\varphi \tag{2.3}$$

and also projection of momentum transfer t

$$t_x = t\cos^2\varphi^*, \qquad t_y = t\sin^2\varphi^* \tag{2.4}$$

$$t = t_x + t_y \approx -p^2\theta^{*2} = -p^2(\theta_x^{*2} + \theta_y^{*2}) \tag{2.5}$$

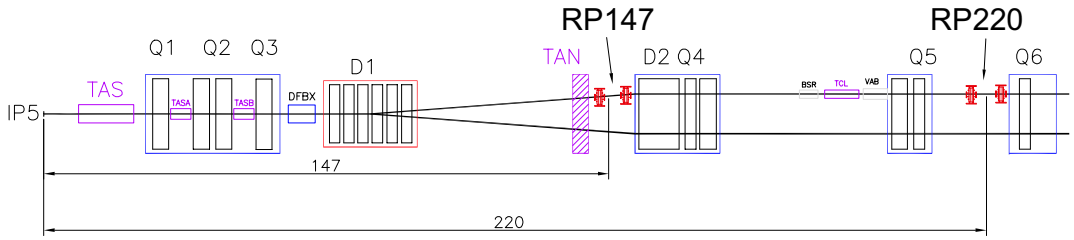

Figure 2.14: The LHC beam line with magnet lattice (quadrupole magnets Q1-Q6, dipoles D1 and D2, correctors, drift spaces...) on one side of the interaction point IP5 and the TOTEM Roman Pots at distances of about 147 m (RP147) and 220 m (RP220).

where low scattering angle approximation has been used in the last relation (see eq. (3.9), the kinematics of two elastically scattered protons will be discussed more in details later in sect. 3.1).

The proton transport through the part of the LHC magnet lattice IP $\rightarrow$ RP (containing around 30 magnets per beam) can be expressed mathematically using *transport matrix*, which is an inhomogeneous Hill's equation in x and y direction for a particle with a momentum loss ξ (more simple case of homogeneous Hill's equation was discussed in sect. 1.3.1)

$$\begin{pmatrix} x \\ \theta_x \\ y \\ \theta_y \\ \Delta p/p \end{pmatrix}_{\mathrm{RP}} = \begin{pmatrix} v_x & L_x & 0 & 0 & D_x \\ \mathrm{d}v_x/\mathrm{d}s & \mathrm{d}L_x/\mathrm{d}s & 0 & 0 & \mathrm{d}D_x/\mathrm{d}s \\ 0 & 0 & v_y & L_y & D_y \\ 0 & 0 & \mathrm{d}v_y/\mathrm{d}s & \mathrm{d}L_y/\mathrm{d}s & \mathrm{d}D_y/\mathrm{d}s \\ 0 & 0 & 0 & 0 & 1 \end{pmatrix} \begin{pmatrix} x \\ \theta_x \\ y \\ \theta_y \\ \Delta p/p \end{pmatrix}_{\mathrm{IP}} \tag{2.6}$$

where the properties of the optics may be expressed by the *dispersion* function $D_{x,y}(s)$ (nominally $D_y(s) = 0$ at LHC) and the two optical functions *effective length* $L_{x,y}(s)$ and *magnification* $v_{x,y}(s)$ (these functions are also called *optical functions*). These two last functions of distance s from the IP are particularly important for proton reconstruction and they are defined by the betatron function $\beta(s)$

$$L_{x,y}(s) = \sqrt{\beta_{x,y}(s)\beta^*_{x,y}}\,\sin\Delta\mu_{x,y}(s)\,, \tag{2.7}$$

$$v_{x,y}(s) = \sqrt{\frac{\beta_{x,y}(s)}{\beta^*_{x,y}}}\,\cos\Delta\mu_{x,y}(s) \tag{2.8}$$

where the phase advance $\Delta\mu_{x,y}(s)$ is defined as

$$\Delta\mu_{x,y}(s) = \int_{\mathrm{IP}}^{\mathrm{RP}} \frac{1}{\beta_{x,y}(s')}\mathrm{d}s'\,. \tag{2.9}$$

The beta function at the LHC interaction point is nominally equal in both the transverse coordinates $\beta^*_x = \beta^*_y = \beta^*$. This parameter β^* is one of the main parameters of the optics influencing proton acceptance by RPs system; it is also used as a "unique" label for a given optics even if there may be more different set of parameters of the magnet settings leading to the same value of β^*. Quite difficult problem is to develop an optics (magnet configuration) which would allow reconstructing *all* the proton kinematic variables and vertex (position) in all coordinates at IP from detected tracks by RP detectors with good resolution for all the variables. Each of the magnet settings is, therefore, optimized for reconstruction of only *some* variables in limited kinematical regions. An example of the (nominal) optical function at two different optics is shown in fig. 2.15.

The aim of experiments similar to TOTEM is to measure the kinematical variables of protons after an interaction in the widest possible range - most importantly momentum transfer t (or equivalently scattering angle θ^*) and momentum loss ξ of diffractively scattered protons at IP. The corresponding distribution of these variables represents important experimental input needed for some further theoretical studies of proton interactions and its structure as it was mentioned in Introduction.

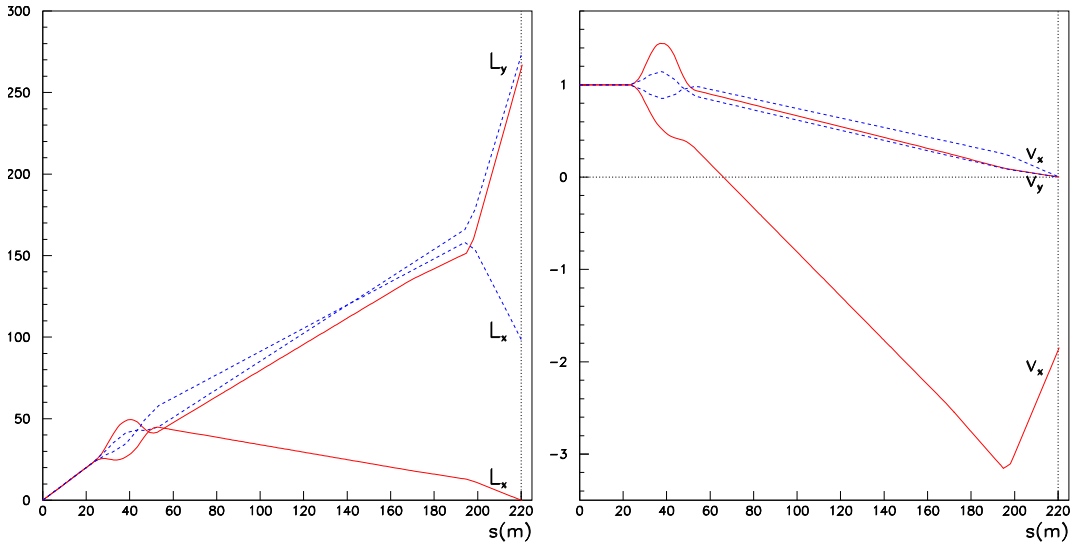

Figure 2.15: Example of (nominal) optical functions for $\beta^* = 90$ m (solid) and 1540 m (dashed) as function of the distance s to IP5: effective length $L_{x,y}$ in meters (left) and magnification $v_{x,y}$ (right); taken from [71].

2.3.1 Determination of optics for elastically scattered protons

TOTEM developed a novel method of machine optics determination: direct LHC optics measurement (which is quite difficult) is improved by making use of angle-position distributions of elastically scattered protons observed in the TOTEM RP detectors. Magnet and beam parameters are varied within some tolerances to match TOTEM observables (constrains). This procedure is, therefore, called *optics matching* or *optics tuning* [44, 117–120]. It is some kind of offline alignment of magnets and their strengths. Determination of the transport matrix for *elastically* scattered protons may be significantly improved by this novel method, e.g., in the case of $\beta^* = 90$ m optics one may reach the precision: $\frac{\delta \mathrm{d}L_x/\mathrm{d}s}{\mathrm{d}L_x/\mathrm{d}s} < 1\%$ and $\delta L_y/L_y < 1\% \rightarrow \delta t/t \approx 0.8 - 2.6\%$ [44, 117–120].

2.3.2 Determination of optics for non-elastically scattered protons

Kinematical variables (most importantly t and ξ) of non-elastically scattered proton may be determined also from detected tracks at RPs, similarly as in the case of elastic scattering. However, non-elastically scattered protons are shifted in horizontal x-direction at RP position due to optics - mainly *dispersion* function $D_x(s)$ of the beam (nominally $D_y(s) = 0$ at LHC). Proton transport from IP to a RP at position s for non-elastically scattered protons is then given by (see eq. (2.6))

$$y(s) = v_y(s).y^* + L_y(s).\theta_y^* \,, \tag{2.10}$$

$$x(s) = v_x(s).x^* + L_x(s).\theta_x^* + \xi D_x(s) \,. \tag{2.11}$$

Generally $v_{x,y}, L_{x,y}$ and D_x are functions of ξ which means that the reconstruction is a non-linear problem and, therefore, there is no "easy" optics matching like in the case of elastically scattered protons mentioned in the previous section. TOTEM can determine

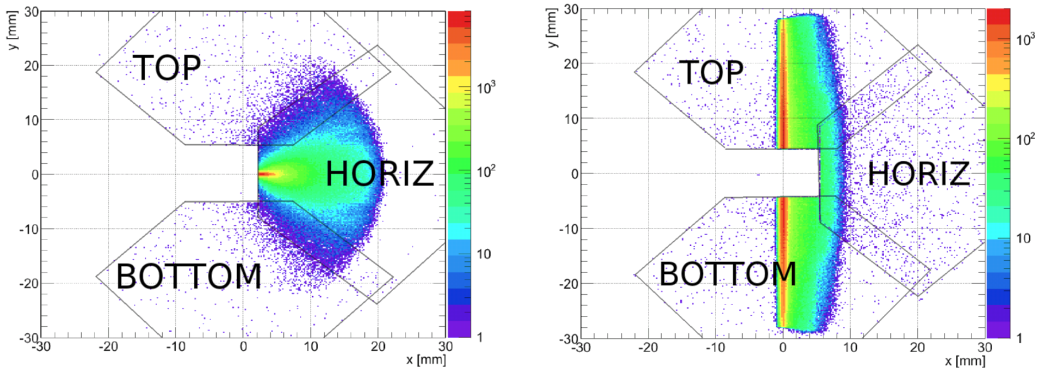

(a) Low $\beta^* = 0.55$ m **(b)** Higher $\beta^* = 90$ m

Figure 2.16: An example of simulated hit maps of protons scattered at the IP and detected by far unit of RP220 for two different optics [39] (one horizontal and two vertical pots, shape of the detectors is also visible, see fig. 2.7).

t and ξ of a non-elastic proton (at least in some cases), too, but the resolution is lower than for elastically scattered protons.

An example of simulated hit distributions of protons detected by far unit of RP220 for two different optics configuration ($\beta^* = 3.5$ m and $\beta^* = 90$ m) taken from [39] is in fig. 2.16. The figure clearly demonstrates the effect of the optics which may enormously influence the detection of scattered protons at the IP (acceptance of RPs detectors).

In the case of low $\beta^* = 0.55$ m (one of the standard optics at LHC) functions L_x and L_y are low and protons are, therefore, shifted in x-direction due to ξ, see eq. (2.11) (shift due to non-zero vertex x^* is not critical due to relatively small transverse IP beam size for low β^*). For the low β^* TOTEM RP220 station has $\xi > 2$ % acceptance. Non-elastically scattered protons are mainly in horizontal RP. Elastically scattered protons may be detected by a vertical RP near $x \approx 0$ only for large scattering angles for such a low β^* optics.

In the case of higher $\beta^* = 90$ m (special optics for RP runs [121, 122]) $L_x = 0$ and L_y is large ($\xi \geq 0$ coverage, $|t_y| > 0.01$ GeV^2). Large transverse beam size $\sigma^{\mathrm{IP}}_{\mathrm{beam}} \approx 200$ μm implies that $v_{x,y}$ are important (deterioration of ξ-resolution). Non-elastically scattered protons are mainly in vertical RPs. Elastically scattered protons are also in RPs in narrow band at $x \approx 0$. This dedicated higher β^* optics changes acceptance of RPs such that much lower elastic scattering angles can be detected; for more details see [39]. One of the property of the 90 m optics developed for TOTEM is that it eliminates the dependence on transverse position of the proton at the collision point (the magnification v_y is close to zero, $\Delta\mu = \pi/2$ and the place of the detection of the protons) - so-called *parallel-to-point* focusing property in y (vertical) coordinate. In the case of such an optics y coordinate of the interaction vertex cannot be measured at all in favour of better determination of scattering angles in y projection θ^*_y [2] at lower values as high effective length L_y pushes the protons vertically into the acceptance of the RP detectors, see also [71]. In one of the planed optics for TOTEM with $\beta^* = 1540$ m, developed in [123], the parallel-to-point focusing condition is required in both x and y transversal directions to reach yet lower values of t of elastic scattering with sufficient resolution. Another high $\beta^* = 1000$ m optics [124] has been already used for TOTEM measurement

[2] i.e., t_y, full scattering angle θ^* is then calculated using some symmetries

which allowed to reach so far the lowest value of $|t|$ at LHC, see sect. 2.5.1.

The acceptance of proton by RP detectors, therefore, in general depends mainly on the following factors: protons kinematics at interaction point (collision energy, momentum loss, scattering angle,...), the optics configuration (magnet settings), position of the RP detectors with respect to the beam and also by any aperture limitations in machine elements between the IP and the RP detectors.

One of the side effect of using higher β^* for changing RPs proton acceptance is that the luminosity proportionally decreases as $L \propto 1/\beta^*$ (see eq. (1.31)) which may bring some advantages as well as disadvantages. As we have mentioned in preceding, it is not easy (or even possible) to optimize an optics for all possible kind of measurements and a given optics (or other LHC or detector settings) is generally suitable only for some kind of measurement.

2.4 Diffractive classes of pp events

In the following only some very basic principles how elastic scattering, single diffraction, double diffraction and so-called central production might be measured will be shown on example of TOTEM (and CMS) detector apparatus. More detailed discussion about measurement of diffractive processes and corresponding technical details may be found, e.g., in [39, 40, 125].

2.4.1 Elastic scattering pp → pp

In the case of elastic scattering (ES) of two protons pp → pp the two outgoing protons are collinear and did not lose any energy (ξ defined in sect. 2.3 being zero), see also fig. 3.1. The two outgoing protons may be detected by TOTEM RPs which are sufficiently far from the interaction point, see fig. 2.17. Corresponding scattering angle (t variable) or other kinematic variables after an elastic interaction of two protons at the interaction point are then determined using information about magnet settings - backward transport to the interaction point as we have mentioned in sect. 2.3. An example of elastic scattering of two protons in $\eta - \varphi$ space (η being pseudorapidity and φ azimuthal angle) is plotted in fig. 2.18. One of the main experimental aim concerning elastic scattering is then measurement of elastic differential cross section

$$\frac{\mathrm{d}\sigma^{\mathrm{el}}(s)}{\mathrm{d}t} \tag{2.12}$$

in the widest possible range of t values and at various collision energies $\sqrt{s}$. The basic steps leading to the determination of this quantity in the case of measurement performed by TOTEM will be briefly summarized in sect. 2.5.2.

2.4.2 Single diffraction pp → pX or Yp

Single diffraction (SD) pp → pX or Yp is a similar process to the elastic scattering except that one of the protons breaks up, producing particles in a limited pseudorapidity

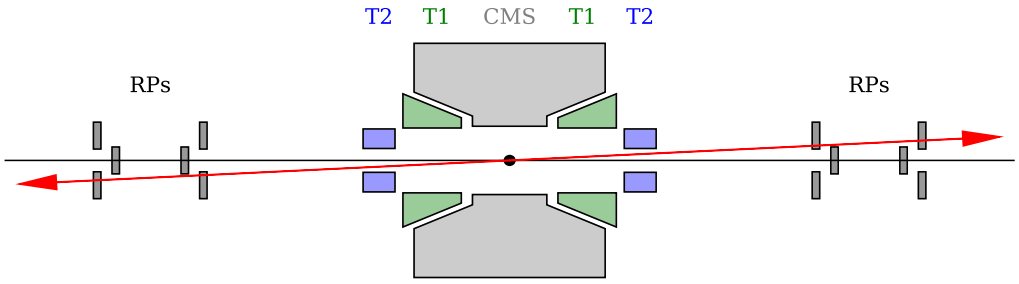

Figure 2.17: Schematic detection of two elastically scattered protons (represented by the two arrows) by TOTEM Roman Pots on each side of the interaction region (represented by black dot at the center). No other particles originating from the same pp elastic interaction at the interaction region are produced.

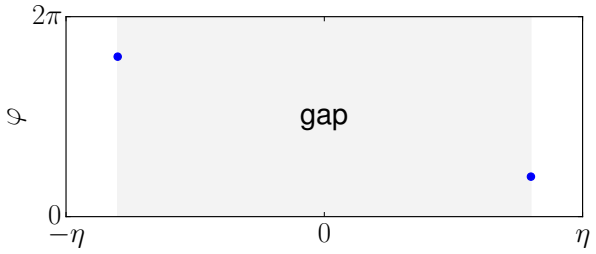

Figure 2.18: $\eta - \varphi$ diagram of an elastic event. Two protons (represented by two dots) are separated by pseudorapidity (angular) gap where no particles are produced.

region. Outgoing proton with a small fraction momentum loss ξ is separated from the diffractive system X (Y) by a pseudorapidity gap $\Delta\eta$ which might be measured, see [126] for a definition of $\Delta\eta$ in the case of a single diffraction without considering (detecting) the leading proton (see also [127]). The average pseudorapidity gap width as a function of momentum loss ξ is commonly calculated using the following formula (see [128] for corresponding derivation, used assumptions and relation to so-called *rapidity* y)

$$\Delta\eta \approx -\ln(\xi). \tag{2.13}$$

The mass of the diffractive system is then calculated as (see again [128] for the corresponding derivation and involved assumptions)

$$M_{\mathrm{SD}} = \sqrt{\xi s}\,. \tag{2.14}$$

An example of single diffraction in $\eta - \varphi$ space is plotted in fig. 2.20.

The leading proton may be detected by RPs and the particles from the diffractive system may be detected by T1 or T2 detectors in the case of TOTEM experiment (if the detector acceptance allows). From the η-acceptance region of T1 and T2 and from the rapidity gap requirement in the case of SD one may classify SD events into four classes as it has been done in fig. 2.19. One can see from the table that the single diffractive events with mass $\Rightarrow$ 3.4 GeV $< M_{\mathrm{SD}} <$ 1.1 TeV can be detected by these two

proton on one side + T2 opposite only + no T1	
M_{SD} = 3.4 - 7 GeV $2 \times 10^{-7} < \xi < 10^{-6}$	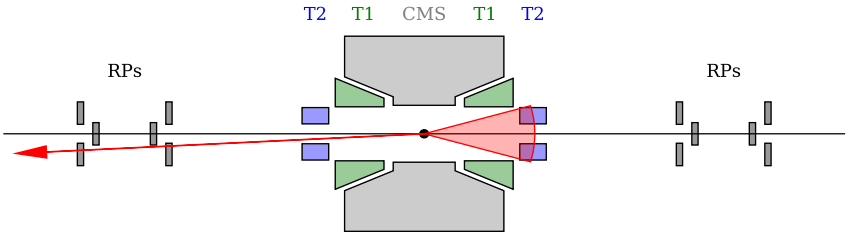
proton on one side + T2 opposite only + T1 opposite only	
M_{SD} = 7 - 350 GeV $10^{-6} < \xi < 0.0025$	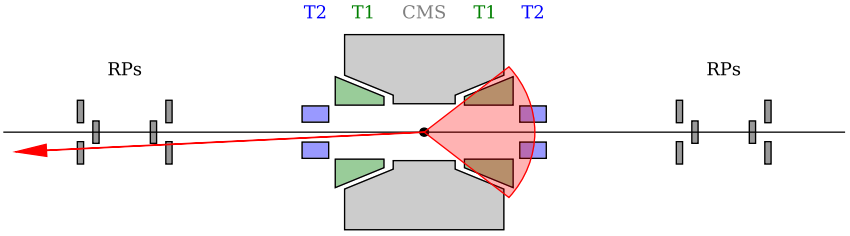
proton on one side + T2 opposite only + both T1	
M_{SD} = 0.35 -1.1 TeV $0.0025 < \xi < 0.025$	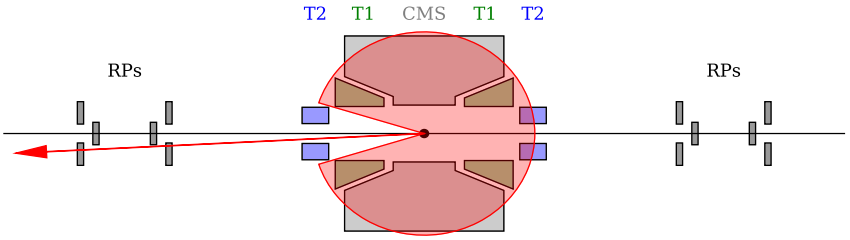
proton on one side + both T2 + both T1	
$M_{SD} > 1.1$ TeV $\xi > 0.025$	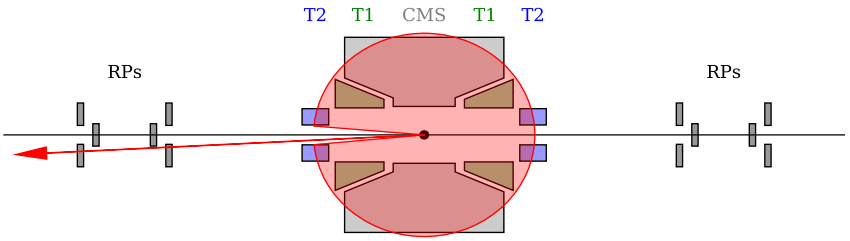

Figure 2.19: Single diffraction classified into 4 mass ranges according to T1 and T2 η-acceptance ranges. It is an example how some events may be divided into groups according to the detector acceptance. The red wedges represent an angular region where some particles may be detected (no other particles being produced outside this region).

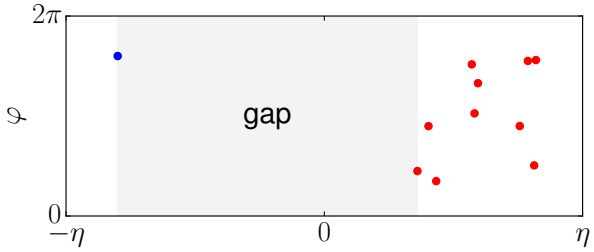

Figure 2.20: A single diffractive event in $\eta - \varphi$ space. One proton is produced on one side from the interaction region while on the other side several particles may be produced and detected. The leading proton and the particles from the diffractive system are separated by a pseudorapidity (angular) gap where no particles are produced.

TOTEM detectors. The scattering angle (t variable) of the single diffractive proton can be again determined using RPs and optics, similarly as in the case of elastic scattering, see sect. 2.3. The ξ variable may be also determined from the optics, if the resolution is sufficient. In that case one may experimentally test relation (2.13). If the resolution of ξ determined from optics is not sufficient, the relation (2.13) is often used to determine ξ from measured pseudorapidity gap (this is especially the case for experiments which do not detect the leading proton at all). From the experimental point of view one would like to measure, e.g., double differential cross section of the single diffraction

$$\frac{\mathrm{d}^2\sigma_{\mathrm{SD}}(s)}{\mathrm{d}t\mathrm{d}\xi} \tag{2.15}$$

in the widest possible range of t and ξ values (at various energies $\sqrt{s}$) but sometimes only partially integrated differential cross section corresponding to a certain ξ range (see, e.g., fig. 2.19) may be determined due to too low statistics or low ξ resolution. From the physics point of view it is good, if also the processes are measured ideally exclusively; if one can determine all the particle types of the diffractive system of the broken proton and their kinematics; this is, however, in general quite difficult and it might be done only in some cases with dedicated detector apparatus.

2.4.3 Double diffraction pp → XY

Double diffraction (DD) pp → XY is similar to single diffraction except that both the protons breaks up, each producing particles in a limited rapidity region. Two diffractive systems X and Y are separated by a rapidity gap which is the essential difference to non double diffractive inelastic events, see fig. 2.21. No particles are produced (detected) in this rapidity gap. The detectors in these regions are thus used as veto, see fig. 2.22. Similarly as in the case of the single diffraction the experimental aim is generally to detect and determine kinematics of all the outgoing particles and their types, measure differential cross section of DD events (or just some selected channels) in dependence on the rapidity gap, etc.

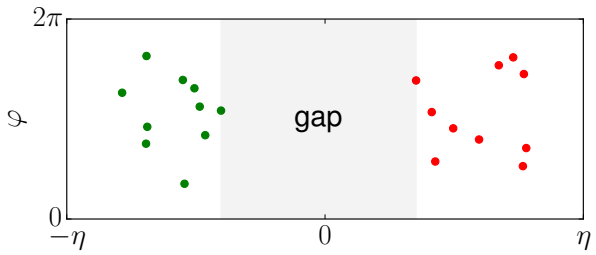

Figure 2.21: A double diffractive event in $\eta - \varphi$ space. Two diffractive systems are separated by a pseudorapidity gap where no particles are produces (the gap distinguish DD events from the non-diffractive inelastic ones).

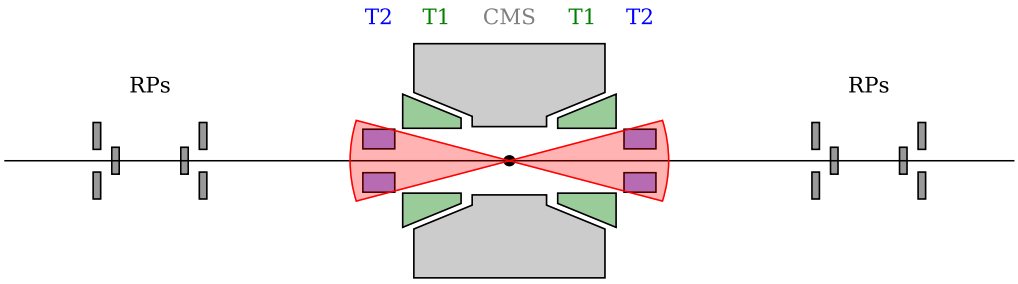

Figure 2.22: Schematic example of a DD event with particles (tracks) in T2 on both sides of the interaction point and no particles in RPs, T1 or CMS (pseudorapidity gap).

2.4.4 Central production pp → pXp

As a central production (CP) is denoted an interaction pp → pXp in which both the leading protons survive the collision (losing only some energy, momentum) and another particles X are produced in a pseudorapidity region separated by a pseudorapidity gap from each of the proton (hence the "central" production), see fig. 2.25. This kind of process is sometimes denoted also as double pomeron exchange (DPE) or central diffraction (CD). This type of events has been observed already at the first hadron collider ISR [129], e.g., the reaction pp → $p\pi^+\pi^-p$ (the two pions produced in the central rapidity region) at $\sqrt{s} = 31$ GeV has been detected and discussed in [130] (see also [131–133]). A process pp → $p(p\pi^+\pi^-)$ is sometimes denoted as single diffraction, even if also the second proton somehow survives the collision and two pions are produced close to it (small rapidity gap). This kind of events may be very important for better understanding of the structure and dynamics of proton as it may be qualitatively very different from the ES, SD and DD events which we have mentioned so far, as *both* the protons survive the collision and "something more" is produced (e.g., the two pions or something else).

One of the experimental challenges is to have sufficient resolution for the double arm proton reconstruction and to measure also the other produced particles. In the case of TOTEM and CMS, the two leading protons may be detected by TOTEM RP system (*two arm proton reconstruction* of both $t_{1,2}$ and $\xi_{1,2}$ using optics), similarly as in the case of single diffraction. One may then try to detect particles from the system X by CMS and also by T1 and T2, see figs. 2.23 and 2.24 with two examples of different topology of

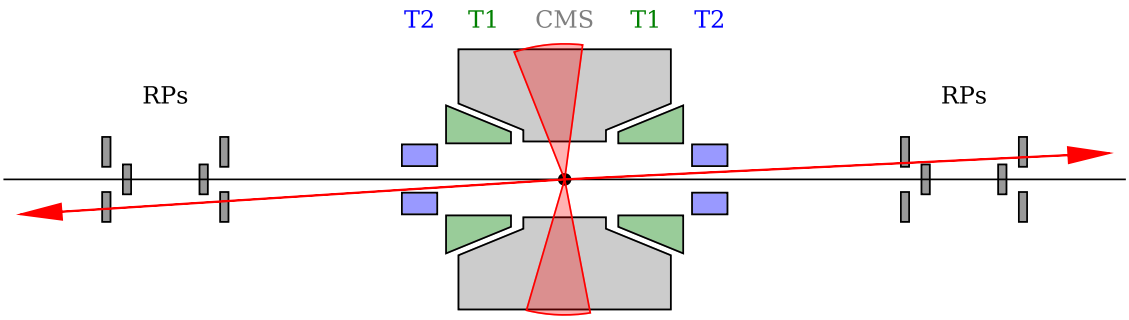

Figure 2.23: Example of a CP event with "bottom-top" proton topology; this proton pair topology is similar to an elastic one (having either "top-bottom" or "bottom-top" topology).

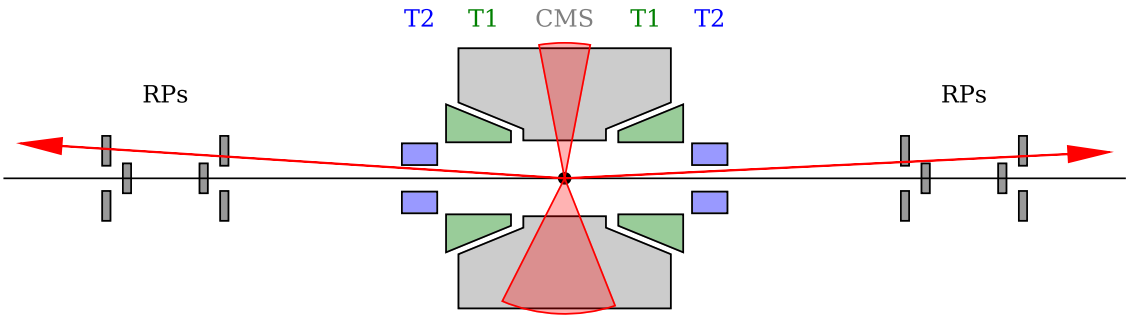

Figure 2.24: Example of a CP event with "top-top" proton pair topology which is quite different from the one of a pair of elastic protons where only "top-bottom" or "bottom-top" topology is possible.

the produced (detected) proton pair in vertical detectors (topologies with *horizontal* RP detectors are possible, too). One may also try to look for *jets* in the diffractive system X (similarly as in SD and DD) which may provide also another important information concerning proton structure and dynamics.

The two arm proton reconstruction of $t_{1,2}$ and $\xi_{1,2}$ using RPs and optics has been done by TOTEM for the first time recently (with relatively low statistics); upgrade of TOTEM detector apparatus is foreseen to increase also statistics of these processes as the cross sections of these processes are relatively small, see [39, 40] for more details.

The understanding of diffractive processes is in general still quite low even if some of them have been observed already at the ISR. In fact, also the term "diffraction" has not very clear meaning (see, e.g., an introduction chapter in [128] for same definitions of this term). This term is used mainly for historical reasons; it was introduced in nuclear high energy physics in analogy with some optics phenomena, even thought any analogy with optics may be quite misleading for description of collisions of two particles. Benefiting from the preceding text one could say for the sake of simplicity

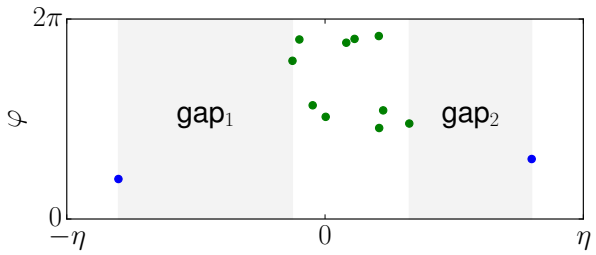

Figure 2.25: $\eta - \varphi$ correlation plot of a CP event pp→ pXp; produced system X is separated by two rapidity gaps.

that "diffractive" processes are mainly those with at least one proton surviving collision (ES, SD or CD) and processes "similar" to them like, e.g., double diffraction mentioned in the preceding. It is also the classification of diffractive events based on the concept of (pseudo)rapidity gaps (as presented in preceding) which should be questioned and studied in more detail, especially with relation to precise measurement of the kinematics of the leading protons and corresponding diffractive systems [39, 40].

2.5 TOTEM results concerning pp collisions

2.5.1 Data taking - LHC Run 1

TOTEM experiment performed several measurements of pp collisions before LS1 (from September 2010 to February 2013) at 2.75, 7 and 8 TeV. As it has been mentioned in the preceding, it is the magnet settings (optics) which changes significantly the acceptance of RP detectors. TOTEM took data at various (dedicated) β^* and at different RP detector positions as it is summarized in table 2.1 (TOTEM has also some data corresponding to proton-lead collisions not mentioned in the table). In 2012 TOTEM and CMS, which are located at the same interaction point, successfully managed to exchange triggers so that also common data taking has been possible (TOTEM and CMS have independent Data AcQuisition (DAQ) systems responsible for storing data from detectors). Dedicated various high β^* runs are needed to detect protons at very low scattering angles. However, this in turn means decreasing the luminosity due to the fact that $L \propto 1/\beta^*$ (see eq. (1.31) and also the end of sect. 2.3). This types of runs are, therefore, not suitable for maximizing overall integrated luminosity (required for looking for some very rare events) but rather for providing very important (complementary) experimental data mainly of diffractive processes for studying proton characteristics. Some proton characteristics may be determined only from diffractive processes (e.g., all contemporary methods determining total pp hadronic cross section require measurement of elastic scattering, as it will be shown in more detail in next chapters). The measurement of SD and CP, including detection of both the protons and possibly also some jets, may provide very important information, too. In the following we shell go briefly through already published physics results by TOTEM collaboration with more emphasis on measurement of elastic scattering as the next chapters will be devoted to theoretical description of this process.

Date	Detector configuration	$\sqrt{s}$ [TeV]	β^* [m]	Some main pp analyses
Sep/Oct 2010	RP at $18\sigma_{\text{beam}}$	7	3.5	ES $2 \lesssim \lvert t\rvert \lesssim 3.5$ GeV^2
Oct 2010	RPs at $7\sigma_{\text{beam}}$ T2	7	3.5	ES $0.36 < \lvert t\rvert < 2.5$ GeV^2 [27]
May 2011	RPs at $5\sigma_{\text{beam}}$; T1, T2	7	1.5	$\mathrm{d}N_{\text{ch}}/\mathrm{d}\eta$ for $5.3 < \lvert\eta\rvert < 6.4$ [29]
Jun 2011	RPs at $10\sigma_{\text{beam}}$; T1, T2	7	90	ES $0.02 < \lvert t\rvert < 0.33$ GeV^2, (luminosity independent) total and inelastic cross sections [28, 32]
Oct 2011	RPs at 4.8 - $6.5\sigma_{\text{beam}}$; T1, T2	7	90	ES $0.005 < \lvert t\rvert < 0.37$ GeV^2, (luminosity independent) total and inelastic cross sections [30–32], SD, DD [34],...
Jul 2012	RPs at 6 - $9.5\sigma_{\text{beam}}$; T1, T2, CMS	8	90	ES $10^{-2} < \lvert t\rvert \lesssim 1.2$ GeV^2, (luminosity independent) total and inelastic cross section [33]; ES $0.027 < \lvert t\rvert < 0.2$ GeV^2 [35]; $\mathrm{d}N_{\text{ch}}/\mathrm{d}\eta$ [43], SD, DD, CP, ... (common data and analysis with CMS and/or TOTEM alone)
Oct 2012	RPs at 3 - $10\sigma_{\text{beam}}$; T1, T2	8	1000	ES at very low $\lvert t\rvert$ ($6 \times 10^{-4} < \lvert t\rvert < 0.2$ GeV^2), study of Coulomb and hadronic interactions, total and inelastic cross sections,...
Feb 2013	RPs, T1, T2, CMS (not all together, various settings)	2.76	11	ES, total and inelastic cross sections,...

Table 2.1: Some of the most important TOTEM pp data taking periods during LHC Run 1 (before LS1) and the corresponding main analysis channels. σ_{beam} denotes transversal size of the beam at a position of a RP - either horizontal or vertical.

2.5.2 Measured elastic differential cross section

In this section the main steps of the measurement of pp elastic differential cross sections which was made by TOTEM collaboration at 7 and 8 TeV and published in [27, 28, 30, 35, 36] (see also [32, 33]) will be briefly summarized. Some steps may vary for different runs and need to be (sometimes) repeated iteratively. The order of the steps mentioned in the following is, therefore, only indicative. We will concentrate on the basic concept only, more details of the measurement may be found also in [38, 116, 134] (for similar measurement at LHC by ATLAS-ALFA see [135–137]). The quoted papers of TOTEM contain much more details concerning the measurement of elastic collisions than it has been ever provided by a similar experiment.

Trigger settings

When two beams collide at LHC one would like to read-out detectors (all their segments) and store data containing information about the collision for subsequent analysis. However, there may be so many collisions (pp interactions or "events") per unit of time that corresponding amount of data from the detectors would be so high that it would not be technically possible to read-out and store all the information (moreover, most of the data would be of very little or no physics importance). For this reason particle detectors have dedicated *trigger system* that selects only the events that are potentially interesting (based on some predefined criteria, e.g., coincidence of some hits in detectors). It usually consists of both hardware and software parts. *Data AcQuisition (DAQ)* system is then responsible for recording only the events selected by the trigger system. In the case of detection of protons by a RP silicon strip detector information about hit strips is stored for each event. Understanding dedicated trigger settings which allows measurement of elastic scattering is, therefore, the first important step in data analysis. Detailed information concerning TOTEM trigger may be found in [138, 139], description of DAQ system is given in [140, 141]; see also [38, 71].

Reconstruction of proton kinematics (alignment and optics)

In this step proton kinematical variables just after an interaction at IP are determined from measured tracks (hits) by RPs. Firstly, strip hits are used to reconstruct a local track in a RP and then global track reconstruction is made for each arm separately. The reconstruction requires mainly very good understanding of the steering magnets guiding the protons from IP to RP detectors - *optics* discussed in sect. 2.3. Precise determination of position of RP detectors with respect to the beam during measurement (order of μm) is needed for good physics performance, too. The corresponding *alignment* of RP detectors is, therefore, done in three steps [38, 134]:

- *beam-based alignment* - During special LHC run a collimator[3] scrapes the beam creating a sharp beam edge; the RPs are then moved one at a time towards the sharp beam edge until an increase in the beam losses is detected downstream of the RPs. This online procedure determines only approximately the position of RP.
- *local track based alignment* - The individual RP detector planes in each RP are aligned with respect to each other using reconstructed tracks in the overlap between the vertical and horizontal RPs as shown in fig. 2.16; this determines relative alignment of each RP unit (offline procedure).

[3] A collimator is a moveable device which may scrape away particles from beam that have gone slightly off track in order to prevent damages to the beam pipe and the magnets.

- *global alignment using elastic events* - The local alignment can not determine common shifts or rotations of the entire RP unit with respect to the beam; these parameters can be constrained by exploiting known symmetries by certain physics processes, most importantly by elastic events (offline procedure).

The alignment and optics are of the key-importance for reconstruction of proton kinematics.

Event selection - elastic tagging
Once a local track reconstruction or even global proton reconstruction is done one may try to select only the elastic events. In that case the basic requirements on the selection following from the definition of elastic events are: 2 anti-collinear protons from the same vertex ($\Rightarrow$ comparison of left and right reconstructed protons), no forward momentum loss of the two protons (optics $\Rightarrow$ correlation hit position vs. track angle at RPs, removal of protons shifted due to beam dispersion as discussed in sect. 2.3).

Background subtraction
The aim of this step is to subtract all non-elastic events which passed the selection cuts (may require additional assumptions, dependence on some models).

Acceptance corrections
The elastic events are detected (and reconstructed) always only in certain limited range of scattering angle θ (t variable) and azimuthal angle φ due to finite size of RP detectors, LHC apertures and optics (see also table 2.1). Moreover, only some elastic events produced in this range are detected by RP detectors, the corresponding event-count in each bin dt has to be accordingly corrected for this reason (using, e.g., φ azimuthal symmetry of elastic scattering $\Rightarrow$ geometrical corrections, beam divergence $\Rightarrow$ correction for missing protons at RP edges,...).

Unfolding of resolution effects (unsmearing)
The aim of this procedure is to determine and eliminate impact on dσ/dt caused by the non-zero beam divergence and the finite detector pitch (see fig. 2.7). The unfolding may require some additional assumptions in some cases.

Corrections of various inefficiencies
There may be various (non-negligible) inefficiencies for which the elastic differential event rate dN/dt need to be corrected for: DAQ inefficiency, trigger inefficiency, uncorrelated one-RP inefficiencies, near-far correlated RP inefficiencies, "pile-up" related inefficiencies (elastic event and another track in a RP) etc., which are discussed more in details, e.g., in [30]. TOTEM data were taken at quite low luminosity leading to also negligible pile-up of physics processes at IP (more than one collision of protons at IP during one bunch crossing); the effect of pile-up, however, may be taken into account in some cases too, see [142] for some explicit formulas.

Luminosity
The luminosity is needed for absolute normalization of the rates, i.e., to transform fully corrected elastic differential rate dN/dt into the elastic differential cross section dσ/dt (see eq. (1.12)). They are currently two methods of luminosity determination relevant to TOTEM data normalization. The luminosity determined using VDM scans

(measured by CMS, see sect. 1.3.2) and TOTEM measurement of luminosity based on optical theorem (this method will be described more in detail in sect. 2.5.3 and sect. 3.5.3).

Besides physics itself (determination of proton characteristics) which will be discussed mainly in next chapters, the measurement of elastic scattering is also very interesting and important tool to improve experimental performance. It is used to improve optics determination of elastically scattered protons (sect. 2.3.1) and, as we have seen in this section, for fine tuning of RP detector alignment. The same alignment may be then used for detection of *non-elastic* protons from SD or CP (it, therefore, indirectly improves measurement precision of these processes). The determination of (differential) cross sections of non-elastic collision processes uses similar steps as in the elastic case which are generally just more complex and complicated; the idea of the steps remains, however, often the same.

The first measured pp elastic differential cross section at LHC at $\sqrt{s} = 7$ TeV by TOTEM at LHC [27] is shown in fig. 2.26 (Oct 2010 data at $\beta^* = 3.5$ m). The measured t-dependence in range $0.36 < |t| < 2.5$ GeV^2 is similar to the one observed earlier at ISR, see fig. 2; namely the dip-bump structure has been observed again by TOTEM at LHC since the era of ISR (where it has been observed for the first time [6]). One can see also a comparison to several contemporary phenomenological models of elastic pp scattering in the fig. 2.26, see also [48]. The measured $|t|$-range at the same energy has been extended to lower values from 0.02 to 0.33 GeV^2 in [28] corresponding to Jun 2011 data at $\beta^* = 90$ m. Even yet lower value of $|t| = 0.00515$ GeV^2 has been reached in [30] corresponding to Oct 2011 data (also $\beta^* = 90$ m) where the RP detectors were closer to the beams then in June 2011, see table 2.1. More details about corresponding comparison of these TOTEM measurements at $\sqrt{s} = 7$ TeV may be found in [30] where measured values of pp elastic differential cross section in the range $0.00515 < |t| < 2.5$ GeV^2 are tabulated together with statistical and systematical uncertainties for each measured point (bin), see fig. 2.27.

TOTEM has measured also nearly exponential differential elastic pp cross-section at $\sqrt{s} = 8$ TeV in the range of four-momentum transfer squared $0.027 < |t| < 0.2$ GeV^2 [35], see fig. 2.28. In a dedicated LHC run with high $\beta^* = 1000$ m optics TOTEM has measured elastic scattering in $|t|$-range from 6×10^{-4} to 0.2 GeV^2 [36] including significantly non-exponential part attributed standardly to Coulomb-hadronic interference, see fig. 2.29. The measured elastic differential cross section at 8 TeV will be used in chapter 4 for obtaining several characteristic of protons at this very high collision energy (using eikonal model).

2.5.3 Determined total, elastic and inelastic hadronic cross sections

Measurement of elastic differential cross section in the widest possible t-range provides very important experimental input for determination of some proton characteristics such as total, elastic and inelastic hadronic integrated cross sections. In this section we summarize corresponding results published by TOTEM collaboration at collision energy of 7 and 8 TeV together with used method which led to the results. These calculations are always model dependent (based on several additional assumptions). Most importantly it is the theoretical description of elastic pp scattering which is essential for such calculations. TOTEM compared 3 different (not completely independent) methods

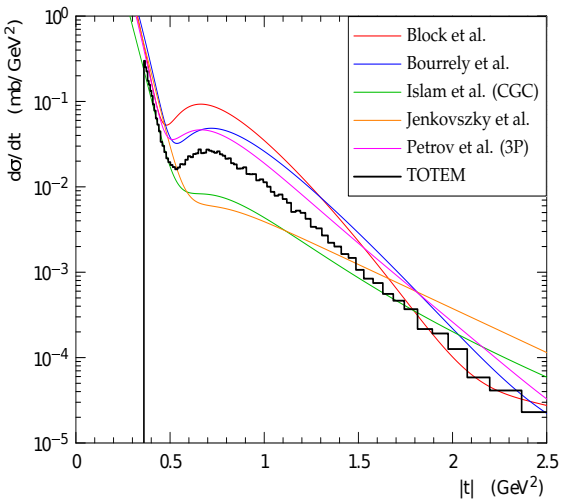

Figure 2.26: First measurement of pp elastic differential cross section at $\sqrt{s} = 7$ TeV by TOTEM (black line) compared to several phenomenological models of elastic scattering [27].

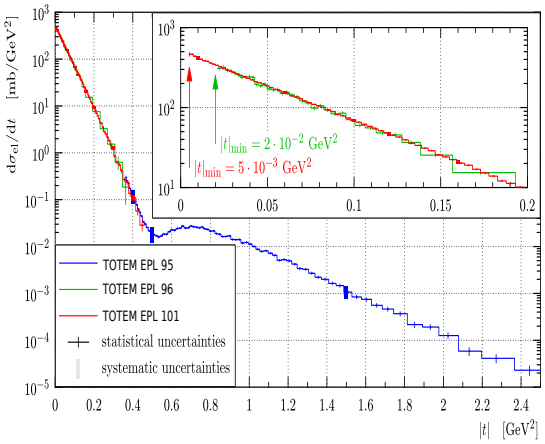

Figure 2.27: Proton-proton elastic differential cross section at $\sqrt{s} = 7$ TeV measured (independently) at three different settings (runs) by TOTEM: blue line - [27] (corresponds to the data in fig. 2.26), green line - [28], red line - [30].

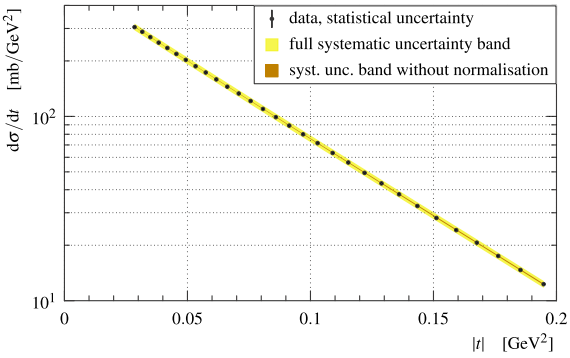

Figure 2.28: Measured elastic pp differential cross section in the region $0.027 < |t| < 0.2$ GeV^2 at $\sqrt{s} = 8$ TeV by TOTEM [35].

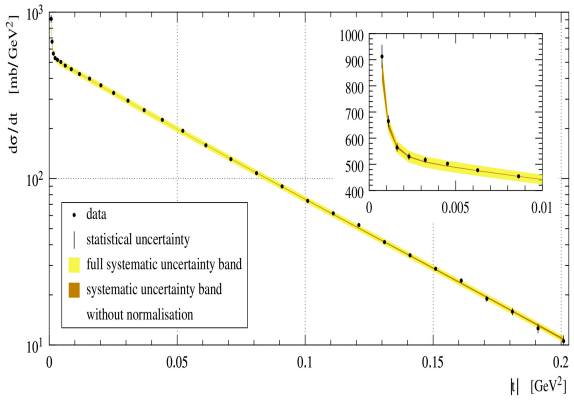

Figure 2.29: Measured elastic pp differential cross section in the region $6 \times 10^{-4} < |t| < 0.2$ GeV^2 at $\sqrt{s} = 8$ TeV by TOTEM [36]. The region includes significantly non-exponential part (see the points corresponding to the lowest measured values of $|t|$) attributed standardly to Coulomb-nuclear interference.

of determination of total hadronic cross section in the similar way how it was done firstly at the ISR in the past; these methods were used similarly by other experiments, too. We shell show some formulas on which the methods are based and how they have been applied by TOTEM. These methods will be discussed in greater detail in sect. 3.5 after explaining the corresponding theoretical background as the whole problem is more delicate than it may seem at first glance.

- **Method OL: Method based on optical theorem and luminosity**

  This method is based on the following formulas

$$\sigma_{\mathrm{OL}}^{\mathrm{tot,N}} = \sqrt{\frac{16\pi(\hbar c)^2}{1+\rho^2}\left.\frac{\mathrm{d}\sigma^{\mathrm{el,N}}}{\mathrm{d}t}\right|_{t=0}}\,, \tag{2.16}$$

$$\sigma^{\mathrm{el,N}} = \int \frac{\mathrm{d}\sigma^{\mathrm{el,N}}}{\mathrm{d}t}\,, \tag{2.17}$$

$$\sigma^{\mathrm{inel}} = \sigma^{\mathrm{tot,N}} - \sigma^{\mathrm{el,N}} \tag{2.18}$$

  where the formula (2.16) for the total hadronic cross section has been derived using optical theorem.

  These formulas were applied by TOTEM at LHC energy of 7 TeV using the measured pp elastic differential cross section mentioned in the previous section (i.e., elastic events measured by TOTEM RPs and the luminosity determined by CMS on the basis of VDM scans), see [30] and also [28]. To apply the formulas it was assumed that the measured differential cross section is given only by hadronic interaction in the given measured region of $|t|$ and the hadronic differential cross section may be extrapolated to $t = 0$ in the unmeasured region of $|t|$ as an exponential function (i.e., with so-called *diffractive slope* being t-independent) for the needs of both the optical theorem in eq. (2.16) and the integration in eq. (2.17). This method requires (due to the optical theorem) dedicated runs with special high β^* optics (see sect. 2.3) which allows detection of elastically scattered protons at very low values of $|t|$. The parameter $\rho = 0.141 \pm 0.007$ (at $\sqrt{s} = 7$ TeV) has been taken from COMPETE [143] extrapolation [144] based on dispersion relations (the parameter ρ, as we will see in chapter 3, is determined usually primarily from Coulomb-nuclear interference but the data at 7 TeV, however, did not allow such determination). It is worth mentioning that the total hadronic cross section given by eq. (2.16) is determined without measuring any inelastic rate (cross section). The key experimental input for this method is measurement of differential cross section of elastic pp scattering in the widest possible t-range.

- **Method TR: Method of total rate**
  This method requires simultaneous measurement of elastic and inelastic event rate and also determination of luminosity for the normalization. The total cross section is calculated according to

$$\sigma_{\mathrm{TR}}^{\mathrm{tot,N}} = \frac{N^{\mathrm{el,N}}}{L} + \frac{N^{\mathrm{inel}}}{L} = \sigma^{\mathrm{el,N}} + \sigma^{\mathrm{inel}} \tag{2.19}$$

  where the integrated elastic hadronic cross section is calculated according to eq. (2.17).

TOTEM determined the value of the total hadronic cross section on the basis of this method under assumptions that the measured elastic differential cross section in the measured t-range is given by hadronic interaction only and that it can be extrapolated to $t = 0$ again as an exponential function. The inelastic rate (cross section) has been measured by T2 and also corrected, on the basis of a model, to take into account also events undetected by T2 (events outside detector acceptance) [31]. Both the elastic and inelastic rates measured by TOTEM were normalized using the luminosity measurement of CMS based on VDM scans. More details about the measurement of the total cross section based on this method of total rate by TOTEM collaboration at 7 TeV may be found in [32].

- **Method OLI: Luminosity independent method**
  This method of total cross section determination is a combination of the two previous ones where the measurement of the luminosity is eliminated. According to this method the total hadronic cross section is given by the formula

$$\sigma_{\mathrm{OLI}}^{\mathrm{tot,N}} = \frac{16\pi(\hbar c)^2}{1+\rho^2} \frac{\left.\frac{\mathrm{d}N^{\mathrm{el,N}}}{\mathrm{d}t}\right|_{t=0}}{N^{\mathrm{el,N}} + N^{\mathrm{inel}}}. \tag{2.20}$$

  Similarly the luminosity may be calculated (determined) according to

$$L_{\mathrm{int}} = \frac{1+\rho^2}{16\pi(\hbar c)^2} \frac{(N_{\mathrm{el,N}} + N_{\mathrm{inel}})^2}{\left.\frac{\mathrm{d}N_{\mathrm{el,N}}}{\mathrm{d}t}\right|_{t=0}} \tag{2.21}$$

  under exactly the same assumptions and from the same simultaneous measurement of elastic and inelastic rate as the total cross section given by eq. (2.20).

  TOTEM applied this method at 7 TeV in [32] under assumption that the measured elastic rate in the measured t-range is given by hadronic interaction only and that it can be extrapolated to $t = 0$ as an exponential function. The $\rho = 0.141 \pm 0.007$ parameter has been taken from the COMPETE preferred extrapolation [144]. The inelastic rate has been corrected on the basis of a model for undetected events by T2.

The values of the total, elastic and inelastic hadronic cross sections determined by TOTEM at energy of 7 TeV on the bases of the three methods are in table 2.2. As we can see, the values are quite similar. The values of the inelastic cross section σ^{inel} may be compared also to the measurements by other LHC experiments (measuring the rate of inelastic events and luminosity, see eq. (1.12)) at $\sqrt{s} = 7$ TeV ("inelastic rate/luminosity") as it was also done in [32]. The inelastic cross section at 7 TeV has been measured by CMS [145], ATLAS [146] and ALICE [147]

$$\begin{aligned}
\sigma_{\mathrm{CMS}}^{\mathrm{inel}} &= (68.0 \pm 2.0^{\mathrm{syst}} \pm 2.4^{\mathrm{lumi}} \pm 4.0^{\mathrm{extrap}})\ \mathrm{mb} \\
\sigma_{\mathrm{ATLAS}}^{\mathrm{inel}} &= (69.1 \pm 2.4^{\mathrm{exp}} \pm 6.9^{\mathrm{extrap}})\ \mathrm{mb} \\
\sigma_{\mathrm{ALICE}}^{\mathrm{inel}} &= (73.2^{+2.0\mathrm{mod}}_{-4.6} \pm 2.6^{\mathrm{lumi}})\ \mathrm{mb}
\end{aligned}$$

see the quoted papers also for the visible cross sections only - without model dependent estimation of undetected events (events outside detector acceptance). These values of the inelastic cross section are similar to those determined by TOTEM using the three methods.

	Method OL [30] (see also [28])	Method OLI [32]	Method TR [32] (see also [31])
$\sigma^{\mathrm{tot,N}}$[mb]	98.6 ± 2.2	98.0 ± 2.5	99.1 ± 4.3
σ^{inel} [mb]	73.2 ± 1.3	72.9 ± 1.5	73.7 ± 3.4
$\sigma^{\mathrm{el,N}}$ [mb]	25.4 ± 1.1	25.1 ± 1.1	25.4 ± 1.1

Table 2.2: Determined values of proton-proton total, inelastic and elastic hadronic cross section at energy of $\sqrt{s} = 7$ TeV by TOTEM using three different methods.

Proton-proton hadronic cross section were determined by TOTEM collaboration using luminosity independent method also at $\sqrt{s} = 8$ TeV [33] (similarly as at 7 TeV) with the result

$$\sigma^{\mathrm{tot,N}} = 101.7 \pm 2.9 \text{ mb},$$
$$\sigma^{\mathrm{inel}} = 74.7 \pm 1.7 \text{ mb},$$
$$\sigma^{\mathrm{el,N}} = 27.1 \pm 1.4 \text{ mb}.$$

The value $\rho = 0.140 \pm 0.007$ at 8 TeV has been taken from COMPETE extrapolation similarly as in the case of $\sqrt{s} = 7$ TeV. The values of the hadronic cross section at energy of 8 TeV are according to these results slightly higher than at 7 TeV. All the mentioned pp hadronic cross sections are plotted in fig. 2.30 together with some similar results at different energies obtained in the past.

The luminosity given by eq. (2.21) has been determined in the similar way how the total cross section has been calculated using eq. (2.20). This method of luminosity determination based on optical theorem has been compared to the independent luminosity determination based on VDM scans (measured by CMS) at LHC energy of $\sqrt{s} = 7$ TeV during October 2011 special LHC run at $\beta^* = 90$ m. Both methods gave similar central values of the luminosity with the uncertainty at the level of 4% for both of the two methods, see [32] for more details about the comparison.

2.5.4 Charged particle pseudorapidity density distribution

So-called *charged particle pseudorapidity distribution* $\mathrm{d}N_{\mathrm{ch}}/\mathrm{d}\eta$ is often used to characterize angular production of (charged) particles in inelastic collisions. This quantity may be defined as the mean number of charged particles per single pp inelastic collision and unit of pseudorapidity η defined by eq. (2.1).

TOTEM has measured this quantity at $\sqrt{s} = 7$ TeV by T2 detector, see figs. 2.31 and 2.32. The measurement corresponds to at least one primary charged particles reconstructed in T2 acceptance region $5.3 < |\eta| < 6.4$. The experimental points (black squares) represent the average of the four T2 quarters with the error bars including both statistical and systematic errors. Main contributions to the systematic error $\sim 10\%$ are subtraction of a large fraction of secondaries from the data, track reconstruction (in)efficiency and misalignment uncertainties. The measurement refers to charged particles with $p_T > 40$ MeV and with mean lifetime greater than 0.3×10^{-10} s, directly produced in pp interactions or in subsequent decays of particles having a shorter lifetime, see [29] and [148] for more details.

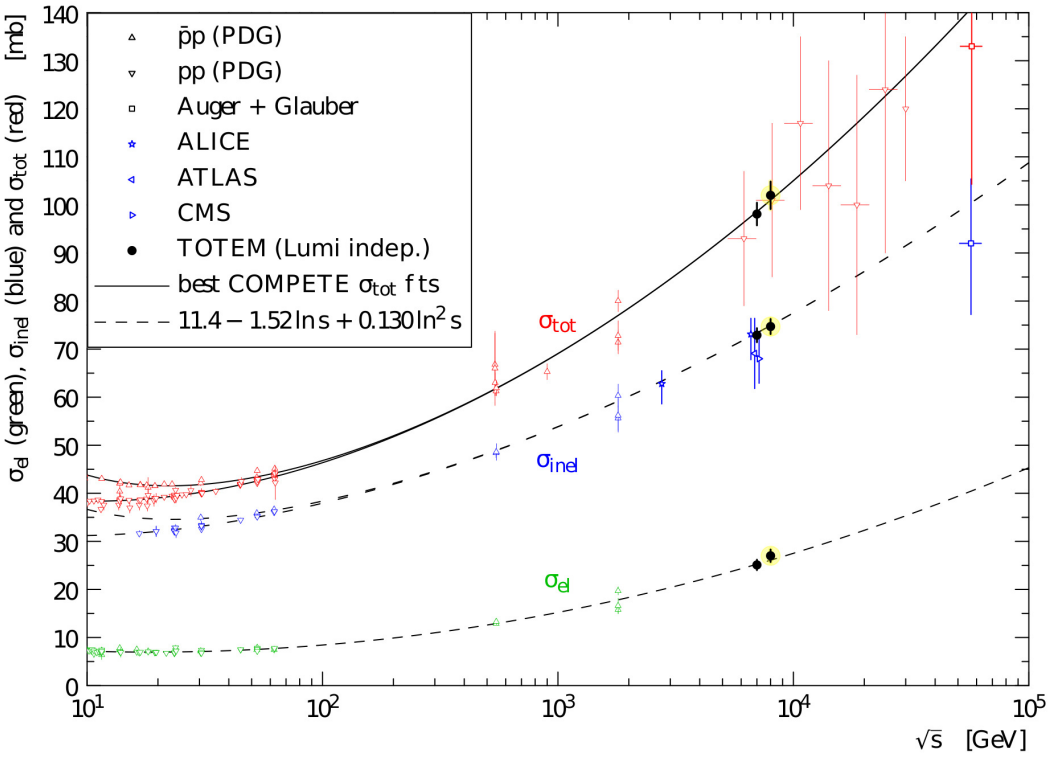

Figure 2.30: Compilation of integrated pp and $\bar{p}p$ hadronic cross sections as a function of energy $\sqrt{s}$ taken from [34]. The continuous black lines (lower for pp, upper for $\bar{p}p$) represent the fits of the total cross-section data by the COMPETE collaboration [144]. The dashed line results from an ad hoc fit of the elastic scattering data. The dash-dotted lines refer to the inelastic cross section and are obtained as the difference between the continuous and dashed fits.

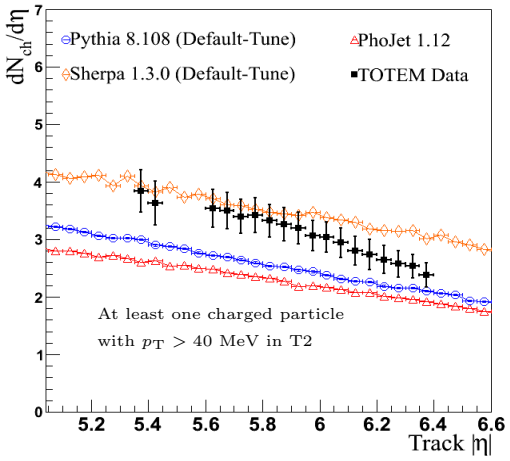

Figure 2.31: Charged particle pseudorapidity density distribution $\mathrm{d}N_{\mathrm{ch}}/\mathrm{d}\eta$ measured by TOTEM T2 detector at 7 TeV. The Phojet, Pythia8 and Sherpa predictions are for charged particles with $p_T >$ 40 MeV in events where at least one primary charged particle is generated in the $5.3 < |\eta| < 6.5$ range [29, 148].

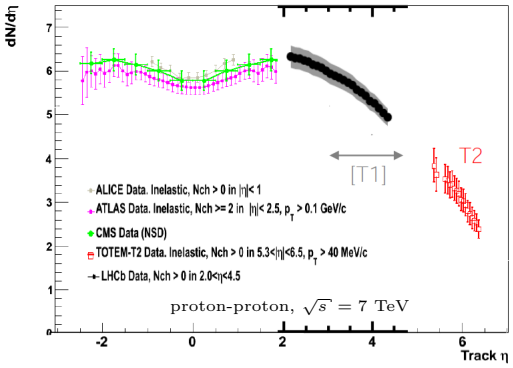

Figure 2.32: Compilation of ALICE, ATLAS, CMS, LHCb and TOTEM experimental results on charged pseudorapidity density distributions for pp inelastic events at 7 TeV [148].

Similar measurement of $\mathrm{d}N_{\mathrm{ch}}/\mathrm{d}\eta$ has been done also at 8 TeV [42]. In this paper it was possible to combine TOTEM and CMS data in one common analysis to better profit from the advantage of having relatively very wide CMS and TOTEM η acceptance region: $|\eta| < 2.2$ and $5.3 < |\eta| < 6.4$. TOTEM experiment further extended this region at 8 TeV when measured $\mathrm{d}N_{\mathrm{ch}}/\mathrm{d}\eta$ within the range $3.9 < \eta < 4.7$ and $-6.95 < \eta < -6.9$ using data collected in a low intensity LHC run with collisions occurring at a distance of 11.25 m from the nominal interaction point [43].

2.5.5 Double diffractive cross section in the forward region

The first double diffractive cross-section measurement in the very forward region has been measured by the TOTEM experiment at the LHC at $\sqrt{s} = 7$ TeV [34]. The very forward TOTEM tracking detectors T1 and T2 (with $|\eta|$ range up to 6.5) were used to select a sample of double diffractive pp events. The cross-section $\sigma_{\mathrm{DD}(4.7<|\eta_{\mathrm{min}}|<6.5)} = (116 \pm 25)\mu$b has been determined for events where at least one particle is detected in each of the T2 detectors and no particles are detected in T1 detectors (both diffractive systems have $4.7 < |\eta|_{\mathrm{min}} < 6.5$). This is, therefore, just a very specific sub-class of DD events. Main source of uncertainty are DD events that have $|\eta_{\mathrm{min}}|$ smaller than corresponds to T1 η-range but with no particles in T1. Improvements may be expected, for example, at 8 TeV combining data from TOTEM and CMS) where it is possible to check the particle activity in the central (CMS) η-range (to decrease dependence on some models). Combined TOTEM and CMS data may allow measuring much greater part of double diffractive cross section with better classification.

Chapter 3

Contemporary descriptions of elastic collisions of (charged) hadrons

The principles of measurement of elastic pp scattering (distribution of scattering angles) have been explained in the preceding. This chapter is devoted to commonly used theoretical descriptions of elastic scattering of charged hadrons (namely pp, resp. $\bar{p}p$) based on elastic scattering amplitudes and the possibilities and limitations of these descriptions.

Kinematics of elastic collision process of two particles is summarized for convenience in sect. 3.1. They are two approaches of describing the elastic scattering of charged hadrons at the present. The first one (historically older) is the approach of West and Yennie which has been commonly used for analysis of experimental data and which contains some important limitations; e.g., it does not take into account dependence of collisions on impact parameter. The second approach is the eikonal model approach which has been introduced to derive some characteristics of collisions also in dependence on impact parameter and enables, therefore, to understand better the whole collisions process. The important assumptions included in both the approaches describing Coulomb-hadronic interference will be emphasized and commented in sects. 3.2 and 3.4. Electromagnetic form factors (determined from ep scattering) entering into the given descriptions will be explained in sect. 3.3.

The understanding of both experimental and theoretical aspects of elastic scattering including corresponding assumptions is a key point for understanding, e.g., contemporary measurement of total hadronic cross section as all the approaches require measurement of elastic scattering (some of them also inelastic). Three different methods (formulas) of total hadronic cross section determination will be, therefore, discussed in detail in sect. 3.5. Sect. 3.6 then contains comments to some widely used parameterizations of elastic hadronic amplitude which is usually determined by fitting it to experimental data.

In chapter 4 the eikonal model approach will be then applied to experimental data of elastic pp scattering at energy of 53 GeV and 8 TeV. It will allow to obtain important numerical values of corresponding quantities characterizing hadronic collisions.

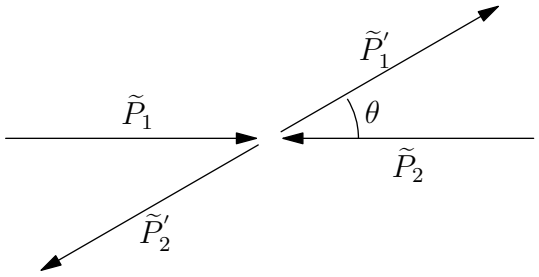

Figure 3.1: Two-body elastic scattering in center of mass system.

3.1 Relativistic kinematics of two-body elastic scattering

In this chapter we shall employ commonly used conventions and formalism to describe relativistic kinematics of two elastically scattered particles, see [8, 128, 149–151] (for classical description of two-body elastic scattering see, e.g., [152]). The four-momentum of a particle may be written as

$$\widetilde{P} = (E, \vec{p}) \tag{3.1}$$

where E is total energy of the particle and $\vec{p}$ is its three-momentum (magnitude of $\vec{p}$ will be denoted as p). Natural units $\hbar = c = 1$ will be made used of. Scalar product of two four-momenta may be defined as

$$\widetilde{P}^2 = g_{\mu\nu}\, p^\mu p^\nu = E^2 - \vec{p}^{\,2} \tag{3.2}$$

where the metric tensor $g_{\mu\nu} = \mathrm{diag}(+1, -1, -1, -1)$.

A special case of two-body reaction is the elastic scattering

$$1 + 2 \to 1' + 2' \tag{3.3}$$

where the structures of the colliding particles remain the same and direction of motion of each colliding particle is changed in agreement to conservation of energy and magnitude of momentum. The four-momentum of the i-th incoming (outgoing) particle is denoted by $\widetilde{P}_i$ ($\widetilde{P}_i'$) for $i = 1, 2$; see fig. 3.1 in the case of center of mass system.

The kinematics of the given process is fully described by two independent variables (if some further characteristics such as spins are not taken into account). It is possible to choose these two parameters among the three Mandelstam variables which are defined as

$$s = (\widetilde{P}_1 + \widetilde{P}_2)^2, \tag{3.4}$$
$$t = (\widetilde{P}_1 - \widetilde{P}_1')^2, \tag{3.5}$$
$$u = (\widetilde{P}_1 - \widetilde{P}_2')^2. \tag{3.6}$$

We shall use s and t kinematic variables as it is common. It is further convenient to choose center of mass system. The variable s has the meaning of the square of the total energy of colliding particles and the variable t is the squared four-momentum transfer in the given reference frame. In the case of pp elastic scattering the magnitude of three-momenta of incoming and outgoing particles (denoted by p, resp. p') are the

same in this reference frame and both the particles have equal masses m. The relations between the center of mass scattering angle θ and three-momentum p (see fig. 3.1) and variables s and t are

$$s = 4(p^2 + m^2)\,, \tag{3.7}$$

$$t = -2p^2(1 - \cos\,\theta) = -4p^2 \sin^2 \frac{\theta}{2}. \tag{3.8}$$

In the approximation of low scattering angles θ, i.e., when $\sin\theta/2 \approx \theta/2$ one may write

$$t \approx -p^2\theta^2, \tag{3.9}$$

which is often used in experiments as all observed elastic scattering angles are relatively very small.

It follows from the relation (3.8) that

$$-4p^2 \leq t \leq 0, \tag{3.10}$$

i.e., the value of t is not positive and its minimal value t_{min} is $-4p^2$, in contrast to s which is always positive. Using eq. (3.7) the value of t_{min} may be expressed also as

$$t_{\mathrm{min}} = -s + 4m^2 \tag{3.11}$$

In high energy limit, i.e., for $s >> m^2$ (or even $s \to \infty$) the mass m may be neglected in formulas (3.7) and (3.11).

Elastic differential cross section of two *spinless* particles in the relativistic theory may be defined in Mandelstam variables s and t as follows (see, e.g., [128, 150] and also Section 3.1 in [149])

$$\frac{\mathrm{d}\sigma(s,t)}{\mathrm{d}t} = \frac{\pi}{sp^2}\,|F(s,t)|^2 \tag{3.12}$$

where we have introduced elastic scattering amplitude $F(s,t)$ in s and t variables and also corresponding normalization in center of mass system (for some other commonly used normalizations see, e.g., [153]; the normalization term is just a matter of definition of the amplitude).

In the given theoretical framework, any collision process is regarded as fully described provided its scattering amplitude is given; it may be a complex function. In the case of hadronic (resp. Coulomb) elastic scattering it is, therefore, necessary to know or establish corresponding amplitude $F^{\mathrm{N}}(s,t)$ (resp. $F^{\mathrm{C}}(s,t)$). Elastic scattering of charged hadrons is being then currently described with the help of a complete elastic scattering amplitude denoted as $F^{\mathrm{C+N}}(s,t)$.

3.2 Approach of West and Yennie

In the case of collisions of two protons (charged hadrons) the measured elastic differential cross section has been standardly described by complete elastic scattering amplitude $F^{\mathrm{C+N}}(s,t)$ (*spin effects neglected*) describing the common influence of both Coulomb and hadron interactions, see eq. (3.12).

According to Bethe [154] (1958) the complete amplitude has been commonly decomposed into the sum of the Coulomb scattering amplitude $F^{\mathrm{C}}(s,t)$ and the hadronic amplitude $F^{\mathrm{N}}(s,t)$ bound mutually with the help of relative phase $\alpha\phi(s,t)$

$$F^{\mathrm{C+N}}(s,t) = F^{\mathrm{C}}(s,t)\,\mathrm{e}^{\mathrm{i}\alpha\phi(s,t)} + F^{\mathrm{N}}(s,t) \tag{3.13}$$

where $\alpha = 1/137.036$ is the fine structure constant[1]. According to the formula (3.13) the complete amplitude $F^{\mathrm{C+N}}(s,t)$ is not given by a mere sum of hadronic and Coulomb amplitude but an *interference* of the two amplitudes is introduced. Bethe further derived with the help of a WKB method[2] in the potential theory for the relative phase the following expression

$$\phi(s,t)_{\mathrm{Bethe}} \approx \pm\frac{2\ln 1.06}{a\sqrt{-t}} \tag{3.16}$$

where parameter a characterizes the dimension of nucleon and the upper (lower) sign corresponds to the scattering of hadrons with the same (opposite) charges. This expresion was derived for a given $F^{\mathrm{N}}(s,t)$ corresponding to a specific collision model of Bethe. Formulas (3.13) and (3.16), therefore, cannot be used for arbitrary t-dependent hadronic amplitude $F^{\mathrm{N}}(s,t)$.

Several authors then tried to derive more general formula for complete amplitude $F^{\mathrm{C+N}}(s,t)$ than the one given by eqs. (3.13) and (3.16). The t dependence of relative phase $\alpha\phi(s,t)$ has been determined on various levels of sophistication. The dependence having been commonly accepted in the past was proposed by West and Yennie [14] (1968) within the framework of Feynman diagram technique (one-photon exchange) in the case of charged *point-like particles* and *partially in the high energy limit* ($s \gg m^2$, m standing for nucleon mass) as

$$\phi_{\mathrm{WY}}(s,t) = \mp\left[\ln\left(\frac{-t}{s}\right) - \int_{-4p^2}^{0}\frac{\mathrm{d}t'}{|t-t'|}\left(1 - \frac{F^{\mathrm{N}}(s,t')}{F^{\mathrm{N}}(s,t)}\right)\right]. \tag{3.17}$$

The upper (lower) sign corresponds to the scattering of particles with the same (opposite) charges. According to eq. (3.17) the t-dependence of the relative phase between the Coulomb and hadronic amplitudes may be calculated from t-dependent hadronic amplitude $F^{\mathrm{N}}(s,t)$ entering into the integrand. In order to derive eq. (3.17) also the Coulomb amplitude has been used (assuming a "known" form from QED, see [14] for details). Note that in order to derive eq. (3.17) only a Coulomb amplitude for point-like scattering particles has been used; no form factors have been taken into account at this stage of calculations (see [14] also for used phase of Coulomb amplitude $F^{\mathrm{C}}(s,t)$).

[1]The fine structure constant α is (in SI units)

$$\alpha = \frac{e^2}{4\pi\epsilon_0\hbar c} \approx \frac{1}{137.036} \tag{3.14}$$

where e is the elementary charge, $\hbar$ is the reduced Planck's constant, c is the speed of light in a vacuum, and ϵ_0 is the permittivity of free space. The fine structure constant expressed in the natural units ($\epsilon_0 = \hbar = c = 1$) is

$$\alpha = \frac{e^2}{4\pi}. \tag{3.15}$$

[2]WKB approximation or WKB method is a method for finding approximate solutions to linear partial differential equations with spatially varying coefficients. It is named after physicists Wentzel, Kramers and Brillouin who developed it in 1926.

The hadronic amplitude $F^{\mathrm{N}}(s,t)$ may be then written using its modulus $\left|F^{\mathrm{N}}(s,t)\right|$ and phase $\zeta^{\mathrm{N}}(s,t)$ as

$$F^{\mathrm{N}}(s,t) = \mathrm{i}\left|F^{\mathrm{N}}(s,t)\right| \mathrm{e}^{-\mathrm{i}\zeta^{\mathrm{N}}(s,t)} \tag{3.18}$$

Formula (3.17) containing the integration over all admissible values of four-momentum transfer squared t' seemed to be complicated when it was proposed. To perform analytical integration it has been assumed for the two following quantities:

- the ratio of real to imaginary part of hadronic amplitude

$$\rho(s,t) = \frac{\mathrm{Re}\, F^{\mathrm{N}}(s,t)}{\mathrm{Im}\, F^{\mathrm{N}}(s,t)} \tag{3.19}$$

- and diffractive slope defined as

$$B(s,t) = \frac{\mathrm{d}}{\mathrm{d}t}\left[\ln\frac{\mathrm{d}\sigma^{\mathrm{N}}}{\mathrm{d}t}(s,t)\right] = \frac{2}{|F^{\mathrm{N}}(s,t)|}\frac{\mathrm{d}}{\mathrm{d}t}\left|F^{\mathrm{N}}(s,t)\right| \tag{3.20}$$

to be t-independent for *all kinematically allowed t values*[3], see [14, 155] and [156, 157]. The diffractive slope being t-independent means that the modulus $\left|F^{\mathrm{N}}(s,t)\right|$ has been taken as purely exponential function of t. With the help of eqs. (3.18) and (3.19) one may obtain relation

$$\tan\zeta^{\mathrm{N}}(s,t) = \rho(s,t) \tag{3.21}$$

which implies that the assumption of t-independent quantity $\rho(s,t)$ is equivalent to requirement of t-independent hadronic phase $\zeta^{\mathrm{N}}(s,t)$.

For the relative phase between the Coulomb and elastic hadronic amplitude the following simplified expression has been then obtained for *small values of t only*:

$$\alpha\phi(s,t) = \mp\alpha\left[\ln\left(\frac{-B(s)t}{2}\right) + \gamma\right] \tag{3.22}$$

where $\gamma = 0.577215$ is Euler constant and B is t-independent diffractive slope. As introduced in [158, 159] some other high energy approximations and limitations were added, too.

Optical theorem relating the imaginary part of elastic hadronic scattering amplitude at $t = 0$ (corresponding to zero scattering angle) to total hadronic cross section

$$\sigma^{\mathrm{tot,N}}(s) = \frac{4\pi}{p\sqrt{s}}\,\mathrm{Im}\, F^{\mathrm{N}}(s,t=0) \tag{3.23}$$

has been then applied to and the complete elastic scattering amplitude (3.13) of Bethe has been written as

$$F^{\mathrm{C+N}}_{\mathrm{WY}}(s,t) = \pm\frac{\alpha s}{t}G_1(t)G_2(t)\,\mathrm{e}^{\mathrm{i}\alpha\phi(s,t)} + \frac{\sigma^{\mathrm{tot}}(s)}{4\pi}p\sqrt{s}\,(\rho(s)+\mathrm{i})\,\mathrm{e}^{B(s)t/2}\,. \tag{3.24}$$

The two quantities $G_1(t)$ and $G_2(t)$ stand here for the electric form factors taken commonly in standard dipole form (see, e.g., [153]) as

$$G^{\mathrm{D}}_{\mathrm{E}}(t) = \left(1 - \frac{t}{\Lambda^2}\right)^{-2} \tag{3.25}$$

[3] These important assumptions have been explicitly pointed out also in 1973 in [155] where the WY approach has been applied to experimental data for the first time.

where $\Lambda^2 = 0.71$ GeV^2. The electric form factors as Fourier–Bessel (FB) transformation of electric charge distribution of colliding hadrons have been put into formula (3.24) by hand. The second term on the right hand side of this equation represents the hadronic amplitude $F^{\mathrm{N}}_{WY}(s,t)$.

The Coulomb differential cross section (including form factors) has been, therefore, taken as

$$\frac{\mathrm{d}\sigma^{\mathrm{C}}(s,t)}{\mathrm{d}t} = \frac{\pi s}{p^2}\frac{\alpha^2}{t^2}G_1^2(t)G_2^2(t), \tag{3.26}$$

i.e., diverging at $t = 0$ [4]. The integrated Coulomb differential cross section over the whole kinematically allowed region of t is infinite due to this divergence at $t = 0$ (which is also a reason why total proton-proton cross section usually automatically refers to short-ranged hadronic interaction for which the cross section is finite). In high energy limit, see eq. (3.7), the Coulomb differential cross section (3.26) may be further simplified to

$$\frac{\mathrm{d}\sigma^{\mathrm{C}}(s,t)}{\mathrm{d}t} = \frac{4\pi\alpha^2}{t^2}G_1^2(t)G_2^2(t). \tag{3.27}$$

The simplified formula (3.24) of WY has been commonly applied to experimental data (using eq. (3.12)) for determination of $\sigma^{\mathrm{tot,N}}$, ρ and B at various energies in very narrow interval of small values of $|t|$ (as the validity of WY approach has been limited only to these small values). The eqs. (3.22) and (3.24) derived by WY were derived in similar form also by Locher [161] even one year earlier (in 1967).

Integrated elastic hadronic cross section may be obtained from established hadronic amplitude $F^{\mathrm{N}}(s,t)$ and eq. (3.12) as follows

$$\sigma^{\mathrm{el,N}}(s) = \int_{t_{\mathrm{min}}}^{0} \frac{\mathrm{d}\sigma^{\mathrm{N}}}{\mathrm{d}t}(s,t)\mathrm{d}t. \tag{3.28}$$

The inelastic cross section may be then defined as

$$\sigma^{\mathrm{inel}}(s) = \sigma^{\mathrm{tot,N}}(s) - \sigma^{\mathrm{el,N}}(s). \tag{3.29}$$

As to the mentioned assumptions and problems included in the simplified formula of WY (3.24), they have been discussed in details in 1989 [156] and later in even more details in 2005 [158] (see also [48], [162] and [157]). In the following main points are summarized.

The assumption concerning neglecting spin dependent effects in unpolarized beams has been discussed, e.g., in [162] and [157]. According to these papers the spin effects have negligible impact in the case of forward elastic hadronic pp scattering at ISR energy range of $\sqrt{s}$, i.e., from 23.5 GeV to 62.5 GeV, and in all high energy elastic hadron scattering. More detailed analysis of elastic collisions in dependence on spin would be surely very interesting as it could bring some new information about the structure of corresponding particles. From experimental (technical) point of view it is, however, much more difficult to prepare spin-polarized beams than spin-unpolarized ones. In the case of pp collision there are some data obtained with spin-polarized protons beams,

[4] The Coulomb scattering is known in literature also as Rutherford scattering, see the treatment of the problem in classical physics (scattering on potential) in [152] (pages 53-55) and [160] (pages 516-519) for analogous calculations in non-relativistic quantum mechanics (QM).

e.g., at RHIC[5]. The influence of spin is usually not taken into account in contemporary description of elastic hadronic scattering as it represents quite complicated problem.

On the other hand the assumptions of t-independent quantities $\rho(s,t)$ and $B(s,t)$ in the whole kinematically allowed region of t are much more important. They are introducing a priory strong limitations on the hadronic amplitude $F^{\mathrm{N}}(s,t)$ without any reasoning. The simplified formula of WY defined by eqs. (3.22) and (3.24) has been used for the analysis of differential cross section data in the interference region only, i.e., in the case of elastic nucleon scattering for $|t| \lesssim 0.05$ GeV^2 at ISR energies (see, e.g., [153, 155], [115, 163–175]). For higher values of $|t|$ it has been believed that the influence of Coulomb scattering may be, on the basis of the simplified formula of WY, completely neglected. Other formulas of hadronic amplitude $F^{\mathrm{N}}(s,t)$ not corresponding to these limiting assumptions have been then commonly used to fit measured elastic differential cross section at higher values of $|t|$. The whole t-dependence of elastic scattering has been, therefore, simultaneously described with the help of two inconsistent (contradictory) approaches as it has been pointed out and further analyzed in, e.g., [49, 157, 176, 177].

The assumed purely exponential t-dependence of the modulus of the hadronic amplitude has been in contradiction to the measured elastic nucleon differential cross section for higher values of $|t|$ where a dip-bump (resp. shoulder) structure has been clearly visible, see fig. 2 in the case of pp (resp. $\bar{\mathrm{p}}$p) elastic scattering. This assumption was introduced before the diffractive structures in elastic hadronic collisions was observed. Measurement of neutron-proton (np) elastic scattering in 1984 provided a (more) direct measurement of the hadronic scattering also at lower values of $|t|$ where some non-purely exponential effects have been observed, see appendix A.1.

It has been further shown in [159] (2007) that already the fact that the relative phase $\phi(s,t)$ between the Coulomb and hadronic amplitude given by the original integral formula (3.17) is real implies that the quantity $\rho(s,t)$ (hadronic phase) has to be t-independent; even the return to the eq. (3.17) does not, therefore, remove a priory limitation on the hadronic phase included in the approach of WY. Similar return to the original integral formula (3.17) has been recently suggested, e.g., in [178]. In this paper the elastic hadronic amplitude has been divided into real and imaginary part and both of them parameterized as an exponential function of t. In such a case, however, the hadronic phase has been allowed to be t-dependent which is in contradiction to the "hidden" assumption of t-independent phase under which the integral formula (3.17) for real phase has been derived.

To take into account space distribution of electric charge (for non point-like hadrons) some electromagnetic form factors have been added by hand to the simplifed formula of WY (3.24) at the end of all the calculations; they have not been taken into account in any previous step of the derivation of the formula. The relevance of such approach should be questioned, too.

It is evident that the description of elastic scattering in the approach of WY has been based on very limiting assumptions simplifying corresponding calculations without any physical motivation (e.g., the dependence of ρ and B on t has not been considered). Dependence of (elastic) hadronic collisions on impact parameter has not been taken into account in the given approach. Any attempt has not been done to study some correlations of initial state characteristics and final state ones which should be the main

[5]RHIC achieved maximal collision energy 500 GeV in 2009 of polarized proton - the highest in the world at that time.

goal of any experimental data analysis.

In elastic collisions one should take into account mainly correlations between impact parameter values of colliding particles and angle deviations (i.e., values of t) of scattered particles. The first attempt in this direction has been done with the help of the eikonal model which will be explained in sect. 3.4. It is, however, convenient to discuss proton electromagnetic form factors in more detail first.

3.3 Electromagnetic proton form factors determined from elastic ep scattering

The proton cannot be taken as point-like object, which represents a modification of the simple Coulomb interaction as its charge is distributed in a larger space. The shape of this distribution and its influence on the corresponding interactions are commonly characterized by elastic electromagnetic form factors, see eq. (3.26). The form factors have been established on the basis of analysis of ep (not pp) scattering. The corresponding elastic ep differential cross section $\frac{\mathrm{d}\sigma}{\mathrm{d}\Omega}$ (in the one-photon exchange) in the laboratory frame has been described by Rosenbluth formula (see [179–183]) which has been rewritten later by Sachs [184] in the form

$$\left(\frac{\mathrm{d}\sigma}{\mathrm{d}\Omega}\right)_{ep} = \left(\frac{\mathrm{d}\sigma}{\mathrm{d}\Omega}\right)_{\mathrm{Mott}} \left\{\frac{1}{1+\tau}\left[G_{\mathrm{E}}^2(Q^2) \; + \; \tau G_{\mathrm{M}}^2(Q^2)\right] + 2\tau G_{\mathrm{M}}^2(Q^2)\tan^2\left(\frac{\theta}{2}\right)\right\} \tag{3.30}$$

where

$$Q^2 = 4\, EE' \sin^2\left(\frac{\theta}{2}\right), \tag{3.31}$$

$$\tau = \frac{Q^2}{4m^2} \tag{3.32}$$

and E and E' are the incident and final electron energies, respectively, which are bound due to the conservation of the total four-momentum by relation

$$E' \; = \; \frac{E}{1+\frac{2E}{m}\sin^2(\frac{\theta}{2})}; \tag{3.33}$$

θ is the scattering angle of the electron in the laboratory frame. G_{E} and G_{M} stand for electric and magnetic form factor. The expression

$$\left(\frac{\mathrm{d}\sigma}{\mathrm{d}\Omega}(E,\theta)\right)_{\mathrm{Mott}} = \frac{\alpha^2}{4E^2\,\sin^4(\frac{\theta}{2})}\,\frac{E'}{E}\,\cos^2\left(\frac{\theta}{2}\right) \tag{3.34}$$

is the Mott formula [185] (in one-photon exchange approximation) for the differential cross section describing the elastic scattering of Dirac electron with point-like and spinless charged particle of proton mass m at incident energy E in the same frame (see, e.g., [180]).

The formula (3.30) contains electric form factor $G_{\mathrm{E}}(Q^2)$ and magnetic form factor $G_{\mathrm{M}}(Q^2)$ which depend only on the square of exchanged momentum transfer

$$t \equiv -Q^2 \tag{3.35}$$

and which should satisfy the initial conditions

$$G_{\rm E}(0) \;=\; G_{\rm M}(0)/\mu_p \;=\; 1; \tag{3.36}$$

here $\mu_p \approx 2.793$ is the proton magnetic moment divided by nuclear magneton.

From early measurements of the elastic ep scattering at lower energies it has been also deduced that electric $G_{\rm E}(t)$ proton form factor can be described by the dipole formula (3.25) and the magnetic one by

$$G_{\rm M}^{\rm D}(t) \approx \mu_p G_{\rm E}^{\rm D}(t)\ . \tag{3.37}$$

Borkowski et al. [186, 187] analyzed elastic ep scattering data at several energies with the help of Rosenbluth differential cross section formula (3.30) where the t-dependencies of both the electric and magnetic form factors have been parametrized by the formulas

$$G_{\rm E}^{\rm B}(t) = \sum_{j=1}^{4} \frac{g_k^{\rm E}}{w_k^{\rm E} - t}, \tag{3.38}$$

$$G_{\rm M}^{\rm B}(t) = \mu_p \sum_{j=1}^{4} \frac{g_k^{\rm M}}{w_k^{\rm M} - t} \tag{3.39}$$

inspired by the vector dominance model. The original values of the parameters $g_k^{\rm E,M}$ and $w_k^{\rm E,M}$ (being different for both the electric and magnetic form factors) may be found in [187] the corresponding electric and magnetic form factors may be denoted as $G_{\rm E}^{\rm BO}(t)$ and $G_{\rm M}^{\rm BO}(t)$. Different shapes of electromagnetic form factor parametrizations have been proposed by Arrington et al. [188, 189] (denoted as $G_{\rm E}^{\rm AR}(t)$ and $G_{\rm M}^{\rm AR}(t)$) and Kelly [190] which has been applied by Puckett [191] (denoted as $G_{\rm E}^{\rm PU}(t)$ and $G_{\rm M}^{\rm PU}(t)$), too.

Extending the measurements of the proton electric and magnetic form factors to higher values of $|t|$ has offered a chance for a better description of the influence of electromagnetic proton structure in the elastic pp collisions at high energies. However, this approach may be considered as fully entitled assuming that the electric and magnetic form factors determined from an analysis of elastic ep scattering are identical with the form factors involved in a description of pp elastic scattering (which should be tested in the future).

The relatively recent determination of t-dependent electric and magnetic form factors has been done by Arrington et al. [189] (see also [182, 188]) in the relatively broad region of $-t \in (0.007, 5.85)$ GeV^2. In this region we may express (refit) the form factors using the parameterizations of Borkowski given by eqs. (3.38) and (3.39). The fitted parameters are in table 3.1; the corresponding electric and magnetic form factors (which we will use extensively later) may be denoted as $G_{\rm E}^{\rm BN}(t)$ and $G_{\rm M}^{\rm BN}(t)$. The mentioned electric and magnetic form factors $G_{\rm E,M}^{\rm AR}(t)$, $G_{\rm E,M}^{\rm PU}(t)$, $G_{\rm E,M}^{\rm BO}(t)$, $G_{\rm E,M}^{\rm BN}(t)$ and $G_{\rm E,M}^{\rm D}(t)$ are shown in figs. 3.2 and 3.3.

The effective electromagnetic form factor squared ($\tau = -t/(4m^2)$)

$$G_{eff}^2(t) = \frac{1}{1+\tau}\left[G_{\rm E}^2(t) + \tau\, G_{\rm M}^2(t)\right]\ , \tag{3.40}$$

appearing in eq. (3.30) has been introduced in [192] for analysis of elastic pp scattering as the term in eq. (3.30) proportional to $\tan^2\left(\frac{\theta}{2}\right)$ can be neglected in linear α approximation (one-photon exchange) [189]. One may define effective electric form factor squared as

$$G_{{\rm E},eff}^2(t) = \frac{1}{1+\tau} G_{\rm E}^2(t) \tag{3.41}$$

k	1	2	3	4
g_k^{E}	0.1344	5.014	-7.922	2.747
w_k^{E}	0.2398	1.135	1.530	2.284
g_k^{M}	0.2987	27.73	-28.15	0.1274
w_k^{M}	0.3276	1.253	1.276	6.361

Table 3.1: The values of parameters specifying the new Borkowski's et al. electromagnetic proton form factors $G_{\mathrm{E}}^{\mathrm{BN}}(t)$ and $G_{\mathrm{M}}^{\mathrm{BN}}(t)/\mu_p$ taken from [189]; here the parameters have been expressed in units of GeV^2.

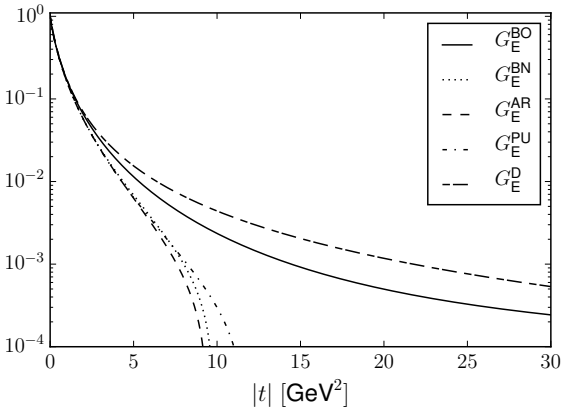

Figure 3.2: Proton electric form factors $G_{\mathrm{E}}(t)$.

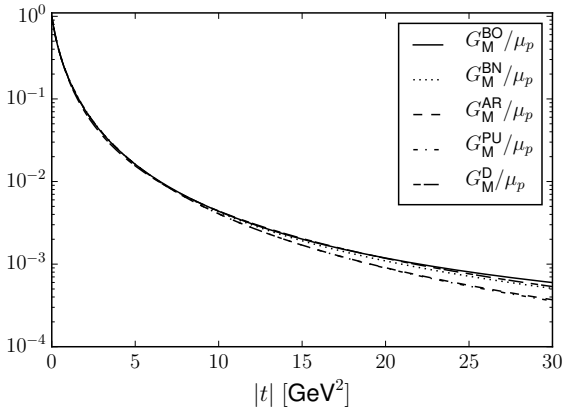

Figure 3.3: Proton magnetic form factors $G_{\mathrm{M}}(t)/\mu_p$ having very similar t-dependence.

and effective magnetic form factor as

$$G_{\mathrm{M},eff}^2(t) = \frac{\tau}{1+\tau} G_{\mathrm{M}}^2(t)\,. \tag{3.42}$$

The graphs of the effective electric form factor $G_{\mathrm{E},eff}^2(t)$, the effective magnetic form factor $G_{\mathrm{M},eff}^2(t)$ and effective electromagnetic form factor $G_{eff}^2(t)$ corresponding to the $G_{\mathrm{E}}^{\mathrm{BN}}(t)$ and $G_{\mathrm{M}}^{\mathrm{BN}}(t)$ (i.e., Borkowski's parameterization with the newly determined values of free parameters) are shown in fig. 3.4. For the comparison also the electric form factor $(G_{\mathrm{E}}^{\mathrm{BO}})^2(t)$ used in [20] is plotted.

Fig. 3.4 shows that the t-dependence of the effective electromagnetic form factor $G_{eff}^2(t)$ in eq. (3.40) is different from that one appearing in original Borkowski's et al. parameterization eq. (3.38) which has been used in analysis of experimental elastic pp data in [20]. One may ask what may be the difference in the result if also magnetic form factor is included. In next section it will be, therefore, shown how to generalize the approach in [20] to take into account the effective electromagnetic form factors in the eikonal model description of elastic pp collisions.

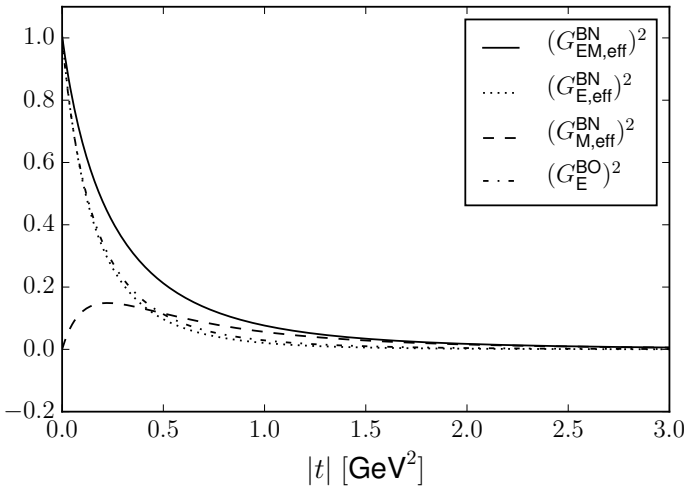

Figure 3.4: Effective form factors corresponding to $G_{\mathrm{E}}^{\mathrm{BN}}(t)$ and $G_{\mathrm{M}}^{\mathrm{BN}}(t)$ (see eqs. (3.40) to (3.42)) and compared to $(G_{\mathrm{E}}^{\mathrm{BO}})^2(t)$.

3.4 Eikonal model approach

3.4.1 Coulomb-hadronic interference formula

One of the fundamental differences between the eikonal model approach and the approach of WY (based on Feynman diagram technique) is that the former one is trying to take into account the influence of impact parameter and establish some characteristics of hadron collisions depending on this fundamental parameter. The complex amplitude of elastic collisions of two *spinless* hadrons has been expressed in the form

$$F(s, q^2 = -t) = \frac{s}{4\pi \mathrm{i}} \int\limits_{\Omega_b} \mathrm{d}^2 b \ \mathrm{e}^{i\vec{q}.\vec{b}} [\mathrm{e}^{2\mathrm{i}\delta(s,b)} - 1] \tag{3.43}$$

where Ω_b represents two-dimensional Euclidean space of impact parameter $\vec{b}$ and $\delta(s, b)$ is so-called eikonal function. The vector $\vec{q}$ is defined as difference $\vec{p} - \vec{p'}$ of particle momenta before and after elastic scattering. In the case of elastic hadronic scattering the first (approximate) form of eq. (3.43) was suggested by Glauber [193] (1959) in *high energy* limit. Mathematically more rigorous derivation of elastic scattering amplitude in the impact parameter representation which respects a finite admissible region of momentum transfers at *finite* collision energies was given by Adachi and Kotani [194–199] (1965-1968) and also by Islam [200, 201] (1968-1976).

The eikonal $\delta(s, b)$ may be calculated from energy-dependent spherically symmetric potential $V(s, r)$ according to [200–202] as

$$\delta(s, b) \sim \int\limits_{b}^{\infty} \frac{V(s, r) r \mathrm{d}r}{\sqrt{r^2 - b^2}}. \tag{3.44}$$

Potential $V(s, r)$ corresponds to potential between particles at momentary mutual

positions during their motions and might be generally represented by a complex function[6]. Due to eq. (3.43) the complete elastic amplitude $F^{\mathrm{C+N}}(s,t)$ of two charged and spinless hadrons is fully determined by the complete eikonal $\delta^{\mathrm{C+N}}(s,b)$. Taking into account the linearity of potential $V(s,r)$ in expression (3.44) and the *additivity of Coulomb and hadronic potentials* complete eikonal $\delta^{\mathrm{C+N}}(s,b)$ is given by the sum of individual eikonals $\delta^{\mathrm{C}}(s,b)$ and $\delta^{\mathrm{N}}(s,b)$ for the Coulomb and hadronic eikonals

$$\delta^{\mathrm{C+N}}(s,b) = \delta^{\mathrm{C}}(s,b) + \delta^{\mathrm{N}}(s,b). \tag{3.45}$$

Due to the fact that potentials in eikonal model are allowed to be complex (having non-zero imaginary part) their additivity is not obvious and it may have deeper implications then the additivity of real potentials in classical physics.

The complete elastic amplitude of charged hadrons in the eikonal model may be rewritten as

$$F^{\mathrm{C+N}}_{\mathrm{eik}}(s,q^2=-t) = \frac{s}{4\pi\mathrm{i}} \int\limits_{\Omega_b} \mathrm{d}^2b \ \mathrm{e}^{\mathrm{i}\vec{q}.\vec{b}}[\mathrm{e}^{2\mathrm{i}(\delta^{\mathrm{C}}(s,b)+\delta^{\mathrm{N}}(s,b))}-1]. \tag{3.46}$$

The Coulomb and hadronic elastic scattering in the eikonal approach is determined by the complete eikonal $\delta^{\mathrm{C+N}}(s,b)$. Due to eq. (3.44) the often mentioned "interference" between the Coulomb and hadronic interactions follows thus in the eikonal model from the mere sum of corresponding potentials.

According to [203] and [204] one may further write

$$\begin{aligned} F^{\mathrm{C+N}}_{\mathrm{eik}}(s,t) &= F^{\mathrm{C}}(s,t) + F^{\mathrm{N}}(s,t) + F^{\mathrm{I}}(s,t) \\ &= F^{\mathrm{C}}(s,t) + F^{\mathrm{N}}(s,t) + \frac{s}{4\pi\mathrm{i}} \int\limits_{\Omega_b} \mathrm{d}^2b \ \mathrm{e}^{\mathrm{i}\vec{q}.\vec{b}}[\mathrm{e}^{2\mathrm{i}\delta^{\mathrm{C}}(s,b)}-1][\mathrm{e}^{2\mathrm{i}\delta^{\mathrm{N}}(s,b)}-1] \end{aligned} \tag{3.47}$$

where the interference term $F^{\mathrm{I}}(s,t)$ have been introduced. Due to the eq. (3.47) the complete elastic scattering amplitude in the eikonal model is, therefore, not given by mere sum of Coulomb $F^{\mathrm{C}}(s,t)$ and hadronic $F^{\mathrm{N}}(s,t)$ scattering amplitudes.

Cahn [204] in 1982 further established phase of Coulomb amplitude $F^{\mathrm{C}}(s,t)$ in the following (formal) way. He started from the Born shape of the Coulomb scattering amplitude

$$F^{\mathrm{C}}_{\mathrm{Born}}(s,t=-q^2) = \mp\frac{\alpha s}{q^2+\mu^2} \tag{3.48}$$

where the upper (lower) sign corresponds to the scattering of the same (opposite) charges and μ is a fictitious rest non-zero mass of a photon standardly used in order to remove infrared divergences; in the final expression one passes to a limit $\mu \to 0$. Using eq. (3.43) coulomb eikonal $\delta^{\mathrm{C}}(s,b)$ has been written as

$$\delta^{\mathrm{C}}(s,b) = \frac{1}{2\pi s} \int\limits_{\Omega_b} \mathrm{d}^2q \, \mathrm{e}^{-\mathrm{i}\vec{q}.\vec{b}} \, F^{\mathrm{C}}_{\mathrm{Born}}(s,q^2) \tag{3.49}$$

which can be simplified to

$$\delta^{\mathrm{C}}(s,b) = \alpha[\ln(1/2b\mu) + \gamma + O(b\mu)] \tag{3.50}$$

[6]The meaning of complex potential in quantum mechanics is, however, not so straightforward as meaning of real potential in classical physics. Imaginary part is sometimes used to open (describe) inelastic scattering while real part describes elastic scattering.

where γ is the Euler constant. The Coulomb amplitude has been obtained when eq. (3.50) has been inserted into eq. (3.43)

$$F^{\mathrm{C}}(s,t=-q^2) = \mp\frac{s\alpha}{q^2}\,\mathrm{e}^{\mathrm{i}\alpha\zeta^{\mathrm{C}}(q^2)} \tag{3.51}$$

where the quantity $\zeta^{\mathrm{C}}(q^2)$ is the phase of the Coulomb amplitude for point-like particles in the eikonal model and is equal to

$$\zeta^{\mathrm{C}}(q^2) = \ln\left(\frac{\mu^2}{q^2}\right). \tag{3.52}$$

Similar (mathematical) procedure of establishing Coulomb phase taking into account dipole form factors may be found also in [204]. Both the modulus and phase of the Coulomb amplitude (3.51) are singular at $t = q^2 = 0$ which causes non-direct application of optical theorem for Coulomb interaction.

Using eqs. (3.51) and (3.52) Cahn was able to rewrite eq. (3.47) in a form similar to the relative phase of WY given by eq. (3.17). In this procedure several limiting assumptions have been introduced as the goal of Cahn was mainly to rederive the relative phase of WY.

However, in course of deriving a formula for complete amplitude $F^{\mathrm{C+N}}(s,t)$ suitable for analysis of experimental data one should not impose any a prior limitation on hadronic amplitude $F^{\mathrm{N}}(s,t)$ without corresponding justification. Mistakenly constrained $F^{\mathrm{N}}(s,t)$ may lead to completely wrong physical conclusions.

Kundrát and Lokajíček in [20] (1994) tried to remove unjustified approximations and limitation imposed mainly on hadronic amplitude $F^{\mathrm{N}}(s,t)$ and to derive more general expression for complete amplitude $F^{\mathrm{C+N}}(s,t)$ which could be then used for analysis of experimental data. According to the paper [20] it is possible to derive from Cahn's eq. (3.47) and Coulomb amplitude in the form given by eq. (3.51) for the complete elastic amplitude $F^{\mathrm{C+N}}(s,t)$ in the eikonal model the following relation

$$F^{\mathrm{C+N}}_{\mathrm{eik}}(s,t) = \pm\frac{\alpha s}{t}G_1(t)G_2(t) + F^{\mathrm{N}}(s,t)[1 \mp \mathrm{i}\alpha\bar{G}(s,t)] \tag{3.53}$$

where

$$\bar{G}(s,t) = \int\limits_{t_{\min}}^{0} \mathrm{d}t' \left\{\ln\left(\frac{t'}{t}\right)\frac{\mathrm{d}}{\mathrm{d}t'}[G_1(t')G_2(t')] - \frac{1}{2\pi}\left[\frac{F^{\mathrm{N}}(s,t')}{F^{\mathrm{N}}(s,t)} - 1\right] I(t,t')\right\} \tag{3.54}$$

and

$$I(t,t') = \int\limits_{0}^{2\pi} \mathrm{d}\Phi'' \frac{G_1(t'')G_2(t'')}{t''}. \tag{3.55}$$

Quantities $G_1(t)$ and $G_2(t)$ in eq. (3.53) stand for form factors reflecting the electromagnetic structure of colliding charged hadrons and $t'' = t + t' + 2\sqrt{tt'}\cos\Phi''$ in eq. (3.55). The minimal kinematically allowed value $t_{\min}$ in (3.54) is given by eq. (3.11) in the case of two hadrons with the same masses m. The upper (lower) sign in (3.53) corresponds then to the scattering of particles with the same (opposite) charges.

Formula (3.53) has been derived for *any s and t value* with the accuracy up to terms *linear in* α. It has been derived with the aim not to put any a priori unreasoned

strong restriction on hadronic amplitude $F^{\mathrm{N}}(s,t)$ (to avoid limitations on $F^{\mathrm{N}}(s,t)$ in the WY approach). The formula (3.53) may be, therefore, used in two distinct ways. Firstly, it is possible to perform an analysis of measured differential cross section in the whole measured t-region (i.e., not only in very limited interval of small values of t as it is in the case of the approach of WY) and to determine corresponding hadronic amplitude $F^{\mathrm{N}}(s,t)$. For this purpose one may chose suitable parametrization of the corresponding modulus and phase and try to determine $F^{\mathrm{N}}(s,t)$ from experimental data as it has been done in [20]. Secondly, the formula (3.53) for complete elastic scattering amplitude $F^{\mathrm{C+N}}(s,t)$ may be used, too, to obtain prediction of measured differential cross section with the help of eq. (3.12) if the hadronic amplitude $F^{\mathrm{N}}(s,t)$ has been specified within a framework of some phenomenological model description (see, e.g., [48] where several model predictions of pp elastic differential cross sections including the influence of Coulomb interaction at the LHC have been made). The former usage of the formula (3.53) will be applied to in chapter 4.

The determination of total hadronic cross section from the hadronic amplitude $F^{\mathrm{N}}(s,t)$ in the eikonal model has been based on optical theorem given by eq. (3.23) similarly as in the approach of WY. The main advantage (and motivation) of the eikonal model over the approach of WY is that it allows studying some characteristic of collisions in dependence on impact parameter as it will be shown in the following.

The use of electromagnetic form factors reflects the influence of both the electric and magnetic charge structures of colliding nucleons. Only the electric form factors given by eq. (3.38) have been used originally in [20] to calculate $F^{\mathrm{C+N}}(s,t)$ according to eq. (3.53) for analysis of experimental data. It has enabled to include in the elastic scattering the influence of electric space structure of colliding protons. Such an approach can be generalized by taking into account also the influence of the proton magnetic form factor, i.e., the interaction of magnetic moment of the proton with Coulomb field of the other colliding proton.

The influence of the magnetic form factors in the case of elastic pp scattering at high energies have been theoretically studied by Block [175, 192]. However, this approach has been based on the application of standard WY complete elastic amplitude containing originally only the dipole electric proton form factors given by eq. (3.25) which have been replaced by effective electromagnetic form factor (3.40) containing also dipole magnetic form factor (3.37). Such an approach, however, contains many limitations and deficiencies as it has been discussed in sect. 3.2.

Unlike the approach of WY (see sect. 3.2) the electromagnetic form factors form the part of Coulomb amplitude from the very beginning in the eikonal model. Due to the integration over all kinematically allowed region of t' in eq. (3.54) the t'-dependence of effective electromagnetic form factors should describe the charges distributions in the largest interval of momentum transfers t' as possible. For some suitable t-dependent parameterizations of electromagnetic proton form factor the integral $I(t,t')$ may be analytically calculated (see sect. 3.4.2) which helps in numerical calculations in application of the eikonal model to experimental data. The elaborated approach then enables to study either the influence of individual effective electric or magnetic form factor or the common influence of both of them.

3.4.2 Analytical expression of integral $I(t,t')$

It has been mentioned in sect. 3.4.1 that the integral involving the electromagnetic proton form factors (3.55) may be calculated analytically for some form factors. It is sufficient to integrate only over a finite region of momentum transfers in formula (3.53) since the whole integral is multiplied by the elastic hadronic amplitude $F^{\rm N}(s,t)$ the modulus of which decreases at high $|t|$ approximately like $|t|^{-4}$ - see, e.g., [205]. The used limited integration region of momentum transfers allows us to use some simpler formulas for the ep form factors enabling us much simpler analytical calculation.

In [20] the integral $I(t,t')$ given by eq. (3.55) was analytically calculated only for *electric* form factor parameterized according to (3.38). The integral may be analytically calculated for more complex t-dependence of *effective electromagnetic* form factor given by eq. (3.40) if the corresponding electric and magnetic form factors are given by eqs. (3.38) and (3.39).

The analytical calculation of the new form of the integral $I(t,t')$ in eq. (3.55) has been calculated with the program Mathematica [206] and equals to the sum of two contributions coming from the electric and magnetic form factors which contain now some kinematical factors ($r_p = -\tau/t = 1/(4m^2)$)

$$I(t,t') \;=\; -\left[\sum_{j,k=1}^{4} g_j^{\rm E} g_k^{\rm E}\; W_{jk}^{\rm E}(t,t')\; I_{jk}^{\rm E}(t,t') \;+\; {r_p\mu_p}^2 \sum_{m,n=1}^{4} g_m^{\rm M} g_n^{\rm M}\; W_{mn}^{\rm M}(t,t')\; I_{mn}^{\rm M}(t,t')\right]. \tag{3.56}$$

The contribution of electric form factor in this equation is given as follows. For $j \neq k$ it holds

$$\begin{aligned} I_{jk}^{\rm E}(t,t') =& 2\pi \left[\frac{(U-1)^3}{\sqrt{U}(U-R)(U-P_j^{\rm E})(U-P_k^{\rm E})} + \frac{(R-1)^3}{\sqrt{R}(R-U)(R-P_j^{\rm E})(R-P_k^{\rm E})}\right. \\ &\left. + \frac{(P_j^{\rm E}-1)^3}{\sqrt{P_j^{\rm E}}(P_j^{\rm E}-U)(P_j^{\rm E}-R)(P_j^{\rm E}-P_k^{\rm E})} + \frac{(P_k^{\rm E}-1)^3}{\sqrt{P_k^{\rm E}}(P_k^{\rm E}-U)(P_k^{\rm E}-R)(P_k^{\rm E}-P_j^{\rm E})}\right], \end{aligned} \tag{3.57}$$

while for $j = k$ one has

$$\begin{aligned} I_{jj}^{\rm E}(t,t') =& 2\pi \left[\frac{(U-1)^3}{\sqrt{U}(U-R)(U-P_j^{\rm E})^2} + \frac{(R-1)^3}{\sqrt{R}(R-U)(R-P_j^{\rm E})^2}\right. \\ &+ \frac{(P_j^{\rm E}-1)^2}{2(U-P_j^{\rm E})^2(R-P_j^{\rm E})^2(P_j^{\rm E})^{3/2}} \\ &\left. \left[U\left(R+5RP_j^{\rm E}-3P_j^{\rm E}(P_j^{\rm E}+1)\right)+P_j^{\rm E}\left(-3R(P_j^{\rm E}+1)+P_j^{\rm E}(5+P_j^{\rm E})\right)\right]\right]. \end{aligned} \tag{3.58}$$

The quantities U, R and $P_j^{\rm E}$ are the functions of t and t' variables defined as

$$U = \frac{(\sqrt{-t}+\sqrt{-t'})^2}{(\sqrt{-t}-\sqrt{-t'})^2}, \qquad R = \frac{1+r_p(\sqrt{-t}+\sqrt{-t'})^2}{1+r_p(\sqrt{-t}-\sqrt{-t'})^2}, \qquad P_j^{\rm E} = \frac{w_j^{\rm E}+(\sqrt{-t}+\sqrt{-t'})^2}{w_j^{\rm E}+(\sqrt{-t}-\sqrt{-t'})^2}. \tag{3.59}$$

Similarly the quantity $W^{\rm E}_{jk}$ is also the function of t and t' variables and equals

$$W^{\rm E}_{jk}(t,t') = \Big[[w^{\rm E}_j + (\sqrt{-t} - \sqrt{-t'})^2][w^{\rm E}_k + (\sqrt{-t} - \sqrt{-t'})^2] \\ [\sqrt{-t} - \sqrt{-t'}]^2[1 + r_p(\sqrt{-t} - \sqrt{-t'})^2]\Big]^{-1} . \tag{3.60}$$

The contribution of magnetic form factor is represented by the second term in eq. (3.56). The integral for $m \neq n$ equals to

$$I^{\rm M}_{mn}(t,t') = 2\pi \left[\frac{(P^{\rm M}_m - 1)^2}{\sqrt{P^{\rm M}_m}(P^{\rm M}_m - R)(P^{\rm M}_m - P^{\rm M}_n)} \right. \\ + \frac{(R-1)^2}{\sqrt{R}(R - P^{\rm M}_m)(R - P^{\rm M}_n)} \\ \left. + \frac{(P^{\rm M}_n - 1)^2}{\sqrt{P^{\rm M}_n}(P^{\rm M}_n - R)(P^{\rm M}_n - P^{\rm M}_m)} \right] \tag{3.61}$$

and for $m = n$ it equals

$$I^{\rm M}_{mm}(t,t') = 2\pi \left[\frac{(R-1)^2}{\sqrt{R}(R - P^{\rm M}_m)^2} + \frac{(P^{\rm M}_m - 1)\left[P^{\rm M}_m(P^{\rm M}_m + 3) - R(3P^{\rm M}_m + 1)\right]}{2\,(P^{\rm M}_m)^{3/2}(R - P^{\rm M}_m)^2} \right] . \tag{3.62}$$

The quantities $P^{\rm M}_m$ and $W^{\rm M}_{mn}$ are the functions of t and t' variables and equal

$$P^{\rm M}_m = \frac{w^{\rm M}_m + (\sqrt{-t} + \sqrt{-t'})^2}{w^{\rm M}_m + (\sqrt{-t} - \sqrt{-t'})^2} \tag{3.63}$$

and

$$W^{\rm M}_{mn} = \Big[[w^{\rm M}_m + (\sqrt{-t} - \sqrt{-t'})^2][w^{\rm M}_n + (\sqrt{-t} - \sqrt{-t'})^2]\,[1 + r_p(\sqrt{-t} - \sqrt{-t'})^2]\Big]^{-1} . \tag{3.64}$$

Then the complete elastic scattering amplitude in the eikonal model describing the common influence of Coulomb and hadron scattering in one-photon exchange approach which is valid at any s and t up to the terms linear in α is generally given by eqs. (3.53) to (3.55) with the quantity $I(t,t')$ given by eqs. (3.56) to (3.64). This form of the complete elastic scattering amplitude will be used for the analysis of pp elastic scattering data in chapter 4.

3.4.3 Unitarity of S matrix and b-dependent profile functions

According to van Hove [207, 208] (1963-1964) the unitarity condition of S matrix ($S^+S = 1$) may be written in terms of t-dependent hadronic amplitude $F^{\rm N}(s,t)$ as (see also [200])

$$\mathrm{Im}\, F^{\rm N}(s,t) = \frac{p}{4\pi\sqrt{s}} \int \mathrm{d}\Omega' F^{\rm N^*}(s,t') F^{\rm N}(s,t'') + G_{\rm inel}(s,t) \tag{3.65}$$

where $\mathrm{d}\Omega' = \sin\vartheta' \mathrm{d}\vartheta' \mathrm{d}\Phi'$, $t = -4p^2 \sin^2\frac{\vartheta}{2}$, $t' = -4p^2\sin^2\frac{\vartheta'}{2}$, $t'' = -4p^2\sin^2\frac{\vartheta''}{2}$ and $\cos\vartheta'' = \cos\vartheta\cos\vartheta' + \sin\vartheta\sin\vartheta'\cos\Phi'$. Variables ϑ, ϑ' and ϑ'' are angles defining

corresponding momentum transfers squared t, t' and t'' in the center-of-mass system and $G_{\mathrm{inel}}(s,t)$ is the so-called inelastic overlap function (introduced by van Hove) representing summation over all possible production (inelastic) states as well as the integration over all other kinematical variables.

The t-dependent elastic hadronic amplitude $F^{\mathrm{N}}(s,t)$ is standardly expressed in b-space using FB transformation as

$$h_{\mathrm{el}}(s,b) = \frac{1}{4p\sqrt{s}} \int_{-\infty}^{0} F^{\mathrm{N}}(s,t) J_0(b\sqrt{-t})\mathrm{d}t \tag{3.66}$$

where J_0 is Bessel function of the first kind of order zero defined as

$$J_0(x) = \frac{1}{2\pi} \int_0^{2\pi} \mathrm{e}^{\mathrm{i}x\cos\varphi}\,\mathrm{d}\varphi. \tag{3.67}$$

Function $g_{\mathrm{inel}}(s,b)$ has been then similarly introduced as FB transformation of $G_{\mathrm{inel}}(s,t)$.

The unitarity condition (3.65) is then usually expressed in impact parameter space as

$$\mathrm{Im}\, h_{\mathrm{el}}(s,b) = |h_{\mathrm{el}}(s,b)|^2 + g_{\mathrm{inel}}(s,b). \tag{3.68}$$

Practically all approaches of hadron-hadron scattering in the impact parameter space have been based on FB transformation (3.66) and unitarity condition (3.68) (see, e.g., [16, 128, 209–214]) as some physical meaning has been attributed to the b-dependent terms in eq. (3.68) using so-called profile functions $D^{\mathrm{X}}(s,b)$ (X=tot, el, inel) defined as

$$D^{\mathrm{el}}(s,b) \equiv 4\,|h_{\mathrm{el}}(s,b)|^2, \tag{3.69}$$

$$D^{\mathrm{tot}}(s,b) \equiv 4\ \mathrm{Im}\, h_{\mathrm{el}}(s,b), \tag{3.70}$$

$$D^{\mathrm{inel}}(s,b) \equiv 4\, g_{\mathrm{inel}}(s,b). \tag{3.71}$$

The factor 4 in eqs. (3.69) to (3.71) follows from our normalization of the scattering amplitudes, see eq. (3.12); the factor may be different in different conventions. This definition of profile functions has been chosen so that cross sections σ^{X} may be obtained by integrating of corresponding profile functions in impact parameter space as

$$\sigma^{\mathrm{X}}(s) = 2\pi \int_0^{\infty} b\mathrm{d}b\ D^{\mathrm{X}}(s,b). \tag{3.72}$$

The factor $2\pi b$ in eq. (3.72) corresponds to the weight of initial states distinguished by impact parameter as mentioned in Introduction; this factor is, therefore, not part of the profile functions. Such definition will be convenient in chapter 5 for easier comparison of our profile functions (obtained from analysis of experimental data in chapter 4) with the earlier results of Miettinen. It should hold for the profile functions due to the unitarity condition (3.68) in b-space

$$D^{\mathrm{tot}}(s,b) = D^{\mathrm{el}}(s,b) + D^{\mathrm{inel}}(s,b). \tag{3.73}$$

However, Adachi and Kotani [194–199] and Islam [200] showed that no direct physical meaning can be attributed to the terms in the unitarity equation (3.68) (i.e., to profile

functions given by eqs. (3.69) to (3.71)) at *finite* collision energies $\sqrt{s}$ due to $\mathrm{Im}\, h_{\mathrm{el}}(s,b)$ being repesented by oscillating function. It has been shown in the quoted paper that it is necessary to distinguish integrations over physical and unphysical region of t in (3.66), i.e., $t \in \langle t_{\mathrm{min}}, 0\rangle$ and $t \in (-\infty, t_{\mathrm{min}}\rangle$ (and similarly also for $g_{\mathrm{inel}}(s,b)$).

The elastic hadron scattering amplitude $h_{\mathrm{el}}(s,b)$ in the impact parameter space at *finite* energies may be then defined by FB transformation of the elastic hadron scattering amplitude $F^{\mathrm{N}}(s,t)$ as (see [194–199], [200–202] and [215, 216] for more details)

$$\begin{aligned} h_{\mathrm{el}}(s,b) &= h_1(s,b) + h_2(s,b) \\ &= \frac{1}{4p\sqrt{s}} \int\limits_{t_{\mathrm{min}}}^{0} F^{\mathrm{N}}(s,t) J_0(b\sqrt{-t})\mathrm{d}t + \frac{1}{4p\sqrt{s}} \int\limits_{-\infty}^{t_{\mathrm{min}}} \lambda(s,t) J_0(b\sqrt{-t})\mathrm{d}t \end{aligned} \tag{3.74}$$

where the first term $h_1(s,b)$ represents the contribution of the FB transformation of $F^{\mathrm{N}}(s,t)$ from the physical region of t and the second one represents the contribution corresponding to the unphysical region of t. The unknown function $\lambda(s,t)$ is assumed to fulfill (obey) some conditions [200]. At infinite energies t_{min} is equal to $-\infty$ in eq. (3.74) according to eq. (3.11). The function $g_{\mathrm{inel}}(s,b)$ has been then similarly defined as FB transformation of the inelastic overlap function $G_{\mathrm{inel}}(s,t)$ such that integration over physical and unphysical region of t-values has been separated: $g_{\mathrm{inel}}(s,b) = g_1(s,b) + g_2(s,b)$.

To obtain non-oscillating profile functions the following definitions have been introduced (instead of eqs. (3.69) to (3.71))

$$D^{\mathrm{el}}(s,b) \equiv 4\,|h_1(s,b)|^2, \tag{3.75}$$

$$D^{\mathrm{tot}}(s,b) \equiv 4\,(\mathrm{Im}\, h_1(s,b) + c(s,b)), \tag{3.76}$$

$$D^{\mathrm{inel}}(s,b) \equiv 4\,(g_1(s,b) + K(s,b) + c(s,b)) \tag{3.77}$$

and the unitarity condition at finite energies has been written in the form

$$\mathrm{Im}\, h_1(s,b) + c(s,b) = |h_1(s,b)|^2 + g_1(s,b) + K(s,b) + c(s,b) \tag{3.78}$$

where the real function $c(s,b)$ has been chosen so that the total and inelastic profile functions have been non-negative and main characteristics of the scattering of the scattering (like total cross section calculated from eq. (3.23)) have remained unchanged, see appendix B for more details. The function $K(s,b)$

$$\begin{aligned} K(s,b) = \frac{1}{16\pi^2 s} &\int\limits_{t_{\mathrm{min}}}^{0} \mathrm{d}t_1 \int\limits_{t_{\mathrm{min}}}^{0} \mathrm{d}t_2 F^{\mathrm{N}*}(s,t_2) F^{\mathrm{N}}(s,t_1) \\ &\times \left[J_0\left(\frac{b}{2p}\sqrt{-t_1(4p^2+t_2)}\right) J_0\left(\frac{b}{2p}\sqrt{-t_2(4p^2+t_1)}\right) - J_0(b\sqrt{-t_1}) J_0(b\sqrt{-t_2}) \right]. \end{aligned} \tag{3.79}$$

is a quite negligible correction that is to be added when unitarity condition at finite energies is to be fulfilled.

In [215] the function $c(s,b)$ has been then parameterized and fitted to experimental data together with hadronic amplitude $F^{\mathrm{N}}(s,t)$. In the following we shall make use of a different approach as we shall choose total profile function $D^{\mathrm{tot}}(s,b)$ in quite fixed

(Gaussian) form as it has usually been assumed; the function $c(s,b)$ may be then determined for a given amplitude $F^{\mathrm{N}}(s,t)$ on the basis of eqs. (3.74) and (3.76). It is, however, convenient to introduce formulas for mean values of impact parameters first.

In [216] mean-square values of impact parameter b (for different collision types) have been defined as (see also some previous attempts in, e.g., [19, 197, 217])

$$\langle b^n \rangle^{\mathrm{X}} = \frac{\int\limits_0^\infty b^n \; w(b) D^{\mathrm{X}}(s,b) \mathrm{d}b}{\int\limits_0^\infty w(b) D^{\mathrm{X}}(s,b) \mathrm{d}b} \tag{3.80}$$

with $n = 2$ and $w(b) = 2\pi b$. It has been shown in [216] that the mean-squares $\langle b^2 \rangle^{\mathrm{X}}$ (defined by eq. (3.80)) of total, elastic and inelastic processes may be determined from the t-dependent elastic hadronic amplitude $F^{\mathrm{N}}(s,t)$. The elastic mean-square $\langle b^2 \rangle^{\mathrm{el}}$ may be written as sum of two terms (see also [218])

$$\begin{aligned} \langle b^2 \rangle^{\mathrm{el}} =& \langle b^2 \rangle^{\mathrm{mod}} + \langle b^2 \rangle^{\mathrm{ph}} \\ =& \frac{4 \int\limits_{t_{\min}}^0 \mathrm{d}t |t| \left(\frac{\mathrm{d}}{\mathrm{d}t} \left| F^{\mathrm{N}}(s,t) \right| \right)^2}{\int\limits_{t_{\min}}^0 \mathrm{d}t \left| F^{\mathrm{N}}(s,t) \right|^2} + \frac{4 \int\limits_{t_{\min}}^0 \mathrm{d}t \left| F^{\mathrm{N}}(s,t) \right|^2 |t| \left(\frac{\mathrm{d}}{\mathrm{d}t} \zeta^{\mathrm{N}}(s,t) \right)}{\int\limits_{t_{\min}}^0 \mathrm{d}t \left| F^{\mathrm{N}}(s,t) \right|^2} \end{aligned} \tag{3.81}$$

where the contributions of the modulus and of the phase have been separated. The first term $\langle b^2 \rangle^{\mathrm{mod}}$ depends only on the modulus of the hadronic amplitude $F^{\mathrm{N}}(s,t)$ while the second term $\langle b^2 \rangle^{\mathrm{ph}}$ may be influenced significantly also by the hadronic phase $\zeta^{\mathrm{N}}(s,t)$.

Similarly, the total mean-square $\langle b^2 \rangle^{\mathrm{tot}}$ and inelastic $\langle b^2 \rangle^{\mathrm{inel}}$ may be evaluated with the help of $F^{\mathrm{N}}(s,t)$ as

$$\langle b^2 \rangle^{\mathrm{tot}} = 4 \left(\frac{\frac{\mathrm{d}}{\mathrm{d}t} \left| F^{\mathrm{N}}(s,t) \right|}{\left| F^{\mathrm{N}}(s,t) \right|} - \tan \zeta^{\mathrm{N}}(s,t) \frac{\mathrm{d}}{\mathrm{d}t} \zeta^{\mathrm{N}}(s,t) \right) \Bigg|_{t=0}, \tag{3.82}$$

$$\langle b^2 \rangle^{\mathrm{inel}} = \frac{\sigma^{\mathrm{tot,N}}(s) \langle b^2 \rangle^{\mathrm{tot}} - \sigma^{\mathrm{el,N}}(s) \langle b^2 \rangle^{\mathrm{el}}}{\sigma^{\mathrm{inel}}(s)}. \tag{3.83}$$

Eqs. (3.81) and (3.83) allow comparison of $\langle b^2 \rangle^{\mathrm{inel}}$ and $\langle b^2 \rangle^{\mathrm{el}}$ corresponding to a given hadronic amplitude $F^{\mathrm{N}}(s,t)$ and, therefore, may provide basic information whether elastic collisions are more peripheral or central than the inelastic ones, as it has been discussed in Introduction.

To compare our results to those of Miettinen (see Introduction) we may chose Gaussian shape of total profile function $D^{\mathrm{tot}}(b)$ corresponding to the commonly assumed one as [177]

$$D^{\mathrm{tot}}(b) = \tilde{a}_2 \, \mathrm{e}^{-\tilde{a}_1 b^2} \tag{3.84}$$

where $\tilde{a}_1$ and $\tilde{a}_2$ are some parameters which may be expressed using eqs. (3.72) and (3.80) as

$$\tilde{a}_1 = \frac{1}{\langle b^2 \rangle^{\mathrm{tot}}}, \tag{3.85}$$

$$\tilde{a}_2 = \frac{\sigma^{\mathrm{tot,N}}}{\pi \langle b^2 \rangle^{\mathrm{tot}}}. \tag{3.86}$$

The total profile function D^{tot} given by eq. (3.84) may be, therefore, determined from given values of $\sigma^{\mathrm{tot,N}}$ and $\langle b^2\rangle^{\mathrm{tot}}$ using optical theorem (3.23) and eq. (3.82), i.e., from t-dependent elastic amplitude $F^{\mathrm{N}}(s,t)$. It means that using FB transformation (3.74) of $F^{\mathrm{N}}(s,t)$ and eq. (3.73) the total, elastic and inelastic profile functions may be determined for a given $F^{\mathrm{N}}(s,t)$ (e.g., from fitting experimental data as it will be done in chapter 4).

Other shapes of the total profile function than the Gaussian one (3.84) should be admitted in principle, too; the whole problem of impact parameter picture of hadron collisions is, however, more complicated than it may seem at first glance, see the following chapters.

3.5 Contemporary methods (formulas) determining total hadronic cross section

In the previous text some important aspects and assumptions included in the contemporary description of the Coulomb and hadronic interactions acting simultaneously in the case of charged hadrons have been discussed. In the following we shell analyze to greater details three different formulas (methods) on the basis of which the total hadronic cross section has been commonly determined from experimental data (see also recent result of TOTEM in sect. 2.5.3). Some additional assumptions included in the corresponding "measurement" will be identified (similarly, as it was partially done for one of the formula in [45]). These assumptions are often tacitly added without sufficient reasoning, even thought they may significantly influence values of several quantities or the interpretation of the given collision process.

3.5.1 Method of total rate (TR method)

One may detect simultaneously elastic and inelastic events (total rate (TR)). Measuring independently also the corresponding luminosity (e.g., by separation scan, see sect. 1.3.2) the total hadronic cross section may be determined with the help of the following formula

$$\sigma_{\mathrm{TR}}^{\mathrm{tot,N}} = \frac{N^{\mathrm{el,N}} + N^{\mathrm{inel}}}{L}. \tag{3.87}$$

However, the usage of this formula is not as straightforward as it may seem at first glance. First of all, one can measure the elastic and inelastic events always only in a certain limited region of detector acceptance - only "visible" rates $N_{\mathrm{vis}}^{\mathrm{el}}$ and $N_{\mathrm{vis}}^{\mathrm{inel}}$. The method of total rate, therefore, also requires

- estimation (extrapolation) of the undetected events (both elastic and inelastic),
- determination of elastic *hadronic* rate $N^{\mathrm{el,N}}$ from the measured one which is strongly influenced by the Coulomb interaction at very low scattering angles; some non-hadronic interaction may play significant role also at other scattering angles especially at lower collision energies.

These model dependent aspects are always determined on the basis of some additional assumptions. Different models may, of course, lead to different values of total hadronic cross section. The models (assumptions) should be, therefore, properly reasoned and studied.

If we use only one assumption that the measured elastic rate is given by hadronic interaction $N_{\mathrm{vis}}^{\mathrm{el}} = N_{\mathrm{vis}}^{\mathrm{el,N}}$ (i.e., Coulomb or any other non-hadronic effects being negligible) then we may derive the following lower limit on the total hadronic cross section

$$\sigma_{\mathrm{TR}}^{\mathrm{tot,N}} > \frac{N_{\mathrm{vis}}^{\mathrm{el}} + N_{\mathrm{vis}}^{\mathrm{inel}}}{L}. \tag{3.88}$$

This limit may provide first estimation of the total cross section independently of some other assumptions such as validity of optical theorem included in the two following methods of total cross section determination.

3.5.2 Method based on optical theorem and luminosity measurement (OL method)

A different method (formula) of total cross section determination has been based on optical theorem (given by eq. (3.23)) and independent luminosity measurement (this method will be, therefore, denoted as OL method). Adding the relation for the elastic hadronic differential cross section (3.12) to the optical theorem the following formula for total cross section may be derived

$$\sigma_{\mathrm{OL}}^{\mathrm{tot,N}} = \sqrt{\frac{16\pi}{1+\rho(t=0)^2}\,\frac{\left.\frac{\mathrm{d}N^{\mathrm{el,N}}}{\mathrm{d}t}\right|_{t=0}}{L}} = \sqrt{\frac{16\pi}{1+\rho(t=0)^2}\left.\frac{\mathrm{d}\sigma^{\mathrm{el,N}}}{\mathrm{d}t}\right|_{t=0}} \tag{3.89}$$

where the $\rho(t=0)$ parameter is defined by eq. (3.19). This method requires simultaneous measuring of

- elastic differential rate,
- and luminosity,

i.e., elastic differential cross section. However, any application of the formula (3.89) also requires

- determination of *hadronic* elastic scattering from the measured elastic differential cross section (measured elastic rate), including, e.g., Coulomb interaction,
- optical theorem and, therefore, also extrapolation of both the modulus ($\frac{\mathrm{d}\sigma^{\mathrm{el,N}}}{\mathrm{d}t}$) and phase ($\rho$ quantity) of the hadronic amplitude to the unmeasurable point at $t = 0$.

There are different approaches which may deal with these model dependent aspects in different ways. The approach of WY and the eikonal approach have been discussed in sects. 3.2 and 3.4. These two approaches determine the total cross section also on the basis of eq. (3.89) and experimental data given by measured elastic differential cross section (requires mainly detection of protons scattered at very low scattering angles in so-called Coulomb-nuclear interference region which requires dedicated accelerator settings, see sect. 2.3). The total hadronic cross section corresponding to the two performed fits in chapter 4 has been calculated on the basis of eq. (3.89).

Current methods based on the formula (3.89) determine total hadronic cross section from elastic processes without measuring (taking into account) the inelastic ones. The inelastic cross section is calculated by subtracting the elastic hadronic cross section from the total one, see eqs. (3.28) and (3.29).

3.5.3 Luminosity independent method (OLI method)

The other formula for total cross section has been derived from the combination of formulas (3.87) and (3.89) when the total cross sections have been identified

$$\sigma_{\mathrm{OLI}}^{\mathrm{tot,N}} = \frac{16\pi}{1+\rho^2} \; \frac{\left.\frac{\mathrm{d}N_{\mathrm{el}}^{\mathrm{N}}}{\mathrm{d}t}\right|_{t=0}}{N_{\mathrm{el}}^{\mathrm{N}} + N_{\mathrm{inel}}}. \tag{3.90}$$

Determination of total cross section is in this method based on optical theorem and does not require luminosity measurement - it will be, therefore, denoted as OLI method. This method has been used for the first time in [164].

Eliminating $\sigma^{\mathrm{tot,N}}$ from (3.87) and (3.89) it has been possible to derive the following formula for the luminosity

$$L_{\mathrm{OLI}} = \frac{1+\rho^2}{16\pi} \; \frac{(N_{\mathrm{el}}^{\mathrm{N}} + N_{\mathrm{inel}})^2}{\left.\frac{\mathrm{d}N_{\mathrm{el}}^{\mathrm{N}}}{\mathrm{d}t}\right|_{t=0}}. \tag{3.91}$$

The quantities which are measured for application of the formula (3.90) (or (3.91)) are only elastic and inelastic rates. The two formulas, however, further require (see comments in sects. 3.5.1 and 3.5.2)

- determination of elastic *hadronic* rate from the measured one (effect of other interactions subtracted),
- optical theorem and, therefore, also extrapolation of both the elastic hadronic rate $\frac{\mathrm{d}N_{\mathrm{el}}^{\mathrm{N}}}{\mathrm{d}t}$ and phase (ρ quantity) to the unmeasurable point at $t = 0$,
- estimation (extrapolation) of the inelastic events which escape detector acceptance.

It is necessary to stress that the formula for total cross section given by eq. (3.90) has been derived under the assumption that the TR and OL methods give the same results, i.e., that $\sigma_{\mathrm{TR}}^{\mathrm{tot,N}} = \sigma_{\mathrm{OL}}^{\mathrm{tot,N}}$. This is in fact an additional assumption that should be carefully tested and verified before applying the luminosity independent method to some data. Such testing requires, however, a luminosity measurement independent of optical theorem (e.g., using VDM scans mentioned in sect. 1.3.2).

3.5.4 Some general aspects of total hadronic cross section determination

The discussed methods of total hadronic cross section determination have several common aspects. It is interesting to see that all the methods require measurement of elastic scattering (some of them also inelastic one). It is also not possible to determine the total cross section only from data without adding another important assumption. The additional assumptions are related mainly to

- determination of elastic *hadronic* scattering from the measured one (it is mainly the Coulomb interaction at very low values of scattering angles which need to be taken into account),
- estimation (extrapolation) of undetected elastic and inelastic events,

- and validity of optical theorem (if applied) and accompanying extrapolation of both the modulus and phase of hadronic amplitude to unmeasurable and limit zero elastic hadronic scattering angle.

The determination of total hadronic cross section, therefore, requires necessarily a reliable model of (elastic) collisions.

However, all the commonly used methods of total cross section determination have been based on only some mathematical-phenomenological models under very limiting, simplifying or even false assumptions, as we have seen, e.g., in the case of WY approach in sect. 3.2 which has been used as standard tool to determine total cross section from region of very low scattering angles.

The OL and OLI methods based on optical theorem (and also the method of total rate) have been applied and compared in [164] (1976) for the first time at ISR energies ranging from energy of 23.5 GeV to 62.7 GeV by CERN-Rome and Pisa-Stony Brook collaborations. The methods based on optical theorem require the value of quantity ρ at $t = 0$, see eqs. (3.89) and (3.90). The value $\rho(t=0)$ was taken in [164] as an external input based on the simplified WY Coulomb-hadronic interference formula (3.24). Also the total hadronic cross section determined by the WY approach has been used (due to a "correction for electromagnetic effects", see Eq. (13) in [164]) for "new" determination (measurement) of total cross section. Such an application of the formulas eqs. (3.89) and (3.90) (OL and OLI methods) is, however, necessary to denote as mistaking (circular) as it does not provide any "new and independent measurement" of total cross section.

Similarly inconsistent application of the OL and OLI methods has been commonly used since that time, see past results on total cross section determination based on optical theorem recently summarized in [110] (see mainly the papers quoted there). The problematic approach may be identified whenever quantity $\rho(t=0)$ is taken from some "external calculations" which determine also total cross section under the same set of assumptions (e.g., combining the numerical results obtained at lower energies based on WY approach with some high energy extrapolations using dispersion relations [128, 219] as it is sometimes suggested; see, e.g., [144]). Taking only the quantity $\rho(t=0)$ in eq. (3.89) or eq. (3.90) for "new" measurement of total cross section is, therefore, misleading. Determination of quantity $\rho(t=0)$ and $\sigma^{\mathrm{tot,N}}$ based on optical theorem are quite inseparable problems.

The quantity $\rho(t=0)$ and total cross section $\sigma^{\mathrm{tot,N}}$ should be determined consistently from one method only (based on one consistent set of assumptions only). In the given theoretical framework all the properties of elastic hadronic collisions are determined from the corresponding scattering amplitude and, therefore, it is necessary to establish the modulus and phase of elastic hadronic amplitude in the widest possible t-range for better understanding of the given process (which was possible to do, at least partially, in the eikonal model approach but not in the approach of WY). All contemporary methods of total cross section determination which do not even try to establish the t-dependent modulus $\left|F^{\mathrm{N}}(s,t)\right|$ and phase $\zeta^{\mathrm{N}}(s,t)$ also cannot, therefore, provide any deeper understanding of the given collision process (namely the behaviour of collisions in the impact parameter space), either. It means that these methods cannot provide any deeper reasoning of the value of total cross section. The measurement of total cross section is as reliable as a collision model on the basis of which the determination has been made (i.e., as much understood the whole physical process is).

Last but not least one should be also aware of the fact that the assumptions under which the optical theorem has been derived have not been practically tested

experimentally. All hitherto experimental tests of optical theorem have corresponded basically only to comparison of values of total hadronic cross sections determined with and without using optical theorem (using the OL and OLI methods of measurement); see, e.g., [220, 221] (πp scattering), [164] (pp scattering) or recent interesting comparison made at much higher energy of 7 TeV by TOTEM [32] (pp scattering) as it was discussed in sect. 2.5.3. However, even if both the values of total cross section may be found to be similar one cannot conclude that the optical theorem is valid (contrary to statements in [220, 221]). The (experimental) testing is more delicate as the derivation and application of the optical theorem is always accompanied by some other strong assumptions, see [51] for detailed study of this topic. One should mainly better understand elastic collisions in dependence on impact parameter as this question is often not addressed at all or with only partial success as we will see in next chapters.

3.6 Elastic hadronic amplitude

For the description of hadron interactions, mainly in the case of deep inelastic scattering processes, QCD has been commonly made use of. However, in the case of elastic and other diffractive processes there has not been any significant progress in spite of enormous effort having been produced. The point is that the perturbative methods, being principally involved in QCD descriptions of hard processes, may be hardly applied to in the case of soft diffractive processes.

This has been especially the case of elastic hadronic amplitude describing the scattering of charged nucleons where differential cross section data have been obtained with relatively large statistics. The observed dip-bump (or shoulder) structure of high-energy data has been usually described with the help of a complex hadronic amplitude $F^{\mathrm{N}}(s,t)$ having the dominant imaginary part in a large region of lower $|t|$ and vanishing at the diffractive minimum. The real part (very small in the region of low deviations) has been introduced to obtain a non-zero value at the diffractive minimum.

This currently accepted dominance of the imaginary part of the hadron elastic amplitude has seemed to be supported by the theorems derived at asymptotic energies and has been introduced on the basis of some *a priori* assumptions (being accepted by most physicists) [222–229]. However, it has been shown [156, 157, 230, 231] that the experimental data, e.g., for pp and $\bar{\mathrm{p}}$p elastic hadron scattering at the ISR energies, have behaved according to these theorems at most only in a very narrow interval of t close to $t = 0$ where the dominance of imaginary part may exist while fundamental deviations may appear in a greater interval. Consequently, the application of the mentioned assumptions to elastic hadron scattering at present energies in a broad interval of momentum transfers can be hardly justified.

The mentioned standard properties of hadronic amplitude might seem, of course, to be justified for the authors of the first papers analyzing the elastic pp scattering at the ISR energies [16, 209–212]; consequently, they obtained the central profile function of elastic hadron scattering $D^{\mathrm{el}}(s,b)$ in the impact parameter space, represented by a Gaussian function narrower than that obtained for inelastic one. All consequences have been denoted as reliable results, even if the colliding protons have had to behave as transparent objects in elastic collisions.

Similar amplitude characteristics have been used as a starting point of many analyses concerning the elastic pp and $\bar{\mathrm{p}}$p scattering at different energies; see, e.g., [232–244]. These authors have tried to determine the elastic hadronic amplitude directly from the

experimental data of $\frac{\mathrm{d}\sigma}{\mathrm{d}t}$ provided the following assumptions were accepted [245]: the elastic hadronic amplitude has been taken as smoothly energy dependent and purely imaginary. Then the imaginary part has been parameterized by a sum of n ($n \leq 5$) differently weighted exponentials in t:

$$\mathrm{Im}\, F^{\mathrm{N}}(s,t) \;=\; \mathrm{Im}\, F^{\mathrm{N}}(s,0) \sum_{j=1}^{n} \alpha_j(s)\, \mathrm{e}^{-\beta_j(s)|t|}. \tag{3.92}$$

The role of the real part has been admitted only as a small partial fraction of corresponding imaginary part, i.e., the number of its contributing terms has been smaller than n (as, e.g., in [234, 235, 239, 245]); or specified with the help of derivative dispersion relations as in [233, 236–238, 242]. Also additional linear logarithmic t-dependencies of all quantities $\beta_j(s)$ and quadratic logarithmic t-dependencies of all quantities $\alpha_j(s)$ have been introduced in order to better reproduce the corresponding differential cross section. Similar behaviour of elastic hadronic amplitude has been also used in papers [240, 241] where the model of stochastic vacuum to the pp and $\bar{\mathrm{p}}$p elastic scattering has been applied to. The individual free parameters specifying the quantities $\alpha_j(s)$ and $\beta_j(s)$ have been determined by fitting measured differential elastic cross section.

However, as the FB transform of $F^{\mathrm{N}}(s,t)$ (see eqs. (B.9) and (3.66)) is additive and as it holds (see formula (6.631.4) in [246])

$$\int_0^\infty \sqrt{-t}\; \mathrm{d}\sqrt{-t}\;\; \mathrm{e}^{-\beta_j(s)|t|}\, J_0(b\sqrt{-t}\,) = \frac{1}{2\beta_j(s)}\, \mathrm{e}^{-b^2/(4\beta_j(s))}, \tag{3.93}$$

final elastic impact parameter profile $D^{\mathrm{el}}(s,b)$ must be interpreted as superpositions of different central Gaussian functions with the maximum at $b = 0$; their shapes being chosen from the very beginning as central. It is already the choice of the parameterization of $F^{\mathrm{N}}(s,t)$ which predetermined the result independently of actual values of the free parameters.

Similar weak t-dependence of hadron phase $\zeta^{\mathrm{N}}(s,t)$ in quite broad internal of lower $|t|$ values and imaginary part of $F^{\mathrm{N}}(s,t)$ being equal to zero at the position of the dip has been used in majority of contemporary published papers practically without any deeper reasoning - see, e.g., [247, 248] and discussion of some other phenomenological models in [48]. It means that in all cases the elastic collisions have been taken as central from the very beginning.

However, the existence of minimum (dip) in the differential cross section observed practically in all elastic hadron collisions (see, e.g., [7]) does not require zero value for imaginary part of the amplitude; *only the sum of the squares of both the real and imaginary parts should be minimal at this point.* The mentioned requirement that the imaginary part should vanish at this point represents much stronger and more limiting condition that the theory and experiment require.

It has not been respected at all, either, that a very different behaviour may be derived with the help of a non-dominant imaginary part as it has been shown already earlier in 1981 [19]. In such a case a quite peripheral behaviour of elastic processes may be derived. It has been shown then in [20, 156, 157, 249–251] that one may obtain a peripheral picture of elastic hadron scattering for pp collisions at the ISR energies (53 GeV) and for $\bar{\mathrm{p}}$p scattering at the energy of 541 GeV if the hadron phase $\zeta^{\mathrm{N}}(s,t)$ changes rather rapidly (see the second term in eq. (3.81)). In peripheral case the imaginary part of

the amplitude goes to zero at value of $|t| \sim 0.1$ GeV^2. It means that the imaginary part of the elastic hadronic amplitude may be dominant only in a very narrow region of momentum transfers near the forward direction; the given behaviour of the hadron phase $\zeta^{\mathrm{N}}(s,t)$ being still in a full agreement with the assertions of the mentioned asymptotic theorems.

If one assumes that the measured elastic differential cross section is given by hadronic interaction (Coulomb effects neglected), i.e., $\frac{\mathrm{d}\sigma}{\mathrm{d}t} = \frac{\mathrm{d}\sigma^{\mathrm{N}}}{\mathrm{d}t}$, then according to eq. (3.12) the measured differential cross section is determined only by the square of the modulus $\left|F^{\mathrm{N}}(s,t)\right|$ of elastic hadronic amplitude. As its phase $\zeta^{\mathrm{N}}(s,t)$ does not enter into the calculations a conveniently parameterized t-dependence of the modulus alone can be used for fitting the experimental data.

On the other hand for the determination of both the real and imaginary parts of elastic hadronic amplitude the knowledge of its modulus is not sufficient; the behaviour of t-dependent phase $\zeta^{\mathrm{N}}(s,t)$ should be known, too. Performing the FB transformation of both of these parts the behaviour of all the profiles in the impact parameter space may be determined. Thus the t-dependence of the phase $\zeta^{\mathrm{N}}(s,t)$ specifies the behaviour of elastic hadron scattering in the impact parameter space.

If in fitting procedure some arbitrarily chosen parameterizations of both the imaginary and real parts have been used as it has been done, e.g., in [232–244], then the dominance of the imaginary part of elastic hadronic amplitude in a much broader region of momentum transfers then needed has been implicitly incorporated; it has led to the central image of elastic hadron collisions. Therefore, more general parameterizations of both the modulus $\left|F^{\mathrm{N}}(s,t)\right|$ and of the phase $\zeta^{\mathrm{N}}(s,t)$ should be preferred than those used in the quoted papers.

Chapter 4

Application of the eikonal model to 53 GeV and 8 TeV pp data

4.1 Fitting procedure

It has been shown in sect. 3.3 that the recent analyses of both the t-dependent electromagnetic proton form factors showed some deviations from standardly used dipole formulas. One may see in fig. 3.4 that the effective electromagnetic form factor has quite different values than the widely used electric one for analysis of pp experimental data. It is clear that the inclusion of magnetic form factor might have an impact also on the results of analysis of elastic pp scattering data at high energies.

We have, therefore, performed new analysis of pp elastic scattering data at the ISR energy of 53 GeV with the help of the eikonal model (see sect. 3.4) similarly as it has been done in [20] but now with the help of *effective electric* form factors (3.41) and *effective electromagnetic* form factors (3.40). Form factors $G_{\mathrm{E}}^{\mathrm{BN}}(t)$ and $G_{\mathrm{M}}^{\mathrm{BN}}(t)$ (i.e., Borkowski's et al. parameterizations (3.38) and (3.39) specified by parameters taken from table 3.1) have been used for this purpose.

For both the form factors the description of pp elastic collision data based on hadronic phase corresponding to the widely used assumptions (namely to the dominance of its imaginary part in quite broad region around $t = 0$) and leading to the central behaviour of elastic collisions has been compared to the alternative peripheral description having different t-dependence of the phase. In the peripheral case some new possibilities corresponding to different values of $\sqrt{\langle b^2\rangle^{\mathrm{el}}}$ have been newly performed.

Conveniently parameterized elastic hadronic amplitude $F^{\mathrm{N}}(s,t)$ have been fitted to the measured pp elastic differential cross section at 52.8 GeV (denoted as 53 GeV) in broad interval $|t| \in \langle 0.00126, 9.75\rangle$ GeV^2 [8] with the help of eq. (3.12) and complete amplitude $F^{\mathrm{C+N}}(s,t)$ given by eqs. (3.53) and (3.54). The data include observed dip at $t_{\mathrm{dip}} = -1.375$ GeV^2, see the data points in fig. 4.1. The aim of the calculations at 53 GeV has been to produce also new numerical results (namely of the b-dependent profile functions) suitable for comparison to corresponding results of Miettinen as many contemporary descriptions of elastic scattering have been based on a quite similar approach.

The results at 53 GeV have been then compared to similar analysis at much higher energy of 8 TeV. Elastic pp differential cross section has been recently measured at LHC by TOTEM at 8 TeV in the region $0.000741 \leq |t| \leq 0.2010$ GeV^2 [36] which contains the Coulomb-hadronic interference region. Nearly exponential elastic pp differential

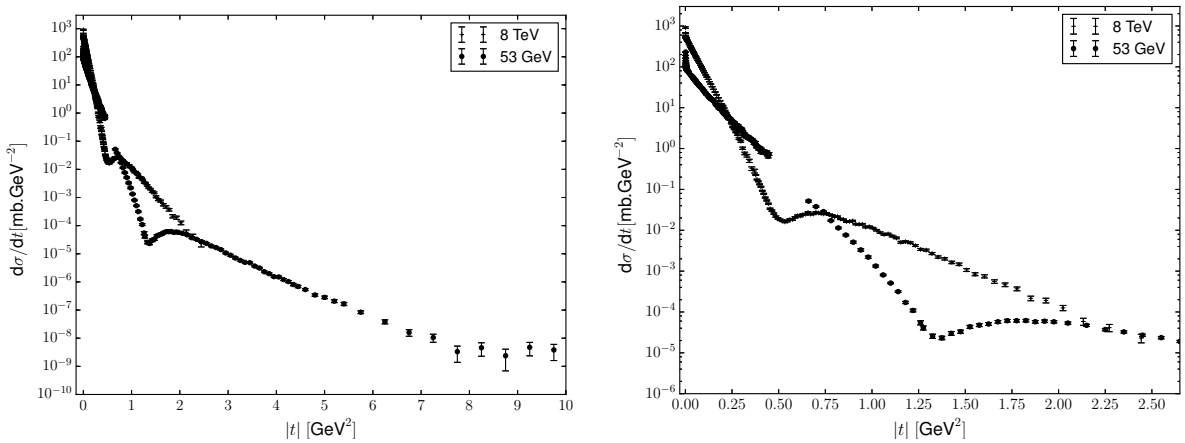

(a) full available t-range **(b)** $|t|$ values up to ≈ 2.5 GeV^2

Figure 4.1: Measured elastic pp differential cross section at 53 GeV and 8 TeV.

cross section at the same energy has been measured by TOTEM [35] in the region $0.027 < |t| < 0.2$ GeV^2 (see fig. 2.28). These two data sets will be combined and continuously extended by renormalized 7 TeV TOTEM data corresponding to the region $0.2 < |t| < 2.5$ GeV^2 [30] which contains dip-bump structure, see fig. 2.26. This compilation of data will be denoted as "8 TeV data" in the following (only statistical errors will be taken into account), see fig. 4.1. The extension by the renormalized 7 TeV data is only an approximation since the measured data at 8 TeV in this region are not (yet) available. This is also one of the reason why we will be more interested in overall character of the elastic collision model fitted to data rather than in determination of exact numerical values of some quantities.

The integral $I(t,t')$ in eq. (3.54) have been analytically calculated using eqs. (3.56) to (3.60) and parameters from table 3.1 and then also compared to corresponding numerical integration. All the fits have been performed by minimizing the corresponding χ^2 function with the help of program MINUIT [52, 54]. Quoted uncertainties have been estimated with the help of HESSE procedure in MINUIT.

4.2 Energy of 53 GeV

4.2.1 Central case

The analysis of experimental data with the help of eqs. (3.53) and (3.54) requires a convenient parameterization of the complex elastic hadronic amplitude $F^{\mathrm{N}}(s,t)$, i.e., its modulus and its phase. The modulus may be parameterized as

$$\left|F^{\mathrm{N}}(s,t)\right| \;=\; (a_1 + a_2 t)\,\mathrm{e}^{b_1 t + b_2 t^2 + b_3 t^3} \;+ (c_1 + c_2 t)\,\mathrm{e}^{d_1 t + d_2 t^2 + d_3 t^3} \;. \tag{4.1}$$

The hadron phase $\zeta^{\mathrm{N}}(s,t)$ corresponding to the widely used assumptions leading to central behaviour of elastic collisions in impact parameter space may be parameterized as (see, e.g., [214])

$$\zeta^{\mathrm{N}}(s,t) = \arctan \frac{\rho_0}{1 - \left|\frac{t}{t_{\mathrm{dip}}}\right|} \tag{4.2}$$

where $t_{\rm dip} = -1.375$ GeV^2 is the position of the dip in data and $\rho_0 = \rho(t=0)$. All parameters specifying the modulus and the phase of elastic hadronic amplitude $F^{\rm N}(s,t)$ may be energy dependent. Similar t-dependence of the hadronic phase has been used in Miettinen's calculations leading to the central behaviour of elastic collisions in dependence on impact parameter. This parameterization reproduces the dominance of imaginary part of elastic hadronic amplitude in a rather broad region of $|t|$ and zero imaginary part at position of the dip ($t = t_{\rm dip}$) commonly assumed in many contemporary phenomenological models (even if no reasoning of such strong and limiting assumptions has been given). Such "standard" form of the phase leads to central behaviour of elastic collisions as it has been demonstrated for several models at the LHC energies in [48], see also sect. 3.6.

The fitted values of all free parameters are in table 4.1 for both the effective electric form factor (Fit I) and effective electromagnetic form factor (Fit II). Both the fits are quite straightforward (the functional t-dependence of the standard phase is very limited) and very similar. Fig. 4.2 shows fitted elastic pp differential cross section $\frac{{\rm d}\sigma^{\rm C+N}}{{\rm d}t}$ together with corresponding Coulomb $\frac{{\rm d}\sigma^{\rm C}}{{\rm d}t}$ and hadronic $\frac{{\rm d}\sigma^{\rm N}}{{\rm d}t}$ differential cross sections. The corresponding elastic hadronic amplitudes for both the fits have dominant imaginary parts in the large region of t around forward direction which decrease with increasing $|t|$ and vanish in the diffraction dip (as commonly assumed), see fig. 4.3.

Determined values of several physically interesting quantities calculated from the fitted hadronic amplitude for each fit may be found in table 4.1. The total hadronic cross section $\sigma^{\rm tot}$ has been calculated using the optical theorem (3.23), integrated elastic hadron cross section $\sigma^{\rm el}$ using the first equation in eq. (B.15) and inelastic $\sigma^{\rm inel}$ as their difference. The values of quantities $\sigma^{\rm tot}$, $\rho(t=0)$ and $B(t=0)$ in table 4.1 may be compared to similar values

$$\sigma^{\rm tot} = 42.38 \pm 0.27 \text{ mb}, \quad \rho(t=0) = 0.078 \pm 0.010, \quad B = 13.1 \pm 0.2 \text{ GeV}^{-2}; \qquad (4.3)$$

determined earlier in [252, 253] on the basis of the simplified WY formula (3.24). However, the simplified WY complete amplitude (3.24) has been applied to only in the very narrow region $|t| \in (0.00126, 0.01)$ GeV^{-2}, while the Fits I and II have been realized in much broader measured region of $|t| \in \langle 0.00126, 9.75\rangle$ GeV^2. While in eq. (3.24) it has been assumed that $\rho(t)$ (or $\zeta^{\rm N}(s,t)$) and $B(t)$ are t-independent the quantities in the Fit I and II are t-dependent, see figs. 4.3 and 4.4. Corresponding t-dependent diffractive slope defined by eq. (3.20) may be found in fig. 4.4. This figure shows that diffractive slope is not constant in the analyzed region of t; therefore one of the assumptions used in derivation of simplified WY complete amplitude (3.24) is not fulfilled. The simplified WY complete amplitude does not hold and it cannot be used for the correct analysis of experimental $\frac{{\rm d}\sigma}{{\rm d}t}$ data.

Values of mean impact parameters $\sqrt{\langle b^2\rangle^{\rm tot}}$, $\sqrt{\langle b^2\rangle^{\rm el}}$, $\sqrt{\langle b^2\rangle^{\rm inel}}$ determined with the help of eqs. (3.81) to (3.83) may be found also in table 4.1. It holds $\sqrt{\langle b^2\rangle^{\rm el}} < \sqrt{\langle b^2\rangle^{\rm inel}}$, i.e., elastic collisions according to this description should correspond in average to lower impact parameters than average impact parameter corresponding to inelastic collisions (~ 0.68 fm against ~ 1.09 fm). This centrality of elastic collisions may be further seen from the profile functions $D^{\rm X}(b)$ calculated as explained at the end of appendix B, see fig. 4.5a. Elastic profile function $D^{\rm el}(b)$ has Gaussian shape with a maximum at $b = 0$. Some other b-dependent functions characterizing hadron collisions in b-space which have been discussed in appendix B may be found in fig. 4.6a. The integrated cross sections $\sigma^{\rm X}$ and mean impact parameters $\sqrt{\langle b^2\rangle^{\rm X}}$ discussed above have been

Fit		I	II
Case		central	central
Form factor		effective electric	effective electromagnetic
ρ_0		0.0763 ± 0.0017	0.0766 ± 0.0017
a_1		12225 ± 24	12237 ± 24
a_2	[GeV^{-2}]	10500 ± 100	10440 ± 110
b_1	[GeV^{-2}]	5.908 ± 0.019	5.909 ± 0.022
b_2	[GeV^{-4}]	3.760 ± 0.075	3.757 ± 0.087
b_3	[GeV^{-6}]	1.750 ± 0.058	1.757 ± 0.069
c_1		-16 ± 21	-24 ± 20
c_2	[GeV^{-2}]	-82 ± 14	-90 ± 11
d_1	[GeV^{-2}]	1.400 ± 0.055	1.425 ± 0.025
d_2	[GeV^{-4}]	0 ± 0.014	0.0038 ± 0.0086
d_3	[GeV^{-6}]	-0.0045 ± 0.0012	-0.00430 ± 0.00081
χ^2/ndf		326.763/205	323.268/205
$\rho(t=0)$		0.0763 ± 0.0017	0.0766 ± 0.0017
$B(t=0)$	[GeV^{-2}]	13.517 ± 0.055	13.514 ± 0.050
σ^{tot}	[mb]	42.70 ± 0.16	42.71 ± 0.15
σ^{el}	[mb]	7.471	7.472
σ^{inel}	[mb]	35.23	35.23
$\sigma^{\mathrm{el}}/\sigma^{\mathrm{tot}}$		0.1750	0.1750
$\mathrm{d}\sigma^{\mathrm{N}}/\mathrm{d}t(t=0)$	[mb.GeV^{-2}]	93.70	93.74
$\sqrt{\langle b^2\rangle^{\mathrm{tot}}}$	[fm]	1.027	1.027
$\sqrt{\langle b^2\rangle^{\mathrm{el}}}$	[fm]	0.6764	0.6764
$\sqrt{\langle b^2\rangle^{\mathrm{inel}}}$	[fm]	1.086	1.086
$D^{\mathrm{tot}}(b=0)$		1.29	1.29
$D^{\mathrm{el}}(b=0)$		0.536	0.536
$D^{\mathrm{inel}}(b=0)$		0.753	0.753

Table 4.1: pp elastic scattering at energy of 53 GeV. Values of free parameters obtained by fitting experimental data with the help of new formula (3.53) and (3.54), and values of physically significant quantities characterizing the standard picture of elastic hadron scattering in the impact parameter space.

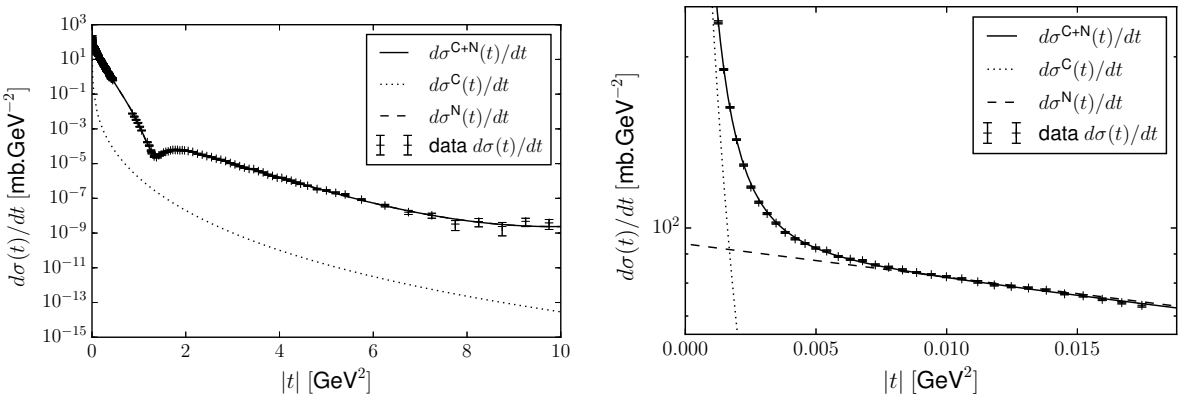

(a) full available $|t|$-range of measured data **(b)** region of very low values of $|t|$

Figure 4.2: Eikonal model of Coulomb-hadronic interaction fitted to measured elastic pp differential cross section at energy of 53 GeV in the interval $|t| \in \langle 0.00126, 9.75\rangle$ GeV^2 for central picture of elastic pp scattering (Fit II). All the Fits I - VIII give very similar figure.

also calculated integrating the corresponding profile functions $D^{\mathrm{X}}(b)$ with the help of eqs. (3.72) and (3.80) leading to the same values.

It is evident from table 4.1 that the fitted quantities characterizing the elastic hadronic amplitudes are practically unchanged when derived with the help of the proton effective electric or the effective electromagnetic form factors.

4.2.2 Peripheral case

Next fits of the same differential cross section data have been performed similarly as in the previous case but now with the different parameterization of elastic hadron phase ($t_0 = 1$ GeV^2)

$$\zeta^{\mathrm{N}}(s,t) = \zeta_0 + \zeta_1 \left|\frac{t}{t_0}\right|^{\kappa} \mathrm{e}^{\nu t} \tag{4.4}$$

enabling to include a fast increase of $\zeta^{\mathrm{N}}(s,t)$ with increasing $|t|$ and, consequently, a peripheral behaviour of elastic hadron scattering.

The parameterization (4.4) is much more general and flexible than (4.2) as it may reproduce quite broad class of t-dependent functions which all fits measured data and lead to either central or peripheral behaviour. To obtain peripherality we have required $\sqrt{\langle b^2\rangle^{\mathrm{el}}} > \sqrt{\langle b^2\rangle^{\mathrm{inel}}}$ and $D^{\mathrm{el}}(b)$ to have its maximum at some non-zero impact parameter b. However, the fit has not been unique. We have, therefore, further required value of parameter ζ_1 to be around 2000 and $\sqrt{\langle b^2\rangle^{\mathrm{el}}}$ to be around 1.6, 1.75 and 1.9 fm and looked for the values of all the free parameters separately in these 3 cases. If all these additional conditions bounding the values of fitted free parameters have been imposed on them corresponding unambiguous fits have been found[1].

[1]Mathematically speaking one had to solve the problem of bounded extrema of the χ^2 function, i.e., of the function of the n free parameters $x = (x_1, ..., x_n)$ which may be solved with the help of penalty functions technique. If at the minimum of the χ^2 the values of the free parameters x are limited at point x_0 by some condition $g(x = x_0)$ then one may add to the minimized χ^2 function additional function $[g(x) - g(x = x_0)]^2 * C_p$, where C_p is some chosen constant value (weight of the penalty function). In the case of several limiting conditions the resulting penalty function is given by the sum of all individual penalty functions which is added to the original χ^2 during minimization. Performing the minimization

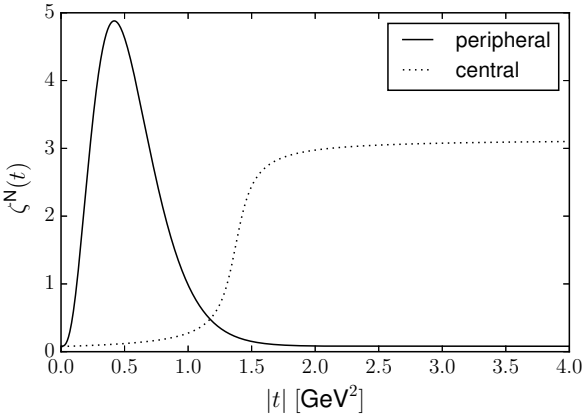

Figure 4.3: Elastic hadron phases $\zeta^{\mathrm{N}}(s,t)$ for central (Fit II) and peripheral (FIT VII) pictures of elastic pp collisions at energy of 53 GeV. Both the Fits I and II leading to centrality of elastic collisions correspond to the same shape of the phase. The peak around 0.5 GeV^2 in the Fits III-VIII corresponding to the peripherality changes slightly its maximum.

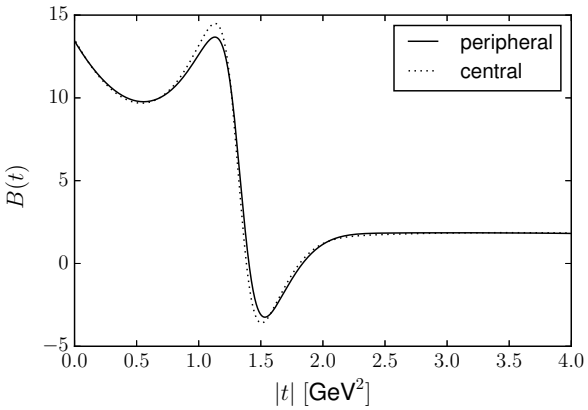

Figure 4.4: t-dependence of elastic hadron diffractive slopes $B(t)$ for standard and peripheral pictures of elastic pp collisions at energy of 53 GeV - Fit II (central) and Fit VII (peripheral), all the other fits give similar figure.

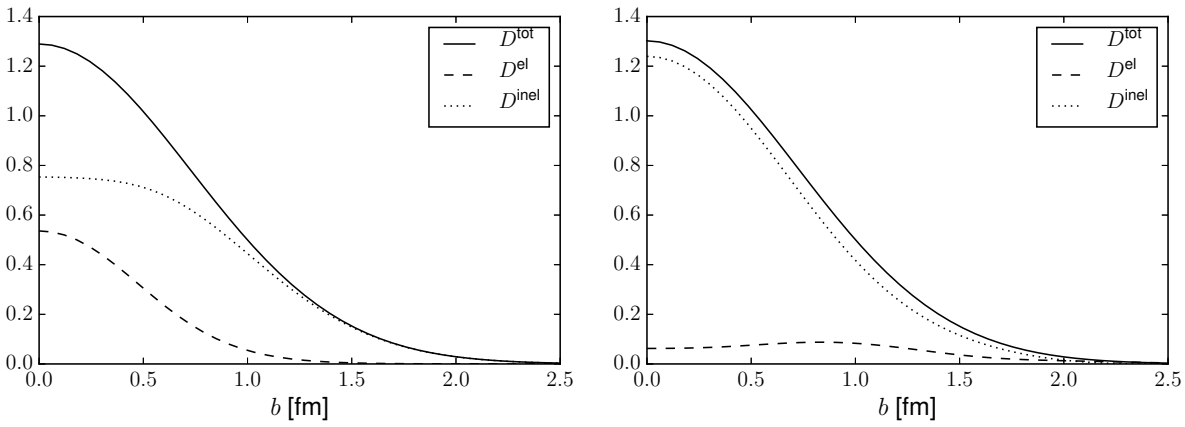

(a) central case **(b)** peripheral case

Figure 4.5: Proton-proton profile functions at 53 GeV in the central and peripheral case determined on the basis of eqs. (3.73), (3.75) and (3.84). Full line corresponds to total profile function, dashed line to elastic one and dotted line to inelastic one.

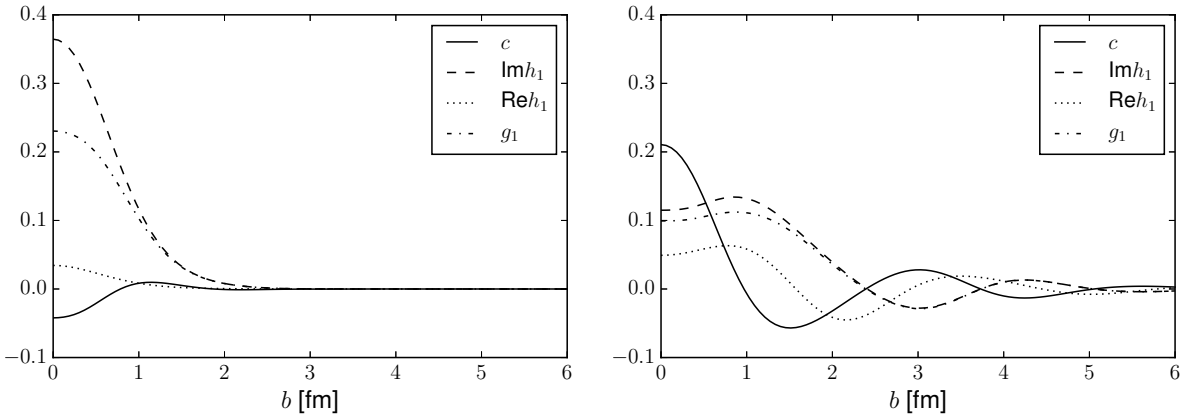

(a) central case **(b)** peripheral case

Figure 4.6: Some additional functions characterizing pp collisions in dependence on impact parameter at 53 GeV in the central and peripheral case.

Table 4.2 contains the results of three fits corresponding to the different values of $\sqrt{\langle b^2\rangle^{\rm el}}$ and the effective electric form factors (Fits III-V). In all the three fits it indeed holds $\sqrt{\langle b^2\rangle^{\rm el}} > \sqrt{\langle b^2\rangle^{\rm inel}}$ as required. Table 4.3 shows the results of the next three analogous fits of peripheral elastic hadron pp collisions but with effective electromagnetic form factor (Fits VI-VIII). These two tables also contain the final values of penalty functions $\Delta\chi^2$ which are small compared to the χ^2 values.

Differential cross sections $\frac{{\rm d}\sigma^{\rm N}}{{\rm d}t}$, $\frac{{\rm d}\sigma^{\rm C}}{{\rm d}t}$ and $\frac{{\rm d}\sigma^{\rm C+N}}{{\rm d}t}$ corresponding to the Fits III-VIII are very similar to those plotted in fig. 4.2; there is not any significant difference between the central and peripheral cases. The diffractive slope $B(t)$ for Fit VII is shown in fig. 4.4; its t-dependence is quite similar for all the central and peripheral pictures of elastic pp scattering discussed here. However, the phases $\zeta^{\rm N}(s,t)$ in the peripheral fits are very different than in the central case already at very small values of $|t|$, see fig. 4.3. It may be interesting to note that the central phase does not fulfill Martin's theorem [254] (derived later in 1997) requiring the real part of elastic hadronic amplitude to be zero at smaller value of $|t|$. The theorem is fulfilled, however, in all the peripheral cases.

For the total $\sqrt{\langle b^2\rangle^{\rm tot}}$ practically the same value of ~ 1.02 fm has been obtained in all the Fits I - VIII. As to the numerically greater values ($\sim 1.6 \div 1.90$ fm) of $\sqrt{\langle b^2\rangle^{\rm el}}$ in the peripheral cases it is given by the second term in eq. (3.81) representing the influence of the phase; inelastic $\sqrt{\langle b^2\rangle^{\rm inel}}$ being correspondingly lower.

The profile functions in fig. 4.5b for the Fit VII. Fig. 4.6b shows some other functions corresponding to the Fit VII and further characterizing hadron collisions in dependence on impact parameter b. Quantitatively similar plots may be obtained also for the other peripheral fits. It may be seen from fig. 4.5 that even if data may be fitted in the central and peripheral cases equally well the behaviour of proton collisions in impact parameter space is completely different. In the peripheral case one may obtain elastic profile function $D^{\rm el}(b)$ having its maximum at some $b > 0$. The non-zero function $c(s,b)$ discussed in sect. 3.6 and shown in fig. 4.6 in the peripheral case enables to define

procedure one can significantly influence the way how the position of the minimum can be achieved. When performing several successive minimizations one has to decrease successively the values of all the penalty constants C_p in such a way that the position of the minimum is being preserved. Using this approach the added value of total penalty function $\Delta\chi^2$ may become finally very small compared to the value of pure χ^2.

non-oscillating and non-negative profile functions. In the central case the function $c(s,b)$ plays much less significant role.

Similarly as in sect. 4.2.1, it has been checked for all the Fits III-VIII that after integration of profile functions $D^{\mathrm{X}}(b)$ according to eqs. (3.72) and (3.80) one obtains the same values of integrated cross sections σ^{X} and mean impact parameters $\sqrt{\langle b^2\rangle^{\mathrm{X}}}$ as in tables 4.2 and 4.3.

Fit		III	IV	V
Case		peripheral	peripheral	peripheral
Form factor		effective electric	effective electric	effective electric
ζ_0		0.0793 ± 0.0018	0.0795 ± 0.0018	0.0801 ± 0.0018
ζ_1		2000 ± 12	2000 ± 12	2000 ± 12
κ		3.256 ± 0.086	3.226 ± 0.082	3.148 ± 0.059
ν	[GeV^{-2}]	7.93 ± 0.39	7.72 ± 0.35	7.69 ± 0.17
a_1		12205 ± 25	12209 ± 23	12225 ± 17
a_2	[GeV^{-2}]	10640 ± 100	10650 ± 100	10630 ± 130
b_1	[GeV^{-2}]	5.877 ± 0.019	5.876 ± 0.020	5.873 ± 0.018
b_2	[GeV^{-4}]	3.528 ± 0.073	3.531 ± 0.075	3.524 ± 0.064
b_3	[GeV^{-6}]	1.579 ± 0.052	1.582 ± 0.054	1.581 ± 0.042
c_1		34 ± 23	31 ± 21	19 ± 17
c_2	[GeV^{-2}]	-43 ± 30	-45 ± 24	-60.6 ± 3.8
d_1	[GeV^{-2}]	1.24 ± 0.24	1.25 ± 0.19	1.353 ± 0.073
d_2	[GeV^{-4}]	-0.013 ± 0.040	-0.012 ± 0.035	0.004 ± 0.026
d_3	[GeV^{-6}]	-0.0046 ± 0.0026	-0.0046 ± 0.0025	-0.0038 ± 0.0023
χ^2/ndf		264.49/202	265.78/202	269.8/202
$\Delta\chi^2$		0.42	0.63	4.1
$\rho(t=0)$		0.0795 ± 0.0017	0.0797 ± 0.0018	0.0802 ± 0.0018
$B(t=0)$	[GeV^{-2}]	13.444 ± 0.042	13.445 ± 0.042	13.443 ± 0.037
σ^{tot}	[mb]	42.79 ± 0.17	42.79 ± 0.15	42.80 ± 0.12
σ^{el}	[mb]	7.512	7.513	7.517
σ^{inel}	[mb]	35.274	35.28	35.29
$\sigma^{\mathrm{el}}/\sigma^{\mathrm{tot}}$		0.1756	0.1756	0.1756
$\mathrm{d}\sigma^{\mathrm{N}}/\mathrm{d}t(t=0)$	[mb.GeV^{-2}]	94.14	94.16	94.22
$\sqrt{\langle b^2\rangle^{\mathrm{tot}}}$	[fm]	1.024	1.024	1.024
$\sqrt{\langle b^2\rangle^{\mathrm{el}}}$	[fm]	1.602	1.736	1.902
$\sqrt{\langle b^2\rangle^{\mathrm{inel}}}$	[fm]	0.8513	0.7933	0.7078
$D^{\mathrm{tot}}(b=0)$		1.30	1.30	1.30
$D^{\mathrm{el}}(b=0)$		0.0611	0.0613	0.0664
$D^{\mathrm{inel}}(b=0)$		1.24	1.24	1.23

Table 4.2: pp elastic scattering at energy of 53 GeV. Values of free parameters obtained by fitting experimental data with the help of formulas (3.53) and (3.54) for complete elastic amplitude with electric effective form factors. Values of physically significant quantities characterizing the peripheral picture of elastic hadron scattering in the impact parameter space.

Fit		VI	VII	VIII
Case		peripheral	peripheral	peripheral
Form factor		effective electromagnetic	effective electromagnetic	effective electromagnetic
ζ_0		0.0798 ± 0.0018	0.0800 ± 0.0018	0.0804 ± 0.0018
ζ_1		2000 ± 12	2000 ± 12	2000 ± 12
κ		3.254 ± 0.073	3.225 ± 0.066	3.175 ± 0.058
ν	[GeV^{-2}]	7.92 ± 0.34	7.70 ± 0.29	7.56 ± 0.23
a_1		12189 ± 15	12190 ± 20	12194 ± 15
a_2	[GeV^{-2}]	10704 ± 91	10720 ± 140	10727 ± 88
b_1	[GeV^{-2}]	5.864 ± 0.020	5.865 ± 0.023	5.864 ± 0.020
b_2	[GeV^{-4}]	3.477 ± 0.073	3.474 ± 0.084	3.468 ± 0.071
b_3	[GeV^{-6}]	1.538 ± 0.051	1.535 ± 0.063	1.533 ± 0.050
c_1		53 ± 11	53 ± 16	52 ± 10
c_2	[GeV^{-2}]	-1.4 ± 7.6	-1 ± 10	-3.1 ± 7.3
d_1	[GeV^{-2}]	0.77 ± 0.14	0.76 ± 0.35	0.79 ± 0.14
d_2	[GeV^{-4}]	-0.061 ± 0.037	-0.062 ± 0.062	-0.061 ± 0.034
d_3	[GeV^{-6}]	-0.0068 ± 0.0029	-0.0068 ± 0.0045	-0.0068 ± 0.0027
χ^2/ndf		259.69/202	260.16/202	263.37/202
$\Delta\chi^2$		1.29	0.31	2.67
$\rho(t=0)$		0.0799 ± 0.0018	0.0802 ± 0.0018	0.0806 ± 0.0018
$B(t=0)$	[GeV^{-2}]	13.417 ± 0.041	13.420 ± 0.048	13.421 ± 0.040
σ^{tot}	[mb]	42.795 ± 0.090	42.80 ± 0.13	42.809 ± 0.087
σ^{el}	[mb]	7.525	7.525	7.527
σ^{inel}	[mb]	35.27	35.28	35.28
$\sigma^{\mathrm{el}}/\sigma^{\mathrm{tot}}$		0.1758	0.1758	0.1758
$\mathrm{d}\sigma^{\mathrm{N}}/\mathrm{d}t(t=0)$	[mb.GeV^{-2}]	94.18	94.21	94.26
$\sqrt{\langle b^2\rangle^{\mathrm{tot}}}$	[fm]	1.023	1.023	1.023
$\sqrt{\langle b^2\rangle^{\mathrm{el}}}$	[fm]	1.612	1.746	1.908
$\sqrt{\langle b^2\rangle^{\mathrm{inel}}}$	[fm]	0.8456	0.7868	0.7023
$D^{\mathrm{tot}}(b=0)$		1.30	1.30	1.30
$D^{\mathrm{el}}(b=0)$		0.0606	0.0625	0.0783
$D^{\mathrm{inel}}(b=0)$		1.24	1.24	1.22

Table 4.3: pp elastic scattering at energy of 53 GeV. Values of free parameters obtained by fitting experimental data with the help of formulas (3.53) and (3.54) for complete elastic amplitude with effective electromagnetic form factors. Values of dynamical quantities characterizing the peripheral picture of elastic hadron scattering in the impact parameter space.

4.3 Energy of 8 TeV

To understand better the dependence of various characteristics of pp collisions on collision energy the eikonal model has been applied also to recent experimental data at 8 TeV (see sect. 4.1) very similarly as it has been done at the energy of 53 GeV. In this 8 TeV case the results corresponding only to effective electromagnetic form factors will be shown.

The hadronic amplitude $F^{\mathrm{N}}(s,t)$ parameterized according to eqs. (4.1) and (4.2) has been fitted to 8 TeV data, see fig. 4.7. In this case the fit (denoted as central) is quite straightforward (unique) as it was at 53 GeV. Using parameterization of $F^{\mathrm{N}}(s,t)$ given by eqs. (4.1) and (4.4) one may again find several peripheral alternatives; only one example fit having been chosen. In both the fits (central and peripheral) values of parameters d_2 and d_3 have been chosen to be zero and not varied during the fit.

The values of all the fitted parameters may be found in table 4.4. In both the central and peripheral cases the fitted hadronic phases $\zeta^{\mathrm{N}}(s,t)$ in fig. 4.8 and diffractive slopes $B(t)$ in fig. 4.9. In the peripheral case one may again observe steep increase of the phase with rising $|t|$ similarly as in at 53 GeV, see fig. 4.3.

In table 4.4 one may further find several interesting hadronic quantities. One may see that it indeed holds $\sqrt{\langle b^2\rangle^{\mathrm{el}}} < \sqrt{\langle b^2\rangle^{\mathrm{inel}}}$ in the denoted central case and $\sqrt{\langle b^2\rangle^{\mathrm{el}}} > \sqrt{\langle b^2\rangle^{\mathrm{inel}}}$ in the peripheral one (as required). The corresponding b-dependent profile functions in fig. 4.10. Some other b-dependent functions further characterizing the collisions in dependence on impact parameter in fig. 4.11.

It may be seen from fig. 4.12 that the "Coulomb-hadronic" t-region is much broader at 53 GeV then at 8 TeV. Only few points corresponding to $\mathrm{d}\sigma^{\mathrm{C+N}}/\mathrm{d}t > \mathrm{d}\sigma^{\mathrm{N}}/\mathrm{d}t$ are available at 8 TeV (and with higher statistical uncertainty than at 53 GeV). It implies much more ambiguity on separation of Coulomb and hadronic effects at 8 TeV than at 53 GeV.

The results concerning the central and peripheral fits of the same experimental data at 8 TeV obtained in this section are consistent with the very recent results determined by TOTEM in [36] where one may find also estimation of uncertainties of various quantities.

Strong dependence on collision energy of some physically significant hadronic quantities characterizing pp collisions may be seen from tables 4.1 to 4.4 where one can compare the numerical values at two very different energies. E.g., the value of total cross section at 8 TeV is more than twice greater than at 53 GeV (≈ 42 mb vs. ≈ 103 mb). The increasing value of proton total cross section with rising collision energy is known already for quite a long time, see also fig. 2.30, but it is still not fully understood. It is, e.g., not clear how the dependence looks like at even higher collision energies (especially in the limit $\sqrt{s} \to \infty$). Measured elastic pp scattering at even higher collision energy may provide important experimental input to solve some of the corresponding open questions[2]. The question of energy dependence of some quantities (e.g., total cross section) should be addressed together with several open fundamental problems in contemporary descriptions of elastic collisions which will be discussed later in chapter 6.

[2]TOTEM at LHC has recently (October 2015) performed measurement of pp elastic scattering at 13 TeV which might be quite useful in this respect.

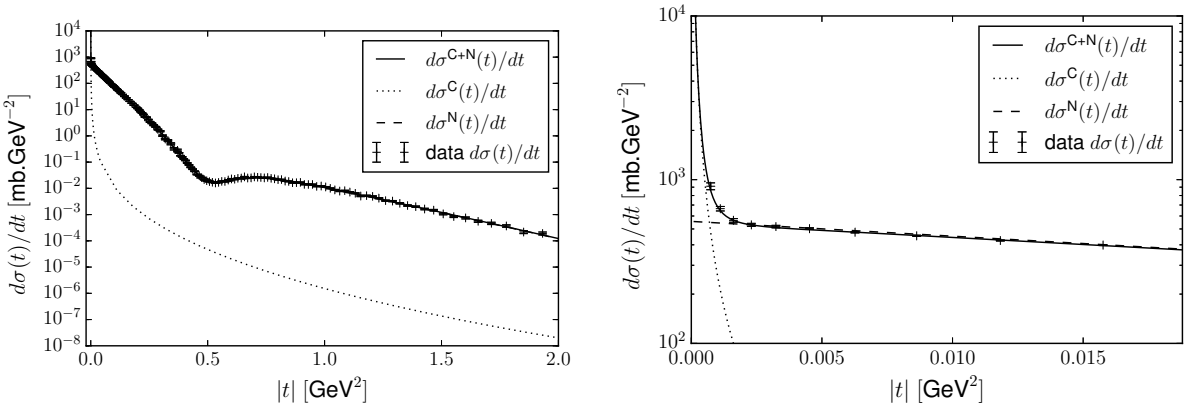

(a) 8 TeV, full fitted t range **(b)** 8 TeV, region of very low values of $|t|$

Figure 4.7: Eikonal model fitted to measured pp elastic differential cross section at energy of 8 TeV in the central case (the peripheral case having similar t-dependence): (a) - full fitted t-range, (b) - zoom to very small values of $|t|$. Individual points - experimental data, full line - Coulomb-hadronic elastic differential cross section $\mathrm{d}\sigma^{\mathrm{C+N}}(t)/\mathrm{d}t$ given by eikonal model and fitted to the experimental data, dotted line - Coulomb differential cross section $\mathrm{d}\sigma^{\mathrm{C}}(t)/\mathrm{d}t$, dashed line - hadronic differential cross section $\mathrm{d}\sigma^{\mathrm{N}}(t)/\mathrm{d}t$.

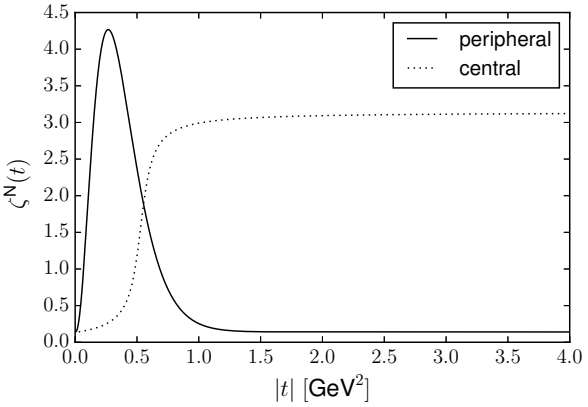

Figure 4.8: Elastic hadron phases $\zeta^{\mathrm{N}}(s,t)$ for central and peripheral pictures of elastic pp collisions at energy of 8 TeV.

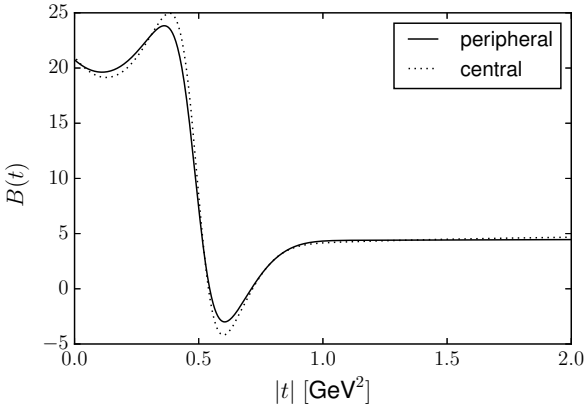

Figure 4.9: t-dependence of elastic hadron diffractive slopes $B(t)$ for central and peripheral pictures of elastic pp collisions at energy of 8 TeV.

Case		central	peripheral
Form factor		effective electromagnetic	effective electromagnetic
ρ_0		1.3488e-1	-
t_{dip}	[GeV^2]	-0.53 (fixed)	-
ζ_0		-	0.14013
ζ_1		-	1.4520e3
κ		-	2.5290
ν	[GeV^{-2}]	-	9.4511
a_1		6.6577e8	6.6046e8
a_2	[GeV^{-2}]	1.6419e9	1.7098e9
b_1	[GeV^{-2}]	8.2651	8.1147
b_2	[GeV^{-4}]	9.1852	7.1060
b_3	[GeV^{-6}]	14.567	11.479
c_1		1.6486e7	2.6603e7
c_2	[GeV^{-2}]	-2.8896e7	-6.8805e6
d_1	[GeV^{-2}]	2.7272	2.3998
d_2	[GeV^{-4}]	0 (fixed)	0 (fixed)
d_3	[GeV^{-6}]	0 (fixed)	0 (fixed)
$\sigma^{\mathrm{tot,N}}$	[mb]	103.4	104.0
$\sigma^{\mathrm{el,N}}$	[mb]	27.7	28.0
σ^{inel}	[mb]	75.7	76.1
$\mathrm{d}\sigma^{\mathrm{N}}/\mathrm{d}t(t=0)$	[mb.GeV^{-2}]	556	564
$\rho(t=0)$		0.135	0.141
$B(t=0)$	[GeV^{-2}]	21.0	20.7
$\sqrt{\langle b^2\rangle^{\mathrm{tot}}}$	[fm]	1.28	1.27
$\sqrt{\langle b^2\rangle^{\mathrm{el}}}$	[fm]	0.879	1.97
$\sqrt{\langle b^2\rangle^{\mathrm{inel}}}$	[fm]	1.40	0.882
$D^{\mathrm{tot}}(b=0)$		2.01	2.05
$D^{\mathrm{el}}(b=0)$		1.02	0.180
$D^{\mathrm{inel}}(b=0)$		0.983	1.87

Table 4.4: Values of free parameters of elastic hadronic amplitude $F^{\mathrm{N}}(s,t)$ in the central and peripheral case as fitted to measured pp elastic differential cross section at 8 TeV and corresponding values of some physically interesting hadronic quantities.

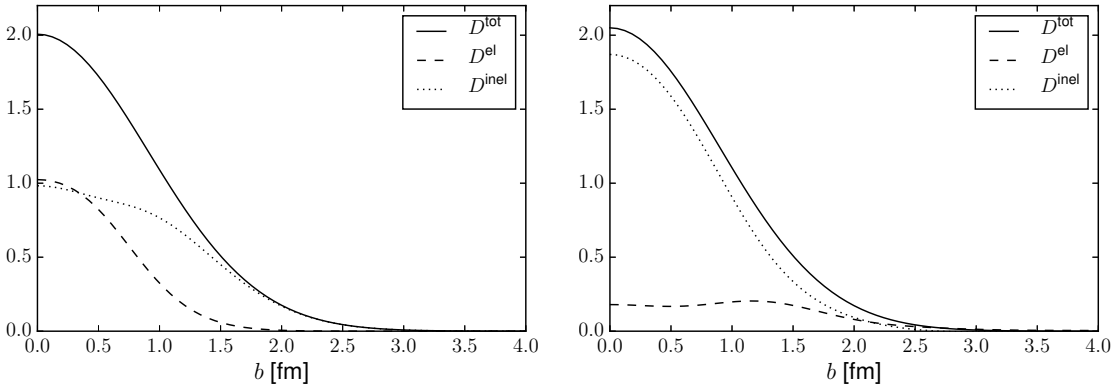

(a) central case **(b)** peripheral case

Figure 4.10: Proton-proton profile functions at 8 TeV in the central and peripheral case. Full line corresponds to total profile function, dashed line to elastic one and dotted line to inelastic one.

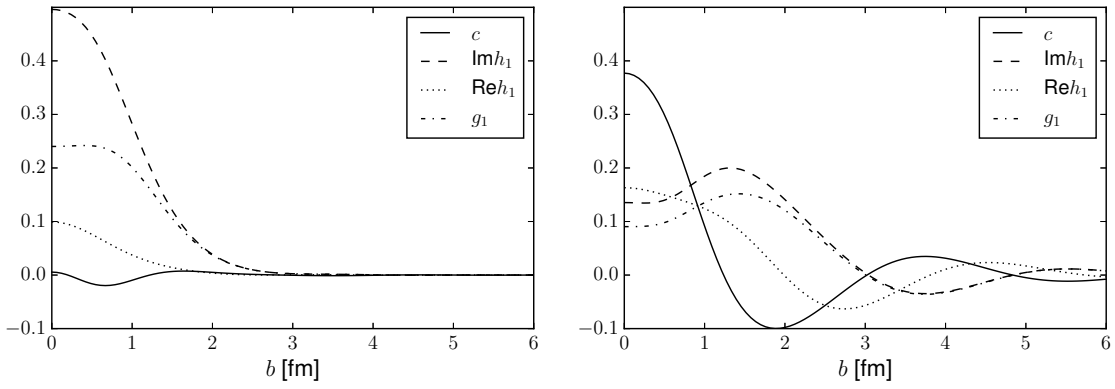

(a) central case **(b)** peripheral case

Figure 4.11: Functions $c(s,b)$, $\text{Im}\, h_1(s,b)$, $\text{Re}\, h_1(s,b)$ and $g_1(s,b)$ in dependence on impact parameter at 8 TeV in the central and peripheral case.

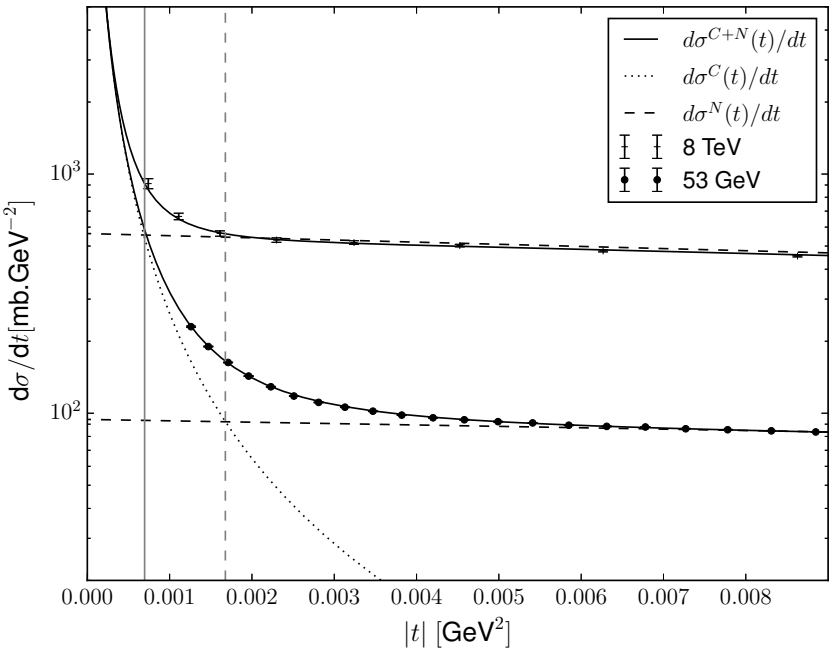

Figure 4.12: Elastic pp differential cross sections at 53 GeV and 8 TeV - region of the lowest measured t values (8 TeV part being above 53 GeV part). Dashed (resp. solid) vertical line corresponds to t value for which $\mathrm{d}\sigma^{\mathrm{C}}/\mathrm{d}t \approx \mathrm{d}\sigma^{\mathrm{N}}/\mathrm{d}t$ at 53 GeV (resp. 8 TeV).

4.4 Summary

The measurement of elastic differential cross section $\frac{\mathrm{d}\sigma}{\mathrm{d}t}$ represents main source of experimental data for the analysis of elastic processes of protons. The goal of quantum-theoretical description consists in separating Coulomb and elastic hadronic collisions and determining elastic hadronic amplitude $F^{\mathrm{N}}(s,t)$, from which conclusions concerning structure (or hadronic interaction) of colliding particles should be derived. However, there has not been any actual theory until now which would reliably determine its corresponding t-dependence.

In the past the simplified approach of West and Yennie has been made use of for separation of Coulomb and hadron interactions. However, this method is not theoretically consistent and is not in sufficient agreement with the measured data. It contains many limitations as it has been discussed in sect. 3.2. It has been applied to the analysis of the data only in a very narrow region of momentum transfers in forward direction and the influence of Coulomb scattering at higher values of momentum transfers has been always neglected by definition. The elastic scattering at higher values of momentum transfer has been always described phenomenologically as purely hadronic scattering. Such a duality approach in the description of elastic hadron collisions can be hardly justified.

The eikonal model approach, based on the complete elastic scattering amplitude $F^{\mathrm{C+N}}(s,t)$ fulfilling eqs. (3.53) to (3.55), provides more reliable basis for analysis of elastic collisions of (charged) hadrons. In principle it is established on the fact that the common influence of the Coulomb and hadronic elastic scattering can be reliably described by the sum of the Coulomb and elastic hadronic eikonals and without any a priori limitation on t-dependence of the elastic hadronic amplitude. However, in such a case

the complex hadronic component $F^{\mathrm{N}}(s,t)$ cannot be uniquely established; in principle, only its modulus may be determined from experimental differential cross section while the t-dependence of its phase has been only partially limited when Coulomb-hadronic interference (the region of very small $|t|$) has been taken into account.

In the majority of published analyses of experimental data the corresponding freedom has been, however, strongly limited by the choice of amplitude parameterization. The imaginary part has been assumed usually to be dominant in a great interval of t and vanishing in the diffractive minimum; with the real part determining the non-zero value of differential cross section in the diffractive minimum; see, e.g., the earlier papers [16, 128, 209–214], [255–263] and also recent papers [232–244, 247, 248, 264]. Only a very small change of phase with rising $|t|$ has been allowed in a great region of $|t|$. The so-called central behaviour in impact parameter space has been then obtained in such a limited case; elastic processes being more central (i.e., existing for very small b even at $b = 0$) than inelastic ones. Transparent elastic processes may be hardly brought to agreement with the existence of inelastic processes when hundreds of particles have been formed at the same energy in many other collision events. Description corresponding to these widely used assumptions has been fitted to experimental data at energy of 53 GeV in sect. 4.2.1 and at 8 TeV in sect. 4.3.

Much more general parameterization of the hadronic amplitude $F^{\mathrm{N}}(s,t)$ has been used in sect. 4.2.2 and sect. 4.3. A rather steep rise of phase $\zeta^{\mathrm{N}}(s,t)$ with increasing $|t|$ already at very small values of $|t|$ has been allowed. It has been possible to obtain strongly peripheral impact parameter profile for elastic processes at both the analysed energies.

It has been shown how to solve the problems concerning the oscillating profiles (at finite energy), even if the given questions require a deeper analysis. The determined total, elastic and inelastic profile functions (under different assumptions) strongly characterize behaviour of proton collisions in dependence on impact parameter. It has been shown, too, at both the analysed energies, that inclusion of the effective electromagnetic form factor into the description instead of just the effective electric one does not substantially influence the determined hadronic quantities. One should be, however, aware that the electromagnetic form factors in ep and pp processes need not be the same, which should be tested in the future.

It is possible to say (against earlier conviction) that there is not any reason against more realistic interpretation of elastic processes when protons are regarded as rather compact (non-transparent) objects. The central and peripheral fits at 53 GeV performed in this chapter will be further discussed and compared to corresponding results of Miettinen in chapter 5.

Chapter 5

Centrality or peripherality of elastic collisions?

Basic experimental characteristic established in elastic collisions of protons has been represented by measured differential elastic cross section. In the case of unpolarized proton beams its t-dependence has exhibited very similar structure in all cases at contemporary high energies: there has been a dip-bump or shoulder structure following the diffraction peak characterizing the behaviour at small $|t|$ (close to $t = 0$) practically for all colliding hadrons [7–12], see the data points at 53 GeV and 8 TeV in fig. 4.1 as example. If the influence of Coulomb interaction (existing mainly in the region of very small deviations) has been separated the elastic hadronic differential cross section has been represented by the modulus of corresponding amplitude (see eq. (3.12)). It means that the modulus of amplitude has been strongly constrained by the given experimental data while the corresponding phase (see eq. (3.18)) has remained in principle undetermined (limited only by optical theorem, imaginary part of amplitude at $t = 0$ corresponding to total hadronic cross section).

It was probably the main reason why in the first analyses the phase of elastic hadronic amplitude was taken as t-independent in a small interval around zero; see the approach of WY [14] (1968) summarized in sect. 3.2 where the phase has been taken as t-independent in the whole region of kinematically allowed values of t. The simplified formula (3.24) of WY was used as standard tool in the era of the ISR mainly for determining total (hadronic) pp cross section from measured elastic scattering at very low values of scattering angle. However, it has been shown later that several important and very limiting assumptions have been involved in the approach of WY, see sect. 3.2. Most importantly, the dependence of elastic collisions on impact parameter has not been taken into account in the approach of WY at all.

The influence of impact parameter value on hadronic collisions was not considered in the first descriptions (phenomenological models) of elastic scattering, even thought the individual collision results depend surely strongly on it. As it has been mentioned in Introduction, one of the first discussion concerning the influence of impact parameter and interpretation of (elastic) hadronic collisions in b-space has been done by Miettinen [15, 16, 209] (1973-1975). According to his papers a rather great ratio of elastic processes should correspond to central collisions; around 6% of all collisions should be elastic even at impact parameter $b = 0$ (i.e., head-on collisions) in the whole ISR energy range (approximately $20 - 60$ GeV).

The given results followed from profile functions (called b-dependent overlap functions

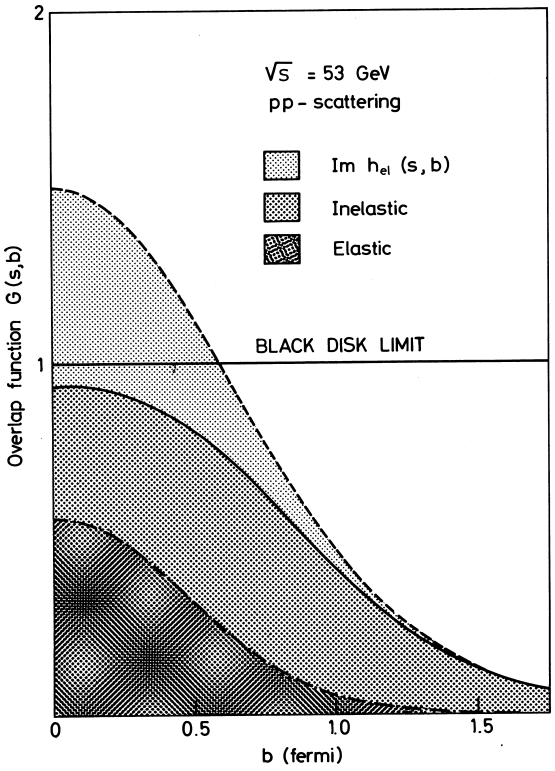

Figure 5.1: Impact structure of pp scattering at $\sqrt{s} = 53$ GeV derived by Miettinen [15]. Characteristics in b space are presented: imaginary part of elastic hadronic amplitude (corresponding to total profile function eq. (3.69) in our notation) and b-dependent elastic and inelastic overlap functions (elastic and inelastic profile functions in our terminology). The "black disc limit" indicates value 1 assumed to correspond to the maximum value of inelastic overlap (profile) function allowed by unitarity (100% absorption).

by Miettinen) determined on the basis of FB transformation (3.66) and unitarity condition (3.68). The inelastic profile function was then identified by Miettinen with inelastic probability function $P^{\text{inel}}(b)$ and subtracted from 1 ("black disc limit" assumed to represent the maximum value of the inelastic profile function allowed by unitarity - 100% absorption).[1] According to fig. 5.1, a Gaussian shape having maximum at $b = 0$ and decreasing with increasing b has been obtained for the profile (probability) functions of inelastic as well as elastic collisions.

It is not, however, clear from [15, 16, 209] why the elastic probability at $b = 0$ was calculated from the inelastic one (it was put $P^{\text{el}}(b{=}0) = 1 - P^{\text{inel}}(b{=}0)$) and not directly taken from elastic profile (probability) function which was also established and which had the value of approximately 50% at $b = 0$ (which is very different value than the previous 6%). It has not been explained, either, why total profile function being the sum of elastic and inelastic profile (probability) functions (imaginary part of elastic hadronic amplitude $\text{Im}\, h_{\text{el}}(s, b)$ in Miettinen's notation, see fig. 5.1) has been significantly greater than 1 at values of $b < 0.6$ fm.

The suggested central character of elastic collisions (according to [15] p. 6: 'hadrons seem to be rather airy objects') was very confusing due to the fact that the single inelastic diffraction seemed to be peripheral (see again [15] or, e.g., Giovannini et al. [17] from 1979). Such significant different physical interpretations of elastic processes and inelastic diffraction processes (mainly single diffractive) having very similar dynamics

[1] Definition of black disc model may be found in [149]. Colliding particles have been represented by discs of finite radius R such that for impact parameters $b < R$ only absorption (inelastic) events have been allowed and for $b > R$ there has not been any hadronic interaction at all. In such a case one would expect corresponding elastic cross section being zero. However, the elastic channel has been opened in the given mathematical description when corresponding elastic scattering amplitude was not chosen to be zero; the elastic cross section in black disc model has been taken as one half of the total cross section corresponding to the disc.

Model	$\sqrt{\langle b^2\rangle^{\mathrm{tot}}}$	$\sqrt{\langle b^2\rangle^{\mathrm{el}}}$	$\sqrt{\langle b^2\rangle^{\mathrm{inel}}}$
Bourelly et al.	1.249	0.876	1.399
Petrov et al. (2P)	1.227	0.875	1.324
Petrov et al. (3P)	1.263	0.901	1.375
Block et al.	1.223	0.883	1.336
Islam et al.	1.552	1.048	1.659

Table 5.1: Values of root-mean-squares of impact parameter (in femtometers) predicted by several contemporary phenomenological models of pp collisions at collision energy of 14 TeV. All the models predict $\sqrt{\langle b^2\rangle^{\mathrm{el}}} < \sqrt{\langle b^2\rangle^{\mathrm{inel}}}$, i.e., central behaviour of elastic hadronic scattering [48, 49].

may hardly correspond to reality. This kind of "transparency" of protons (in elastic collisions) has been denoted as a puzzling question, too, already at that time (see, e.g., Giacomelli and Jacob [18], 1979) as it may be hardly accepted for collisions of two matter objects (when in other collision events hundreds of other fundamental particles may be produced).

The result of Miettinen concerning behaviour of collisions in impact parameter space (shape of profile functions) has followed mainly from assumptions that have limited the phase $\zeta^{\mathrm{N}}(s,t)$ as he used hadronic phase of the "standard" shape, see our comments next to eq. (4.2); in his papers the used parameterizations, fitted parameters and several other details of his calculations have not been, unfortunately, explicitly mentioned. It is, therefore, not so surprising that our profile functions in the central case shown in chapter 4 (obtained in eikonal approach) are similar to that of Miettinen (see fig. 4.5a and fig. 5.1); both the approaches have been based on very similar assumptions (some differences existing but with quite minor impact on the result).

Very similar approach as that of Miettinen has been commonly used up to now by many other authors. Different parameterizations of the ("standard") hadronic phase $\zeta^{\mathrm{N}}(s,t)$ which assume (under influence of WY approach) the dominance of imaginary part of elastic hadronic amplitude at $t = 0$ and in a quite wide region of higher values of $|t|$ have always been applied to. This is also, e.g., the case of recently published papers [243, 264] where one may find (elastic) profile functions at 53 GeV very similar to those of Miettinen. As to some other contemporary descriptions of elastic scattering suggested by other authors they have been analyzed at the LHC energies in [48]. All these models assume the "standard" form of the hadronic phase; all of them also lead to the centrality of elastic collisions as it has been demonstrated in [48], see table 5.1 for corresponding values of root-mean-squares of impact parameter.

In [19] (1981) it has been shown that the assumptions of t-independent hadronic phase (t-independent quantity ρ) and purely exponential modulus $\left|F^{\mathrm{N}}(s,t)\right|$ (t-independent diffractive slope B) included in the simplified formula (3.24) of WY have led to the given central character of elastic collisions. It is evident that the centrality of elastic collisions has been derived on the basis of a number of assumptions (having influenced mainly the phase) that have not been sufficiently specified and reasoned; the b-dependence of elastic collisions having not been considered at all.

The following question has been then solved in [19] (in 1981), i.e., what t-dependence of the phase $\zeta^{\mathrm{N}}(s,t)$ is to be if elastic processes might be interpreted as peripheral (or even more generally what must be changed in a given theoretical framework to obtain

more acceptable behaviour of elastic collisions in dependence on impact parameter). It has been shown that peripheral interpretation of hadronic collisions may be obtained if the phase has strong t-dependence (see also [249] from 1987). The result concerning peripherality in [19] has been obtained without taking into account Coulomb-hadron interference. In chapter 4 it has been shown that one may obtain similar result if Coulomb interaction has been included on the basis of interference formula (3.53), see figs. 4.3 and 4.8 (and also [20] from 1994 and [251] from 1992).

To interpret elastic hadron collisions as peripheral has gained support also in the analysis of elastic hadron processes between light nuclei. Franco and Yin [265, 266] (1985-1986) studied the elastic scattering of α particles on various targets (^1H, ^2H, ^3He, ^4He). They tried to reproduce the momentum transfer distribution of elastic collisions of the two objects composed of individual nucleons using the Glauber model approach [193, 267]. As an input they used the "elementary" nucleon-nucleon elastic scattering amplitude, assuming (in the first approximation) to be the same for all possible combinations of nucleons involved in the scattering. The data were selected in order to have practically the same energy per one nucleon. They obtained an agreement with experimental data in all considered types of scattering if they introduced the strongly t-dependent elementary elastic hadron phase of the form $\zeta^{\mathrm{N}}(s,t) = \frac{\tilde{\gamma}\, t}{2} + \mathrm{const}$ with $|\tilde{\gamma}| > 10$ GeV^{-2}. Such a simple t-dependence of the phase together with a purely exponential t-dependence of the corresponding modulus was chosen in order to perform analytically all the needed integrals involved in the Glauber model approach. Their elementary nucleon - nucleon elastic scattering amplitude had imaginary part vanishing at $|t| \leq 0.1$ GeV^2, which corresponded to the result obtained in [19, 156, 157].[2]

The formulas (3.81), (3.83) and (3.82) determining root-mean-squares of impact parameter $\sqrt{\langle b^2 \rangle}$ corresponding to elastic, inelastic or total hadronic events have been derived in [216] (2002). They have allowed testing whether a given t-dependent hadronic amplitude $F^{\mathrm{N}}(s,t)$ leads to central or peripheral behaviour of elastic collisions without the need to establish the whole profile functions, see sect. 3.4.3. In the quoted paper it has been shown that similar results to the behaviour of pp collisions in the impact parameter space mentioned up to now were obtained in the case of elastic $\bar{\mathrm{p}}$p scattering at energy of 541 GeV, too (see also [20]).

The mean impact parameters of total, elastic and inelastic processes $\sqrt{\langle b^2 \rangle^{\mathrm{X}}}$ have been defined with the help of eq. (3.80) where $n = 2$ and $w(b) = 2\pi b$. The factor $w(b) = 2\pi b$ has corresponded to the assumed weight of initial two-particle states (of their impact parameter values) in corresponding experiment. Such a definition of mean impact parameters has been commonly used in the past [19, 197, 216, 217] as it has been assumed that the profile functions had some meaning of probabilities or distributions of impact parameter value b. This definition of mean impact parameter with $w(b) = 2\pi b$ depends, however, rather strongly on the b-dependent frequency of produced two-particle collisions.

For discussion of centrality and peripherality of elastic collisions (reflecting different instant structures and orientations of colliding particles) it seems, however, to be more suitable to put $w(b) = 1$ in eq. (3.80). Comparison of the corresponding numerical values of mean impact parameters with $w(b) = 2\pi b$ and $w(b) = 1$ in the central Fit II and peripheral Fit VII discussed in chapter 4 may be found in table 5.2. One may see that

[2] The technique similar to the Glauber approximation has been also used by Franco [203] (1973) in re-deriving the WY integral formula for the relative phase (3.17) appearing in the Coulomb-hadronic interference.

Fit		II	II	VII	VII
Case		central	central	peripheral	peripheral
$w(b)$		1	$2\pi b$	1	$2\pi b$
$\sqrt{\langle b^2\rangle^{\rm tot}}$	[fm]	0.726	1.03	0.723	1.02
$\sqrt{\langle b^2\rangle^{\rm el}}$	[fm]	0.473	0.676	1.19	1.75
$\sqrt{\langle b^2\rangle^{\rm inel}}$	[fm]	0.800	1.09	0.647	0.787
$\langle b\rangle^{\rm tot}$	[fm]	0.579	0.910	0.577	0.907
$\langle b\rangle^{\rm el}$	[fm]	0.376	0.595	0.956	1.47
$\langle b\rangle^{\rm inel}$	[fm]	0.655	0.977	0.532	0.937

Table 5.2: Comparison of different definitions of mean impact parameter values corresponding to total, elastic and inelastic scattering calculated on the basis of eq. (3.80) for $n = 1, 2$ and $w(b) = 1$ or $w(b) = 2\pi b$ in the central Fit II and peripheral Fit VII of pp data at 53 GeV discussed in chapter 4.

the values are quite different; both the definitions have also different physical meaning.

One may also calculate in both the fits the mean impact parameters using $n = 1$ instead of $n = 2$ in eq. (3.80) (for both the weights $w(b)$) as it is common in mathematics for definition of mean value of random variable. The numerical values of $\langle b\rangle^{\rm X}$ might be then compared to values of $\sqrt{\langle b^2\rangle^{\rm X}}$, see table 5.2. The values of "mean impact parameters" might be very different according to chosen definition. For the two fits from chapter 4 the mean impact parameter corresponding to elastic collisions remains lower (greater) than for the inelastic case in the central (peripheral) fit independently of the chosen definition.

It has been shown in chapter 4 that measured elastic differential cross section at given energy may be fitted as central or peripheral according to assumptions (or parametrizations) influencing t-dependence of phase; the corresponding profile functions commonly interpreted as some probabilities or distribution functions of impact parameter might be very different. One of the main and very basic problems lies in the fact that the theory of elastic collisions has been introduced in particle physics with strict analogy to description of some optics phenomena (light meeting an obstacle of a given profile which describes its absorptive properties), see [128]. However, in the case of particle physics it has never been shown in sufficient details why the profile functions should have the meaning of distribution functions of impact parameter of total, elastic or inelastic events or that they should have meaning of some probabilities. The physical meaning of the commonly calculated profile functions in particle physics is quite unclear.

It is evident that a number of important open questions and problems exists, which should be solved before one will be able to get some really reasoned conclusions concerning the structures of corresponding particles; some of them will be discussed in next section. There is not, however, any doubt that it is the analysis based on impact parameter representation of incoming collision states that has opened quite new insight.

Chapter 6

Open problems in contemporary descriptions of elastic collisions

In the preceding we have tried to show main results concerning proton structure and corresponding characteristics derived from elastic collision data on the basis of eikonal model introduced in [20]. The results of elastic collisions have been interpreted on the basis of eikonal model, of course, also in the framework of other theoretical approaches. In these cases the eikonal model has not been used, however, for a construction of the complete elastic scattering amplitude $F^{\mathrm{C+N}}(s,t)$ (i.e., for description of common influence of both Coulomb and elastic hadronic scattering, see sect. 3.4) but for a construction of elastic hadronic amplitude $F^{\mathrm{N}}(s,t)$ only. The Coulomb effect has been usually added using the WY approach described in sect. 3.2.

One of the recent attempts [268–270] to interpret elastic hadronic scattering has been done within the standard Regge pole model; it has been endeavored to determine the final hadronic effect as the sum of eikonal contributions corresponding to the exchange of different (pomerons or others) trajectories. All of the individual contributions have had a typical central Gaussian shape in the impact parameter space which has held for the resulting eikonal $\delta^{\mathrm{N}}(s,b)$, too. Corresponding elastic profile function $D^{\mathrm{el}}(s,b)$ has had, therefore, also Gaussian shape leading to central behaviour of elastic collisions in dependence on impact parameter [48]. Hadronic amplitude $F^{\mathrm{N}}(s,t)$ has been then determined on the basis of eq. (3.43). The influence of Coulomb scattering has been finally described within the standard WY approach.

The analysis of results obtained in elastic collision experiments at LHC has been done on the basis of similar Reggeon trajectories also in papers [271] and [272]. The corresponding model has been more complex being based on three channel eikonal model trying to describe also single diffraction collision. The limitation concerning the existence of central elastic collisions has remained, as in the previous case.

Similar eikonal model approach has been used, too, in so-called QCD-inspired model of Block et al. [273–276]. Also in this case the eikonal model has been used for specifying the elastic hadronic amplitude $F^{\mathrm{N}}(s,t)$ on the basis of eikonal function $\delta^{\mathrm{N}}(s,b)$ and eq. (3.43). The interaction between hadrons has been defined in terms of the interactions of their constituents (quarks and gluons) corresponding to hadronic eikonal function. The model has been applied to elastic pp scattering at 7 TeV LHC energy [276]. Very similar multichannel eikonal approach has been also used in the already mentioned paper [264].

All these models have been proposed, of course, earlier; it has been demonstrated

in [48] that they have given central elastic scattering; no attention has been devoted to this fact in original papers, even if some b-dependent characteristics have been calculated. In both the kinds of these eikonal approaches (Regge and QCD-inspired models) the peripheral interpretation might be undoubtedly obtained, too, if they were correspondingly generalized.

In the corresponding experiments we need to establish the complex scattering amplitude $F^{\mathrm{N}}(s,t)$ from the measured elastic differential cross section. However, from experimental data it is possible to determine practically the modulus of this amplitude only; the shape of phase has not practically any relation to experimental data. Its t-dependence has been usually strongly limited by other (often latent) assumptions. However, the t-dependence of phase determines central or peripheral character of the collisions. The given behaviour has been then strongly influenced by a very limited parametrization of free (fitted) functions in the standard approach, while in the model applied to in chapter 4 much more broader parametrization of elastic collisions has been made use of.

However, the results derived from corresponding experimental data have been influenced also by some theoretical assumptions contradicting experimental conditions. The attention to one mistaking assumption (admission of infinite impact parameter) has been called in [36] concerning the recent results at 8 TeV obtained by TOTEM experiment at the LHC at CERN. In the quoted paper the comparison of standard central behaviour of elastic collisions with the peripheral one obtained with the help of the eikonal model discussed in this paper has been presented, too.

There are, however, other problems and open questions in contemporary theory of collision processes which will be introduced and discussed in the following:

1. *Coulomb interaction and experimental conditions*
   In experimental analysis it is always necessary to "subtract" the effect of Coulomb interaction of charged particles which is currently done under assumptions being in partial disagreement with corresponding experiments.

   (a) *(Non)divergence at $t = 0$*
   The Coulomb differential cross section has always been assumed to be given by eq. (3.26), i.e., diverging at $t = 0$. Contemporary Coulomb-hadronic interference formulas include integration over the corresponding diverging t-dependence of Coulomb amplitude (which has been also the case of both eqs. (3.24) and (3.53)). However, such a dependence does not correspond to conditions in any relevant experiment as the singular point $t = 0$ may exist only for events corresponding to infinite impact parameter value while in real experiments corresponding values are to be less than micrometers.

   (b) *Multiple collisions*
   In real experiments very small deviations (scattering angles) should be described rather as the sum of multiple Coulomb scattering of one particle at higher yet possible impact parameters and of standard Coulomb scattering of two colliding particles. It means that also the t-dependence of elastic hadronic cross section in the region of the smallest measured deviations might be strongly influenced by subtraction of the given Coulomb interaction effect. The effect of multiple scattering was discussed already by Rutherford, Geiger and Marsden when they started to interpret first fixed-target experiments in 1911, see [1]. It has been taken into account in some other analyses of

fixed-target experiments in order to determine corresponding characteristic of only single scattering. It should be considered also in colliding-beam experiments.

(c) *Electromagnetic form factors*
The dependence of Coulomb interactions on impact parameter has not been satisfactorily taken into account probably not only in elastic pp scattering but also in elastic ep scattering for determination of electromagnetic proton form factors (e.g., in [189] the influence of impact parameter on particle collisions not having been mentioned at all, either).

2. *Different mechanism of Coulomb and strong forces*
One should ask, too, whether the standardly used Coulomb-hadronic interference formulas have described the given collision data in full agreement with reality when the corresponding forces have had very different characteristics. The Coulomb force acts at any distance being efficient practically during the whole evolution time while the hadronic force should be interpreted rather as a contact force being efficient for a very short time interval at very small impact parameter values only. One should, therefore, ask how much the contact hadronic interaction may be influenced by earlier Coulomb interaction acting at greater distances.

3. *Weak interaction*
The existence of some weak forces (their range being probably limited similarly as for strong ones) has been standardly considered in the description of fundamental particles but until now the elastic hadron collisions have been interpreted as superpositions of strong and Coulomb interactions only. Considering corresponding problems in a much broader context (see, e.g., probable dimension of hydrogen atom and the distances of hadronic objects in solid substances [24]) one may come to the conclusion that the proton might interact also weakly at greater distances, the strongly interacting matter being surrounded by other matter interacting only weakly. One should, therefore, ask whether the hadronic collisions are not influenced more by such a weak interaction than by Coulomb force.

4. *Properties of S matrix and structure of Hilbert space*
It is also the usual definition of S operator that should be newly analyzed and tested. If the collision processes are to be represented in a Hilbert space correctly the initial and final states should be represented by vectors in two mutually orthogonal subspaces (see, e.g., [277, 278] and also [24, 279, 280]). The given Hilbert structure has been, however, excluded by Bohr in 1927 [281] who asked for the Hilbert space representing the evolution of any physical system to be spanned always on one basis of Hamiltonian eigenvectors (instantaneous states of incoming and outgoing particle pairs having always been represented by the same vector). The S matrix in Bohr's Hilbert space may, therefore, hardly represent the transition probabilities from initial state to final one

$$P_{i\to f} = |\langle f|\, S\, |i\rangle|^2 \tag{6.1}$$

as it is usually assumed. There is also problem with the interpretation of S matrix unitarity. It will be probably necessary to define a transition operator between incoming and outgoing states (i.e., between two mutually orthogonal

Hilbert subspaces) caused by a "contact" force; however, it will be hardly possible to ask for it to be unitary (see [51]).

5. *Optical theorem*
All contemporary models of elastic hadron collisions have been based on validity of optical theorem which correlates the total cross section to the value of imaginary part of elastic amplitude at one point ($t = 0$), see eq. (3.23). The theorem has been taken from optics and applied to strong interaction collisions while any proof of its validity in strong interactions (particle physics) has not been given until now, see [51] (and also [50, 282, 283]) for detailed discussion. It has been shown in [51] that the attempts to prove optical theorem in particle physics assume unitarity of S matrix (given by eq. (3.65)) and initial state(s) not properly distinguished according to impact parameter. Another problem is related to the fact that the so-called "non-interacting" final states have been arbitrarily interchanged with elastic states at $t = 0$. Both the cases correspond to zero scattering angle but the corresponding states have completely different frequencies in experiments, which has not been respected and taken into account. Detailed discussion of these problems and some others may be found in [51] where one may find also historical context (see also [284]). The impact of the constraining optical theorem in contemporary models is not quite clear as it is accompanied by other assumptions. It has, however, strongly influenced contemporary extrapolations of elastic hadronic amplitude to $t = 0$ (choice of its parameterizations) since its first application to experimental data. One should, therefore, look for description without this limitation and make corresponding comparisons.

6. *Determination of b-dependent probability functions of hadron collisions*
If the colliding objects are not spherically symmetrical and randomly oriented in space in the time of collision then one may expect that the particles collide elastically at a given value of impact parameter with some probability $P^{\rm el}(b)$. Miettinen tried to identify (without any justification) profile functions with the corresponding probabilities but without sufficient reasons. Even if profile functions (or other b-dependent quantities) have been calculated by many authors up to now it has been quite rare to find in corresponding papers at least some comments related to the actual meaning of these functions. Their relation to clearly defined b-dependent probabilities of corresponding collisions has not been given, which has strongly limited the possibilities of interpreting measured collision data, see chapter 5.

7. *Distribution of elastic scattering angles for a given impact parameter*
In description of elastic collisions one should take into account correlations between impact parameter value of colliding particles and angle deviations (values of t) of scattered particles, i.e., correlations between initial and final elastic states. Two particles may interact elastically at impact parameter b with probability $P^{\rm el}(b)$ and be scattered with a value of t in (rather broad) t-range. The corresponding t-distribution at each value of b may be denoted as $d_b(t)$. This t-distribution is different from that corresponding to t-dependent differential cross section (3.12) (elastic hadronic amplitude $F^{\rm N}(s,t)$) as the later one does not correspond to only one value of b. Standardly used FB transformation (3.66) and (3.74) connecting t-dependent elastic hadronic amplitude with b-dependent may, therefore, hardly

provide basis for determination of the functions $P^{\mathrm{el}}(b)$ and $d_b(t)$.

It is evident, due to the mentioned problems, that the usually applied theory of elastic collisions has remained practically in its initial stage. Many assumptions have been made use of to obtain agreement with some experimental data without testing their conformity with other experimental observations. Any assumptions concerning the structures of colliding objects have not been practically tested.

Any progress in the given area may consist evidently in abandoning corresponding mistaking assumptions and in analyzing systematically the dependence of collisions on impact parameter. Assumptions without clear physical meaning (arbitrarily chosen mathematical conditions like, e.g., a priori assumed t-dependence of elastic hadronic amplitude) should be substituted by new assumptions with direct relation to corresponding possible particle structures; purely mathematical-phenomenological descriptions should be substituted by ontological models of physical reality, see [285]. The outcome of collision models fitted to experimental data should have clear relation to particle structure while, e.g., the quantity $\rho(t = 0)$ commonly calculated up to now under influence of the approach of WY (see sect. 3.2) does not have such property. Any model of elastic collisions (even if based possibly on very different assumptions) should analyze collisions in dependence on impact parameter and be able to determine b-dependent probability function $P^{\mathrm{el}}(b)$ and the t-distribution $d_b(t)$ that might be further discussed as they strongly reflect the structure of colliding particles. It is necessary to evaluate newly all assumptions concerning description of elastic scattering, which includes the commonly applied optical theorem, too.

In the next chapter a very preliminary version of a model corresponding to the mentioned requirements will be presented. It is based on simple assumptions concerning some b-dependent collision characteristics that might be expected on the basis of ontological approach that represents the backgrounds of classical physics.

Chapter 7

New probabilistic model of elastic collisions

We have seen in chapter 6 that one of the main problems of contemporary descriptions of elastic particle collisions has been related to the fact that the influence of impact parameter has not been systematically taken into account. Some b-dependent functions have been derived but their physical meaning have been very unclear. Even if the given physical process has been commonly denoted as probabilistic the corresponding probabilities in dependence on impact parameter (or transition probabilities of initial state to final one) have not been determined from corresponding experimental data.

To overcome the mentioned difficulties new probabilistic model of elastic particle (proton) collisions has been recently proposed in [24] (some very first ideas may be found in [23]). In the quoted papers the model has been applied for guidance to a smaller part of elastic pp collisions data obtained at CERN ISR at the center-of-mass collision energy of 52.8 GeV (denoted also as 53 GeV).

In the following the model for short-ranged hadron (proton) collisions will be described to a greater detail (see sect. 7.1) and applied to the experimental data in wider region of $|t|$ values, see sect. 7.2. Some new open questions will be then discussed in sect. 7.3. Several concluding remarks will be contained in sect. 7.4.

7.1 Model formulation

7.1.1 Basic ideas

To obtain some further information about structure of particles from their mutual elastic collisions at given collision energy three important points concerning description of this physical process in dependence on impact parameter should be taken into account:

1. *Different frequency of initial two particle collision states distinguished by impact parameter*
   Initial two particle collision states are distributed according to experimental conditions and the corresponding b-distribution need to be taken into account correspondingly in descriptions of elastic collisions in order not to mix events at different impact parameters (see also comments related to factor $w(b)$ in chapter 5).

2. *b-dependent probabilities of collisions*
   In the collisions of two hadrons (protons) at higher energies two different (elastic

and inelastic) processes may exist. In standard ontological approach the collisions at very small impact parameter values should be mainly inelastic, while at higher impact parameters the elastic processes should prevail. No hadronic collisions should then exist at impact parameter values greater than $b^{\max}$ corresponding to maximum dimensions of colliding objects (range of short-ranged hadronic interaction). If the colliding hadrons are taken as normal matter objects, e.g., of ellipsoid-like shape (differently oriented in the space) then we may assume, too, that b-dependent probability of hadronic (elastic or inelastic) interaction $P^{\mathrm{tot}}(b)$ will be a non-increasing function of $b \in \langle 0, b^{\max}\rangle$. It is also natural to expect similarly that the ratio of elastic to total probability $P^{\mathrm{rat}}(b)$ at given b will be non-decreasing in the same impact parameter interval. The probability of elastic collision $P^{\mathrm{el}}(b)$ at given impact parameter is then given by product of the two monotone functions

$$P^{\mathrm{el}}(b) = P^{\mathrm{rat}}(b)\, P^{\mathrm{tot}}(b)\,. \tag{7.1}$$

The probability of inelastic processes as a function of impact parameter b may be then defined as (conservation of probability)

$$P^{\mathrm{inel}}(b) = P^{\mathrm{tot}}(b) - P^{\mathrm{el}}(b). \tag{7.2}$$

For short-ranged (contact) hadronic processes it should always hold $P^{\mathrm{tot}}(b) = P^{\mathrm{el}}(b) = P^{\mathrm{inel}}(b) = 0$ for any $b \geq b^{\max}$. It is evident that it should hold further: $P^{\mathrm{rat}}(b) = 1$ and $P^{\mathrm{tot}}(b) = 0$ at $b = b^{\max}$, and $P^{\mathrm{rat}}(b) = 0$ and $P^{\mathrm{tot}}(b) = 1$ at $b = 0$ (head on collisions). The values of the probabilities $P^{\mathrm{tot}}(b)$, $P^{\mathrm{el}}(b)$, $P^{\mathrm{inel}}(b)$ and function $P^{\mathrm{rat}}(b)$ may lie in the interval $\langle 0, 1\rangle$ in dependence on $b \in \langle 0, b^{\max}\rangle$.

3. *Distribution of elastic scattering angles for a given impact parameter*
   It is necessary to admit (for non-spherical particles) that initial two particle states characterized by a given b value may pass in the case of elastic processes to a continuous set of t values (if $P^{\mathrm{el}}(b) > 0$, the elastic probabilities at the limits of the given interval will tend to zero). The corresponding t-distribution $d_b(t)$ of t values for given impact parameter b (discussed in chapter 6) will have maximum at certain value of $t(b)$.

It is generally assumed that all hadrons consist of other objects that are bound strongly together. It holds also for protons which means that some changeable *internal structures* are to exist, which may influence the results in individual collisions, too. The contemporary models describe the corresponding processes practically in a phenomenological way representing individual colliding objects by one common average mathematical function. It will be shown in the following that more realistic description may be obtained if the existence of different internal structures will be taken into account. The measured elastic differential cross section of two colliding hadrons should be then interpreted as the sum of elastic collision channels corresponding to different combinations of internal hadron states.

There are, therefore, two main assumptions in the new model of elastic (hadron) collisions based fully on ontological approach:

1. hadrons may exist in different internal states which may behave differently in mutual collisions

2. the probability function $P^{\mathrm{tot}}(b)$ should be non-decreasing and the function $P^{\mathrm{rat}}(b)$ non-increasing in the interval $\langle 0, b^{\max}\rangle$ for each corresponding collision channel

The model will be described in more details in the following.

7.1.2 Frequencies and maximal dimensions of hadron states

We shall assume that the collision characteristics may be significantly influenced also by the instantaneous states of colliding hadrons and denote the corresponding probabilities (frequencies) of these states as p_k ($\sum_k p_k = 1$) for one particle and p_l ($\sum_l p_l = 1$) for the second one. If two particles of *different* types (e.g., proton and pion) collide then the individual probabilities of corresponding collision channels $r_{k,l}$ are equal to $p_k p_l$. In the case of two particles of the *same* type (e.g., two protons) one may write

$$r_{k,l} = \begin{cases} p_k p_l & \text{if } k = l \\ \\ 2 p_k p_l & \text{if } k \neq l,\ k < l \end{cases} . \tag{7.3}$$

The factor 2 in the last relation follows from the fact that for $k \neq l$ the cases with interchanged collision types k, l and l, k are the same and the corresponding probabilities may be summed, but in such a case it is necessary to introduce convention $k < l$ to count each *distinct* collision type only once. The two indexes k and l in $r_{k,l}$ may be, therefore, substituted for convenience by only one index j using a one-to-one correspondence $(k, l) \leftrightarrow j$. It holds $\sum_j r_j = 1$ if we sum over all possible collision types.

If we take the strong interaction as contact one (short-ranged) the maximum effective impact parameter for which two hadrons may still interact in their mutual collisions is equal to

$$b_{k,l}^{\max} = (d_k + d_l)/2. \tag{7.4}$$

where d_k (d_l) represents maximum size (dimension) that the corresponding hadron structure may exhibit. The two indexes k and l in $b_{k,l}^{\max}$ may be again substituted for convenience by only one index j ($b_{k,l}^{\max} \leftrightarrow b_j^{\max}$). The value of $b_j^{\max}$ may be, therefore, different for each j collision channel; it holds also for the b-dependent probabilities and other functions introduced in sect. 7.1.1.

7.1.3 Impact parameter and corresponding values of scattering angle

For the sake of simplicity we shell assume in the following that the value $t_j(b)$ represents the only t value for a given impact parameter and collision channel. The corresponding monotonic inverse function may be denoted as $b_j(t)$. The t-distribution $d_{b,j}(t)$ for a given j-th collision channel (as well as t-distribution $d_b(t)$ corresponding to all j channels and which has been mentioned in chapter 6) is given by a Dirac delta function in this special (simplified) case.

7.1.4 (Differential) cross sections and other hadronic quantities

It is then possible to write for elastic hadronic differential cross section corresponding to j-th collision channel

$$\frac{\mathrm{d}\sigma_j^{\mathrm{N}}(t)}{\mathrm{d}t} = 2\pi b_j(t) \frac{\mathrm{d}b_j(t)}{\mathrm{d}t} P_j^{\mathrm{el}}\left(b_j(t)\right) \tag{7.5}$$

where the factor $2\pi b$ represents frequency (weight $w(b)$) of initial collision states distinguished by impact parameter if the colliding particles are distributed uniformly in cross plane. This assumption represents good approximation in the case of short-ranged hadronic interactions in collision experiments where non-zero collision probabilities correspond to impact parameters less than several femtometers; the problem would be more complicated in the case of long-ranged Coulomb interaction. The elastic hadronic differential cross section of colliding protons is then given by the sum of individual contributions of all individual collision types

$$\frac{\mathrm{d}\sigma^{\mathrm{N}}(t)}{\mathrm{d}t} = \sum_j r_j \frac{\mathrm{d}\sigma_j^{\mathrm{N}}(t)}{\mathrm{d}t}. \tag{7.6}$$

The values of individual integrated cross sections may be calculated from corresponding probabilities for given j-th collision channel as (collision type $X = \mathrm{tot}, \mathrm{el}$ or inel)

$$\sigma_j^{\mathrm{X,N}} = 2\pi \int_0^{b_j^{\max}} b\mathrm{d}b \; P_j^{\mathrm{X}}(b). \tag{7.7}$$

Total, elastic and inelastic hadronic cross sections averaged over all j collision channels are then given by

$$\sigma^{\mathrm{X,N}} = \sum_j r_j \sigma_j^{\mathrm{X,N}}. \tag{7.8}$$

If two hadrons collide at given impact parameter b then the mean (overall) probability of individual collision kinds will be expressed as a weighted sum of all the individual hadronic collision channels

$$P^{\mathrm{X}}(b) = \sum_j r_j P_j^{\mathrm{X}}(b). \tag{7.9}$$

Function $P^{\mathrm{rat}}(b)$ mentioned in sect. 7.1.1 may be then defined using eqs. (7.1) and (7.9). Integrated cross sections given by eq. (7.8) may be written also as

$$\sigma^{\mathrm{X,N}} = 2\pi \int_0^{b^{\max}} b\mathrm{d}b \; P^{\mathrm{X}}(b). \tag{7.10}$$

To characterize further the behaviour of hadronic collisions in impact parameter space on the basis of the probabilistic model one may define n-th moment ($n > 1$) of impact parameter b for different processes ($X = \mathrm{tot}, \mathrm{el}$ or inel) in individual collision channels as

$$\langle b^n \rangle_j^{\mathrm{X}} = \frac{\int_0^{\infty} b^n \; w(b) P_j^{\mathrm{X}}(b)\mathrm{d}b}{\int_0^{\infty} w(b) P_j^{\mathrm{X}}(b)\mathrm{d}b} = \frac{\int_0^{b_j^{\max}} b^n \; w(b) P_j^{\mathrm{X}}(b)\mathrm{d}b}{\int_0^{b_j^{\max}} w(b) P_j^{\mathrm{X}}(b)\mathrm{d}b} \tag{7.11}$$

and corresponding averages over j for different processes as (using eq. (7.9))

$$\langle b^n \rangle^{\mathrm{X}} = \frac{\int_0^{\infty} b^n \; w(b) P^{\mathrm{X}}(b)\mathrm{d}b}{\int_0^{\infty} w(b) P^{\mathrm{X}}(b)\mathrm{d}b} = \frac{\sum_j r_j \int_0^{b_j^{\max}} b^n \; w(b) P_j^{\mathrm{X}}(b)\mathrm{d}b}{\sum_j r_j \int_0^{b_j^{\max}} w(b) P_j^{\mathrm{X}}(b)\mathrm{d}b}. \tag{7.12}$$

The mean impact parameters given by eqs. (7.11) and (7.12) may be again calculated for comparison with the factor (weight) $w(b) = 1$ and $w(b) = 2\pi b$ as it was discussed in chapter 5.

7.1.5 Coulomb and hadron interaction

If two protons collide then in addition to hadronic force the elastic collision process is influenced significantly also by Coulomb interaction mainly in the region of very small $|t|$ values. There is, however, great difference between these two kinds of interactions. While the Coulomb interaction acting also at rather great distances is usually taken as being well described with the help of potential formed by electrically charged matter objects the potential interpretation may be denoted as only approximate in the case of strong interactions, as it is evident that this interaction is to be taken practically as zero at any distance greater than dimensions of corresponding objects. Some new possibility of describing this contact characteristics of this strong force should be looked for.

The Coulomb and hadronic collision kinds may be taken, therefore, practically as mutually independent at *high* collision energies. The corresponding probabilities of the Coulomb or hadronic collisions in dependence on impact parameter may be summed for any impact parameter value at high collision energies (at least in a good approximation). The hadronic interaction is described using the j collision channels. To describe also the Coulomb effects separately for these collision channels would be needlessly complicated as the given contribution concerns rather small values of $|t|$ where only very small differences between individual channels may be expected. Consequently, we shall write for the elastic differential cross section which takes into account also Coulomb effect:

$$\begin{aligned}\frac{\mathrm{d}\sigma^{\mathrm{C+N}}(t)}{\mathrm{d}t} &= \frac{\mathrm{d}\sigma^{\mathrm{N}}(t)}{\mathrm{d}t} + \frac{\mathrm{d}\sigma^{\mathrm{C}}(t)}{\mathrm{d}t} \\ &= \sum_j r_j \frac{\mathrm{d}\sigma_j^{\mathrm{N}}(t)}{\mathrm{d}t} + \frac{\mathrm{d}\sigma^{\mathrm{C}}(t)}{\mathrm{d}t}\end{aligned} \tag{7.13}$$

where the Coulomb differential cross section will be established in sect. 7.2 directly as a part of fitted experimental data (measured $\mathrm{d}\sigma^{\mathrm{C+N}}(t)/\mathrm{d}t$).

In such a case it is, of course, necessary to devote sufficient attention to the parameterization of corresponding Coulomb part of fitting formula. It will be admitted to play a role only in the interval of very small values of $|t|$. It is further necessary to realize that it is not possible to use usual t-dependence of Coulomb differential cross section (3.26) requiring infinite value at $t = 0$ as such t value may occur only at impact parameter values going to infinity. However, in any real collision experiments the corresponding impact parameter values are limited by maximal distances between individual colliding objects in corresponding targets. It is evident that a great part of corresponding events will then represents the results of several subsequent collisions, see one of the problems discussed in chapter 6. Consequently, the region of very small (practically unmeasurable) values of $|t|$ may be represented approximately by a constant (maximum) value of $\mathrm{d}\sigma^{\mathrm{C}}(t)/\mathrm{d}t$ followed by steeper decrease with rising $|t|$. Single Coulomb scattering should then exist, which should be respected in the given formula, too.

There is no doubt that such a description of Coulomb effect is currently only very phenomenological and more detailed study should be devoted to interpretation of measured elastic differential cross section at very low values of $|t|$ in the future as will be further commented later in sect. 7.3.

7.2 Application of the probabilistic model to experimental pp data at 53 GeV

7.2.1 Choice of data and parameterizations of corresponding functions

As we have already mentioned, the given probabilistic model has been applied in [23] and then also in [24] to the pp data represented by measured elastic differential cross section obtained earlier at CERN ISR [8] at the energy of 52.8 GeV (denoted also as 53 GeV). The eikonal model has been applied to the same data in chapter 4. It has been shown in [24] that two proton states exhibiting the largest dimensions may be responsible for the part of measured elastic differential cross section data corresponding to $|t| \in \langle 0.00126, 1.25\rangle$ GeV^2 ($|t| = 0.00126$ GeV^2 being the lowest measured value at the given collision energy). In the following a more detailed analysis will be presented. We will show that if a further (third) proton state is taking into account then we may describe the measured elastic differential cross section in wider interval of $|t| \in \langle 0.00126,\ 5.\rangle$ GeV^2 which includes also observed dip-bump structure around $t = -1.375$ GeV^2.

If one proton in a k-state (k=1,2,3) collides with another proton in a l-state (l=1,2,3) we may define collision channel j using one-to-one correspondence $(k,l) \leftrightarrow j$ (where $k < l$) which will be used in the following: $(1,1) \leftrightarrow 1$, $(1,2) \leftrightarrow 2$, $(2,2) \leftrightarrow 3$, $(1,3) \leftrightarrow 4$, $(2,3) \leftrightarrow 5$ and $(3,3) \leftrightarrow 6$. We have thus 6 different hadronic collision channels that will be used to fit the given part of measured elastic differential cross section.

To apply the model to experimental data represented by measured elastic pp differential cross section it is necessary to parameterize suitably all corresponding functions needed to calculate Coulomb-nuclear differential cross section given by eq. (7.13). Our aim consists in describing truly the corresponding dependences. Consequently, our parametrization will be rather general. First of all flexible representations of all monotonous functions $P_j^{\mathrm{tot}}(b)$, $P_j^{\mathrm{rat}}(b)$ and $b_j(t)$ must be chosen; the following parameterizations will be used for the 6 individual collision channels

$$P_j^{\mathrm{tot}}(b) = \begin{cases} 1 & \text{if } 0 \le b \le \mu_{j,0} \\ \dfrac{(1+\mu_{j,3})}{\mathrm{e}^{\left(\mu_{j,1}(b-\mu_{j,0})\right)^{\mu_{j,2}}} + \mu_{j,3}} & \text{if } \mu_{j,0} < b < b_j^{\max} \\ 0 & \text{if } b \ge b_j^{\max} \end{cases} \tag{7.14}$$

$$P_j^{\mathrm{rat}}(b) = \frac{(1+\nu_{j,2})}{\mathrm{e}^{\left(\nu_{j,0}(b_j^{\max}-b)\right)^{\nu_{j,1}}} + \nu_{j,2}} \tag{7.15}$$

$$b_j(t) = b_j^{\max}\left(\frac{2}{\pi}\arccos\left[\left(\frac{|t|}{\lambda_{j,0}}\right)^{1/\lambda_{j,2}}\right]\right)^{1/\lambda_{j,1}} \tag{7.16}$$

where $\mu_{j,0..3}$, $\nu_{j,0..2}$ and $\lambda_{j,0..2}$ are free parameter sets that are to be determined from experimental data for each collision channel ($j = 1, ..., 6$) together with free parameters p_k and d_k ($k = 1, 2, 3$).

The remaining function which needs to be parameterized in applying our model to experimental data is Coulomb differential cross section $\mathrm{d}\sigma^{\mathrm{C}}(t)/\mathrm{d}t$. The following

parameterization has been chosen

$$\frac{\mathrm{d}\sigma^{\mathrm{C}}(t)}{\mathrm{d}t} = (\eta_0 + \eta_1|t|)\frac{1+\eta_2}{\mathrm{e}^{(\eta_3|t|)^{\eta_4}} + \eta_2} + \zeta_u(\zeta_0|t|)^{\zeta_1}\frac{1+\zeta_2}{\mathrm{e}^{(\zeta_3|t|)^{\zeta_4}} + \zeta_2} \tag{7.17}$$

where $\zeta_u = 1$ mb.GeV^{-2} and $\eta_{0..4}$ and $\zeta_{0..4}$ are additional free parameter sets.

In the presented preliminary model of hadron (pp) collisions some quite new physical ideas are considered and tested to initiate further study with the help of other experimental data (e.g., at different collision energies or for different particles). The number of free parameters used in the corresponding analysis may seem to be rather high. However, if the goal does not consist in testing some simplified mathematical model but actual complex physical mechanism is to be truly described the number of parameters should be regarded as quite irrelevant, especially if the possibilities of a new model in description of experimental data are to be demonstrated.

7.2.2 Elastic differential cross sections

The probabilistic model of elastic pp collisions characterized by eq. (7.13) has been fitted to experimental data at the given energy in the interval of $|t| \in \langle 0.00126,\, 5.\rangle$ GeV^2. Elastic hadronic differential cross sections $\mathrm{d}\sigma_j^{\mathrm{N}}(t)/\mathrm{d}t$ given by eq. (7.5) are plotted for all 6 distinct collision channels in fig. 7.1. The proper contributions of individual hadronic channels to measured differential cross section have been obtained after multiplying the pictured dependences by corresponding probabilities r_j. The complete differential cross section $\mathrm{d}\sigma^{\mathrm{C+N}}(t)/\mathrm{d}t$ represented in the figure by full line is in good agreement with the experimental data.

Separated Coulomb and nuclear elastic differential cross sections at lower values of $|t|$ are plotted in fig. 7.2. One may see that at very low values of $|t|$ the Coulomb effect prevails and exhibits some strong decreasing $|t|$-dependence. The elastic hadronic differential cross section rises from zero value of $|t|$ which is completely different t-dependence than the commonly assumed (quasi)exponential dependence in all contemporary models based on optical theorem (optical theorem not having been applied to in our probabilistic model for the reasons given in chapter 6). In the region of very small values of $|t|$ it holds $\mathrm{d}\sigma^{\mathrm{N}}(t)/\mathrm{d}t \approx r_1 \mathrm{d}\sigma_1^{\mathrm{N}}(t)/\mathrm{d}t$. The hadronic effect is then responsible for all higher values of $|t|$.

The dip-bump structure in the measured elastic differential cross section is shown in fig. 7.3. It is formed by hadronic collision channels $j = 4, 3$ and 5 in our fit; their proper contributions after multiplying by r_j being plotted.

The Coulomb interaction being responsible mainly for the lowest values of $|t|$ may be then described by formula (7.17) with the following values of free parameters:

$$\begin{aligned}
\eta_0 &= 1070 \text{ mb.GeV}^{-2},\\
\eta_1 &= 1.63 \times 10^6 \text{ mb.GeV}^{-4},\\
\eta_2 &= 388,\\
\eta_3 &= 1.42 \times 10^6 \text{ GeV}^{-2},\\
\eta_4 &= 0.291
\end{aligned}$$

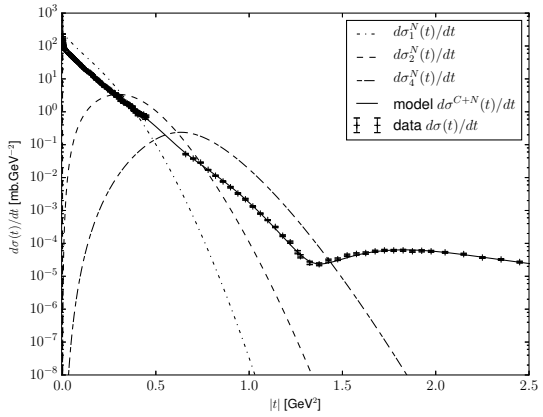

(a) $\mathrm{d}\sigma_j^{\mathrm{N}}(t)/\mathrm{d}t$ for $j = 1, 2, 4$

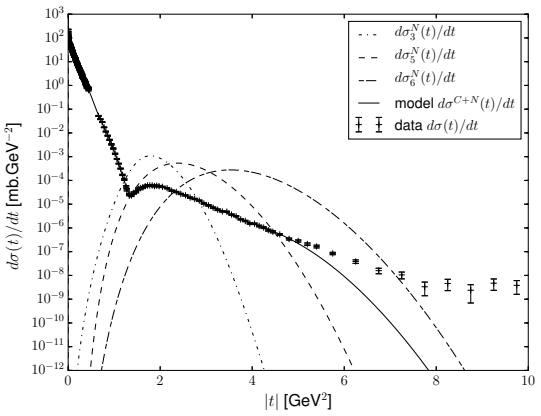

(b) $\mathrm{d}\sigma_j^{\mathrm{N}}(t)/\mathrm{d}t$ for $j = 3, 5, 6$

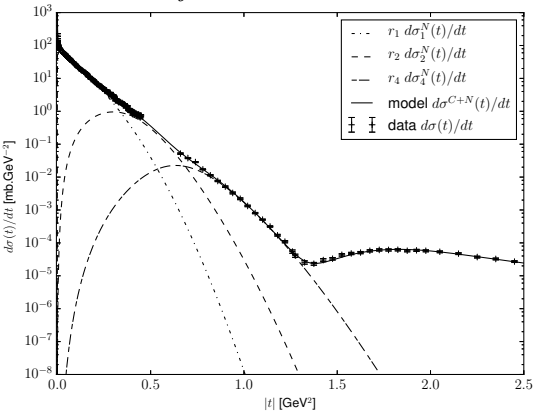

(c) Contributions $r_j \mathrm{d}\sigma_j^{\mathrm{N}}(t)/\mathrm{d}t$ for $j = 1, 2, 4$

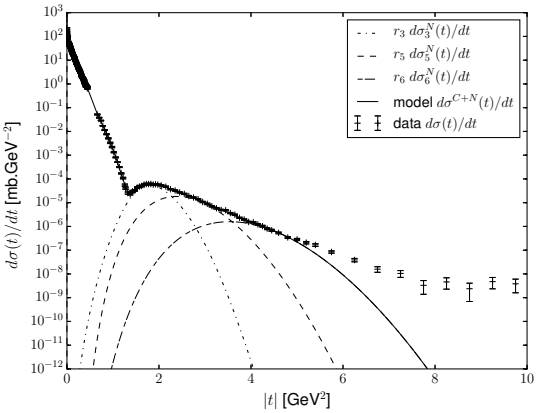

(d) Contributions $r_j \mathrm{d}\sigma_j^{\mathrm{N}}(t)/\mathrm{d}t$ for $j = 3, 5, 6$

Figure 7.1: Proton-proton elastic differential cross sections at energy of 53 GeV in probabilistic model. Individual points - experimental data, full line - probabilistic model fitted to experimental data, other lines - individual hadronic collision channels (top - individual differential cross sections $\mathrm{d}\sigma_j^{\mathrm{N}}(t)/\mathrm{d}t$, bottom - hadronic contributions $r_j \mathrm{d}\sigma_j^{\mathrm{N}}(t)/\mathrm{d}t$ to the differential cross $\mathrm{d}\sigma^{\mathrm{C+N}}(t)/\mathrm{d}t$).

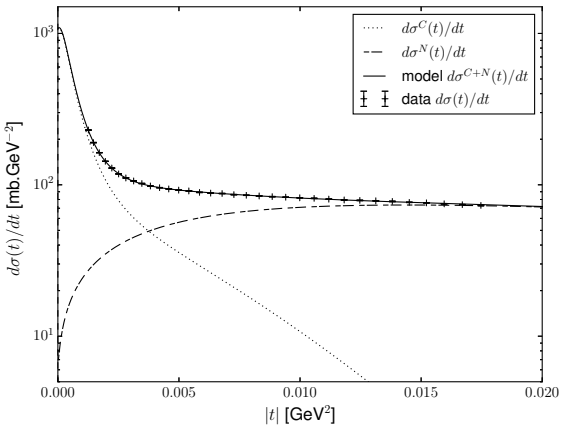

Figure 7.2: Separated Coulomb and nuclear effects in elastic pp scattering at 53 GeV; region of $|t|$ close to zero.

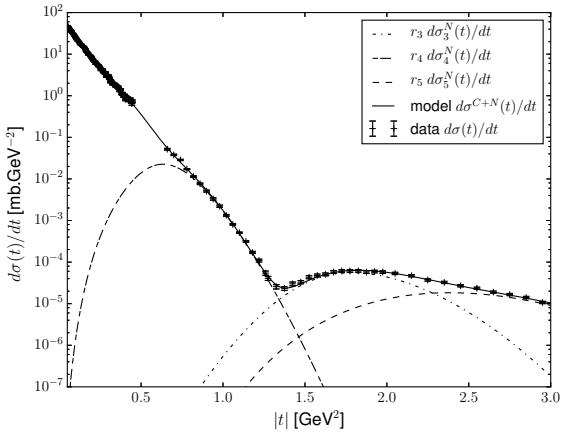

Figure 7.3: t-region around dip-bump structure in elastic pp scattering at 53 GeV; collision channels $j = 3, 4$ and 5.

and

$$\begin{aligned}\zeta_0 &= 4.00 \times 10^8 \mathrm{GeV}^{-2},\\ \zeta_1 &= 0.291,\\ \zeta_2 &= 1.46 \times 10^{-2},\\ \zeta_3 &= 176\ \mathrm{GeV}^{-2},\\ \zeta_4 &= 1.33\,.\end{aligned}$$

The numerical values of free parameters and other quantities characterizing the hadronic part will be presented in the following.

7.2.3 Characteristics of individual hadronic channels

The maximal dimensions of individual proton structures established on the basis of fitting the probabilistic model to the given experimental data are

$$d_1 = 1.976 \text{ fm}, \quad d_2 = 1.960 \text{ fm}, \quad d_3 = 1.948 \text{ fm}$$

and the corresponding probabilities are

$$p_1 = 0.63, \quad p_2 = 0.23, \quad p_3 = 0.076\,.$$

The probabilities of individual collision channels given by parameters r_j, see eq. (7.3), are shown in table 7.1. Corresponding maximal effective impact parameters $b_j^{\max}$ at which protons may still interact strongly (calculated with the help of eq. (7.4)) are shown in table 7.1, too; they equal approximately 2 fm, being slightly different for individual collision channels j. Total, elastic and inelastic hadronic cross sections having been calculated on the basis of eq. (7.7) for all considered collision channels j are also given in table 7.1.

According to our very rough model the proton at the moment of interaction with another proton may be in one of the three considered internal states with probability $p_1 + p_2 + p_3 = 0.93$. It means that in 7% of cases the proton is to be in different internal

j			1	2	3	4	5	6	$\sum_{j=1}^{6}$
k,l			1,1	1,2	2,2	1,3	2,3	3,3	
r_j		[1]	0.39	0.28	0.051	0.095	0.034	0.0057	0.86
$b_j^{\max}$		[fm]	1.976	1.968	1.960	1.962	1.954	1.948	-
$\sigma_j^{\mathrm{tot,N}}$		[mb]	87.0	60.4	58.6	46.8	35.2	32.4	-
$\sigma_j^{\mathrm{el,N}}$		[mb]	17.2	1.03	8.02×10^{-4}	8.64×10^{-2}	6.48×10^{-4}	4.65×10^{-4}	-
$\sigma_j^{\mathrm{inel,N}}$		[mb]	69.7	59.4	58.6	46.8	35.2	32.4	-
$r_j\sigma_j^{\mathrm{tot,N}}$		[mb]	34.1	17.1	3.00	4.44	1.20	0.186	60.0
$r_j\sigma_j^{\mathrm{el,N}}$		[mb]	6.76	0.291	4.104×10^{-5}	8.19×10^{-3}	2.22×10^{-5}	2.67×10^{-6}	7.06
$r_j\sigma_j^{\mathrm{inel,N}}$		[mb]	27.3	16.8	3.00	4.43	1.20	0.186	52.9
$\frac{r_j\sigma_j^{\mathrm{tot,N}}}{\sum_{j=1}^{6} r_j\sigma_j^{\mathrm{tot,N}}}$		[1]	0.57	0.29	0.050	0.074	0.020	3.1×10^{-3}	1
$\frac{r_j\sigma_j^{\mathrm{el,N}}}{\sum_{j=1}^{6} r_j\sigma_j^{\mathrm{el,N}}}$		[1]	0.96	0.041	5.8×10^{-6}	1.2×10^{-3}	3.1×10^{-6}	3.8×10^{-7}	1
$\frac{r_j\sigma_j^{\mathrm{inel,N}}}{\sum_{j=1}^{6} r_j\sigma_j^{\mathrm{inel,N}}}$		[1]	0.52	0.32	0.057	0.084	0.028	3.5×10^{-3}	1
$\langle b\rangle_j^{\mathrm{tot}}$	$w=1$	[fm]	0.833	0.696	0.684	0.612	0.531	0.509	-
$\langle b\rangle_j^{\mathrm{el}}$	$w=1$	[fm]	1.59	1.50	1.55	1.34	1.25	1.21	-
$\langle b\rangle_j^{\mathrm{inel}}$	$w=1$	[fm]	0.746	0.689	0.684	0.611	0.531	0.509	-
$\sqrt{\langle b^2\rangle_j^{\mathrm{tot}}}$	$w=1$	[fm]	0.964	0.806	0.791	0.708	0.616	0.591	-
$\sqrt{\langle b^2\rangle_j^{\mathrm{el}}}$	$w=1$	[fm]	1.59	1.50	1.55	1.34	1.25	1.21	-
$\sqrt{\langle b^2\rangle_j^{\mathrm{inel}}}$	$w=1$	[fm]	0.862	0.798	0.791	0.707	0.616	0.590	-
$\langle b\rangle_j^{\mathrm{tot}}$	$w=2\pi b$	[fm]	1.12	0.933	0.915	0.819	0.714	0.684	-
$\langle b\rangle_j^{\mathrm{el}}$	$w=2\pi b$	[fm]	1.59	1.50	1.55	1.34	1.25	1.21	-
$\langle b\rangle_j^{\mathrm{inel}}$	$w=2\pi b$	[fm]	0.996	0.923	0.915	0.818	0.714	0.684	-
$\sqrt{\langle b^2\rangle_j^{\mathrm{tot}}}$	$w=2\pi b$	[fm]	1.18	0.992	0.971	0.870	0.760	0.727	-
$\sqrt{\langle b^2\rangle_j^{\mathrm{el}}}$	$w=2\pi b$	[fm]	1.60	1.50	1.55	1.34	1.25	1.21	-
$\sqrt{\langle b^2\rangle_j^{\mathrm{inel}}}$	$w=2\pi b$	[fm]	1.06	0.980	0.971	0.869	0.761	0.727	-

Table 7.1: Values of some physically significant quantities characterising proton-proton collisions (individual hadronic collision channels) obtained as a result of the probabilistic model fitted to corresponding experimental data at energy of 53 GeV.

$w(b)$		1	$2\pi b$
$\langle b\rangle^{\mathrm{tot}}$	[fm]	0.752	1.02
$\langle b\rangle^{\mathrm{el}}$	[fm]	1.58	1.59
$\langle b\rangle^{\mathrm{inel}}$	[fm]	0.703	0.946
$\sqrt{\langle b^2\rangle^{\mathrm{tot}}}$	[fm]	0.877	1.09
$\sqrt{\langle b^2\rangle^{\mathrm{el}}}$	[fm]	1.59	1.59
$\sqrt{\langle b^2\rangle^{\mathrm{inel}}}$	[fm]	0.816	1.01

Table 7.2: Comparison of different definitions of mean impact parameter values corresponding to total, elastic and inelastic hadronic scattering calculated on the basis of eq. (7.12) for $n = 1, 2$ and $w(b) = 1$ or $w(b) = 2\pi b$ in the probabilistic model fitted to pp data at 53 GeV.

states. As to the collision processes the given 6 hadronic channels correspond to the probability $\sum_{j=1}^{6} r_j = p_1^2 + 2p_1p_2 + p_2^2 + 2p_1p_3 + 2p_2p_3 + p_3^2 = 0.86$. The additional internal states may be responsible for measured differential cross section outside the t-range considered by us (for $|t| > 5.$ GeV^2); partially also in combination with the three already considered proton states.

It means that the actual total and inelastic cross sections will be higher than the values introduced in table 7.1: $\sigma^{\mathrm{tot,N}} > \sum_{j=1}^{6} r_j \sigma_j^{\mathrm{tot,N}} = 60.0$ mb (resp. $\sigma^{\mathrm{inel}} > \sum_{j=1}^{6} r_j \sigma_j^{\mathrm{inel}} = 52.9$ mb), while the increase of elastic hadronic cross section will be negligible: $\sigma^{\mathrm{el,N}} \approx \sum_{j=1}^{6} r_j \sigma_j^{\mathrm{el,N}} = 7.06$ mb. The contributions of collision channels $j = 3, .., 6$ to $\sigma^{\mathrm{el,N}}$ are negligible, see table 7.1. The values of integrated cross sections corresponding to averaged values over the 6 collision channels may be compared to the values from our previous analysis based on the eikonal model, see table 7.2.

The b-dependent monotonous functions $P_j^{\mathrm{tot}}(b)$, $P_j^{\mathrm{rat}}(b)$ and $b_j(t)$ given by eqs. (7.14) to (7.16) for all the hadronic channels are plotted in fig. 7.4. The corresponding values of free parameters may be found in table 7.3. The basic properties of probabilities of total, elastic and inelastic events in dependence on impact parameter are quite similar for all the 6 collision channels and may be demonstrated using hadronic collision channel $j = 1$ which also contributes the most to the average behaviour of hadron collisions (averaged over the 6 collision channels) as it is the most frequent collision channel.

The three monotonous functions for $j = 1$ are shown in fig. 7.5 where also probabilities $P_1^{\mathrm{el}}(b)$ and $P_1^{\mathrm{inel}}(b)$ have been added. The greater change concerns the function $P_1^{\mathrm{el}}(b)$ (defined by eq. (7.1)); its maximum value (0.8 at around $b = 1.6$ fm) diminishes rather strongly for greater j values. This value $b = 1.6$ fm represents also approximate average value of impact parameter for elastic processes, see the values for $j = 1$ in table 7.1 and the average values over all the 6 considered j channels in table 7.2. The plot also shows that the probability of inelastic collision $P_1^{\mathrm{inel}}(b)$ and the total probability $P_1^{\mathrm{tot}}(b)$ are practically equal to 1 for impact parameters lower than approximately 1.4 fm; the probability $P_1^{\mathrm{el}}(b)$ of elastic events being practically zero in this interval. For all considered elastic hadronic channels the non-zero values of $P_1^{\mathrm{el}}(b)$ exist at impact parameters greater than approximately 0.75 fm, which may represent an additional important information in studying more detailed proton structure.

Probabilities of total, elastic and inelastic hadronic collision $P^{\mathrm{X}}(b)$ and ratio $P^{\mathrm{rat}}(b)$ given by eqs. (7.1) and (7.9) are plotted in fig. 7.6. Probability $P^{\mathrm{tot}}(b)$ is 0.86 at $b = 0$ which corresponds to $\sum_{j=1}^{6} r_j$, i.e., to the fact that only 3 internal proton states (6 collision channels) have been considered in our fit. As one can see from the plot the elastic probability $P^{\mathrm{el}}(b)$ is maximal at $b = 1.6$ fm which corresponds again to the already mentioned mean impact parameter of elastic collisions.

To characterize further basic behaviour of hadronic collisions in the impact parameter space one may calculate mean values of impact parameter for total, elastic and inelastic collisions according to eq. (7.11) for $n = 1, 2$ and weight $w(b)$ equal to 1 or $2\pi b$ with result shown in table 7.1. It holds $\langle b \rangle_j^{\mathrm{el}} > \langle b \rangle_j^{\mathrm{inel}}$ and $\sqrt{\langle b^2 \rangle_j^{\mathrm{el}}} > \sqrt{\langle b^2 \rangle_j^{\mathrm{inel}}}$ for each j-th collision channel. The same relation holds also for corresponding average values calculated using eq. (7.12), see table 7.2, i.e., elastic collisions are in average more peripheral than inelastic collisions (independently of used definition of mean impact parameter in this case). Values of mean impact parameters in table 7.2 may be compared to corresponding values in table 5.2 obtained on the basis of the eikonal model applied to the same experimental data.

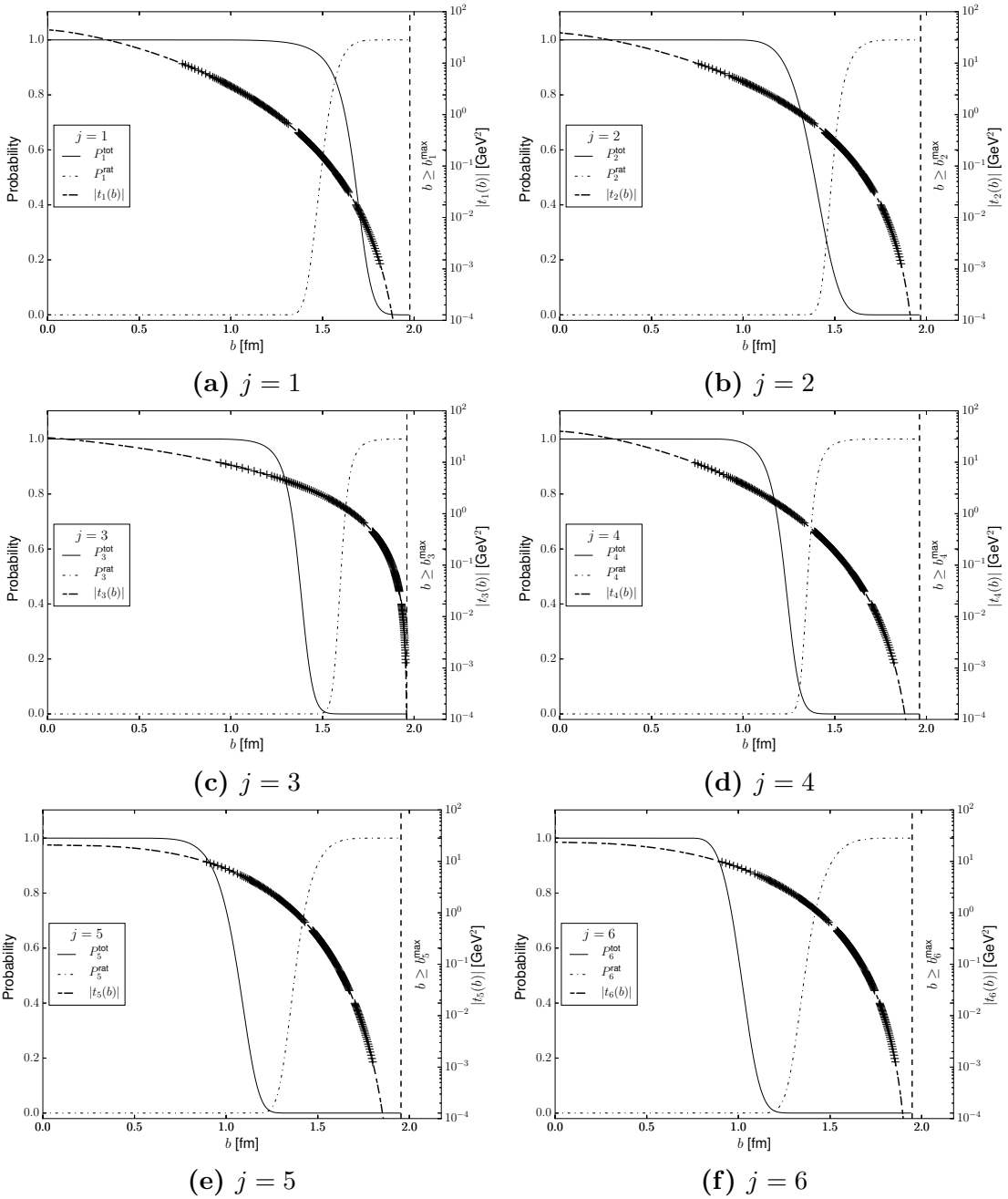

Figure 7.4: The shapes of all parameterized monotonous functions for individual collision channels fitted to experimental data. Full lines - $P_j^{\text{tot}}(b)$, dash-dotted line - $P_j^{\text{rat}}(b)$, dotted lines - $|t_j(b)|$; individual points - experimental values of $|t|$ corresponding to b values in individual channels.

		j	1	2	3	4	5	6
$P_j^{\mathrm{tot}}(b)$	$\mu_{j,0}$	[fm]	0.543	0.857	0.850	0.814	0.270	0.723
	$\mu_{j,1}$	[fm^{-1}]	1.05	1.78	2.85	3.53	1.27	3.24
	$\mu_{j,2}$	[1]	6.72	5.35	3.42	3.02	8.26	3.80
	$\mu_{j,3}$	[1]	25.1	0.151	50.2	21.1	0.975	0.241
$P_j^{\mathrm{rat}}(b)$	$\nu_{j,0}$	[fm^{-1}]	1.98	2.26	4.31	2.03	1.78	1.84
	$\nu_{j,1}$	[1]	8.16	6.77	3.42	6.49	6.91	5.64
	$\nu_{j,2}$	[1]	0.0993	4.27	93.3	50.7	1.51	2.67
$b_j(t)$	$\lambda_{j,0}$	[GeV^2]	44.3	38.4	30.0	40.0	20.7	23.4
	$\lambda_{j,1}$	[1]	0.703	0.686	0.597	0.712	1.44	1.19
	$\lambda_{j,2}$	[1]	4.38	3.64	1.76	4.11	5.56	4.03

Table 7.3: Values of free parameters of monotonous functions $P_j^{\mathrm{tot}}(b)$, $P_j^{\mathrm{rat}}(b)$ and $b_j(t)$ characterising hadronic pp collisions at 53 GeV in the impact parameter space for all 6 considered collision types given by parametrizations (7.14), (7.15) and (7.16).

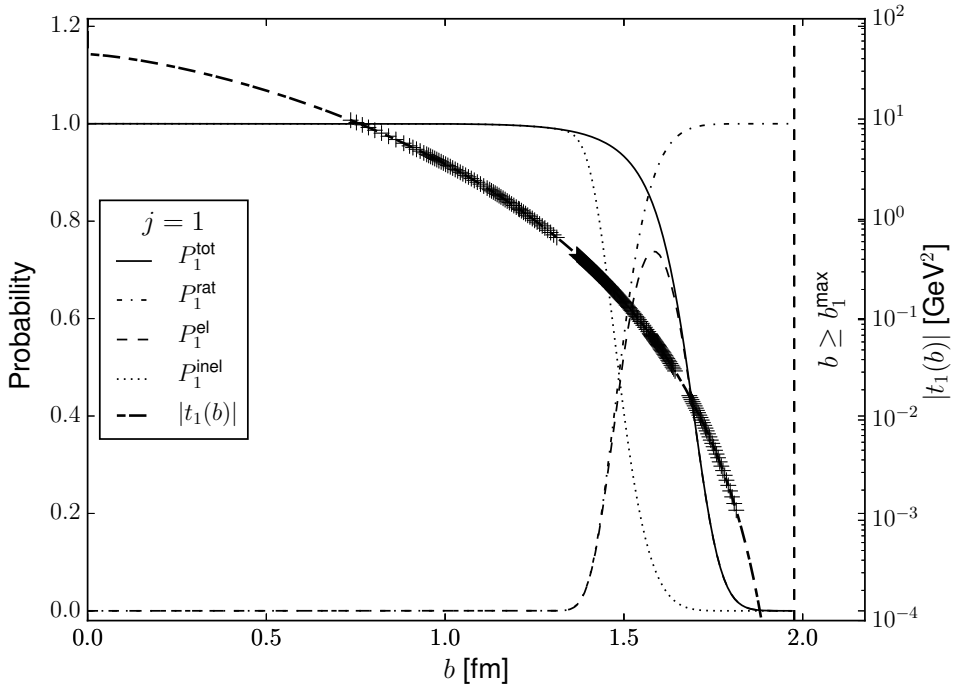

Figure 7.5: Probabilities in dependence on impact parameter b for hadronic collision state $j = 1$ and function $|t_1(b)|$; individual points represent then impact parameter values corresponding to the interval of measured values of $|t|$ (calculated with the help of $|b_1(t)|$ function).

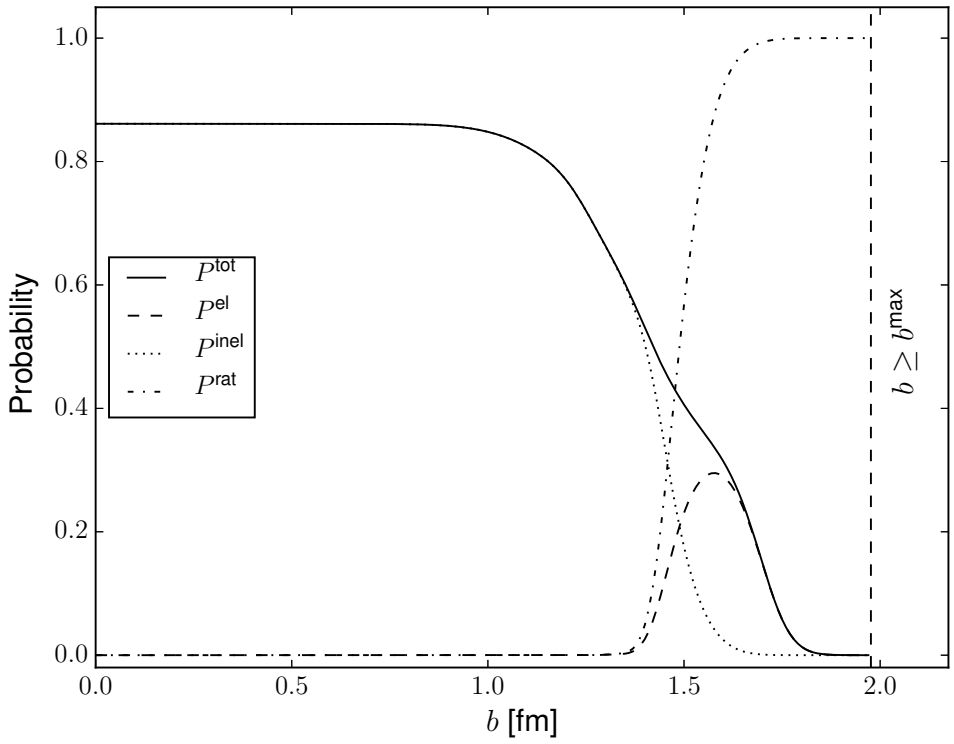

Figure 7.6: Probabilities of total, elastic and inelastic hadronic collision $P^{\mathrm{X}}(b)$ and function $P^{\mathrm{rat}}(b)$ calculated on the basis of eqs. (7.1) and (7.9) representing corresponding average probabilities over all hadronic collision channels considered in the fit.

7.3 Some open questions

The given numerical results in the presented form of the probabilistic model may be, of course, influenced rather strongly by our very rough approximation neglecting the distributions of transversal momenta at individual impact parameter values as it was discussed in sect. 7.1.3. It is possible, too, that in fact a greater number of different collision channels will correspond to the given t-range of differential cross section than in the case considered by us. The presented results must be, therefore, taken only as quite orientation ones. Our rough model shows, however, that the given probabilistic model represents a quite new way how to interpret the structures of protons more realistically.

One may expect that after introducing the t-distributions $d_{b,j}(t)$ for each j collision channel and for any b the model will be much more flexible and that the ambiguity during fitting will increase. It will be necessary to look for good agreement between results derived from experiments of other kinds, too.

In the new collision model some assumptions concerning the b-dependent probabilities has been formulated from the very beginning. It is then interesting to compare eqs. (7.2) and (7.10) for b-dependent probabilities to eqs. (3.72) and (3.73) for b-dependent profile functions as they have the same form. The b-dependent profile functions calculated on the basis of unitarity condition and FB transformation given by eqs. (3.66) and (3.68) have several properties as the b-dependent probability functions but the profile functions cannot be identified with the probabilities as it has been discussed in chapters 5 and 6.

If all known results concerning the fundamental particles are taken into account (including the results obtained on the basis of the probabilistic model) then the main question concerns the proper internal structure of proton. It is possible to assume that any fundamental particle consisting of some other constituents (some quasi-quarks) should exhibit internal evolution, which is required practically by the existence of different decay modes of unstable particles. It seems that during this evolution hadrons may exist also in the form of different parton pairs; these partons consisting of very (super) strongly bound quasi-quarks while the binding forces between them correspond approximately to known strong force. Otherwise, the corresponding hadrons may form a compact structure of very small dimensions. If an internal parton pair exists the corresponding hadron may be in the form of, e.g., ellipsoid of greater external changing dimensions. This variable dimensional size of proton may be then characterized by the functions $P_j^{\mathrm{tot}}(b)$ derived with the help of our probabilistic model.

Consequently, at least two kinds of forces should exist in any hadron, some super strong forces between quasi-quarks and some other (weaker) forces between corresponding partons (corresponding approximately to standard strong forces). However, these forces may be hardly defined with the help of a potential; a new description according to corresponding characteristics should be looked for (some kind of contact forces). If an excited hadron consists of a parton pair and the sum of rest masses of the two partons is less than that of corresponding hadron the hadron may decay (in an appropriate internal arrangement). In the case of stable hadrons (e.g., protons) the elastic collision evolution may become evident only by the different maximal dimensions (d_k) of individual structures or by different characteristics, e.g., by functions $P_j^{\mathrm{X}}(b)$ and $b_j(t)$. The corresponding parton pairs should change quite randomly; each alternative existing in average with probabilities p_k.

One should ask, of course, how the forces existing between individual partons and being practically equivalent to usual strong forces may be described. As already

mentioned they cannot by represented with the help of a potential as it is commonly assumed now (see also sect. 3.4). Corresponding potential should be surely equal to zero when the given partons are not in mutual contact. However, even if two partons are mutually bound (forming an oscillating closed system) it may happen in the case of unstable particles that this force may be coincidentally exceeded by internal energy of corresponding partons. The given property might influence partially also the elastic processes in the time when a contact force acts between two partons belonging to different colliding hadrons. Suitable description of this physical situation might represent quite new problem in the theory of fundamental particles.

Also the existence of different proton (hadron) states may open quite new question concerning the standard quantum theory. It is evident, e.g., that it is not possible to explain how different quantum states of hydrogen atom may be formed when an electron of very low energy is attracted to proton. It is necessary to take into account some mutual repulsive force (or a similar corresponding assumption) that should have to be efficient (in addition to attractive Coulomb interaction) at rather small distances corresponding to the dimensions of hydrogen atom.

However, a better explanation might be given by the impenetrability of both the attracted objects and by the existence of some weak adhesive contact force between electron and proton. In such a case the existence of possible different internal proton states might play important role and one should ask, e.g., whether the states derived from elastic collision data might be brought into correspondence to the energy spectrum of absorbed or emitted photons. It would be interesting to study similarly elastic collisions of anti-protons (and also $\bar{p}p$) and energy spectrum and other properties of anti-hydrogen which are currently studied by, e.g., Antihydrogen Laser PHysics Apparatus (ALPHA)[1] and Antihydrogen TRAP (ATRAP) experiments at CERN. Another interesting physical phenomena to study could be charge exchange collisions of various particles (mainly neutron-proton), see appendix A.2. It could shed more light on some questions related to both matter and anti-matter.

The other important problem concerns the region of very low scattering deviations. In our fit the Coulomb interaction is significant for measured values at $|t| < 0.015$ GeV^2; hadronic interaction prevails at higher values. However, only a purely phenomenological parametrization of the Coulomb differential cross section (7.17) has been used in our fit; much more detailed analysis should be devoted to this t region in the future. One should mainly ask how big role may be played by multiple Coulomb collisions in elastic collisions in the given region of t at given collision energy. In considering corresponding problems in a much broader context (see, e.g., probable dimension of hydrogen atom and the distances of hadronic objects in solid substances [24]) one may come to the conclusion that the proton might interact also weakly at greater distances; the strongly interacting matter being surrounded by other matter interacting only weakly. Consequently, much more detailed analysis of elastic processes of different particles at various energies (both low and high) in dependence on impact parameter will be required to estimate the forces corresponding to the Coulomb, weak and strong interactions.

The probabilistic model of elastic pp collisions was applied to experimental data at one collision energy of 53 GeV at the present. It will be important to apply it also to other data measured at other energy values to establish actual energy dependence of main characteristics. Especially the energy dependence of total probability of hadronic interactions $P_j^{\mathrm{tot}}(b)$ on impact parameter might represent very important information.

[1] ALPHA and ALFA are two different experiments (collaborations).

The corresponding analysis of elastic collision data with the help of new ontological model has opened in principle two new problems: existence of different internal proton (hadron) states and the question concerning actual dimension of individual protons. The answers to the given question might open also a quite new way in solving problems of contemporary quantum theory [24].

7.4 Summary

The probabilistic model of elastic collisions used in the preceding has been based in principle on two basic assumptions. Firstly, protons should exist in different states which behave slightly differently in mutual collisions and, secondly, that the functions $P_j^{\mathrm{tot}}(b)$ and $P_j^{\mathrm{rat}}(b)$ are monotonous in agreement with the standard ontological view concerning the corresponding closed matter objects.

The model proposed originally in [23] and later improved in [24] has been extended to describe greater part of differential elastic proton-proton cross section. It has been shown that the t-dependence of measured differential cross section in the region of $|t| \in \langle 0.00125,\, 5.\rangle$ GeV^2 (which includes also observed nontrivial dip-bump structure) may be explained on the basis of three most probable proton structures. To describe also the part corresponding to yet higher values of $|t|$ it will be necessary to take also other less probable proton states into account. All these structures seem to exhibit only very slightly different maximum dimensions (approximately 2 fm) but they behave rather differently in mutual collisions. The given structures are assumed to change randomly during internal proton evolution.

The given model has allowed deriving some further important characteristics, too, without adding any other assumptions; e.g., to derive the probabilities of different proton structures and the values of different kinds of cross sections in individual collision channels. Some values (e.g., total hadronic cross section) are, of course, different from those derived in the papers published in the past. One reason may consist in that our approach has been based for the sake of simplicity on a very rough approximation when for any impact parameter only the average value of momentum transfer has been taken into account and not the whole interval of corresponding t-values (see sect. 7.1.3).

However, these differences might have more serious reason, too. All earlier results (concerning elastic proton scattering) have involved some important assumptions that have not been sufficiently reasoned. They have been based, e.g., on the validity of optical theorem for hadronic interactions or on the standard diverging t-dependence of Coulomb differential cross section in the region of very small $|t|$ values (existing at infinite impact parameter values only, which does not correspond to experimental conditions) or on other problematic assumptions discussed in details in chapter 6 (in fact, the results obtained from the probabilistic model significantly helped to identify some main problems).

Even if the probabilistic model is only preliminary (it has not yet addressed all the problems and suggestions discussed in chapter 6) it has opened a new way how to interpret structure and interaction of fundamental particles in dependence on impact parameter. It is formulated and based only on assumptions and quantities of clear physical meaning which might be further discussed and tested.

Conclusion

In previous chapters different theoretical as well as experimental aspects of elastic pp collisions have been discussed in greater details with the aim to provide better insight into the given physical process.

In chapters 1 and 2 one could learn that the measurement of (elastic) pp collisions by TOTEM at the LHC is actually quite complex and requires understanding of the used detector apparatus as well as the accelerator. Good understanding of the measurement is also necessary for proper interpretation of the given physical process.

The description of elastic collisions of charged hadrons suggested by original West-Yennie model has influenced significantly many recent descriptions of elastic scattering in interpreting the b-dependence of elastic collisions, even if the corresponding dependence on impact parameter has not been tested and taken originally into account at all. Main limitations of the WY approach have been summarized in sect. 3.2. This approach has been used commonly in past for determination of total hadronic cross section (often denoted as "measurement" even if many unreasoned assumptions have been involved). More relevant value of the total cross section and all other characteristics of protons may be obtained when elastic scattering processes will be better understood.

The eikonal model described in sect. 3.4 has allowed studying the characteristics of elastic collisions of charged hadrons in dependence on impact parameter. In chapter 4 the model has been applied to experimental data at ISR energy of 53 GeV (for comparison of results obtained in the past) and at much higher energy of 8 TeV measured recently by TOTEM experiment at the LHC at CERN. Mean impact parameters corresponding to total, elastic and inelastic collisions have been determined at both the energy values together with corresponding profile functions characterising the collision frequency in dependence on impact parameter. It has been shown that the numerical results depend strongly not only on collision energy but also on some additional assumptions included in the given model. Two diverse types of fits have been performed at both the energies to demonstrate different interpretation possibilities of the given physical process. One has corresponded to commonly used assumptions included in many phenomenological models which lead to central character of elastic collisions. The second type of fits has explicitly showed that experimental data may be described equally well while the interpretation of the collisions in dependence on impact parameter is completely different - elastic collisions being more peripheral than inelastic ones.

Eikonal model analysis of experimental data with the help of eqs. (3.53) to (3.55) has been done already earlier in [20]. However, several different alternatives of the peripheral behavior at 53 GeV have been newly shown in chapter 4. In [20] only *electric* form factors have been taken into account. It has been also newly shown that addition of *magnetic* form factors does not lead to significant change of determined amplitude $F^{\mathrm{N}}(s,t)$ (at both 53 GeV and 8 TeV). For the purpose of this analysis integral $I(t,t')$ defined by eq. (3.55) has been calculated also analytically for one suitable parameterization of the

electromagnetic form factors, see sect. 3.4.2. The whole eikonal model approach has been revisited and prepared (see also [21]) for the analysis of pp elastic scattering at the LHC energies, see the very first results of similar analysis of 8 TeV data measured by TOTEM in [36]. One may see very significant change of several quantities characterizing proton collisions with rising energy by comparing the results of the performed eikonal model analysis at 53 GeV and 8 TeV.

The eikonal model has allowed determining some characteristics in dependence on impact parameter but the relation of some b-dependent functions (e.g., profile functions) to corresponding b-dependent probabilities $P^{\mathrm{el}}(b)$ and t-distribution for a given impact parameter $d_b(t)$ has not been established with sufficient reliability. It means that even if the collision process has been denoted as probabilistic the corresponding probabilities have not been determined. It has been shown, however, that the often proclaimed centrality of elastic collisions between fundamental particles has followed from a series of assumptions that may hardly correspond to situation in matter reality as it was pointed out for the first time already in 1981, see chapter 5. Some other fundamental open problems contained in all contemporary descriptions of elastic collisions have been identified and formulated to a greater detail in chapter 6, see also [22, 51]. It is possible to say that the main source of problems has been related to the fact that the dependence of elastic collisions on impact parameter has not been systematically taken into account and studied in corresponding analyzes (models) of experimental data.

As to the fundamental particles it is possible to say, too, that at the present significant progress may be expected from the study of elastic collisions. More general models trying to solve the newly identified problems in chapter 6 and allowing testing some new assumptions concerning the influence of impact parameter values on elastic collisions should be looked for. One should keep in mind that some quantities (e.g., total hadronic cross section) have always been determined on the basis of measured elastic collisions, see detailed discussion in sect. 3.5. New view and new possibilities will be opened by comparing the results obtained with the help of these models to the contemporary results. Some first steps in this direction have been done in chapter 7 where the new preliminary probabilistic model of elastic collisions in dependence on impact parameter has been introduced.

Bibliography

[1] E. Rutherford, "LXXIX. The scattering of α and β particles by matter and the structure of the atom", Philosophical Magazine Series 6 **21**, 669–688 (1911).

[2] E. L. Feinberg and I. Pomerančuk, "High energy inelastic diffraction phenomena", Il Nuovo Cimento (1955-1965) **3**, 652–671 (1956).

[3] M. L. Good and W. D. Walker, "Diffraction dissociation of beam particles", Phys. Rev. **120**, 1857–1860 (1960).

[4] U. Amaldi, P. Bryant, P. Darriulat, and K. Hubner, eds., *40th Anniversary of the First Proton-Proton Collisions in the CERN Intersecting Storage Rings (ISR). Proceedings, Colloquium, Geneva, Switzerland, January 18, 2011*, CERN-2012-004, arXiv:1206.4876 (2012).

[5] P. Desgrolard, M. Giffon, and E. Martynov, "Elastic pp and $\bar{p}p$ scattering in the modified additive quark model", The European Physical Journal C - Particles and Fields **18**, 359–367 (2000).

[6] A. Bohm et al., "Observation of a diffraction minimum in the proton-proton elastic scattering at the ISR", Phys. Lett. B **49**, 491–496 (1974).

[7] M. K. Carter, P. D. B. Collins, and M. R. Whalley, "Compilation of Nucleon-Nucleon and Nucleon-Antinucleon Elastic Scattering Data", RAL-86-002 (1986).

[8] J. Bystricky et al., "Nucleon nucleon and kaon nucleon scattering", edited by H. Schopper, part of Landolt-Börnstein - Group I Elementary Particles, Nuclei and Atoms, Vol. 9a, doi:10.1007/b19945 (1980).

[9] W. F. Baker et al., "Observation of structure in large-momentum-transfer $\pi^- p$ elastic scattering at 200 GeV/c", Phys. Rev. Lett. **47**, 1683–1686 (1981).

[10] R. Rubinstein et al., "Large-momentum-transfer elastic scattering of $\pi^\pm$, $K^\pm$, and $p^\pm$ on protons at 100 and 200 GeV/c", Phys. Rev. D **30**, 1413–1432 (1984).

[11] Z. Asad et al., "Pion-proton elastic scattering at 20 and 50 GeV/c incident momenta in the momentum transfer range $0.7 < |t| < 8.0$ $(\mathrm{GeV/c})^2$", Phys. Lett. B **118**, 442–446 (1982).

[12] Z. Asad et al., "New results on kaon-proton elastic scattering at large momentum transfers", Phys. Lett. B **123**, 265–268 (1983).

[13] C. Broll, "A study of the reaction pp $\rightarrow$ p(n π^+) at the CERN intersecting storage rings", Ann. Phys. (Les Ulis) **1**, 5–72 (1976).

[14] G. B. West and D. R. Yennie, "Coulomb interference in high-energy scattering", Phys. Rev. **172**, 1413–1422 (1968).

[15] H. Miettinen, "Impact structure of diffraction scattering", CERN-TH-1864 (1974).

[16] H. Miettinen, "Geometrical description of hadronic collisions", Acta Physica Polonica **B6**, 625 (1975).

[17] A. Giovannini, G. Mantovani, and S. Ratti, "Old And New Variables, Old And New Optical Concepts In High-energy Hadron Hadron Interactions", La Rivista del Nuovo Cimento **2N10**, 1–99 (1979).

[18] G. Giacomelli and M. Jacob, "Physics at the CERN ISR", Phys. Rept. **55**, 1–132 (1979).

[19] V. Kundrát, M. Lokajíček, and M. V. Lokajíček, "Are elastic collisions central or peripheral?", Czech. J. Phys. **B31**, 1334 (1981).

[20] V. Kundrát and M. V. Lokajíček, "High-energy scattering amplitude of unpolarized and charged hadrons", Z. Phys. **C63**, 619–630 (1994).

[21] J. Procházka and V. Kundrát, "Eikonal model analysis of elastic hadron collisions at high energies", arXiv: hep-th/1606.09479 (2016).

[22] J. Procházka, M. V. Lokajíček, and V. Kundrát, "Dependence of elastic hadron collisions on impact parameter", Eur. Phys. J. Plus **131**, 147 (2016), see also arXiv: hep-ph/1509.05343 (2015).

[23] M. V. Lokajíček and V. Kundrát, "Elastic pp scattering and the internal structure of colliding protons", arXiv: hep-ph/0909.3199 (2009).

[24] M. V. Lokajíček, V. Kundrát, and J. Procházka, "Schrödinger equation and (future) quantum physics", in *Advances in quantum mechanics*, edited by P. Bracken (InTech Publisher, 2013), pp. 105–132.

[25] J. Procházka, "Elastic hadron scattering at high energies", Bachelor thesis (Charles University, Prague, 2007).

[26] J. Procházka, "Elastic proton collisions at high energies", MA thesis (Charles University, Prague, 2009).

[27] TOTEM Collaboration, "Proton-proton elastic scattering at the LHC energy of $\sqrt{s} = 7$ TeV", Europhys. Lett. **95**, 41001 (2011).

[28] TOTEM Collaboration, "First measurement of the total proton-proton cross section at the LHC energy of $\sqrt{s} = 7$ TeV", Europhys. Lett. **96**, 21002 (2011).

[29] TOTEM Collaboration, "Measurement of the forward charged-particle pseudorapidity density in pp collisions at $\sqrt{s} = 7$ TeV with the TOTEM experiment", Europhys. Lett. **98**, 31002 (2012).

[30] TOTEM Collaboration, "Measurement of proton-proton elastic scattering and total cross-section at $\sqrt{s} = 7$ TeV", Europhys. Lett. **101**, 21002 (2013).

[31] TOTEM Collaboration, "Measurement of proton-proton inelastic scattering cross-section at $\sqrt{s} = 7$ TeV", Europhys. Lett. **101**, 21003 (2013).

[32] TOTEM Collaboration, "Luminosity-independent measurements of total, elastic and inelastic cross-sections at $\sqrt{s} = 7$ TeV", Europhys. Lett. **101**, 21004 (2013).

[33] TOTEM Collaboration, "A luminosity-independent measurement of the proton-proton total cross-section at $\sqrt{s} = 8$ TeV", Phys. Rev. Lett. **111**, 012001 (2013).

[34] TOTEM Collaboration, "Double diffractive cross-section measurement in the forward region at LHC", Phys. Rev. Lett. **111**, 262001 (2013), see also CERN-PH-EP-2013-170, arXiv:1308.6722.

[35] TOTEM Collaboration, "Evidence for non-exponential elastic proton-proton differential cross section at low $|t|$ and $\sqrt{s} = 8$ TeV by TOTEM", Nucl. Phys. B **899**, 527–546 (2015), see also CERN-PH-EP-2015-083, arXiv:1503.08111.

[36] TOTEM Collaboration, "Measurement of elastic pp scattering at $\sqrt{s} = 8$ TeV in the Coulomb-nuclear interference region – determination of the ρ-parameter and the total cross-section", CERN-PH-EP-2015-325 (2015).

[37] TOTEM Collaboration, "Status of the TOTEM experiment at LHC", Nuclear Instruments and Methods in Physics Research A **718**, 21–25 (2013).

[38] TOTEM Collaboration, "Performance of the TOTEM detectors at the LHC", International Journal of Modern Physics A **28**, 1330046 (2013), see also CERN-PH-EP-2013-173, arXiv:1310.2908.

[39] TOTEM Collaboration, *TOTEM Upgrade Proposal*, CERN-LHCC-2013-009, LHCC-P-007 (Geneva, June 2013).

[40] CMS and TOTEM Collaborations, "CMS-TOTEM Precision Proton Spectrometer: Technical Design Report", CERN-LHCC-2014-021, TOTEM-TDR-003, CMS-TDR-13 (2014).

[41] TOTEM Collaboration, "Timing Measurements in the Vertical Roman Pots of the TOTEM Experiment: Technical Design Report", CERN-LHCC-2014-020, TOTEM-TDR-002 (2014).

[42] CMS and TOTEM Collaborations, "Measurement of pseudorapidity distributions of charged particles in proton-proton collisions at $\sqrt{s} = 8$ TeV by the CMS and TOTEM experiments", Eur. Phys. J. C **74**, 3053 (2014).

[43] TOTEM Collaboration, "Measurement of the forward charged particle pseudorapidity density in pp collisions at $\sqrt{s} = 8$ TeV using a displaced interaction point", Eur. Phys. J. **C75**, 126 (2014), see also CERN-PH-EP-2014-260, arXiv:1411.4963.

[44] TOTEM Collaboration, "LHC optics measurement with proton tracks detected by the Roman pots of the TOTEM experiment", New Journal of Physics **16**, 103041 (2014), see also CERN-PH-EP-2014-066, arXiv:1406.0546.

[45] J. Procházka (TOTEM Collaboration), "Total pp cross section at TOTEM", in Proceedings of the Workshop Forward Physics at the LHC, La Biodola, Elba Island, Italy, May 27-29, 2010, edited by F. Ferro and S. Lami, arXiv: hep-ex/1012.5169 (2010), pp. 36–43.

[46] J. Procházka (TOTEM Collaboration), "Diffraction and Forward Physics at TOTEM", Workshop on QCD at Cosmic Energies - VI, Paris, France, 14 - 17 May (2013), https://indico.cern.ch/event/252570/.

[47] J. Procházka, "Elastic pp scattering at 8 TeV in the Coulomb-nuclear interference region measured by TOTEM", LHCC students poster session, CERN, Mar (2016), `https://indico.cern.ch/event/491582/`.

[48] J. Kašpar, V. Kundrát, M. Lokajíček, and J. Procházka, "Phenomenological models of elastic nucleon scattering and predictions for LHC", Nucl.Phys. **B843**, 84–106 (2011).

[49] V. Kundrát, M. Lokajíček, J. Kašpar, and J. Procházka, "Problems of phenomenological description of elastic pp scattering at the LHC; predictions of contemporary models", in Proceedings of the Workshop Forward Physics at the LHC, La Biodola, Elba Island, Italy, May 27-29, 2010, edited by F. Ferro and S. Lami, arXiv: hep-ex/1012.5169 (2010), pp. 26–35.

[50] M. V. Lokajíček, V. Kundrát, and J. Procházka, "Elastic hadron scattering and optical theorem", arXiv: 1403.1809 (2014).

[51] J. Procházka, V. Kundrát, and M. V. Lokajíček, "Elastic scattering of hadrons without optical theorem", arXiv: 1502.00468 (2015).

[52] R. Brun and F. Rademakers, "ROOT: An object oriented data analysis framework", Nucl. Instrum. Meth. **A389**, 81–86 (1997), see also `http://root.cern.ch`.

[53] E. Jones, T. Oliphant, P. Peterson, et al., *SciPy: open source scientific tools for Python*, `scipy.org`, 2001–.

[54] F. James and M. Roos, "Minuit - a system for function minimization and analysis of the parameter errors and correlations", Computer Physics Communications **10**, 343–367 (1975).

[55] *Subversion (version control system)*, `subversion.apache.org`.

[56] H. Krekel et al., *Pytest (full-featured python testing tool)*, `pytest.org`.

[57] *Jenkins (automation server)*, `jenkins.io`.

[58] L. Evans and P. Bryant, "LHC Machine", Journal of Instrumentation **3**, S08001 (2008).

[59] The LHC study group, *The Large Hadron Collider: Conceptual Design*, edited by T. S. Pettersson and P. Lefevre, CERN-AC-95-05 LHC (Geneva, Oct. 1995).

[60] O. S. Bruning et al., eds., *LHC Design Report Volume I: The LHC Main Ring* (CERN, Geneva, 2004).

[61] O. S. Bruning et al., eds., *LHC Design Report Volume II: The LHC Infrastructure and General Services* (CERN, Geneva, 2004).

[62] M. Benedikt et al., eds., *LHC Design Report Volume III: The LHC Injector Chain* (CERN, Geneva, 2004).

[63] J. Bosser et al., "LHC beam instrumentation: Conceptual design report", CERN-LHC-PROJECT-REPORT-370 (2000).

[64] K. Hanke, M. Chanel, and K. Schindl, "The PS Booster hits 40", CERN Courier **52N7**, 33–37 (2012).

[65] ALICE Collaboration, "The ALICE experiment at the CERN LHC", Journal of Instrumentation **3**, S08002 (2008).

[66] ATLAS Collaboration, "The ATLAS Experiment at the CERN Large Hadron Collider", Journal of Instrumentation **3**, S08003 (2008).

[67] CMS Collaboration, "The CMS experiment at the CERN LHC", Journal of Instrumentation **3**, S08004 (2008).

[68] LHCb Collaboration, "The LHCb detector at the LHC", Journal of Instrumentation **3**, S08005 (2008).

[69] LHCf Collaboration, "The LHCf detector at the CERN Large Hadron Collider", Journal of Instrumentation **3**, S08006 (2008).

[70] MoEDAL Collaboration, "Technical Design Report of the MoEDAL Experiment", CERN-LHCC-2009-006, MoEDAL-TDR-001 (2009).

[71] TOTEM Collaboration, "The TOTEM experiment at the CERN Large Hadron Collider", Journal of Instrumentation **3**, S08007 (2008).

[72] ATLAS Collaboration, *ATLAS Forward Detectors for Measurement of Elastic Scattering and Luminosity*, Technical Design Report ATLAS-TDR-18 CERN-LHCC-2008-004 (CERN, Geneva, 2008).

[73] K. Wille, *The physics of particle accelerators: an introduction* (Oxford University Press, Oxford, 2000).

[74] E. J. N. Wilson, *An Introduction to Particle Accelerators* (Oxford University Press, Oxford, 2001).

[75] H. Wiedemann, *Particle accelerator physics*, 3rd ed. (Springer-Verlag Berlin Heidelberg, 2007).

[76] D. Brandt, ed., *Intermediate accelerator physics. Proceedings, CERN Accelerator School, Zeuthen, Germany, September 15-26, 2003*, CERN-2006-02 (2006).

[77] D. Möhl, "Sources of emittance growth", in Intermediate accelerator physics. Proceedings, CERN Accelerator School, Zeuthen, Germany, September 15-26, 2003, edited by D. Brandt, CERN-2006-02 (2006), pp. 245–269.

[78] F. Roncarolo, "Accuracy of the transverse emittance measurements of the CERN Large Hadron Collider", PhD thesis (SB, Lausanne, 2005).

[79] J. Wenninger, "Energy Calibration of the LHC Beams at 4 TeV", CERN-ATS-2013-040 (2013).

[80] R. Schmidt and W. Herr, "Experience at CERN with luminosity monitoring and calibration, ISR, SPS proton antiproton collider, LEP, and comments for LHC...", in LHC Lumi Days: LHC Workshop on LHC Luminosity Calibration, 13 - 14 Jan 2011, edited by H. Burkhardt, M. Ferro-Luzzi, A. Macpherson, and M. Mangano, CERN-Proceedings-2011-001 (CERN, 2011), pp. 95–97.

[81] O. Napoly, "The luminosity for beam distributions with error and wake field effects in linear colliders", Part. Accel. **40**, 181–203 (1993).

[82] W. Herr and B. Muratori, "Concept of luminosity", in Intermediate accelerator physics. Proceedings, CERN Accelerator School, Zeuthen, Germany, September 15-26, 2003, edited by D. Brandt, CERN-2006-02 (2006), pp. 361–378.

[83] W. Kozanecki et al., "Interaction-point phase-space characterization using single-beam and luminous-region measurements at PEP-II", Nucl. Instrum. Meth. **A607**, 293–321 (2009).

[84] S. M. White, "Determination of the absolute luminosity at the LHC", CERN-THESIS-2010-139, LAL-10-154, PhD thesis (Orsay, Universite Paris-Sud 11, 2010).

[85] V. Balagura, "Notes on van der Meer Scan for absolute luminosity measurement", Nucl. Instrum. Meth. **A654**, 634–638 (2011).

[86] C. Møller, "General properties of the characteristic matrix in the theory of elementary particles I., K. Dan. Vidensk. Selsk.", Mat. Fys. Medd. (1945).

[87] D. Belohrad, "Beam charge measurements", CERN-BE-2011-019 (2011).

[88] G. Anders et al., "LHC bunch current normalisation for the April-May 2010 luminosity calibration measurements", CERN-ATS-Note-2011-004 PERF, BCNWG Note 1 (2011).

[89] A. Alice et al., "LHC bunch current normalisation for the October 2010 luminosity calibration measurements", CERN-ATS-Note-2011-016 PERF, BCNWG Note 2 (2011).

[90] G. Anders et al., "Study of the relative LHC bunch populations for luminosity calibration", CERN-ATS-Note-2012-028 PERF, BCNWG Note 3 (2012).

[91] A. Alici et al., "Study of the LHC ghost charge and satellite bunches for luminosity calibration", CERN-ATS-Note-2012-029 PERF, BCNWG Note 4 (2012).

[92] S. van der Meer, "Calibration of the effective beam height in the ISR", CERN-ISR-PO-68-31, ISR-PO-68-31 (1968).

[93] C. Rubbia, "Measurement of the luminosity of p$-\bar{p}$ collider with a (generalized) Van der Meer Method", CERN-p$\bar{p}$-Note-38 (1977).

[94] H. Burkhardt and P. Grafstrom, "Absolute luminosity from machine parameters", CERN-LHC-PROJECT-REPORT-1019 (2007).

[95] S. Mättig, "Luminosity measurement with the ATLAS detector", PhD thesis (Hamburg, University of Hamburg, 2012).

[96] M. Ferro-Luzzi, "Proposal for an absolute luminosity determination in colliding beam experiments using vertex detection of beam-gas interactions", Nucl. Instrum. Meth. **A553**, 388–399 (2005).

[97] LHCb Collaboration, "Prompt K_s^0 production in pp collisions at $\sqrt{s} = 0.9$ TeV", Phys.Lett. **B693**, 69–80 (2010).

[98] C. Barschel, "Precision luminosity measurement at LHCb with beam-gas imaging", CERN-THESIS-2013-301, PhD thesis (RWTH Aachen U., 2014).

[99] CMS Collaboration, "Measurement of CMS Luminosity", CMS-PAS-EWK-10-004 (2010).

[100] CMS Collaboration, "Absolute luminosity normalization", CERN-CMS-DP-2011-002 (2011).

[101] CMS Collaboration, "Absolute calibration of luminosity measurement at CMS: summer 2011 update", CMS-PAS-EWK-11-001 (2011).

[102] CMS Collaboration, "Absolute calibration of the luminosity measurement at CMS: winter 2012 update", CMS-PAS-SMP-12-008 (2012).

[103] CMS Collaboration, "CMS Luminosity Based on Pixel Cluster Counting - Summer 2012 Update", CMS-PAS-LUM-12-001 (2012).

[104] CMS Collaboration, "CMS Luminosity Based on Pixel Cluster Counting - Summer 2013 Update", CMS-PAS-LUM-13-001 (2013).

[105] CMS Collaboration, "Luminosity Calibration for the 2013 Proton-Lead and Proton-Proton Data Taking", CMS-PAS-LUM-13-002 (2014).

[106] ATLAS Collaboration, "Improved luminosity determination in pp collisions at $\sqrt{s} = 7$ TeV using the ATLAS detector at the LHC", Eur.Phys.J. **C73**, 2518 (2013).

[107] P. Hopchev, "Absolute luminosity measurements at LHCb", CERN-THESIS-2011-210, PhD thesis (Grenoble U., Grenoble, 2011).

[108] H. Burkhardt, M. Ferro-Luzzi, A. Macpherson, and M. Mangano, eds., *LHC Lumi Days: LHC Workshop on LHC Luminosity Calibration, 13 - 14 Jan 2011*, CERN-Proceedings-2011-001, CERN (CERN, Geneva, 2011).

[109] LHCb Collaboration, "Precision luminosity measurements at LHCb", Journal of Instrumentation **9**, P12005 (2014), see also LHCB-PAPER-2014-047, CERN-PH-EP-2014-221, arXiv:1410.0149.

[110] P. Grafström and W. Kozanecki, "Luminosity determination at proton colliders", Progress in Particle and Nuclear Physics, doi:10.1016/j.ppnp.2014.11.002 (2014).

[111] TOTEM Collaboration, *Total cross section, elastic scattering and diffraction dissociation at the LHC: TOTEM Letter of Intent*, CERN-LHCC-97-049, LHCC-I-11 (CERN, Geneva, 1997).

[112] TOTEM Collaboration, *Total Cross Section, Elastic Scattering and Diffraction Dissociation at the LHC: TOTEM Technical Proposal*, CERN-LHCC-99-007, LHCC-P-5 (Geneva, Mar. 1999).

[113] TOTEM Collaboration, *Total cross-section, elastic scattering and diffraction dissociation at the Large Hadron Collider at CERN: TOTEM Technical Design Report*, CERN-LHCC-2004-002, TOTEM-TDR-001 (CERN, Geneva, 2004).

[114] TOTEM Collaboration, *Total cross-section, elastic scattering and diffraction dissociation at the Large Hadron Collider at CERN: Addendum to the TOTEM Technical Design Report*, TOTEM-TDR-001-add-1, CERN-LHCC-2004-020 (CERN, Geneva, 2004).

[115] U. Amaldi et al., "The Energy dependence of the proton proton total cross-section for center-of-mass energies between 23 and 53 GeV", Phys. Lett. B **44**, 112–118 (1973).

[116] H. Niewiadomski, "Reconstruction of Protons in the TOTEM Roman Pot Detectors at the LHC", CERN-THESIS-2008-080, PhD thesis (University of Manchester, Manchester, 2008).

[117] F. Nemes and H. Niewiadomski, "LHC optics measurement with proton tracks detected by the Roman pots of the TOTEM experiment", CERN-TOTEM-NOTE-2015-001 (2015).

[118] F. Nemes and H. Niewiadomski, "LHC optics measurement with proton tracks detected by the Roman pots of the TOTEM experiment", CERN-TOTEM-NOTE-2015-001 (2015).

[119] F. Nemes, "Elastic scattering of protons at the TOTEM experiment at the LHC", PhD thesis (Eötvös Loránd University, Budapest, Oct. 2015).

[120] F. Nemes, H. Niewiadomski, and H. Burkhardt, "LHC optics determination with proton tracks measured in the Roman pots detectors of the TOTEM experiment", in Proceedings of IPAC2012, Louisiana, USA, May 20-25 (2012), pp. 136–138.

[121] TOTEM Collaboration, "Early TOTEM running with the 90 m optics", CERN-LHCC-2007-013/G-130 (2007).

[122] H. Burkhardt and S. White, "High-β^* optics for the LHC", CERN-LHC-Project-Note-431 (2010).

[123] A. Verdier, "TOTEM optics for LHC V6.5", CERN-LHC-Project-Note-369 (2005).

[124] H. Burkhardt et al., "Commissioning and operation at beta* = 1000 m in the LHC", CERN-ACC-2013-0187 (2013).

[125] The CMS and TOTEM diffractive and forward physics working group, "Prospects for diffractive and forward physics at the LHC", LHCC-G-124, CERN-LHCC-2006-039-G-124, CMS-Note-2007-002, TOTEM-Note-2006-005, CERN-TOTEM-Note-2006-005 (2006).

[126] J. Welti, "Event classification and estimation of low mass diffraction at the TOTEM experiment at the LHC", MA thesis (University of Helsinki, Helsinky, Finland, 2011).

[127] J. C. Collins, "Light cone variables, rapidity and all that", arXiv:hep-ph/9705393 (1997).

[128] V. Barone and E. Predazzi, *High-Energy Particle Diffraction* (Springer, 2002).

[129] L. Baksay et al., "Evidence for double pomeron exchange at the CERN ISR", Phys.Lett. **B61**, 89 (1976).

[130] M. Della Negra et al., "Study of Double Pomeron Exchange in pp Collisions at $\sqrt{s} = 31$ GeV", Phys.Lett. **B65**, 394–396 (1976).

[131] D. Drijard et al., "Double pomeron exchange in the reaction pp $\to$ pp$\pi^+\pi^-$ at ISR energies", Nucl. Phys. B **143**, 61–80 (1978).

[132] J. Armitage et al., "A study of the reaction p + p $\to$ p + p + X at ISR energies", Phys. Lett. B **82**, 149–154 (1979).

[133] W. Meyer, "Pomeron interactions at the ISR", Nucl. Phys. B - Proceedings Supplements **12**, 135–148 (1990).

[134] J. Kašpar, "Elastic scattering at the LHC", CERN-THESIS-2011-214, PhD thesis (Charles University, Prague, 2011).

[135] ATLAS Collaboration, "Measurement of the total cross section from elastic scattering in pp collisions at $\sqrt{s} = 7$ TeV with the ATLAS detector", Nucl. Phys. **B889**, 486–548 (2014), see also arXiv:1408.5778 and ATLAS-CONF-2014-040.

[136] S. A. Khalek, "Measurement of the total proton-proton cross section with ATLAS at LHC", LAL-13-375, PhD thesis (Orsay, 2013).

[137] ATLAS Collaboration, "Measurement of the total cross section from elastic scattering in *pp* collisions at $\sqrt{s} = 8$ TeV with the ATLAS detector", CERN-EP-2016-158, arXiv:1607.06605 (2016).

[138] J. Kopal, "TOTEM trigger system", in 2013 International Conference on Applied Electronics (AE), Pilsen 10-12 September 2013 (2013).

[139] J. Kopal, "Development of the TOTEM trigger system", PhD thesis (University of West Bohemia, Pilsen, Mar. 2015).

[140] M. Quinto, "Design development and characterization of 2nd level trigger system for very forward detector at LHC", Presented 18 Mar 2015, CERN-THESIS-2014-300, PhD thesis (Bari University, 2014).

[141] A. Fiergolski, "Vol. 28 - Hardware implementation of the track identification algorithm in the Scalable Readout System for the TOTEM experiment", CERN-ACC-2015-0050, PhD thesis (Warsaw University of Technology, Feb. 2015).

[142] M. Deile, "Pileup probabilities and events per bunch-crossing", CERN-TOTEM-NOTE-2007-002 (2007).

[143] V. Ezhela et al., "Overview of the COMPETE program", arXiv:hep-ph/0212398, 47–61 (2002).

[144] J. Cudell et al., "Benchmarks for the forward observables at RHIC, the Tevatron Run II and the LHC", Phys.Rev.Lett. **89**, 201801 (2002).

[145] CMS Collaboration, "Measurement of the inelastic proton-proton cross section at $\sqrt{s} = 7$ TeV", CERN-PH-EP-2012-293, arXiv: hep-ph/1210.6718 (2011).

[146] ATLAS Collaboration, "Measurement of the Inelastic Proton-Proton Cross-Section at $\sqrt{s} = 7$ TeV with the ATLAS Detector", Nature Commun. **2**, 463 (2011).

[147] ALICE Collaboration, "Measurement of inelastic, single- and double-diffraction cross sections in proton–proton collisions at the LHC with ALICE", arXiv: hep-ph/1208.4968, CERN-PH-EP-2012-138 (2011).

[148] M. Berretti, "Measurement of the forward charged particle pseudorapidity density in pp collisions at $\sqrt{s} = 7$ tev with the TOTEM experiment", CERN-THESIS-2012-231, PhD thesis (Siena University, Sept. 2012).

[149] B. E. Y. Svensson, "High-energy phenomenology and Regge poles, Proceeding of the 1967 CERN school of physics Vol. II", CERN-TH-776 (1967).

[150] H. M. Pilkuhn, *The interaction of hadron* (North-Holland, 1967).

[151] H. M. Pilkuhn, *Relativistic quantum mechanics* (Springer, 2005).

[152] L. D. Landau and E. M. Lifshitz, *Course of Theoretical Physics Volume 1: Mechanics*, second edition, english translation (Pergamon Press, 1969).

[153] M. M. Block and R. N. Cahn, "High-energy $p\bar{p}$ and pp forward elastic scattering and total cross sections", Rev. Mod. Phys. **57**, 563–598 (1985).

[154] H. A. Bethe, "Scattering and polarization of protons by nuclei", Ann. Phys. **3**, 190–240 (1958).

[155] U. Amaldi et al., "Measurements of the proton-proton total cross section by means of Coulomb scattering at the CERN intersecting storage rings", Phys. Lett. B **43**, 231–236 (1973).

[156] V. Kundrát and M. Lokajíček, "Critical comments on the standard description of elastic hadron scattering", Phys. Lett. B **232**, 263–265 (1989).

[157] V. Kundrát and M. Lokajíček, "Description of high-energy elastic hadron scattering in both the Coulomb and hadronic domains", Mod. Phys. Lett. A **11**, 2241–2250 (1996).

[158] V. Kundrát and M. Lokajíček, "Interference between Coulomb and hadronic scattering in elastic high-energy nucleon collisions", Phys. Lett. B **611**, 102–110 (2005).

[159] V. Kundrát, M. Lokajíček, and I. Vrkoč, "Limited validity of West and Yennie integral formula for elastic scattering of hadrons", Phys. Lett. **B656**, 182–185 (2007).

[160] L. D. Landau and E. M. Lifshitz, *Course of Theoretical Physics Volume 3: Quantum Mechanics - non-relativistic theory*, second (revisited) edition, english translation (Pergamon Press, 1965).

[161] M. P. Locher, "Relativistic treatment of structure in the coulomb interference problem", Nucl. Phys. B **2**, 525–531 (1967).

[162] V. Kundrát, *Elastic hadron scattering at high energies*, Doctor of Mathematical and Physical sciences Thesis, Institute of Physics AV CR, 1996.

[163] V. Bartenev et al., "Real part of the proton-proton forward-scattering amplitude from 50 to 400 GeV", Phys. Rev. Lett. **31**, 1367–1370 (1973).

[164] CERN-Pisa-Rome-Stony Brook Collaboration, "New measurements of proton-proton total cross section at the CERN intersecting storage rings", Phys. Lett. B **62**, 460–466 (1976).

[165] L. Baksay et al., "Measurements of the proton-proton total cross section and small angle elastic scattering at ISR energies", Nucl. Phys. B **141**, 1–28 (1978).

[166] E. Nagy et al., "Measurements of elastic proton-proton scattering at large momentum transfer at the cern intersecting storage rings", Nuclear Physics B **150**, 221–267 (1979).

[167] L. A. Fajardo et al., "Real part of the forward elastic nuclear amplitude for pp, $\bar{p}p$, π^+p, π^-p, K^+p, and K^-p scattering between 70 and 200 GeV/c", Phys. Rev. D **24**, 46–65 (1981).

[168] D. Favart et al., "Measurement of $\bar{p}p$ Elastic Scattering at $\sqrt{s} = 52.8$ GeV at the CERN Intersecting Storage Rings", Phys. Rev. Lett. **47**, 1191–1194 (1981).

[169] N. Amos et al., "Comparison of small-angle $p\bar{p}$ and pp elastic scattering at 52.8 GeV center-of-mass energy at the CERN intersecting storage rings", Physics Letters B **120**, 460–464 (1983).

[170] G. Carboni et al., "Precise measurements of proton-antiproton and proton-proton total cross sections at the CERN intersecting storage rings", Nuclear Physics B **254**, 697–736 (1985).

[171] D. Bernard et al., "The real part of the proton-antiproton elastic scattering amplitude at the centre of mass energy of 546 GeV", Physics Letters B **198**, 583–589 (1987).

[172] M. Bozzo et al., "Low momentum transfer elastic scattering at the CERN proton-antiproton collider", Physics Letters B **147**, 385–391 (1984).

[173] M. Bozzo et al., "Elastic scattering at the CERN SPS collider up to a four-momentum transfer of 1.55 GeV^2", Physics Letters B **155**, 197–202 (1985).

[174] C. Augier et al., "A precise measurement of the real part of the elastic scattering amplitude at the S$\bar{p}p$S", Physics Letters B **316**, 448–454 (1993).

[175] M. M. Block, "Hadronic forward scattering: Predictions for the Large Hadron Collider and cosmic rays", Phys. Rept. **436**, 71–215 (2006).

[176] V. Kundrát, M. Lokajíček, and D. Krupa, "High-energy elastic hadron collisions and space structure of hadrons", in Proceedings of the 8th International Conference on Elastic and Diffractive Scattering, Protvino, Russia, Jun 28 - Jul 2, 1999, edited by P. V. A. Petrov and A. V. Prokudin, arXiv:hep-ph/0001047 (2000), pp. 333–338.

[177] V. Kundrát, J. Kašpar, and M. V. Lokajíček, "Theoretical aspects of high energy elastic nucleon scattering", in Proceedings of the 13th International Conference on Elastic and Diffractive Scattering, Switzerland, CERN, Jun 29 - Jul 3, 2009, edited by M. Deile, D. d'Enterria, and A. De Roeck, arXiv:hep-ph/1002.3527 (2010), pp. 35–41.

[178] A. Kohara, E. Ferreira, and T. Kodama, "Amplitudes and observables in pp elastic scattering at $\sqrt{s} = 7$ TeV", Eur. Phys. J. **C73**, 2326 (2013).

[179] M. N. Rosenbluth, "High energy elastic scattering of electrons on protons", Phys. Rev. **79**, 615–619 (1950).

[180] A. W. Thomas and W. Weise, *The structure of the nucleon* (WILEY-VCH, 2001).

[181] P. Jain and S. Mitra, "Proton electromagnetic form factors at large momentum transfer", Pramana **66**, 703–708 (2006).

[182] J. Arrington, C. D. Roberts, and J. M. Zanotti, "Nucleon electromagnetic form factors", Journal of Physics G: Nuclear and Particle Physics **34**, S23 (2007).

[183] V. Punjabi et al., "The structure of the nucleon: Elastic electromagnetic form factors", Eur. Phys. J. A **51**, 79 (2015).

[184] R. G. Sachs, "High-energy behavior of nucleon electromagnetic form factors", Phys. Rev. **126**, 2256–2260 (1962).

[185] N. F. Mott, "The collision between two electrons", Proceedings of the Royal Society of London A: Mathematical, Physical and Engineering Sciences **126**, 259–267 (1930).

[186] F. Borkowski et al., "Electromagnetic form-factors of the proton at low four-momentum transfer", Nucl. Phys. **A222**, 269–275 (1974).

[187] F. Borkowski, G. G. Simon, V. H. Walther, and R. D. Wendling, "Electromagnetic form factors of the proton at low four-momentum transfer (II)", Nuclear Physics B **93**, 461–478 (1975).

[188] J. Arrington, "Extraction of two-photon contributions to the proton form factors", Phys. Rev. C **71**, 015202 (2005).

[189] J. Arrington, W. Melnitchouk, and J. A. Tjon, "Global analysis of proton elastic form factor data with two-photon exchange corrections", Phys. Rev. C **76**, 035205 (2007).

[190] J. J. Kelly, "Simple parametrization of nucleon form factors", Phys. Rev. C **70**, 068202 (2004).

[191] A. J. R. Puckett, "Final results of the GEp-III experiment and the status of the proton form factors", arxiv:1008.0855 [nucl-ex] (2010).

[192] M. M. Block, "Are we really measuring the phase of the nuclear scattering amplitude?", Phys. Rev. D **54**, 4337–4343 (1996).

[193] R. J. Glauber, "High energy collision theory", in *Lectures in Theoretical Physics*, Vol. 1, edited by W. E. Brittin and L. C. Dunham (Interscience Publishers N.Y., 1959), pp. 315–414.

[194] T. Adachi and T. Kotani, "An impact parameter formalism", Progress of Theoretical Physics Supplement **E65**, 316–331 (1965).

[195] T. Adachi and T. Kotani, "Unitarity relation in an impact parameter representation", Progress of Theoretical Physics Supplement **37**, 297–305 (1966).

[196] T. Adachi, "An impact parameter formalism. II", Progress of Theoretical Physics **35**, 463–484 (1966).

[197] T. Adachi and T. Kotani, "An impact parameter formalism. III", Progress of Theoretical Physics **35**, 485–507 (1966).

[198] T. Adachi and T. Kotani, "An impact parameter representation of the scattering problem", Progress of Theoretical Physics **39**, 430–452 (1968).

[199] T. Adachi and T. Kotani, "An impact parameter representation of the scattering problem", Progress of Theoretical Physics **39**, 785–816 (1968).

[200] M. M. Islam, "Impact parameter description of high energy scattering", in Lectures in Theoretical Physics, Vol. 10B, edited by A. O. Barut and W. E. Brittin (1968), pp. 97–156.

[201] M. M. Islam, "Impact parameter representation from the Watson-Sommerfeld transform", Nucl. Phys. B **104**, 511–532 (1976).

[202] M. M. Islam, "Bethe's formula for coulomb-nuclear interference", Phys. Rev. **162**, 1426–1428 (1967).

[203] V. Franco, "Coulomb-nuclear interference", Phys. Rev. D **7**, 215–217 (1973).

[204] R. Cahn, "Coulombic-hadronic interference in an eikonal model", Zeitschrift für Physik C Particles and Fields **15**, 253–260 (1982).

[205] A. Donnachie and P. Landshoff, "Total cross sections", Physics Letters B **296**, 227–232 (1992).

[206] S. Wolfram, *Mathematica: A system for doing mathematics by computer* (Addison Wesley, 1991).

[207] L. van Hove, "A phenomenological discussion of inelastic collisions at high energies", Nuovo Cimento **28**, 798–817 (1963).

[208] L. van Hove, "High-energy collisions of strongly interacting particles", Rev. Mod. Phys. **36**, 655–665 (1964).

[209] E. H. De Groot and H. I. Miettinen, "Shadow approach to diffraction scattering", Invated talk presented at the VIIIth Recontre de Moriond, Merible-les-Allues 1973, RL-73-003 (1973).

[210] U. Amaldi, M. Jacob, and G. Matthiae, "Diffraction of Hadronic Waves", Ann. Rev. Nucl. Part. Sci. **26**, 385–456 (1976).

[211] U. Amaldi and K. R. Schubert, "Impact parameter interpretation of proton-proton scattering from a critical review of all ISR data", Nuclear Physics B **166**, 301–320 (1980).

[212] R. Castaldi and G. Sanguinetti, "Elastic scattering and total cross section at very high energies", Annual Review of Nuclear and Particle Science **35**, 351–395 (1985).

[213] D. S. Ayres et al., "Impact-parameter analysis of elastic scattering from 50 to 175 GeV/c", Phys. Rev. D **14**, 3092–3102 (1976).

[214] J. L. Bailly et al., "An impact parameter analysis of proton-proton elastic and inelastic interactions at 360 GeV/c", Z. Phys. C **37**, 7–16 (1987).

[215] V. Kundrát, M. V. Lokajíček, and D. Krupa, "Nucleon high-energy profiles", in Proceedings of the 9th International Conference on Elastic and Diffractive Scattering, Průhonice, Czech Republic, June 9-15, 2001, edited by V. Kundrát and P. Závada, `http://inspirehep.net/record/593128` (2002), pp. 247–256.

[216] V. Kundrát, M. V. Lokajíček, and D. Krupa, "Impact parameter structure derived from elastic collisions", Phys. Lett. B **544**, 132–138 (2002).

[217] M. Ida, "Phenomelogical analysis of the high-energy collisions of elementary particles", Prog. Theor. Phys. **28**, 945 (1962).

[218] F. S. Henyey and J. Pumplin, "Measuring the geometrical size of multiparticle processes", Nucl. Phys. **117**, 235–249 (1976).

[219] R. J. Eden, "Theorems on high energy collisions of elementary particles", Rev. Mod. Phys. **43**, 15–35 (1971).

[220] P. Eberhard, "Tests of the optical theorem", Nucl. Phys. B **48**, 333–342 (1972).

[221] P. Eberhard et al., "A test of the optical theorem", Phys. Lett. B **53**, 121–124 (1974).

[222] L. V. Hove, "An extension of Pomeranchuk's theorem to diffraction scattering", Physics Letters **5**, 252–253 (1963).

[223] L. V. Hove, "Exchange contributions to high energy scattering and imaginary character of the elastic amplitude", Physics Letters **7**, 76–77 (1963).

[224] A. A. Logunov, N. V. Hieu, I. T. Todorov, and O. A. Khrustalev, "Asymptotic relations between cross sections in local field theory", Physics Letters **7**, 69–71 (1963).

[225] A. A. Logunov, N. van Hieu, and I. T. Todorov, "Asymptotic relations between scattering amplitudes in local field theory", Annals of Physics **31**, 203–234 (1965).

[226] H. Cornille and A. Martin, "A *pomeranchuk* theorem for elastic diffraction peaks", Phys. Lett. **B40**, 671–674 (1972).

[227] H. Cornille and A. Martin, "Asymptotic equality of cross sections for line-reversed reactions", Nuclear Physics B **48**, 104–116 (1972).

[228] A. Martin, "Asymptotic behaviour of the real part of the scattering amplitude at t unequal 0", Lett. Nuovo Cim. **7S2**, 811–812 (1973).

[229] G. Auberson, T. Kinoshita, and A. Martin, "Violation of the Pomeranchuk theorem and zeros of the scattering amplitudes", Phys. Rev. D **3**, 3185–3194 (1971).

[230] V. Kundrát and M. V. Lokajíček, "Geometrical scaling in high-energy hadron collisions", Phys. Rev. D **31**, 1045–1050 (1985).

[231] V. Kundrát and M. Lokajíček, "Applicability of Martin's equations in high-energy elastic hadron scattering", Phys. Rev. D **55**, 3221–3224 (1997).

[232] P. A. S. Carvalho and M. J. Menon, "Evidence for eikonal zeros in the momentum transfer space", Phys. Rev. D **56**, 7321–7324 (1997).

[233] P. A. S. Carvalho, A. F. Martini, and M. J.Menon, "Eikonal representation in the momentum-transfer space", Eur. Phys. J. C **39**, 359 (2005).

[234] M. J. Menon, "Topics on high-energy elastic hadron scattering", Brazilian Journal of Physics **35**, 100–121 (2005).

[235] M. J. Menon, "On the França and Hama analysis of elastic hadron scattering", Brazilian Journal of Physics **37**, 9–12 (2007).

[236] R. F. Avila, S. D. Campos, M. J. Menon, and J. Montanha, "Phenomenological analysis connecting proton-proton and antiproton-proton elastic scattering", Eur. Phys. J. **C47**, 171–186 (2006).

[237] R. F. Avila, S. D. Campos, M. J. Menon, and J. Montanha, "On model-independent analyses of elastic hadron scattering", Brazilian Journal of Physics **37**, 675–677 (2007).

[238] R. F. Avila and M. J. Menon, "Eikonal zeros in the momentum transfer space from proton-proton scattering: An Empirical analysis", Eur. Phys. J. **C54**, 555–576 (2008).

[239] G. L. Pereira da Silva, M. J. Menon, and R. F. Avila, "Proton profile function at 52.8 GeV", Int. J. Mod. Phys. **E16**, 2923–2926 (2007).

[240] E. Ferreira and F. Pereira, "Hadronic sizes and observables in high-energy scattering", Phys. Rev. D **56**, 179–183 (1997).

[241] F. Pereira and E. Ferreira, "Eikonal profile functions and amplitudes for pp and $\bar{p}p$ scattering", Phys. Rev. D **59**, 014008 (1998).

[242] S. D. Campos, "Phenomenological Analysis of pp and $\bar{p}p$ Elastic Scattering Data in the Impact Parameter Space", Int. J. Mod. Phys. **A25**, 1937–1950 (2010).

[243] D. A. Fagundes, M. J. Menon, and G. L. P. Silva, "Model-independent data reductions of elastic proton-proton scattering", Eur. Phys. J. **C71**, 1637 (2011).

[244] D. A. Fagundes and M. J. Menon, "Applicability of a Representation for the Martin's Real-Part Formula in Model-Independent Analyses", Int. J. Mod. Phys. **A26**, 3219–3247 (2011).

[245] H. M. França and Y. Hama, "Energy dependence of the eikonal in $p-p$ elastic collisions", Phys. Rev. D **19**, 3261–3267 (1979).

[246] I. S. Gradshteyn and I. M. Ryzhik, *High-Energy Particle Diffraction* (Academic Press, San Diego, 1980).

[247] A. I. Shoshi, F. D. Steffen, and H. J. Pirner, "S-matrix unitarity, impact parameter profiles, gluon saturation and high-energy scattering", Nuclear Physics A **709**, 131–183 (2002).

[248] M. G. Ryskin, A. D. Martin, and V. A. Khoze, "Soft diffraction at the LHC: A Partonic interpretation", Eur. Phys. J. **C54**, 199–217 (2008).

[249] V. Kundrát, M. Lokajíček, and D. Krupa, "Momentum-transfer dependence of the elastic-amplitude phase in high-energy hadron scattering", Phys. Rev. D **35**, 1719–1722 (1987).

[250] V. Kundrát, M. Lokajíček, and D. Krupa, "Role of the phase and impact-parameter picture of $\bar{p}p$ elastic scattering at CERN Collider energy $\sqrt{s} = 546$ GeV", Phys. Rev. D **41**, 1687–1690 (1990).

[251] V. Kundrát, M. Lokajíček, and D. Krupa, "High-energy elastic hadron scattering in Coulomb and hadronic regions", Phys. Rev. D **46**, 4087–4090 (1992).

[252] U. Amaldi et al., "The real part of the forward proton proton scattering amplitude measured at the cern intersecting storage rings", Physics Letters B **66**, 390–394 (1977).

[253] U. Amaldi et al., "Precision measurement of proton-proton total cross section at the cern intersecting storage rings", Nuclear Physics B **145**, 367–401 (1978).

[254] A. Martin, "A theorem on the real part of the high-energy scattering amplitude near the forward direction", Physics Letters B **404**, 137–140 (1997).

[255] P. Heckman and R. Henzi, "Overlap function analysis of pp elastic scattering data at ISR energies", Phys. Lett. **B41**, 189–191 (1972).

[256] F. S. Henyey, R. Hong Tuan, and G. L. Kane, "Impact parameter study of high energy elastic scattering", Nucl. Phys. **B70**, 445–460 (1974).

[257] R. Henzi and P. Valin, "The inelastic differential cross-section in impact parameter space at ISR energies", Phys. Lett. **B48**, 119–124 (1974).

[258] R. Henzi and P. Valin, "On elastic proton proton diffraction scattering and its energy dependence", Nucl. Phys. **B148**, 513 (1979).

[259] R. Henzi and P. Valin, "Towards a blacker, edgier and larger proton", Phys. Lett. **B132**, 443–448 (1983).

[260] R. Henzi and P. Valin, "On the validity of Martin's real part formula", Phys. Lett. **B149**, 239 (1984).

[261] R. Henzi and P. Valin, "Does the proton look BEL at super-t and super colliders?", Phys. Lett. **B160**, 167 (1985).

[262] R. Henzi and P. Valin, "What is elastic scattering past the diffraction dip telling us?", Z. Phys. **C27**, 351–364 (1985).

[263] R. Henzi, "Energy dependence of diffraction maxima, interaction radius and absorption of proton", Nucl. Phys. **B104**, 52 (1976).

[264] P. Lipari and M. Lusignoli, "Interpretation of the measurements of total, elastic and diffractive cross sections at LHC", Eur. Phys. J. C, 73:2630 (2013).

[265] V. Franco and Y. Yin, "Elastic scattering of α particles and the Phase of the nucleon-nucleon scattering amplitude", Phys. Rev. Lett. **55**, 1059–1061 (1985).

[266] V. Franco and Y. Yin, "Elastic collisions between light nuclei and the phase variation of the nucleon-nucleon scattering amplitude", Phys. Rev. C **34**, 608–618 (1986).

[267] R. J. Glauber, "Multiple diffraction theory of high-energy collisions", in *High-energy physics and nucleon structure*, edited by G. Alexander (North-Holland, Amsterdam, 1967), p. 311.

[268] V. Petrov and A. Prokudin, "The first three pomerons...", Eur. Phys. J. C **23**, 135–143 (2002).

[269] V. Petrov, E. Predazzi, and A. Prokudin, "Coulomb interference in high-energy pp and $\bar{p}p$ scattering", Eur. Phys. J. C **28**, 525–533 (2003).

[270] V. A. Petrov and A. Prokudin, "Three Pomerons versus D0 and TOTEM data", Phys. Rev. D **87**, 036003 (2013).

[271] M. G. Ryskin, A. D. Martin, and V. A. Khoze, "Proton opacity in the light of lhc diffractive data", Eur. Phys. J. C **72**, 1–8 (2012).

[272] V. A. Khoze, A. D. Martin, and M. G. Ryskin, "T dependence of the slope of the high energy elastic pp cross section", Journal of Physics G: Nuclear and Particle Physics **42**, 025003 (2015).

[273] M. M. Block, E. M. Gregores, F. Halzen, and G. Pancheri, "Photon-proton and photon-photon scattering from nucleon-nucleon forward amplitudes", Phys. Rev. D **60**, 054024 (1999).

[274] M. M. Block and F. Halzen, "Forward hadronic scattering at 7 TeV: An update on predictions for the LHC", Phys. Rev. D **83**, 077901 (2011).

[275] M. M. Block and F. Halzen, "Forward hadronic scattering at 8 TeV: Predictions for the LHC", Phys. Rev. D **86**, 014006 (2012).

[276] M. M. Block, L. Durand, P. Ha, and F. Halzen, "Eikonal fit to pp and $\bar{p}p$ scattering and the edge in the scattering amplitude", Phys. Rev. D **92**, 014030 (2015).

[277] P. D. Lax and R. S. Phillips, *Scattering theory* (Academic Press, 1967).

[278] P. D. Lax and R. S. Phillips, *Scattering theory for automorphic functions* (Princeton University Press, 1976).

[279] M. V. Lokajíček, "Einstein-Bohr controversy after 75 years, its actual solution and consequences", in Some Applications of Quantum Mechanics, edited by M. R. Pahlavani (2012), pp. 409–424.

[280] M. V. Lokajíček, V. Kundrát, and J. Procházka, "Two different physical interpretations of Schroedinger equation", arXiv: quant-ph/1305.5503v2 (2014).

[281] N. Bohr, "The quantum postulate and the recent development of atomic theory", Nature **121**, 580–590 (1928).

[282] M. V. Lokajíček and V. Kundrát, "Optical theorem and elastic nucleon scattering", arXiv: hep-ph/0906.3961 (2009).

[283] M. V. Lokajíček and V. Kundrát, "Optical theorem and elastic nucleon scattering", in Proceedings of the 13th International Conference on Elastic and Diffractive Scattering, Switzerland, CERN, Jun 29 - Jul 3, 2009, edited by M. Deile, D. d'Enterria, and A. De Roeck, arXiv:hep-ph/1002.3527 (2010), pp. 62–66.

[284] R. G. Newton, "Optical theorem and beyond", American Journal of Physics **44**, 639–642 (1976).

[285] M. V. Lokajíček, "Phenomenological and ontological models in natural science", Concepts of Physics **4**, 657–670 (2007), see also arXiv:0710.3225 [physics.hist-ph].

[286] A. Arefiev et al., "Measurement of np elastic scattering at high energies and very small momentum transfers", Nucl. Phys. B **232**, 365–397 (1984).

[287] C. E. DeHaven et al., "Neutron-Proton Elastic Scattering from 70 to 400 GeV/c", Phys. Rev. Lett. **41**, 669–672 (1978).

[288] M. N. Kreisler, M. B. Davis, M. J. Longo, and D. D. O'Brien, "Neutron-proton charge-exchange scattering from 8 to 29 GeV/c", Nucl. Phys. B **84**, 3–54 (1975).

[289] G. N. Watson, *A treatise on the theory of Bessel functions* (Cambridge University Press, 1962).

[290] T. M. MacRobert, "Fourier integrals", Proc. Roy. Soc. Edinburgh Sect. A **51**, 116–126 (1931).

[291] T. M. MacRobert, "IV. Some applications of contour integration", The London, Edinburgh, and Dublin Philosophical Magazine and Journal of Science **38**, 45–51 (1947).

[292] I. N. Sneddon, *Fourier Transforms* (McGraw-Hill Co., 1951).

Appendix A

Some older experimental results

A.1 Neutron-proton elastic scattering

The np elastic differential cross section has been also measured for incident neutron momenta $100 - 400$ GeV/c in the very low $|t|$ range from 6×10^{-6} to 5×10^{-1} $(\mathrm{GeV/c})^2$ in the (NA-6) experiment at CERN SPS [286] (1984), see fig. A.1. The np data of this experiment provided a first direct measurement of the hadronic scattering for $|t| < 10^{-2}$ $(\mathrm{GeV/c})^2$ (being non-purely exponential). The data for $|t| < 10^{-4}$ $(\mathrm{GeV/c})^2$ were consistent with a rise attributed to *Schwinger scattering*, caused by the interaction of the neutron magnetic moment with the proton, see fig. A.2.

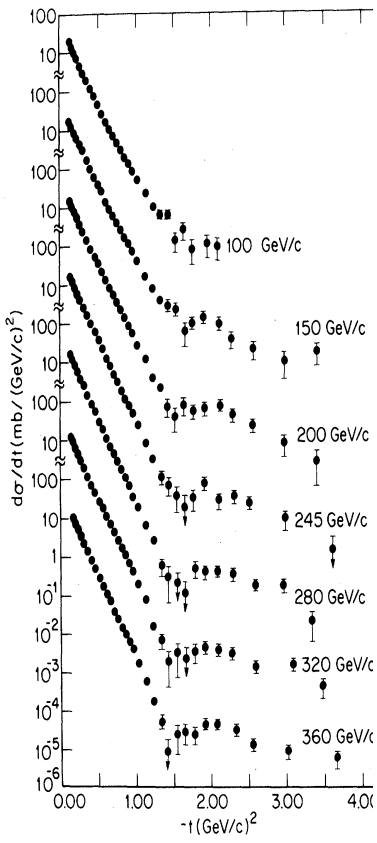

Figure A.1: Neutron-proton elastic differential cross sections in the range $0.15 \lesssim |t| \lesssim 3.6$ GeV^2 for seven incident momentum bins [287]; the momenta indicated are the center of the bins (collision energy $\sqrt{s}$ is two times higher). The data also exhibits a dip at $|t| \approx$ 1.4 GeV^2 for incident momenta above 200 GeV; the dip is more pronounced if the momentum increases.

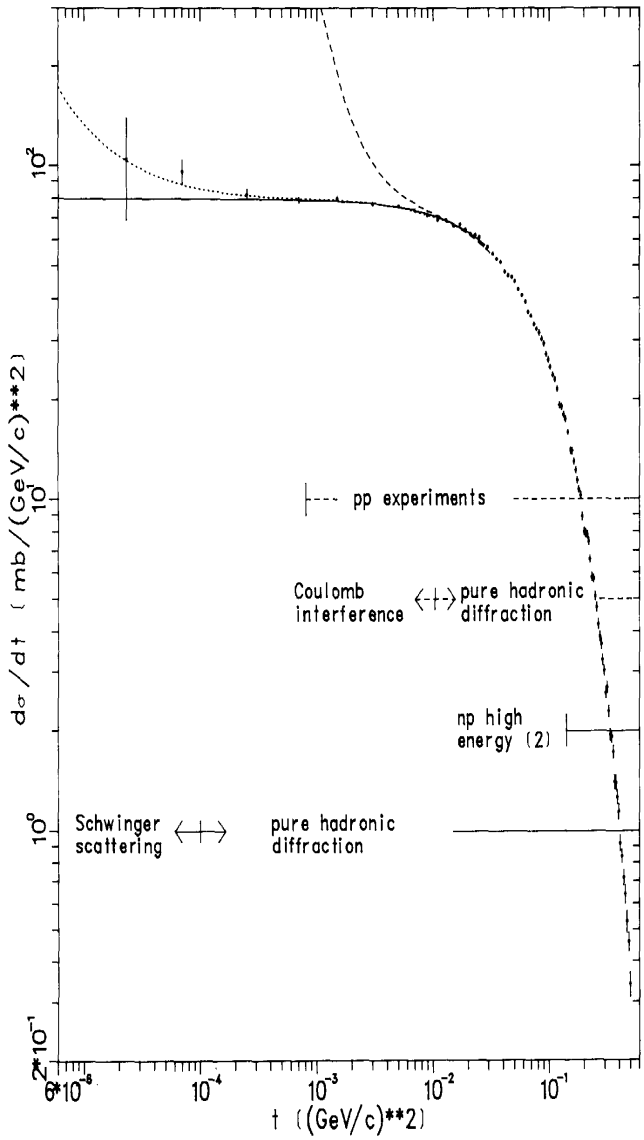

Figure A.2: Neutron-proton elastic differential cross section measured in the NA-6 experiment [286] for incident neutron momenta from 100 to 400 GeV (data points). Dashed line - calculated pp elastic differential cross section (including Coulomb interaction dominating at $|t| < 10^{-2}$ GeV^2). Dotted line - calculated Schwinger np scattering (involving the interaction between the magnetic moment of the neutron and the proton charge). Solid line - purely exponential elastic hadronic differential cross section as assumed in the two previous cases.

A.2 Neutron-proton charge exchange

One of the very interesting type of process is also *charge exchange* in, e.g., neutron-proton collision

$$np \to pn \ . \tag{A.1}$$

It represents an interaction in which electric charge is somehow transfered from the incident proton to the neutron which leads to abnormal (backward) scattering angles not expected at high energies in elastic scattering where no charge is exchanged. The differential cross sections for neutron-proton charge exchange scattering have been measured, e.g., in an experiment performed at the Brookhaven Alternation Gradient Synchrotron before 1975 [288] for incident neutron momenta between 8 and 29 GeV and for four-momentum transfer $|t|$ between 0.002 and 1.0 GeV^2. A neutron beam with a broad momentum spectrum was scattered from liquid hydrogen target in this experiment.

Charge exchange reactions are discussed also, e.g., in these proton-proton collisions:

$$pp \to n + \Delta^{++} \to n + p\pi^+ \tag{A.2}$$
$$pp \to \Delta^0 + \Delta^{++} \to n\pi^0 + p\pi^+ \tag{A.3}$$
$$pp \to \Delta^0 + \Delta^{++} \to p\pi^- + p\pi^+ \tag{A.4}$$

or also in the case of

$$p\pi^- \to n\pi^0. \tag{A.5}$$

Such processes indicate, e.g., that the distribution of electric charge inside proton is quite different than the distribution of hadronic matter. It could help also in considerations concerning the different states derived on the basis of the new probabilistic model discused in chapter 7.

Appendix B

Impact parameter representation of elastic hadronic amplitude at finite energies

The function $h_{\rm el}(s,b)$ defined by eq. (3.66) determines the impact parameter profile in the limit of s going to *infinity* as the FB transformation introducing the impact parameter representation of elastic scattering amplitude requires the amplitude to be defined for all values of t from the interval $(-\infty, 0\rangle$ [194–200]. For *finite* energy values the function $F^{\rm N}(s,t)$ may be specified, however, in the kinematically allowed interval only: $t \in \langle t_{\rm min}, 0\rangle$, where $t_{\rm min} = -s + 4m^2$ and m is the nucleon mass in the case of elastic nucleon scattering. It should hold $F^{\rm N}(s, t_{\rm min}) = 0$.

In the following we shall follow the approach proposed in [200]. One may write

$$\sqrt{-t} \;=\; 2p\,y\,, \qquad y \;=\; \sin\frac{\theta}{2}, \tag{B.1}$$

where θ stands for elastic scattering angle in the center-of-mass system. Let us define then the function $A(s,y)$ by relation

$$A(s,y) = \begin{cases} F^{\rm N}(s,y) & 0 \le y < 1 \\ \lambda(s,y) \equiv \lambda_R(s,y) + {\rm i}\;\lambda_I(s,y) & 1 < y < \infty \end{cases} \tag{B.2}$$

where $\lambda(s,y)$ is unknown complex function the real and imaginary parts of which are supposed to have following properties:

- $\int\limits_1^\infty y^{1/2}\lambda_{R,I}(s,y){\rm d}y$ are absolutely convergent,
- $\lambda_{R,I}(s,y)$ are of bounded variation for $1 < y < \infty$.

Then according to Hankel theorem [289] the amplitude $A(s,y)$ has FB transformation for $0 < y < \infty$

$$A(s,y) = \frac{\sqrt{s}}{2p}\int\limits_0^\infty \beta{\rm d}\beta\; J_0(\beta y)\; h(s,\beta), \tag{B.3}$$

$$h_{\rm el}(s,\beta) = \frac{2p}{\sqrt{s}}\int\limits_0^\infty y{\rm d}y\; J_0(\beta y)\; A(s,y); \tag{B.4}$$

here we have introduced a new variable $\beta = 2pb$.

More detailed insight to inverse FB transformation offers MacRoberts theorem [290–292] which may be formulated as follows. Let the function $F(s,y)$ is holomorphic in the interval $p < y < q$ and let the function $a(s,\beta)$ can be expressed by the integral

$$a(s,\beta) = \frac{2p}{\sqrt{s}} \int_p^q y\mathrm{d}y \; J_\nu(\beta y) \; F(s,y) \tag{B.5}$$

for $0 \le p < q \le \infty$ and $\mathrm{Re}\,\nu > -1$ then

$$A(s,y) = \frac{\sqrt{s}}{2p} \int_0^\infty \beta\mathrm{d}\beta \; J_\nu(\beta y) \; a(s,\beta) = \begin{cases} F(s,y) & \text{for } \; p < y < q, \\ 0 & \text{for } \; 0 < y < p \;\; \text{or} \;\; y > p. \end{cases} \tag{B.6}$$

MacRobert's theorem may be used to the FB transformation of function $F(s,y)$ as the elastic hadronic amplitude $F^{\mathrm{N}}(s,y)$ is the holomorphic function inside Lehman's ellipse with foci -1 and 1 (see, e.g., [219]).

Then the original elastic scattering amplitude $F^{\mathrm{N}}(s,t)$ is given by relation

$$F^{\mathrm{N}}(s,t) = 2p\sqrt{s} \int_0^\infty b\mathrm{d}b \; J_0(b\sqrt{-t}\,) \; h_{\mathrm{el}}(s,b), \tag{B.7}$$

which is the representation of elastic scattering amplitude in the impact parameter space. With the help of relation (B.2) the inverse relation to the relation (B.7) has a form

$$h_{\mathrm{el}}(s,\beta) = h_1(s,\beta) + h_2(s,\beta), \tag{B.8}$$

where

$$h_1(s,\beta) = \frac{2p}{\sqrt{s}} \int_0^1 y\mathrm{d}y \; J_0(\beta y) \; F^{\mathrm{N}}(s,y) \tag{B.9}$$

and

$$h_2(s,\beta) = \frac{2p}{\sqrt{s}} \int_1^\infty y\mathrm{d}y \; J_0(\beta y) \; \lambda(s,y). \tag{B.10}$$

The function $\lambda(s,y)$ as well as its FB image $h_2(s,\beta)$ are in general complex functions.

Similar relations may be derived also for the inelastic processes. Starting from the unitarity condition (3.65) in t variable (expressed now in y variable) and performing the FB transformation of the real inelastic overlap function $G_{\mathrm{inel}}(s,y)$ one may obtain

$$g_{\mathrm{inel}}(s,\beta) = g_1(s,\beta) + g_2(s,\beta), \tag{B.11}$$

where

$$g_1(s,\beta) = \frac{2p}{\sqrt{s}} \int_0^1 y\mathrm{d}y \; J_0(\beta y) \; G_{\mathrm{inel}}(s,y) \tag{B.12}$$

and

$$g_2(s,\beta) = \frac{2p}{\sqrt{s}} \int_1^\infty y\mathrm{d}y \; J_0(\beta y) \; \mu(s,y) \tag{B.13}$$

where the real function $\mu(s,y)$ must fulfill the same conditions as real and imaginary parts of function $\lambda(s,y)$.

The representation of elastic hadronic amplitude in the impact parameter space, i.e., $h_1(s,\beta)$ in the physical region, should contain the same amount of physical information as the original amplitude $F^{\mathrm{N}}(s,t)$. With the help of the optical theorem given by eq. (3.23) the total cross section may be expressed using the b-dependent function $h_1(s,b)$ as [194–200]

$$\sigma^{\mathrm{tot}}(s) = \frac{4\pi}{p\sqrt{s}}\ \mathrm{Im}\, F^{\mathrm{N}}(s,t=0) = \frac{2\pi}{p^2}\int\limits_0^\infty \beta \mathrm{d}\beta\ \mathrm{Im}\, h_1(s,\beta) = 2\pi\int\limits_0^\infty b\mathrm{d}b\ 4\,\mathrm{Im}\, h_1(s,b); \tag{B.14}$$

and also the integrated elastic cross section may be written as

$$\sigma^{\mathrm{el}}(s) = \frac{8\pi}{s}\int\limits_0^1 y\mathrm{d}y\ |F^{\mathrm{N}}(s,y)|^2 = \frac{2\pi}{p^2}\int\limits_0^\infty \beta\mathrm{d}\beta\ |h_1(s,\beta)|^2 = 2\pi\int\limits_0^\infty b\mathrm{d}b\ 4|h_1(s,b)|^2. \tag{B.15}$$

The integrated inelastic cross section ($\sigma^{\mathrm{inel}} = \sigma^{\mathrm{tot}} - \sigma^{\mathrm{el}}$) is then given by relation [194–200]

$$\sigma^{\mathrm{inel}}(s) = \frac{2\pi}{p^2}\int\limits_0^\infty \beta\mathrm{d}\beta\ g_1(s,\beta) = 2\pi\int\limits_0^\infty b\mathrm{d}b\ 4g_1(s,b). \tag{B.16}$$

The unitarity equation in the impact parameter space can be written in a generalized form as [194–200]

$$\mathrm{Im}\, h_1(s,\beta) = |h_1(s,b)|^2 + g_1(s,\beta) + K(s,\beta) \tag{B.17}$$

where the correction function $K(s,\beta)$ is limited by a condition

$$\int\limits_0^\infty \beta\mathrm{d}\beta\ K(s,\beta) = 0. \tag{B.18}$$

Also the functions $h_2(s,\beta)$ and $g_2(s,\beta)$ are limited by the similar conditions [194–200], i.e.,

$$\int\limits_0^\infty \beta\mathrm{d}\beta\ h_2(s,\beta) = 0, \qquad \int\limits_0^\infty \beta\mathrm{d}\beta\ g_2(s,\beta) = 0. \tag{B.19}$$

The function $K(s,\beta)$ equals [194–199]

$$K(s,\beta) = \frac{1}{16\pi^2 s}\int\limits_{t_{\mathrm{min}}}^0 \mathrm{d}t_1 \int\limits_{t_{\mathrm{min}}}^0 \mathrm{d}t_2\ F^{N*}(s,t_2)\ F^{\mathrm{N}}(s,t_1)\ M(\beta;t_1,t_2) \tag{B.20}$$

where

$$M(\beta;t_1,t_2) = J_0\left(\beta\sqrt{t_1\left(\frac{t_2}{t_{\mathrm{min}}}-1\right)}\right) J_0\left(\beta\sqrt{t_2\left(\frac{t_1}{t_{\mathrm{min}}}-1\right)}\right) - J_0(\beta\sqrt{-t_1})J_0(\beta\sqrt{-t_2}). \tag{B.21}$$

The function $K(s,\beta)$ vanishes at $\beta = 0$ and $b \to \infty$; and also at asymptotic energies ($t_{\min} \to -\infty$) [194–200]. Detailed analysis of high energy elastic pp scattering [48] has showed that the value of function $K(s,b)$ is very small and may be neglected.

The shape of elastic amplitude in the impact parameter space $h_{\rm el}(s,\beta)$ determined by eq. (B.8) depends on the t-dependence of elastic hadronic amplitude $F^{\rm N}(s,t)$ in the unphysical region of t. As shown by Islam [201] the uniqueness of the $F^{\rm N}(s,t)$ can be achieved if two t-dependent parts of the amplitude $F^{\rm N}(s,t)$ in the physical and unphysical regions are bounded by the Sommerfeld-Watson transformation. The elastic amplitude $h_{\rm el}(s,\beta)$ in the impact parameter space oscillates at larger β values; the oscillations disappear at infinite energies only.

The representation of the scattering amplitude in the impact parameter space has been defined in [194–200] as an analogy to partial wave analysis. From the requirement of equivalence of both these representations the question arises which conditions imposed on the elastic hadronic amplitude $F^{\rm N}(s,t)$ guarantee the existence of its impact parameter representation. It has been shown in [194–200] that the finiteness of the integrated elastic cross section (B.15) at finite energies guarantees its existence.

It has been shown in [20] that $\mathrm{Im}\, h_1(s,b)$ and $g_1(s,b)$ obtained with the help of the FB transformation oscillate at larger values of impact parameter b due to the fact that the region of kinematically allowed values of momentum transfers t at finite energies is limited and the region for $t < t_{\min}$ is not taken into account. The oscillations appear not only in the case of peripheral behaviour of elastic hadron scattering where they are very significant but also in the case of central behaviour. The physical meaning may be, therefore, hardly attributed to the functions $4\,\mathrm{Im}\, h_1(s,b)$ and $4g_1(s,b)$ in eqs. (B.14), (B.16) and (B.17), even if their integrals represent corresponding cross sections, see also [201]. Only the non-negative function $4|h_1(s,b)|^2$ has been denoted as elastic profile function. According to [49, 176, 177, 215, 216] non-negative (non-oscillating) total and inelastic profile functions at finite energies may be defined if a convenient real function $c(s,b)$ is added to both the sides of the unitarity equation (B.17). In such a case one obtains eq. (3.78). It is then possible to define at finite energies total, elastic and inelastic profile functions $D^{\rm X}(s,b)$ (X=tot, el, inel) according to eqs. (3.75) to (3.77) and rewrite the unitarity condition in b-space in the form given by eq. (3.73). The shape of $D^{\rm tot}(s,b)$ and $D^{\rm inel}(s,b)$ might be then modified to become non-negative; the shape of elastic profile remains the same. The function $c(s,b)$ should, however, fulfill some additional conditions. The total and inelastic cross section given by eq. (3.72) (see eqs. (B.14) to (B.16)) remains unchanged if

$$\int_0^\infty b\,\mathrm{d}b\; c(s,b) = 0. \tag{B.22}$$

The other physical quantities which should be preserved are the mean squared values of the total and inelastic impact parameters, i.e., function $c(s,b)$ should not change the quantities $\langle b^2\rangle^{\rm tot}$ and $\langle b^2\rangle^{\rm inel}$ defined according to eq. (3.80). These quantities will be preserved if also

$$\int_0^\infty b^3\,\mathrm{d}b\; c(s,b) \;=\; 0. \tag{B.23}$$

By definition all the mentioned processes (total, elastic and inelastic) are realized by strong interactions which are of finite ranges. Therefore both the integrals appearing in

eq. (3.80) should be convergent. Condition $\beta^{1/2}h_1(s,\beta) \in L^2(0,\infty)$ guarantees that all three integrals (for total, elastic or inelastic type X) in the denominator of eq. (3.80) are convergent; for the inelastic case also on the basis of unitarity condition given by eq. (B.17) (the influence of the correction function $K(s,\beta)$ as it has been mentioned can be neglected). However, this condition does not guarantee the convergence of the integrals in the nominator of eq. (3.80); in order to achieve this we have to require the validity of stronger condition, i.e., that $\beta^{3/2}h_1(s,\beta) \in L^2(0,\infty)$. Due to the unitarity equation the remaining two integrals corresponding to the elastic and inelastic scattering will be convergent, too.

The function $c(s,b)$ should fulfill, therefore, the following conditions: it must remove the oscillations (provide the non-negative function $D^{\mathrm{tot}}(s,b)$) and fulfill eq. (B.22) and eq. (B.23).

It follows then from the Islam's approach [201] that the two conditions given by eqs. (B.22) and (B.23) are fulfilled when

$$c(s,b) \;=\; -\;\mathrm{Im}\,h_2(s,b), \tag{B.24}$$

where $h_2(s,b)$ is defined by eq. (B.10) and is based on analytical continuation of complex amplitude $F^{\mathrm{N}}(s,t)$ that fulfills the condition

$$F^{\mathrm{N}}(s,t_{\mathrm{min}}) \;=\; 0. \tag{B.25}$$

It means also that one can hardly determine the function $c(s,b)$ quite exactly on the basis of the conditions above and experimental data of elastic scattering corresponding always to very limited t-region (see also [49, 177]). The functions $c(s,b)$ and profile functions $D^{\mathrm{X}}(b)$ may be determined if some other assumptions are added, see the end of sect. 3.4.3.

List of Figures

List of Tables

Acronyms

ALFA Absolute Luminosity For ATLAS. A project under ATLAS with similar physics aims as the ones of TOTEM experiment.

ALICE A Large Ion Collider Experiment. An LHC experiment at CERN, see sect. 1.2.

ALPHA Antihydrogen Laser PHysics Apparatus. An experiment at CERN aiming to compare hydrogen atoms with their antimatter equivalents – antihydrogen atoms (similar to ATRAP experiment).

ATLAS A Toroidal LHC ApparatuS. An LHC experiment at CERN, see sect. 1.2.

ATRAP Antihydrogen TRAP. An experiment at CERN aiming to compare hydrogen atoms with their antimatter equivalents – antihydrogen atoms (similar to ALPHA experiment).

BSRT Beam Synchrotron Radiation Telescope. A device for measuring transversal beam profile.

CD central diffraction. See CP.

CERN European Organization for Nuclear Research. Conseil Européen pour la Recherche Nucléaire (Geneva, Switzerland).

CMS Compact Muon Solenoid. An LHC experiment at CERN, see sect. 1.2.

COMPETE COmputerised Models, Parameter Evaluation for Theory and Experiment. A collaboration whose program was defined in [143].

CP central production. A process pp $\rightarrow$ pXp where both protons survive but lose certain momentum and a system of particles X is created. The definition often also requires the system X to be separated from the two protons by two rapidity gaps. This process is sometimes denoted also as central diffraction (CD) (or double pomeron exchange (DPE) which suggest an intepretation).

CSC Cathode Strip Chamber. Multiwire proportional chamber with segmented cathode read-out. A detector technology chosen for T1 detector.

CT-PPS CMS-TOTEM Precision Proton Spectrometer. Joint CMS and TOTEM project which is intended to add precision proton tracking and timing detectors in the very forward region on both sides of CMS at about 200m from the IP, see [40].

CTS Current Terminating Structure. Part of the TOTEM RP silicon strip detector used to collect the current generated in the highly damaged region at the cut edge and so avoids its diffusion into the sensitive detector volume, see sect. 2.2.3.

DAQ Data AcQuisition. Refers to software and/or hardware systems responsible for recording data during measurement.

DCCT Direct Current Current Transformers. A beam instrumentation for measuring of overall beam charge.

DD double diffraction. A process pp $\rightarrow$ XY which is similar to single diffraction (SD) except that both the protons breaks up, each producing particles in a limited rapidity region.

DPE double pomeron exchange. See CP.

ES elastic scattering. A process pp $\rightarrow$ pp with two outgoing collinear protons which did not lose energy.

FB Fourier–Bessel. Refers to Fourier–Bessel transformation.

FBCT Fast Bunch Current Transformers. A beam instrumentation for measuring of relative bunch charge.

GEM Gas Electron Multiplier. Type of gaseous ionization detector. A detector technology used for T2 detector.

HERA Hadron-Electron Ring Accelerator. A particle accelerator at DESY in Hamburg.

IP Interaction Point. Used commonly in the sama meaning as IR.

IR Interaction Region. A place where two opossite beams may collide in LHC (IR1, IR2, IR5 or IR8) sometimes also used for indication of a LHC octant as shown in fig. 1.7. Also known as Intersection Region or Intersection Point.

ISR Intersecting Storage Rings. A past accelerator (storage rings) which was at CERN; the world's first proton (hadron) collider.

LHC Large Hadron Collider. An accelerator at CERN, see sect. 1.1.

LHCb Large Hadron Collider beauty. An LHC experiment at CERN, see sect. 1.2.

LHCf Large Hadron Collider forward. An LHC experiment at CERN, see sect. 1.2.

LINAC2 LINear ACcelerator 2. A linear proton accelerator at CERN, see sect. 1.1.

LS1 Long Shutdown 1. Refers to first long shutdown of LHC which started in first quoter of 2013 and took $\sim$2 years.

MoEDAL Monopole and Exotics Detector at the LHC. An LHC detector (experiment) at CERN, see sect. 1.2.

NA-6 North Area 6. A past experiment at CERN SPS which measured neutron-proton elastic scattering at very small scattering angles.

np neutron-proton. Refers to a collision of neutron and proton.

OL Optical theorem Luminosity. Refers to a method of total cross section determination based on optical theorem and luminosity, see sect. 3.5.2.

OLI Optical theorem Luminosity Independent. Refers to luminosity independent method of total cross section determination based on optical theorem, see sect. 3.5.3.

pp proton-proton. Refers to a collision of two protons.

$\bar{p}$p antiproton-proton. Refers to collision of antiproton and proton.

PS Proton Synchrotron. An accelerator at CERN, see sect. 1.1.

PSB Proton Synchrotron Booster. An accelerator at CERN, see sect. 1.1.

QCD quantum chromodynamics. Relativistic quantum field theory of strong interactions.

QM quantum mechanics. Non-relativistic quantum theory based on Schrödinger equation (also known as quantum physics).

RF Radio Frequency. Refers to radio frequency system (RF system) used to accelerate charged particles, see chapter 1.

RHIC Relativistic Heavy Ion Collider. A heavy-ion colliders which is able to collide some other particles including spin-polarized proton beams at high energies (Run-9 achieved center-of-mass energy of 500 GeV on 12 February 2009 - the highest in the world). It is located at Brookhaven National Laboratory (BNL) in New York, USA.

RP Roman Pot. A moveable device which can be equipped by detetors to measure particles very close to a particle beam.

RP147 Roman Pot. TOTEM RP station at distance of about 147 m from interaction point IP5, see fig. 2.2.

RP220 Roman Pot. TOTEM RP station at distance of about 220 m from interaction point IP5, see fig. 2.2.

Run 1 Run 1. LHC running period during 2009 – 2013, before LS1.

SD single diffraction. A process pp $\rightarrow$ pX or Yp which is similar to elastic scattering (ES) except that one of the protons breaks up, producing particles in a limited rapidity region.

Sp$\bar{p}$S The SPS operated as a proton–antiproton instead of proton-proton collider from 1981 to 1984 - it was, therefore, called Sp$\bar{p}$S.

SPS Super Proton Synchrotron. An accelerator at CERN, see sect. 1.1.

SUSY supersymmetry. A theory proposing symmetry of nature relating particles which have integer-valued spin (bosons) to particles having a half-integer spin (fermions).

T1 Telescope 1. One of the TOTEM detector detecting charged particles originating from inelastic collisions.

T2 Telescope 2. One of the TOTEM detector detecting charged particles originating from inelastic collisions.

TEVATRON It was a circular particle accelerator in the USA, at the Fermi National Accelerator Laboratory (Fermilab) that accelereted protons and antiprotons to energies of up to 1 TeV (which is the reason for its name).

TOTEM TOTal, Elastic and diffractive cross section Measurement. An LHC experiment at CERN, see sect. 1.2 and chapter 2.

TR total rate. Refers to rate of elastic and inelastic events.

VDM van der Meer. Refers to beam separation scans pioneered by Simon van der Meer, see sect. 1.3.2.

WS Wire Scanner. A device for measuring transversal beam profile.

WY West and Yennie. Authors of one of the Coulomb and hadronic interference formulas, see sect. 3.2.